National Library of Canada
Acquisitions and Bibliographic Services Branch
395 Wellington Street
Ottawa, Ontario
K1A 0N4

Bibliothèque nationale du Canada
Direction des acquisitions et des services bibliographiques
395, rue Wellington
Ottawa (Ontario)
K1A 0N4

Your file Votre référence

Our file Notre référence

NOTICE

The quality of this microform is heavily dependent upon the quality of the original thesis submitted for microfilming. Every effort has been made to ensure the highest quality of reproduction possible.

If pages are missing, contact the university which granted the degree.

Some pages may have indistinct print especially if the original pages were typed with a poor typewriter ribbon or if the university sent us an inferior photocopy.

Reproduction in full or in part of this microform is governed by the Canadian Copyright Act, R.S.C. 1970, c. C-30, and subsequent amendments.

AVIS

La qualité de cette microforme dépend grandement de la qualité de la thèse soumise au microfilmage. Nous avons tout fait pour assurer une qualité supérieure de reproduction.

S'il manque des pages, veuillez communiquer avec l'université qui a conféré le grade.

La qualité d'impression de certaines pages peut laisser à désirer, surtout si les pages originales ont été dactylographiées à l'aide d'un ruban usé ou si l'université nous a fait parvenir une photocopie de qualité inférieure.

La reproduction, même partielle, de cette microforme est soumise à la Loi canadienne sur le droit d'auteur, SRC 1970, c. C-30, et ses amendements subséquents.

Canada

SOME ASPECTS OF PLATEAU PERMAFROST, QINGHAI-XIZANG (TIBET) PLATEAU, CHINA, AND A COMPARISON WITH THE MACKENZIE DELTA REGION, CANADA

by

Baolai Wang
Ottawa-Carleton Geoscience Centre
University of Ottawa
Ottawa, Ontario, Canada

Thesis Presented to the School of Graduate Studies and Research in Partial Fulfilment of the Requirements for the Degree of Doctor of Philosophy in Geology

ISBN 0-315-83845-0

UNIVERSITÉ D'OTTAWA
UNIVERSITY OF OTTAWA

Doctor of Philosophy — University of Ottawa

(Geology) — (Ottawa, Canada)

Thesis Title: Some Aspects of Plateau Permafrost, Qinghai-Xizang (Tibet) Plateau, China, and A Comparison with the Mackenzie Delta Region, Canada

Author: Baolai Wang

(B.Sc. Hebei Institute of Geology, People's Republic of China

(M.Sc. Lanzhou Institute of Glaciology and Geocryology, Chinese Academy of Sciences)

Supervisor: Dr. H.M. French

Pages: xvi, 224

Examining committee:

Dr. S.A. Harris (University of Calgary)

Dr. P.J. Williams (Carleton University)

Dr. B. Lauriol (University of Ottawa)

Dr. P.G. Johnson (University of Ottawa)

ABSTRACT

Differences in permafrost conditions between the Qinghai-Xizang (Tibet) Plateau and the Mackenzie Delta region primarily relate to their Quaternary histories and their current climates. For example, the Tibetan Plateau has experienced uplift of at least 3,000 m during the last 2 million years. Under the present climatic conditions, the lower altitudinal limit of the plateau permafrost in the north is at 4,150 m a.s.l. This suggests that if the Plateau were 1,000 m lower than its present elevation, there would be no permafrost. During the Quaternary, the Tibetan Plateau remained unglaciated. This has meant that little water was available for the formation of massive ground ice, in contrast to the Mackenzie Delta region.

Located at 68-69° N, the Mackenzie Delta region experiences a combination of low air temperature in winter, a long solar night and a short thaw period in summer. The result is a relatively thin active layer. Located at 30-34° N, the Tibetan Plateau experiences much higher solar insolation, and a diurnal temperature rhythm. The thickness of the active layer is much greater than in the Mackenzie Delta region and varies between 1.3 and 3 m or more.

Permafrost on the Tibetan Plateau is much warmer and thinner than that in the Mackenzie Delta region. One consequence is that it is more sensitive to any changes in climate and surface conditions.

Deep ground temperatures in the Pleistocene Mackenzie Delta indicate a recent warming trend, while a cooling trend in the Modern Delta likely relates to local factors such as channel shifting and emergence and/or sedimentation in the Mackenzie River.

Water bodies are a cause of geothermal disturbances common to both regions. Numerical simulation of rapid coastal retreat in the Mackenzie Delta region indicates that subsea permafrost is at least 3°C warmer than adjacent terrestrial permafrost. On the Tibetan Plateau, faulting also disturbs the geothermal regime.

Measurements of *in situ* permafrost creep in the Fenghuo Shan area are one indicator of the warmer permafrost temperatures on the Tibetan Plateau. The average creep velocity ranges from 0.16 cm/year at 2.8 m depth to 0.54 cm/year at 1.6 m depth. These velocities are greater than those recently obtained from the High Arctic of Canada and are approximately of the order of magnitude as those obtained in the Mackenzie Valley. Inter-continental comparison of creep data suggests that climate controls the regional (large scale) magnitude of creep, and that ground ice is a local factor controlling creep rate in a particular area or site. A constitutive relationship (secondary creep power flow law) was applied to the field creep data; and creep parameters A and n were determined for each of the three different depths in the West Valley, Fenghuo Shan area, Tibetan Plateau.

ACKNOWLEDGEMENTS

I would like to acknowledge the support and encouragement given me by a number of organizations and individuals, without which this thesis would not have been written. I was on a China Foreign Scholarship provided by the Chinese Academy of Sciences during the first year of my study at the University of Ottawa. I thank the Lanzhou Institute of Glaciology and Geocryology (LIGG) of the Chinese Academy of Sciences for nominating me for that scholarship. Field work in the Mackenzie Delta region was financially supported by the Natural Science and Engineering Research Council of Canada (grant A-8367 to H.M. French) and the University of Ottawa Northern Research Group. Logistic support for the field work in the Mackenzie Delta region was kindly provided by the Polar Continental Shelf Project (project 37-75), Department of Energy, Mines and Resources, and the Inuvik Research Centre of the Science Institute of Northwest Territories, Canada. The *in situ* creep project on the Qinghai-Xizang (Tibet) Plateau has been financially supported by the National Natural Science Foundation of China. Logistic support for the field work on the Tibet Plateau has been provided by the Lanzhou Institute of Glaciology and Geocryology, the Qinghai-Xizang Plateau Research Station at Golmud, and the Fenghuo Shan Permafrost Research Station of the Northwest Institute of Railway, China.

In particular, I wish to acknowledge Dr. H.M. French, my thesis supervisor, for providing me with guidance and support, and for polishing my English. Professor Guodong Cheng, director of the

LIGG, has provided me with much inspiration and encouragement since I became a permafrost student in 1983. He was also instrumental in planning the logistics of the *in situ* permafrost creep project on the Tibet Plateau. Professor Yizhi Huang, director of the Golmud Research Station, kindly provided drilling equipment for the creep project.

Thanks are extended to professors Youwu Zhou, Boliang Tong, and Dongxin Guo of the LIGG, my M.Sc. thesis supervisors, for their continuing encouragement. A number of my colleagues at the LIGG have provided me with support through correspondence over the years. Field assistance given by Yi Sheng, Haomo Wang, and Yujie Wang is very much appreciated. The *in situ* creep measurements on the Tibet Plateau have been undertaken by Jingsen Zhang and Rongkang Qu. I thank all the staff members of the Golmud Research Station for their hospitality.

I also wish to acknowledge Mr. Gary White, manager of the Inuvik Research Centre for his support at Inuvik, and some of my fellow graduate students in the Department of Geology, University of Ottawa - Frank Brunton, Geof Burbidge, and Julian Murton for their hospitality and friendship. They made my study in Ottawa more enjoyable.

The thesis examiners Drs. P.J. Williams, S.A. Harris, P.G. Johnson, and B.Lauriol provided me with valuable comments and suggestions to improve the thesis. I thank them all.

At last, but most importantly, I acknowledge my wife, Jian-Qi, for her support and understanding.

TABLE OF CONTENTS

PART FOUR: SYNTHESIS

LIST OF FIGURES

LIST OF TABLES

Tables Page

PART ONE

BACKGROUND

CHAPTER ONE - AIMS AND OBJECTIVES

1.1 Introduction

Permafrost is a product of the long-term energy exchanges between the atmosphere and the ground. Permafrost is here defined as ground remaining at or below 0°C in temperature for at least two years (ACGR 1988, p63). This definition is based on temperature only, irrespective of the state of any moisture that might be present. The definition is generally accepted in North America (e.g. French 1976; Lachenbruch 1968; Péwé 1983; Washburn 1981; Williams and Smith 1989). This contrasts with the former USSR and People's Republic of China, where permafrost has been defined as earth material containing ice for at least 3 year's duration (e.g. Tsytovich 1975; Lanzhou Institute of Glaciology, Geocryology and Desert Research 1975).

More than 20% of the land area of the world is underlain by permafrost (Melnikov and Tolstikhin 1988; Péwé 1983). The former Soviet Union possesses the largest extent of permafrost in the world; it is estimated that about 11 x 10^6 km^2 of permafrost exists in that country, about 49% of its territory (Melnikov and Tolstikhin 1988; Tsytovich 1975). The second largest area of permafrost is in Canada. About 50% of Canada (5.7 x 10^6 km^2) is underlain by permafrost (Fig. 1.1). The People's Republic of China ranks third, with an area of 2.15 x 10^6 km^2 being underlain by permafrost (Fig. 1.2). This is 22.3% of its entire territory (Lanzhou Institute of Glaciology and Geocryology 1988). In addition, more than 80% of Alaska is underlain by permafrost, and alpine permafrost with areas of >100,000 km^2 occurs in the western

contiguous United States (Péwé 1983). Smaller permafrost bodies occur in Scandinavia, Greenland, Antarctic and the various alpine mountains throughout the world.

Permafrost environments occur in two contrasting and overlapping geographical regions; namely, high-latitude and high altitude areas (Harris 1986, 1988). Accordingly, permafrost can be classified into one of the following categories: 1) polar (or latitudinal) permafrost, e.g. permafrost in the arctic regions, 2) alpine permafrost, e.g. permafrost in mountainous regions, 3) plateau permafrost, e.g. extensive permafrost at high elevations, such as on the Qinghai-Xizang (Tibet) Plateau of China; and 4) subsea permafrost, e.g. on the continental shelf of the Laptev sea, Siberia and Beaufort Sea, North America. The differentiation between plateau permafrost and alpine permafrost is especially important when dealing with the Tibet Plateau, since conditions in the latter are quite different to the well-known alpine environments of mid-latitudes. For example, when one arrives on the top of the Qinghai-Xizang (Tibet) Plateau, the traveller does not see many rugged mountain ridges or glaciated peaks. Instead, the plateau surface is rather flat. That is why Chinese scientists have named the broad areas between the mountain ranges the 'high plains'. An important feature that differentiates the Plateau from alpine environments is that unconsolidated sediments on the Plateau may exceed 1,000 m in thickness (Guo *et al.* 1982). Recently, the term 'mountain permafrost' has been used to include both alpine and plateau permafrost (e.g. Cheng and Dramis 1992; Harris and Corte

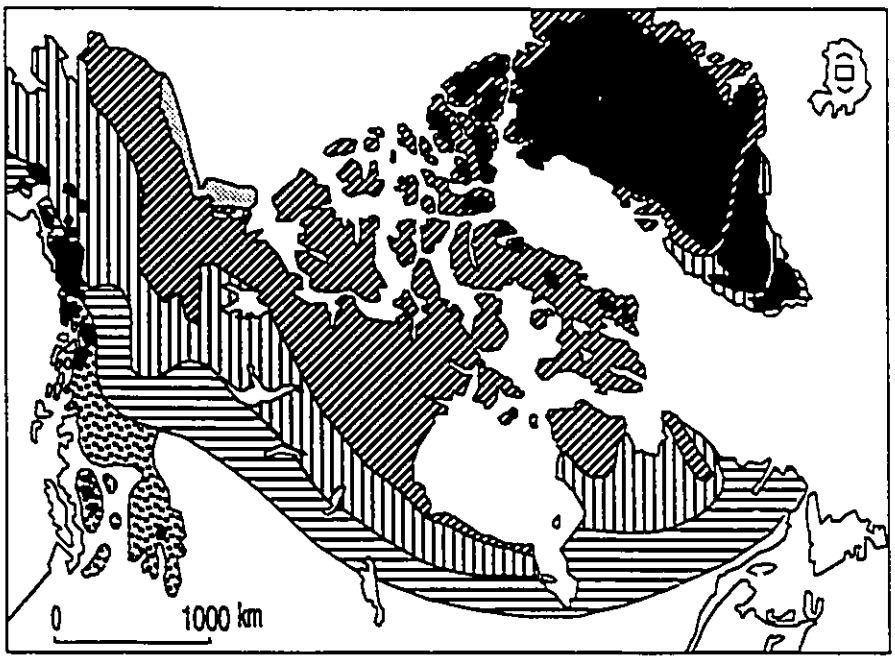

Zone of continuous permafrost (>80% of area underlain by permafrost)

Zone of discontinuous permafrost: subzone of widespread discontinuous permafrost (30 to 80% of area underlain by permafrost)

Zone of discontinuous permafrost: subzone of sporadic discontinuous permafrost (<30% of area underlain by permafrost)

Alpine permafrost

Known subsea permafrost

Perennial ice cap

Figure 1.1 Permafrost in Canada (Source: ACGR 1988).

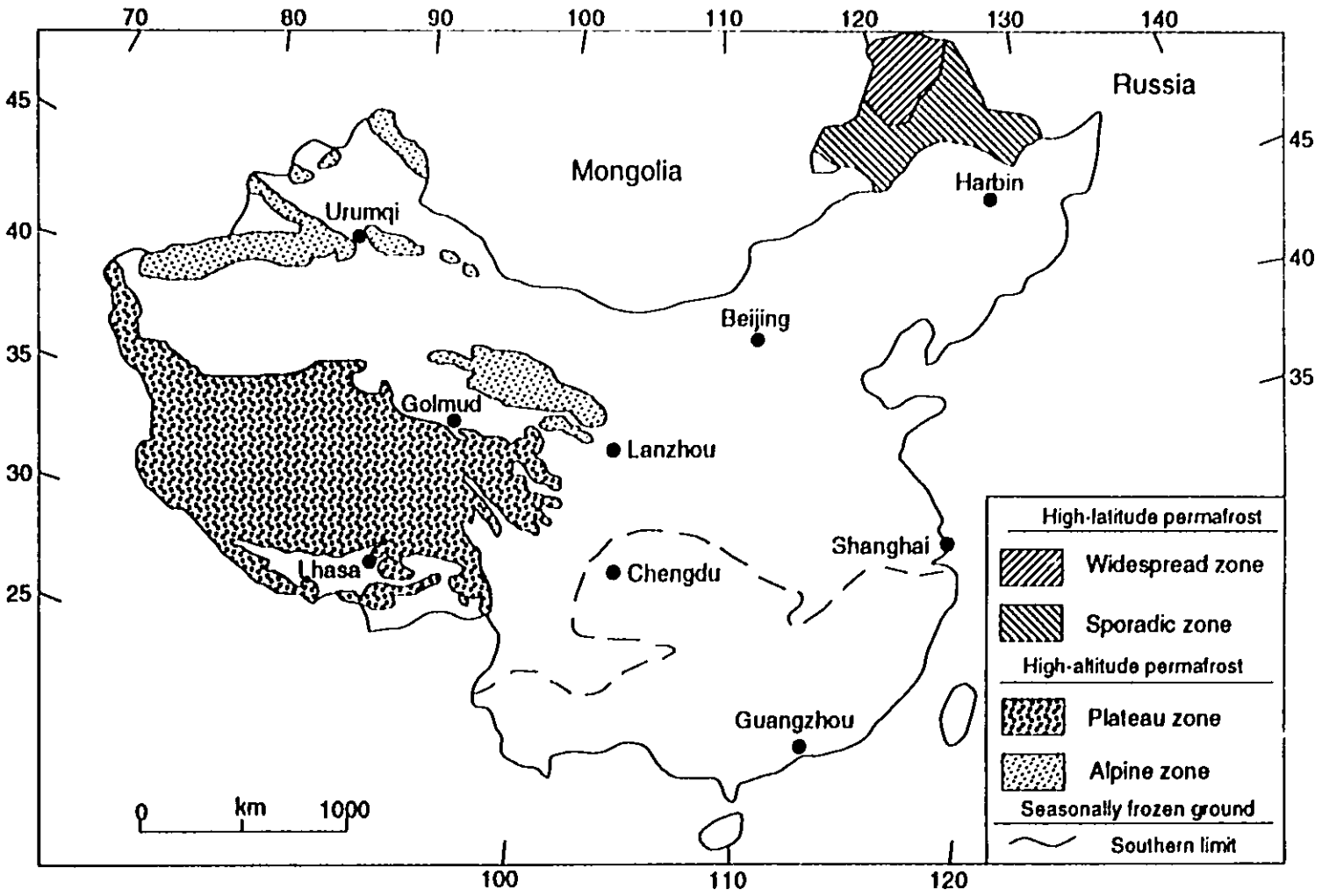

Fig. 1.2 Permafrost and seasonally frozen ground in China (Modified from: Lanzhou Institute of Glaciology and Geocryology 1988).

1992).

The Qinghai-Xizang Plateau is often referred to as 'the roof of the world'. Glaciologists and geocryologists in China refer to it as the 'the third pole' of the earth because, in its simplest terms, permafrost is a result of its high elevation.

The earliest Chinese publication on permafrost described investigations carried out along the Trans-Plateau Highway (Chinese Academy of Sciences 1965), and the first text on permafrost in China appeared in 1975, written by the Lanzhou Institute of Glaciology, Geocryology and Desert Research (1975). Since then, a large literature has appeared, much of it in the Journal of Glaciology and Geocryology and in the Proceedings of various Chinese Conferences.

1.2 Aims and Objectives

This thesis discusses the permafrost conditions on the Qinghai-Xizang Plateau, China and in the Mackenzie Delta region NWT, Canada. It compares the geocryological conditions of the two areas and characterizes their geothermal regimes and the nature and significance of thermal disturbances. The Mackenzie Delta region is relatively well known in the western permafrost literature on account of the ice-rich nature of its permafrost, resulting in numerous pingos, ice wedges and massive ice bodies (see Mackay 1962, 1963a, 1971, 1973, 1979). It is also an area in which detailed field measurements of geomorphic processes have been undertaken (e.g. Mackay 1975, 1979, 1989, 1990a, 1990b). The

Quaternary history is equally well known (e.g. Rampton 1988). However, it is mistakenly regarded as a 'classic' or 'typical' periglacial environment and is widely used as an example in textbooks (e.g. French 1976; Washburn 1979). In reality, the Mackenzie Delta is a rather unique permafrost environment, since it is essentially a deltaic region of numerous lakes, thick deposits of unconsolidated Quaternary sediments, and an abundant and luxurious tundra, and shrub-tundra ecosystem. The so-called typical periglacial environment characterized by 'rock rubble' or 'frost-shatter zones' (e.g. Büdel 1982) does not apply to the Mackenzie Delta.

By contrast, the Qinghai-Xizang Plateau (29-36°N) is poorly known in the North American and European permafrost literature. It is also not typical of the well known alpine periglacial regions of the world since it is at a low latitude and experiences a dry continental climate. The Qinghai-Xizang Plateau lies between the lofty Himalayas to the south and Quidam Basin to the north. The Plateau has an average altitude of 4,500 m a.s.l., and is the highest extensive land area on Earth. It is also the coldest part of the middle latitudes of the world. Permafrost is widespread on the Plateau, with its total area being 1.5×10^6 km^2.

Two specific aims of the thesis are:

1) To compare permafrost conditions in both areas in order to gain a better understanding of how differences in Quaternary history and climate result in different permafrost environments. Unique characteristics of permafrost conditions of an area are

often more apparent and easier to understand when a comparison is made with other regions. For example, Brown (1967) recognized some of the unique characteristics of permafrost in both Siberia and northern Canada by comparing glacial history, climate, and terrain conditions of both areas.

2) To examine geothermal regimes and disturbances in both areas by examining surface energy exchanges, active-layer development, and geothermal gradients, and to discuss the palaeoclimatic implications of deep ground temperatures. The geothermal regime is an important parameter since it determines the sensitivity and response of permafrost to disturbances and any changes in climate.

In addition to these two aims described above, a field component included the measurement of *in situ* permafrost creep on the Qinghai-Xizang (Tibet) Plateau. The aims here are to provide *in situ* creep data relevant to engineering activities on the Plateau and to compare typical permafrost creep rates of low latitude plateau permafrost with those reported from high latitude permafrost of northern Canada. A further aim is to determine creep parameters from the field data, as defined by the secondary (steady state) creep flow law. The rationale for this field component lies in the fact that, although laboratory studies on frozen soil creep have been carried out for a number of years, there is still a need for long-term creep data obtained at low stresses and relatively warm temperatures. This is because most experimental tests have been performed at very low temperatures (down to -30°C) (e.g.

Parameswaran 1982) and stress levels more than 300 kPa (e.g. McRoberts 1988), which are far greater than those experienced in the field by piles and natural slopes (e.g. Morgenstern 1981, 1985). Furthermore, with few exceptions, laboratory creep tests were run over short time periods and terminated before the onset of the secondary creep stage. This also contradicts field conditions where piles and slopes undergo long-term and low-stress secondary creep. Pile design and slope-stability analysis are usually concerned with rheological properties of permafrost at warmer temperatures (e.g. -1 to -5°C), since engineering structures often encounter safety problems within this temperature range due to excessive creep deformation.

Permafrost creep also plays a role in slope processes in areas underlain by permafrost. According to Mackay (1988), permafrost creep may contribute towards rampart formation of pingos especially during the collapse stages that would accompany climatic amelioration. Permafrost creep has been observed in the downslope curvature of ice wedges (Bozhinskiy and Konishchev 1982; Gasanov 1981). A recent review by Lewkowicz (1988) indicates that one of the advances in periglacial slope process studies is the recognition of permafrost creep as a potentially important denudational process in regions with 'warm' permafrost.

The safe operation of the Trans-Plateau Highway and the oil pipelines on the Plateau have been of primary concern of permafrost scientists and engineers in China. The highway has been repaired many times, but permafrost-related problems have never been

entirely solved. There is also a possibility that a proposed trans-plateau railway will be built in the future. If this were realized, there would be a great need for *in situ* creep data.

On the Tibet Plateau, *in situ* creep occurs in a warm permafrost environment; thus, creep data obtained are of great interest to both engineering design and slope analysis.

1.3 History of Permafrost Investigations in the Mackenzie Delta and on the Qinghai-Xizang (Tibet) Plateau

Early permafrost investigations in Canada in the 1960's were largely centred upon the Mackenzie Valley and Delta. Many field studies are still conducted in the Mackenzie Delta region, largely because of the proximity of the PCSP (Polar Continental Shelf Project) base at Tuktoyaktuk and the Inuvik Research Centre. It is not necessary to outline these activities since they are well known in the Canadian permafrost literature (e.g. see Proceedings of the Fifth Canadian Permafrost Conference 1990).

Early observations of periglacial phenomena in the Himalayas-Tibet Plateau region were made by foreign expeditions (Troll 1958). As early as 1925, Odell reported the occurrence of patterned ground phenomena at 5100 m a.s.l. in the Mt Everest region (Odell 1925). Solifluction, stone streams, and patterned ground were some of the major subjects of early observations (e.g., Heim 1936; Heim and Gansser 1939). Heim also noticed that the lower elevational limit of frost soil (permafrost ?) on the Plateau decreased from south to

north. But during that time, permafrost on the Plateau was not specifically mentioned.

Although descriptions of snow, ice and frozen ground appear in ancient Chinese literature of 2,000 years ago, scientific permafrost investigations on the Qinghai-Xizang Plateau are very recent. They are closely related to the development of the Lanzhou Institute of Glaciology and Geocryology, Chinese Academy of Sciences. In 1958, the Chinese Academy of Sciences organized a 'Snow-Ice Research Group'. This led to the establishment in 1965 of the Lanzhou Institute of Glaciology, Geocryology and Desert Research. In 1978 this Institute was split into the Lanzhou Institute of Glaciology and Geocryology, and Lanzhou Institute of Desert Research (Shi 1988).

The first permafrost investigations conducted by scientists on the Qinghai-Xizang Plateau were initiated in the 1960's (Shi 1988). Two years of fieldwork suggested that predominantly continuous permafrost was extensive in the area between the Kunlun Shan to the north and the Tangula Shan to the south. A resulting memoir, published in 1965 by the China Science Press, included papers on periglacial geomorphology (Du and Xie 1965), ground ice (Wu 1965a), groundwater (Wu 1965b), vegetation (Sun 1965), and permafrost conditions (Tong 1965; Zhou 1965).

Anticipated construction of the railway and the operation of the existing Trans-Plateau Highway provided the need for more detailed information on engineering, geologic and hydrogeologic conditions on the Plateau. A consequence was the comprehensive

permafrost investigations conducted during the late 1960's and 1970's by joint groups, largely focussing on engineering geology and hydrogeology (e.g. Qiu 1980). Unfortunately, because of the so-called 'cultural revolution', very few papers were published during the period between the first memoir, published in 1965, and the first issue of the Journal of Glaciology and Geocryology, published in 1979. Some of these early results have been published later in the Journal of Glaciology and Geocryology and in some conference proceedings (e.g. Lanzhou Institute of Glaciology and Geocryology 1982a, 1982b, 1983a, 1983b, 1989a. 1989b).

Permafrost investigations on the Plateau have largely centred on the Trans-Plateau Highway corridor because of easy accessibility. A permafrost map (1:600,000) along the highway produced in 1980 (e.g. Guo 1981; Tong *et al.* 1982, 1983) summarizes information obtained during the period 1960 - 1979. Prior to this map, only some zonation maps had been compiled, showing the local distribution of permafrost (e.g. Tong 1965; Zhou 1965). Investigations focussing on ground ice were carried out mainly from 1977 to 1980 in order to provide information for the construction and design of engineering facilities on the Plateau (Qinghai-Xizang Highway Research Group 1983; Li, Lie 1982; Li and Xing 1980).

Permafrost conditions on the Plateau are now summarized by many investigators (e.g. Wang *et al.* 1979; Zhou and Guo 1982, 1983). Tong and Li (1983) and Cheng (1988) give good accounts of the factors influencing permafrost. Frost blisters and pingos on the Plateau have been studied by Cheng (1979), Cheng and Qiu

(1983), Wang (1983a) and Wang and Yao (1981); ground wedges by Guo (1979), Liang and Cheng (1984) and Zhang (1983); thermokarst by Wang (1983b, 1986, 1990); and rock glaciers by Cui (1983). Other investigations relate to the ground thermal regime (e.g. Wang and Li 1983); taliks (e.g. Guo *et al.* 1982; Qiu 1982; Qiu and Guo 1983); permafrost history (e.g. Ding and Guo 1982; Guo 1988; Pu *et al.* 1982; Zhang and Cai 1981; Wang 1989; Wang and Zhang 1985); plateau permafrost zonation (e.g. Cheng and Wang 1982; Cheng and Wu 1984); hydrogeology (e.g. Hu and Xu 1982; Zhai 1982); solar radiation (e.g. Kou *et al.* 1982; Zeng *et al.* 1982); frost heave (e.g. Tong Changjiang 1982, 1983; Tong and Yu 1983); and physio-mechanical properties of permafrost (e.g. Wang Yaqing 1983; Wu 1979, 1982; Wu *et al.* 1982, 1983a, 1983b; Zhu *et al.* 1982a, 1982b).

CHAPTER TWO - REGIONAL BACKGROUND

2.1 Introduction

Permafrost terrain in the Mackenzie Delta region and on the Qinghai-Xizang Plateau represents important and different types of permafrost environment. Besides climate, permafrost occurrence is controlled mainly by such factors as vegetation, soil/rock type, topography, etc. Differences in these factors may cause quite different permafrost conditions (e.g. Brown 1967, 1969, 1978; Cheng 1988; Melnikov and Tolstikhin 1988; Smith 1975a, 1976). Under certain circumstances these variables break the regional climatic patterns and determine the presence/absence and/or thermal regime of permafrost. Therefore, this chapter provides regional background to both the Mackenzie Delta region and the Qinghai-Xizang Plateau, and supplies information on relevant physiography, Quaternary history, vegetation, permafrost history and geocryology.

2.2 Mackenzie Delta Region

2.2.1 Physiography

The Mackenzie Delta region lies between latitudes 68° and 70°N., immediately south of the Arctic Ocean. Most of the region is flat and below 60 m in elevation. It includes two major physiographic regions: 1) the Modern Mackenzie River Delta and 2) the Pleistocene Coastal Plain, which lies to the east of the Modern Delta and the Caribou Hills (Figure 2.1). This general area has been described systematically by Fyles *et al.* (1972), Mackay (1963a, 1978), and Rampton (1988). The surficial geology of this

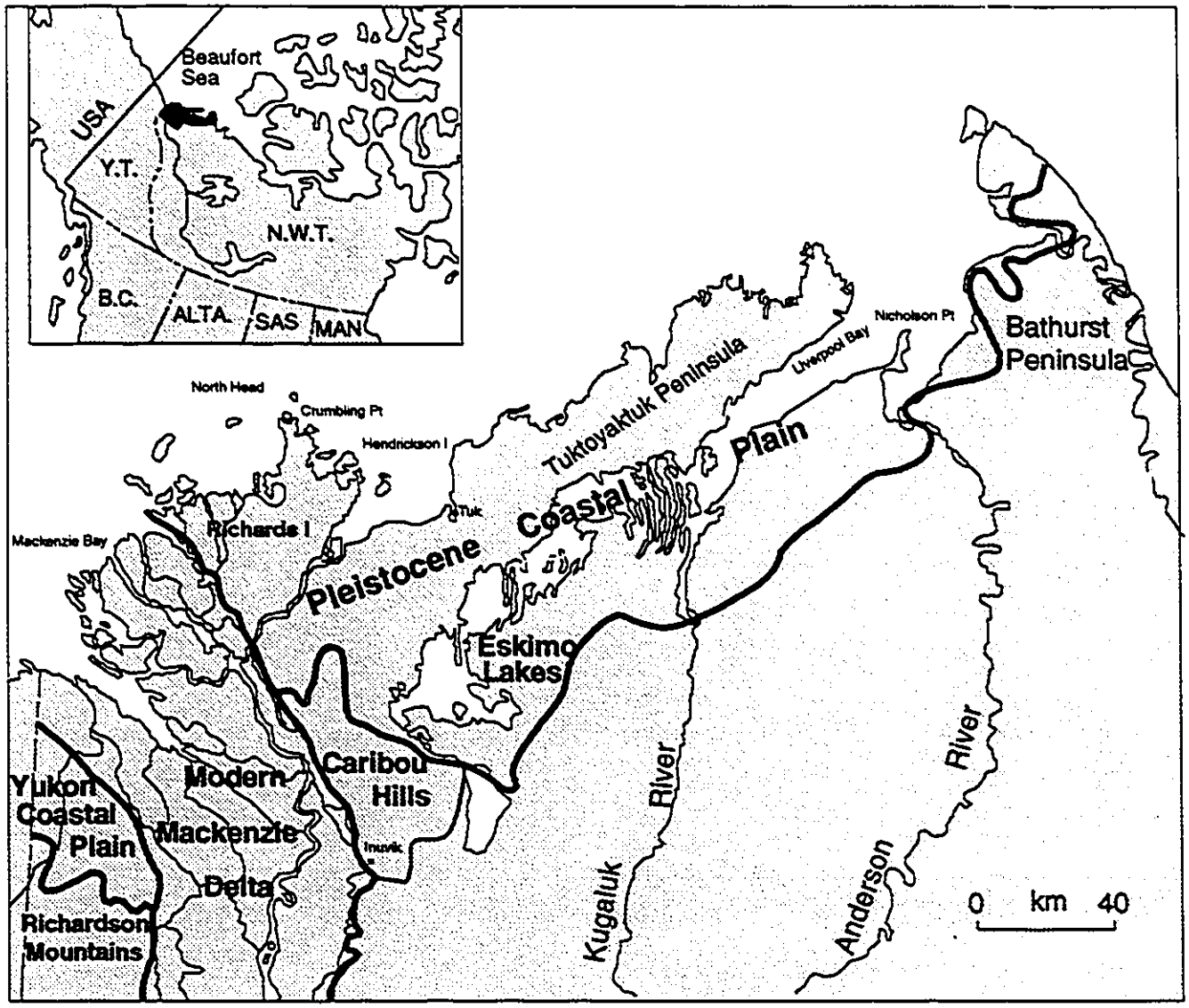

Figure 2.1 Location map and physiographic divisions of the Mackenzie Delta region (Source: Rampton 1988).

area is illustrated in Figure 2.2.

The Mackenzie Delta region is characterized by a sub-arctic tundra climate (Burns 1973a, 1973b). The mean annual air temperature (MAAT) in the study area ranges between -9°C and -12°C, and the mean annual ground surface temperature from -3.0 to -9.0°C (Judge 1973). The mean annual air temperature range is between 26 and 30°C. The annual total precipitation ranges between 150 and 300 mm, and the net radiation between 10 and 20 kly/yr. Only a weak latitudinal zonation (i.e. the higher the latitude, the lower is the air temperature) exists in the region.

Modern Delta

The Modern Delta is about 200 km long and 65 km wide. The floodplain decreases from an altitude of about 10 m a.s.l. at the south to sea level at the north. All of the delta is susceptible to flooding. The higher southern portion may flood at breakup, usually in early June, whereas the seaward part may flood either at breakup or in association with storm surges in summer or early fall (Mackay 1978).

The delta surface (Figure 2.3a) is a complex network of lakes and anastomosing channels (Heginbottom and Tarnocai 1983). Lakes cover more than 30% of the upper part of the delta, 15-30% of the middle part, and less than 15% of the distal part (Mackay 1963a). J.R. Mackay believes that most lakes in the Mackenzie Delta are of floodplain rather than thermokarst origin. On the other hand, as argued by Fyles *et al.* (1972), lakes are most abundant in the

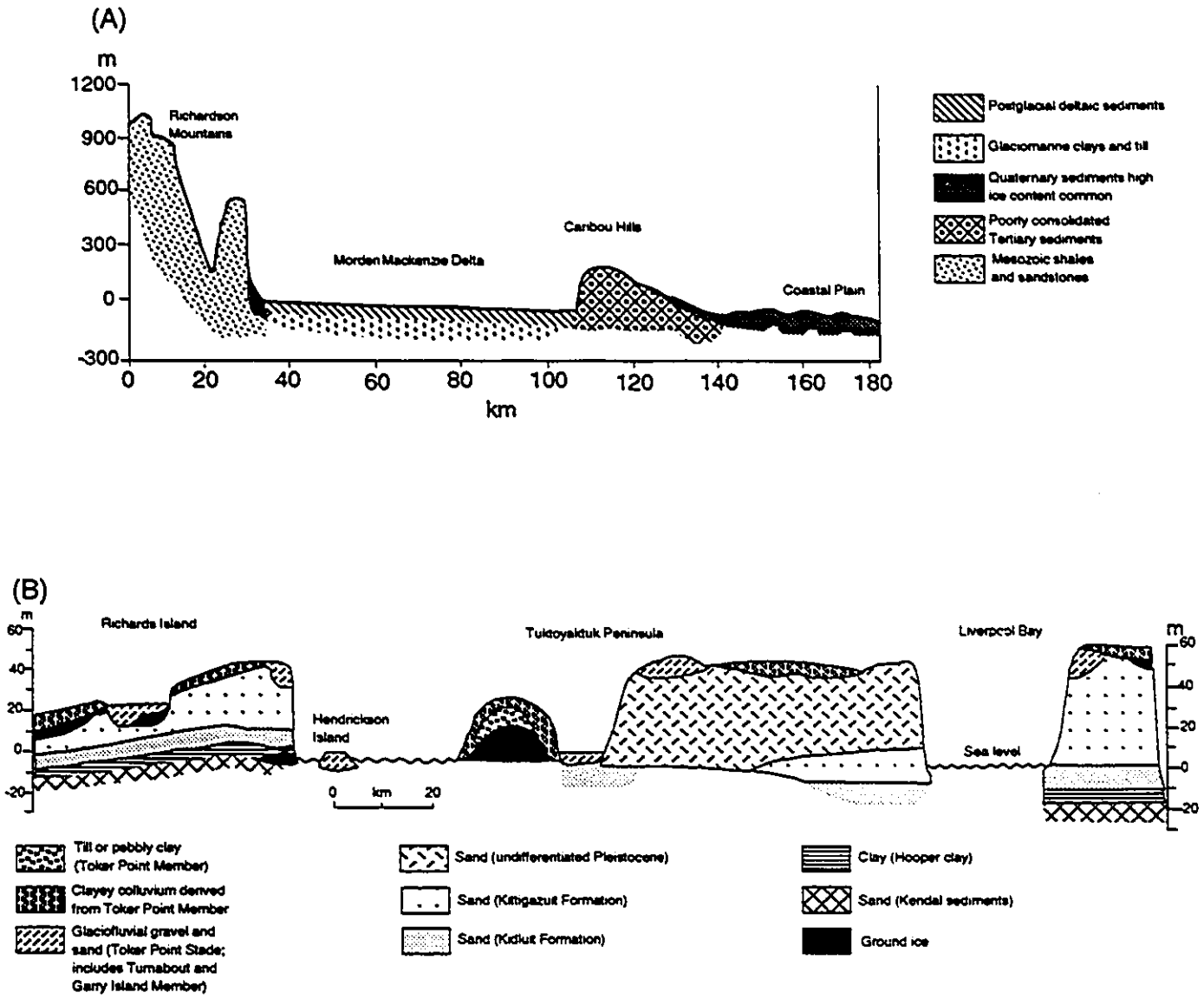

Figure 2.2 (A) Diagrammatic representation of the stratigraphic succession, Pleistocene Coastal Plain (Source: Rampton 1972), and (B) a geological cross-section from Richardson Mountains to the Pleistocene Coastal Plain (Source: Rampton 1988).

A

B

Figure 2.3 Landscape of (A) the modern Mackenzie Delta, and (B) the Pleistocene Delta.

southern part of the delta where permafrost, vegetation, and drainage conditions favour thermoerosion and subsidence.

The Modern Delta is postglacial in age. A radiocarbon date of 6,900 years B.P. has been obtained from a depth of 38 m at a site 8 km southwest of Inuvik (Johnston and Brown 1963, 1964). Probably most of the upper 30 m of the delta sediments has been deposited in the past 5,000 years (Mackay 1978).

Pleistocene Coastal Plain

The Pleistocene Coastal Plain (Figure 2.3b), previously termed the Pleistocene Coastlands (Mackay 1963a), the Pleistocene Mackenzie Delta (Mackay 1962), and the Tuktoyaktuk Coastlands (Rampton 1988), borders the eastern edge of the Modern Delta and the Caribou Hills. To the south is the northern limit of the Anderson Plain (Figure 2.1). The coastal plain includes Tuktoyaktuk Peninsula, the southern side of the Eskimo lakes, Richards Island, and a group of offshore Islands (Mackay 1978). The Coastal Plain has been described by Mackay (1963a, 1978) as consisting ".... mainly of Pleistocene marine and fluvial sands, silts, gravels and clays, veneered for the most part with glacial till. Most of the area lies below altitudes of 60 m with about 50% below 30 m".

Much of the sediment was probably deposited by an ancestral Mackenzie River during interglacial periods when sea level was 10 to 20 m higher than the present coastal plain. Most of the Pleistocene Coastal Plain, with the possible exception of the eastern third of the Tuktoyaktuk Peninsula, has been glaciated

(Mackay 1978; Rampton 1988). However, the Late Wisconsinan ice extended little, if any, distance across the Tuktoyaktuk Peninsula.

2.2.2 Quaternary Geology

The Quaternary history of the Pleistocene Coastal Plain has been summarized by Rampton (1988). Most of the coastal plain in the lower Mackenzie Delta region lies within the limits of continental glaciation. During the Mason River glaciation of Middle Pleistocene age, northwesterly moving continental ice halted on Cape Bathurst Peninsula, leaving an unglaciated terrain to the north (Figure 2.4).

Northwesterly flowing ice again covered most of the area during the Toker Stade of Early Wisconsinan age. The Laurentide Ice Sheet persisted in the southern Mackenzie Delta and Sitidgi Lake areas (Figure 2.4), depositing till (Sitidgi Member). During this time, glaciers were confined mainly to the trench underlying the Modern Mackenzie Delta and adjacent lowlands. Much of the continental shelf was exposed during the Late Wisconsinan and earlier glaciations, allowing permafrost to develop (Heginbottom and Tarnocai 1983). During the Middle Wisconsinan, the Laurentide Ice Sheet was subject to melting because of climatic amelioration, but the extent of the ice at that time is a matter of debate (Dredge and Thorleifson 1987).

Numerical modelling of permafrost aggradation in the Mackenzie Delta indicates an Early Wisconsinan and Late Wisconsinan surface temperature of about -18°C and a Middle Wisconsinan rise to -8°C,

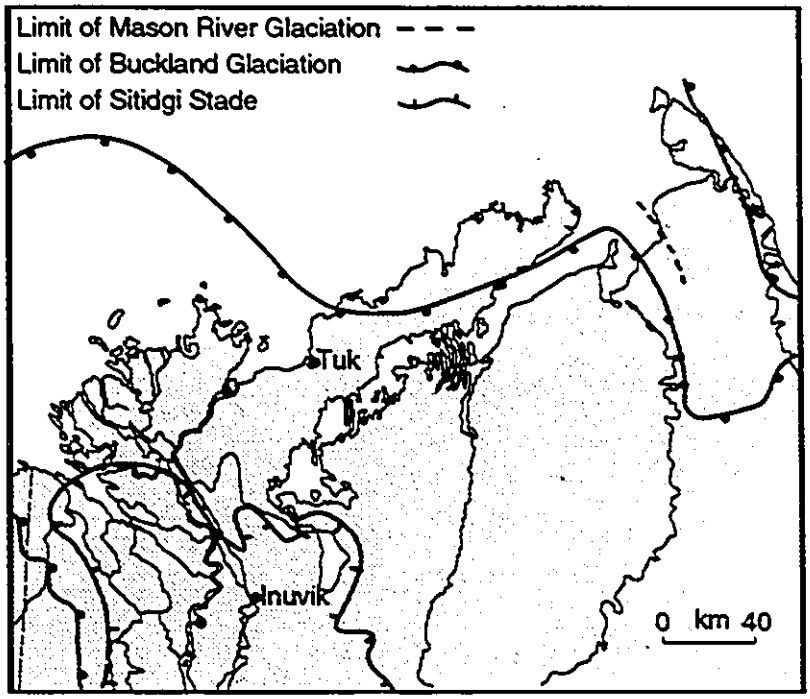

Figure 2.4 Glacial limits during the Middle Pleistocene Mason River Glaciation, the Early Wisconsinan (Buckland Glaciation) and the Late Wisconsinan (Sitidgi Stade Glaciation) Glaciations (Source: Rampton 1988).

similar to the mean surface temperature today (Allen *et al.* 1988a, 1988b).

Thermokarst was extremely active in this area during the regional climatic optimum between 8,500 and 4,000 yrs B.P.(Rampton 1988; Harry *et al.* 1988). Thermokarst proceeds primarily through the development and expansion of thaw slides and slumps.

The Modern Delta has formed since the retreat of the Late Wisconsinan ice. Silt and clay is being deposited in the Mackenzie Canyon and other glacially eroded channels that traverse the continental shelf (Heginbottom and Tarnocai 1983).

2.2.3 Vegetation

Vegetation patterns (Figure 2.5) in the Mackenzie Delta have been discussed by many investigators (e.g. Lambert 1972; Mackay 1963a; Ritchie 1972, 1984; Tarnocai and Hill 1978). The Modern Delta may be divided into three distinct zones (Figure 2.6): a southern boreal forest portion, a central forest-tundra zone and a tundra area at the mouth of the Delta. These zones grade from one to another and seldom possess sharp boundaries (Lambert 1972). The Modern Delta, because of active alluvial activity and the tempering effect of Mackenzie River waters, has a vegetation cover significantly different from the surrounding terrain. In the southern part of the Delta, the vegetation is dominated by white spruce (**Picea glauca**) and balsam poplar (**Populus balsamifera**). Spruce stands are present in the Delta region well north of their extent in adjacent areas. Shrubs such as alder (**Alnus** sp) and

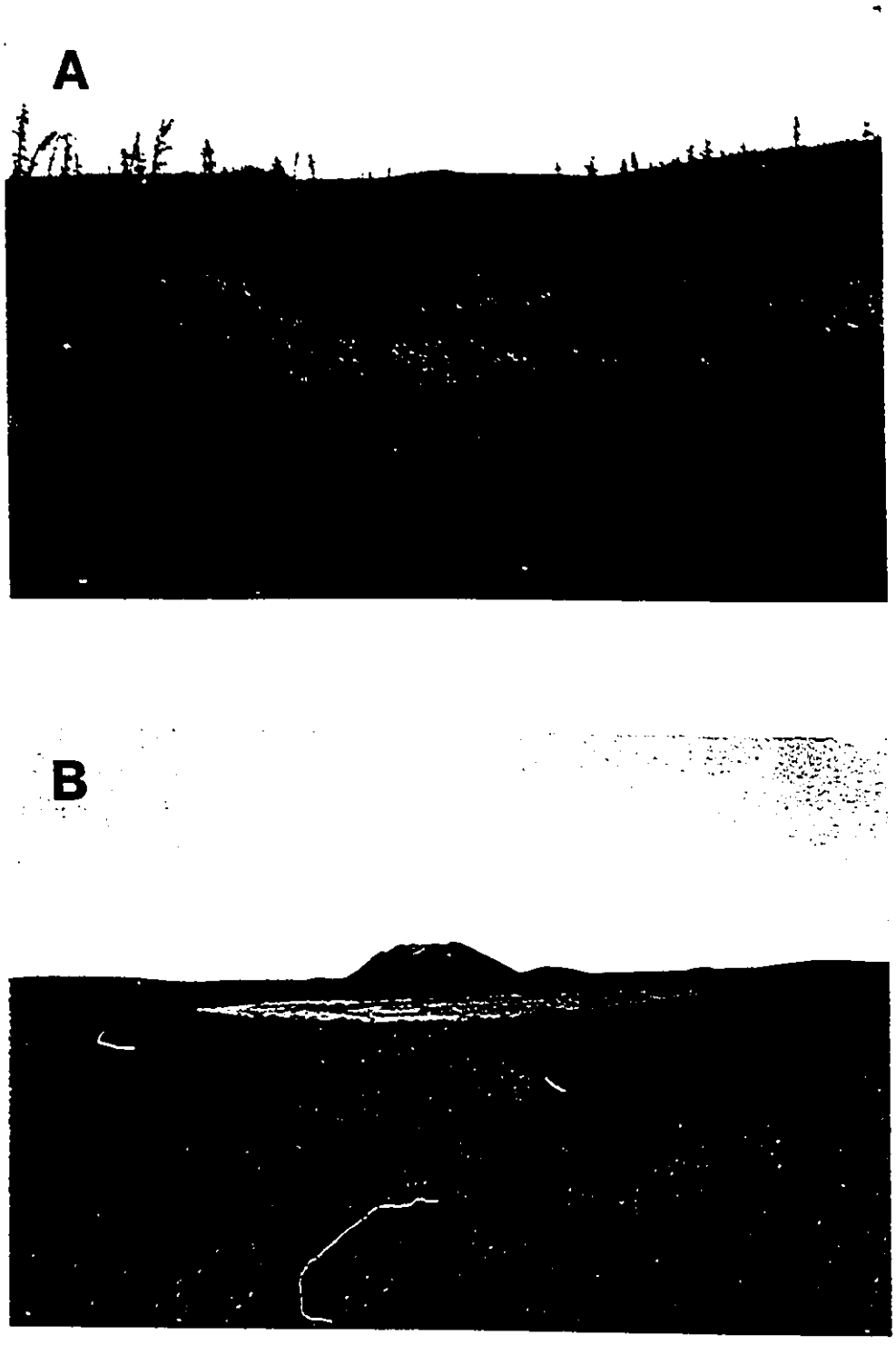

Figure 2.5 Vegetation in the Mackenzie Delta region: A - Boreal forest near Inuvik, and B - Tundra near Tuktoyaktuk (Ibuyk pingo in the background).

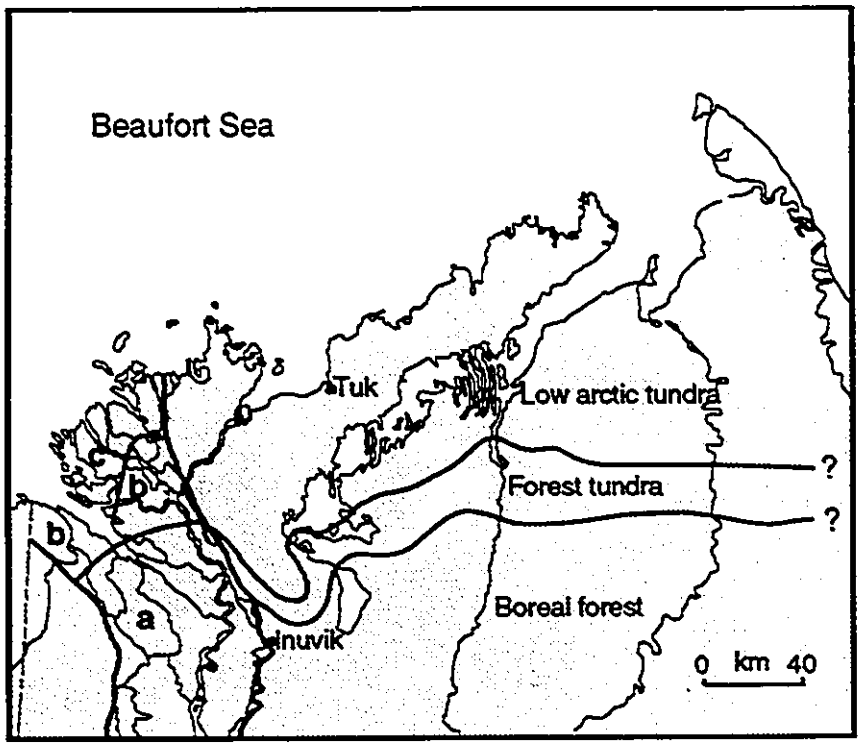

a - Treed with spruce
b - Shrubs and poplar
c - Sedges and willows

Figure 2.6 Vegetation of the Mackenzie Delta region (Source: Rampton 1988).

willow (**Salix** sp.) are important components of the vegetation because of their role in plant succession following deposition of alluvium. The central part of the delta is dominated by willow and alder, although low areas are characterized by aquatic vegetation. Poplar extends into this belt, well beyond the limit of spruce. The outer islands are covered mainly by sedges (**Carex** sp.) and willows and are subject to frequent flooding.

The Pleistocene Coastal Plain also contains three vegetation zones: boreal forest, forest tundra, and shrub-tundra. Shrub tundra, described by Mackay (1963a) as being composed of "scrub willow and ground birch", covers much of the southern limit of the low arctic tundra zone. This community is dominated by dwarf birch (**Betula glandulosa**), willow (mainly **Salix glauca**), and numerous heaths (cf. **Vaccinium** spp., **Ledum decumbens, Empetrum nigrum**).

The forest tundra is the narrow transition belt where boreal forest gives way to low arctic tundra. Trees are scattered and in clumps amongst the dense shrub cover dominated by scrub birch, willows, and heaths. The northern treeline is formed by clumps and individuals of white spruce (**Picea glauca**).

South of Inuvik and Sitidgi Lake, boreal forest, albeit quite open near its northern extent, is present. The forest is dominated by black spruce (**Picea mariana**), white spruce (**Picea glauca**), birch (**Betula** sp) and poplar (**Populus** sp.) (Ritchie 1984).

By 13,000 years B.P., the Tuktoyaktuk Peninsula was ice-free, as the ice retreated to the southeast (Dyke and Prest 1986, 1987). Ritchie (1972, 1984) has reported upon the vegetation evolution of

this area following the retreat of the ice sheet in terms of the pollen stratigraphy. Pollen analyses suggest an extension northward into the Tuktoyaktuk Peninsula of continuous spruce forest between 8,500 and 4,000 B.P.. Ritchie (1984) concludes that the mean daily temperature for the warmest months was about 5°C higher than at present, and that the growing season was about 30 days longer than present. Such an amelioration in climate would require a displacement of the median July position of the Arctic Front about 350 km north of its present position.

2.2.4 Permafrost history and geocryology

Permafrost history

The permafrost history of the Mackenzie Delta region is closely associated with its Quaternary history because at some time during the Quaternary, ice sheets covered all of the region except for the northeast corner of Bathurst Peninsula (Mackay 1978).

It has been postulated that the temperature beneath much of the Laurentide Ice Sheet was below 0°C (e.g. Brown 1967; Mackay and Black 1973). Consequently, although permafrost was probably widespread, it was also thin due to ice-bottom temperatures being close to 0°C. Permafrost may have been thicker towards the margins of the ice sheets. Investigations indicate that much of the permafrost in the Mackenzie Delta region is more than 40,000 years old (Mackay *et al.* 1972), and probably more than 100,000 years old (Mackay 1978). Recent numerical paleoclimatic modelling suggests

that permafrost has aggraded since the end of the Sangamonian (75,000 years B.P.) when surface temperatures were approximately -1°C (Figure 2.7). It is also possible that pre-Sangamonian permafrost thawed completely during the interglacial, or was much more restricted and thinner than today.

Although detailed information on the chronology of permafrost is still sketchy, it is certain that the Pleistocene Coastal Plain was free of glacial ice much earlier than the Modern Delta. Thus, the Pleistocene Coastal Plain has been subject to low air temperature imposed on an unprotected ground surface for a much longer time than the Modern Delta, resulting in permafrost that is thicker, older and colder.

Geocryology

The Mackenzie Delta region lies within the zone of continuous permafrost (Figure 1.1). More than 80% of the area is underlain by permafrost. In the Modern Delta, permafrost is usually less than 100 m in thickness (Smith 1976)) and in its youngest parts, where the sediments are just above sea level, permafrost is only tens of metres thick, and ground temperatures may be as high as -1 to -2 °C (Mackay 1978). However, in the Pleistocene Coastal Plain, permafrost depths range from about 300 to 600 m or more, and mean annual ground temperatures are between -6 to -9°C (Judge 1973).

The Mackenzie Delta region has one of the world's largest concentration of pingos. The great majority (about 1350) are in the Pleistocene Delta, but only a small number (about 80) occur in the

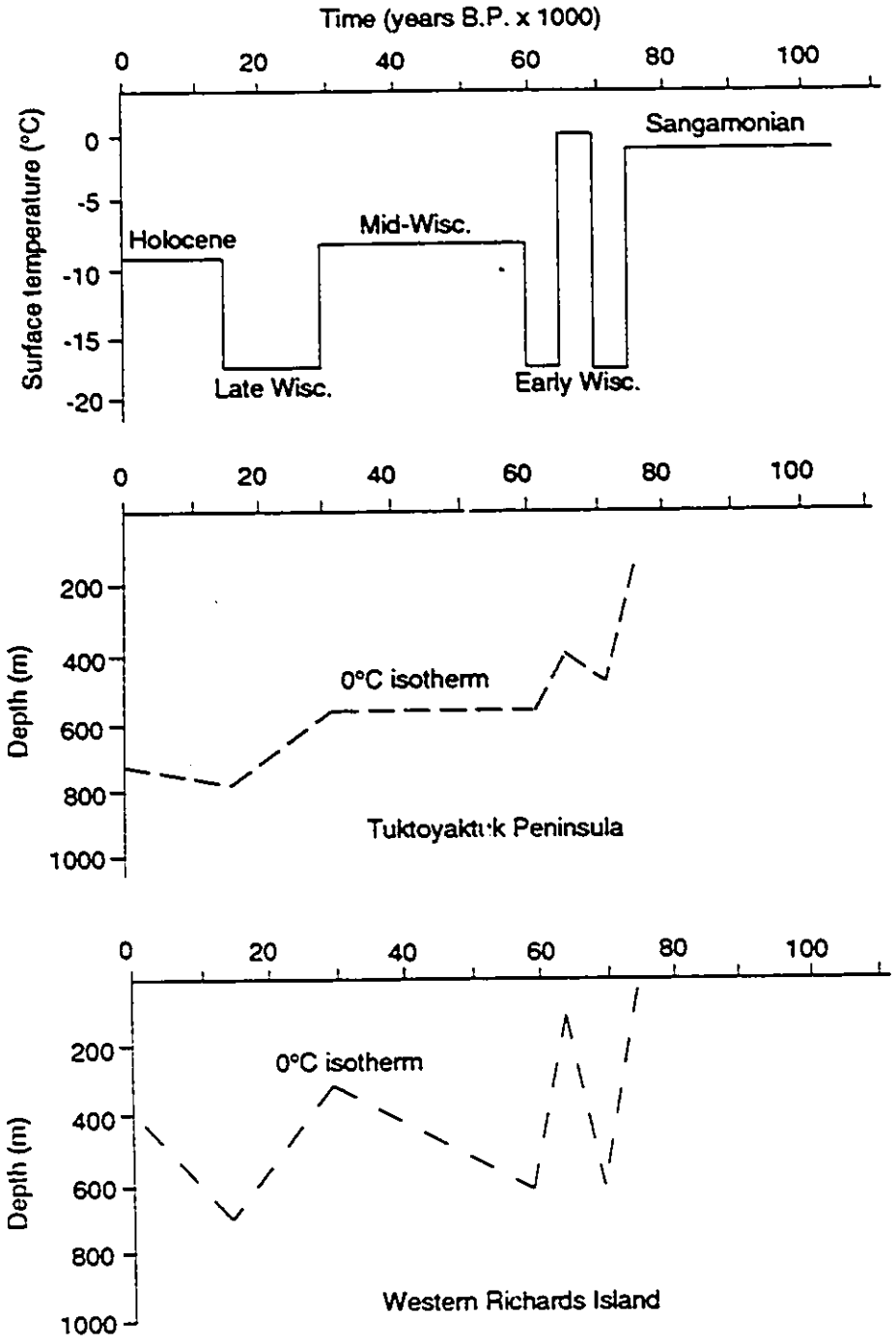

Figure 2.7 Simulated surface temperature history and variation of 0°C isotherm with depth, Mackenzie Delta region (According to: Allen *et al.* 1988a,1988b).

Modern Delta (Mackay 1978). Ice wedges are widespread, and are best developed on poorly drained flats. Along some coastal exposures, relict ice wedges can be seen at a depth of 2 to 5 m, the tops having thawed during the hysithermal warm period. Syngenetic and epigenetic ice wedges have been known for a long time (e.g. French and Gozdzik 1988). Mackay (1990a) recognised a third type of ice wedges in the Mackenzie Delta region, namely, anti-syngenetic ice wedges. A final interesting characteristic is that many large tabular ground ice bodies are exposed along the coast of the region (e.g. French and Harry 1990; Mackay 1971; Mackay and Dallimore 1992).

Many of the geomorphic features of the region are of thermokarst origin (Rampton 1974; Harry *et al.* 1988). A substantial proportion of the lakes are partly thermokarst in nature (Mackay 1978; 1992). Many lakes have been impounded by damming as a result of ice-wedge growth and have later become drained from ice-wedge erosion (Mackay 1978). Sediments with high ice content have been the cause of rapid coastal retreat where the mean rate of retreat may exceed 8 m/yr.

2.3 Qinghai-Xizang Plateau

2.3.1 Physiography

The physiography of the Qinghai-Xizang Plateau (Figure 2.8) is different from the Mackenzie Delta region in terms of both topography and landscape. The name 'Qinghai-Xizang Plateau' is

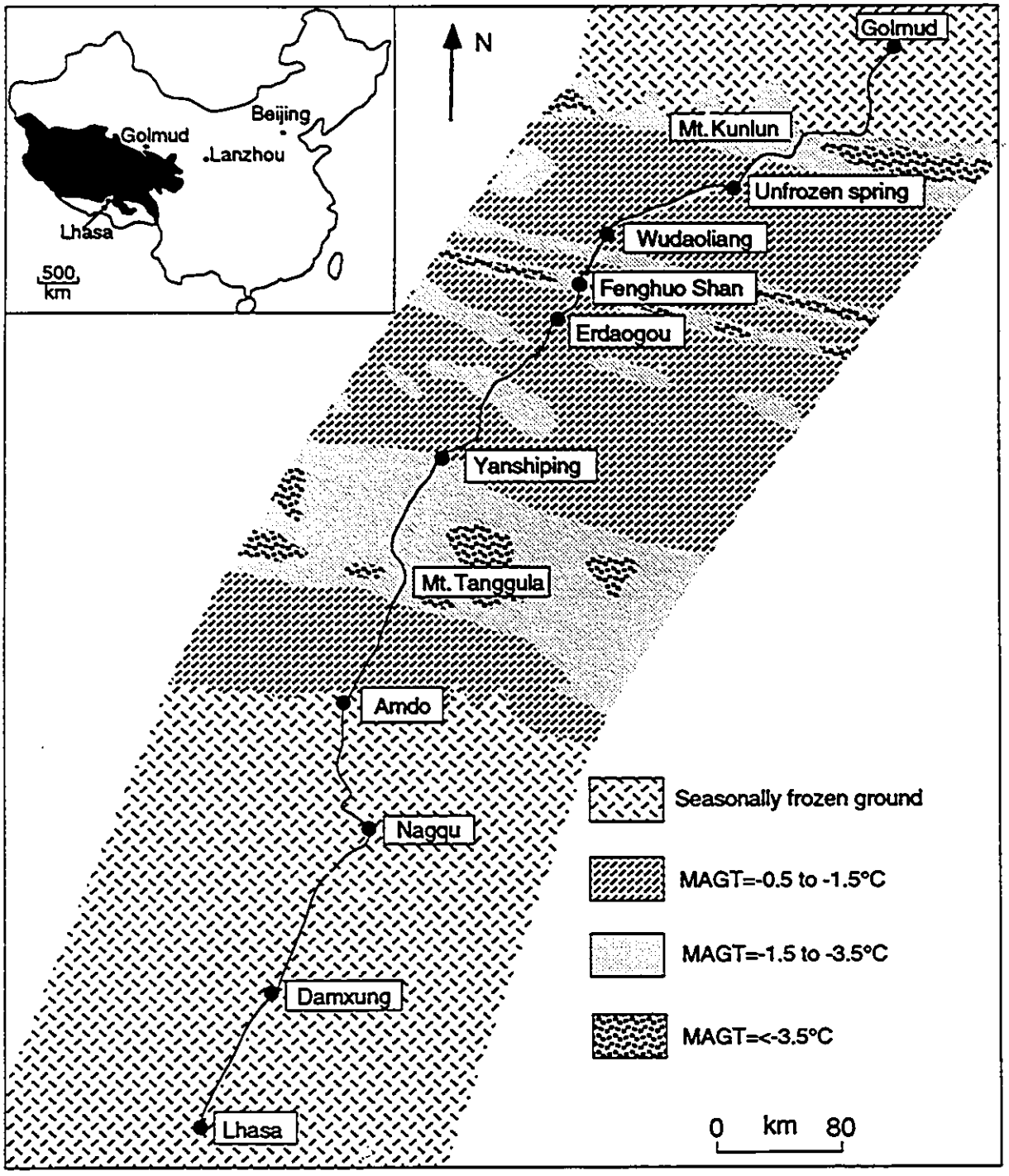

Figure 2.8 Location map of the Qinghai-Xizang (Tibet) Plateau permafrost area in China (shaded area in the inset map) and the permafrost distribution along the Trans-Plateau Highway corridor, MAGT=mean annual ground temperature (according to Tong *et al*. 1982).

derived from the fact that this Plateau is located between Xizang (Tibet) Autonomous Region to the south and Qinghai Province to the north. In Chinese literature this name is abbreviated as 'Qing-Zang Plateau' (e.g. Cheng and Qiu 1983; Tong and Li 1983; Wang *et al.* 1979; Zhou 1965). The total area of the Plateau is approximately 2.2 million km^2 (Zeng *et al.* 1982), with 75% of it being underlain by permafrost. Permafrost conditions mapped adjacent to the Trans-Plateau Highway are illustrated in Figure 2.8 (after Tong et al. 1982). On the Plateau, relative relief may be as much as 500 m. This is especially true in the middle portion of the Plateau. In general, the Plateau is characterized by hills, flats and inter-hill valleys (Figure 2.9). Typical rugged mountains can hardly be seen on the Plateau. Many large rivers of continental Asia originate from this Plateau, including the Yangtze River, the largest river in China. Since the precipitation on the Plateau is meagre, and evaporation is several times greater than precipitation, lakes on the Plateau cannot be maintained by precipitation. Instead, lakes are maintained largely by snow and glacier ice-melt or by springs, and runoff is concentrated in the summer and fall periods. Taliks (either open or closed) exist beneath those lakes, and some of the lakes are oriented in an east-west direction (Tong and Li 1983). Snowline elevations on the higher mountains vary between 5,000 to 6,000 m a.s.l.

The mean annual air temperature (MAAT) in the permafrost areas of the Plateau is between -2 and -6.6°C, and the ground surface temperature between 0 and -4.3°C (Xie 1982). The annual range of

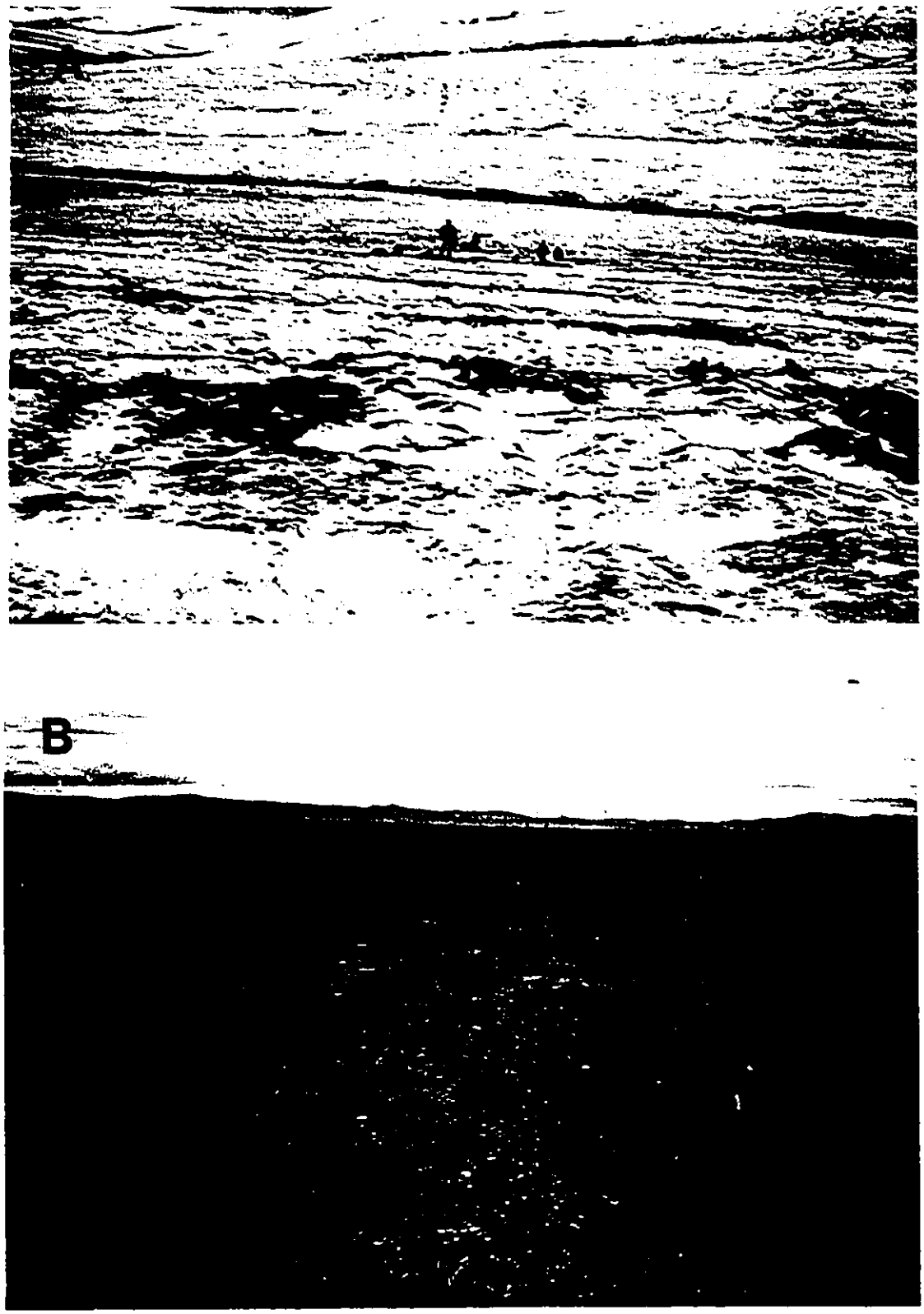

Figure 2.9 Typical landscape on the Qinghai-Xizang Plateau: (A) - hills and valleys, and (B) - the 'high plain' .

temperature is from 15 to 24°C, and the net radiation from 60 to 80 kly/yr, much higher than in the Mackenzie Delta region. The annual total precipitation ranges from 200 to 600 mm, but evaporation is more than 1,300 mm (Zhang 1983). The MAAT on the Qinghai-Xizang Plateau changes with both latitude and altitude (Ding and Xu 1982; Xu *et al.* 1981). The lapse rate of the MAAT on the Plateau ranges between 0.44 and 0.55°C/100 m, with an average of 0.5 °C/100 m (Xie and Zeng 1983).

2.3.2 Quaternary history

The Quaternary history of the Qinghai-Xizang Plateau is directly related to its continuing uplift during the last 2 million years, triggered by the collision between the Indian and Eurasian Plates during the Tertiary. Various lines of evidence, including karst topography, flora and fauna, and pollen within lakes on the Plateau, indicate that during the Pliocene, the area was tropical or subtropical, with an average altitude of about 1,000 m a.s.l. (Li *et at.* 1979).

The Plateau started to uplift at the end of the Pliocene, and now its altitude ranges from 4,500 to 5,000 m a.s.l. Thus, the Tibetan Plateau has experienced uplift of at least 3,500 m during the Quaternary. Especially rapid uplift occurred in the Late Pleistocene with rates of more than 10 mm yr^{-1} (an uplift of 1,500 to 2,000 m over about 130 ka, see Figure. 2.10).

The Quaternary deposits vary greatly in thickness, from several metres to 1,000 m (Guo *et al.* 1982). This is because

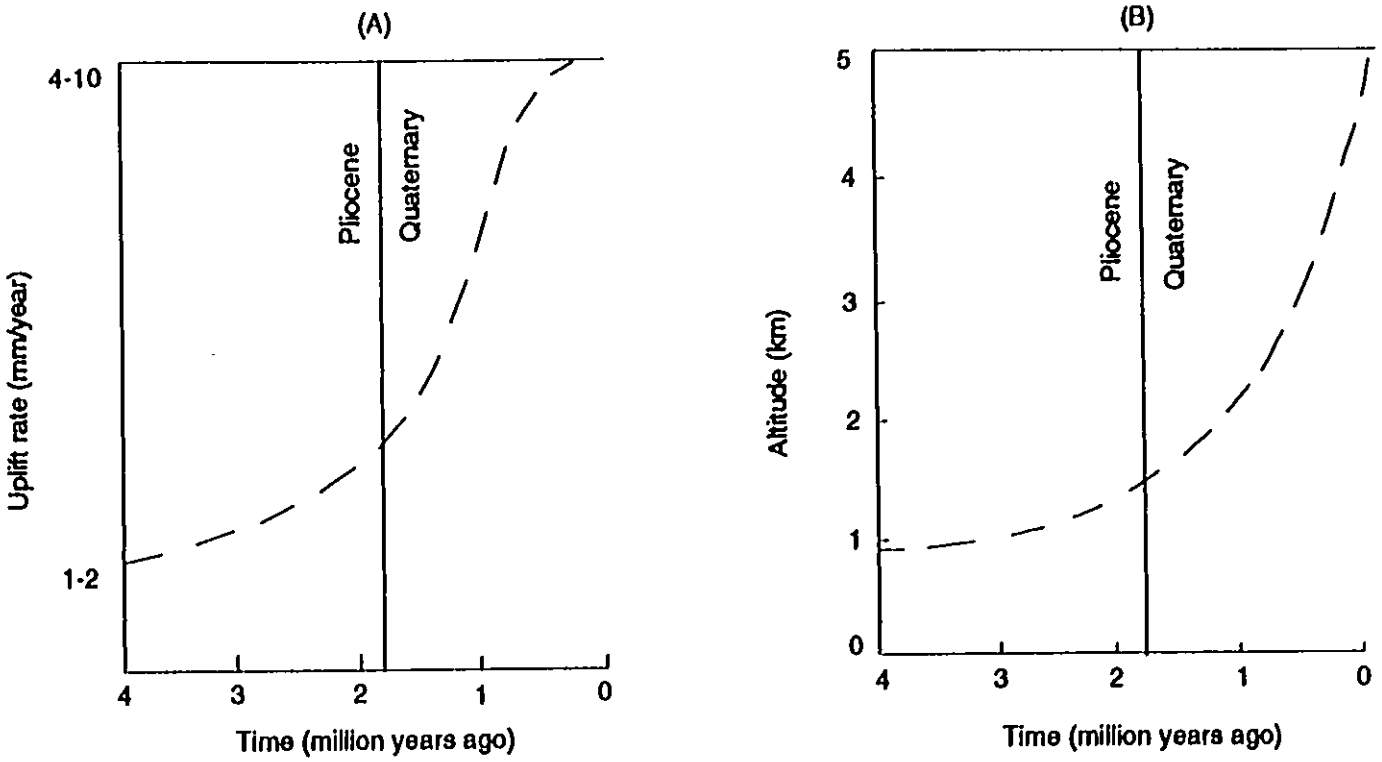

Figure 2.10 Changes in uplift rate and altitude of the Qinghai-Xizang Plateau since the Pliocene Epoch.
(A) Estimated uplift rate during the last 4 million years, showing increasing rate during the Quaternary Period.
(B) Increase in altitude of the Plateau, as inferred from geologic evidence (Source: Skinner and Porter 1989).

differential movement (i.e. faulting) has accompanied the uplift of the Plateau. A geological cross-section through the Plateau is given in Fig. 2.11.

Investigations of contemporary and Quaternary glaciations on the Plateau have been made since 1950's. Various lines of evidence suggest that during the Pleistocene, no ice sheet covered the Plateau. Only scattered mountain glaciers developed (Fig. 2.12A), with valley glaciers rarely extending far from the surrounding mountain ranges (Shi *et al.* 1990). Although M. Kuhle (1985) proposed a unified ice sheet model for the Qinghai-Xizang Plateau (Fig. 2.12B), this is not generally accepted by glaciologists and Quaternary geologists in China.

According to Shi *et al.* (1990), the extent of mountain glaciation varied from time to time during the Pleistocene because of the fluctuation of climate, but glaciers did <u>not</u> coalesce to form a unified ice sheet covering the entire Plateau. The reason is that, before the Late Pleistocene, the Plateau was not high enough for the ice sheet to form. During the Late Pleistocene, the altitude of the Plateau progressively increased, and air temperatures lowered. At the same time, the monsoon climate was replaced by a continental climate because of the barrier effect of the Himalayas which prevented moist ocean air of the Indian Ocean from reaching the Plateau. Therefore, the Plateau became progressively drier, and no adequate water source existed for the expansion of mountain glaciers.

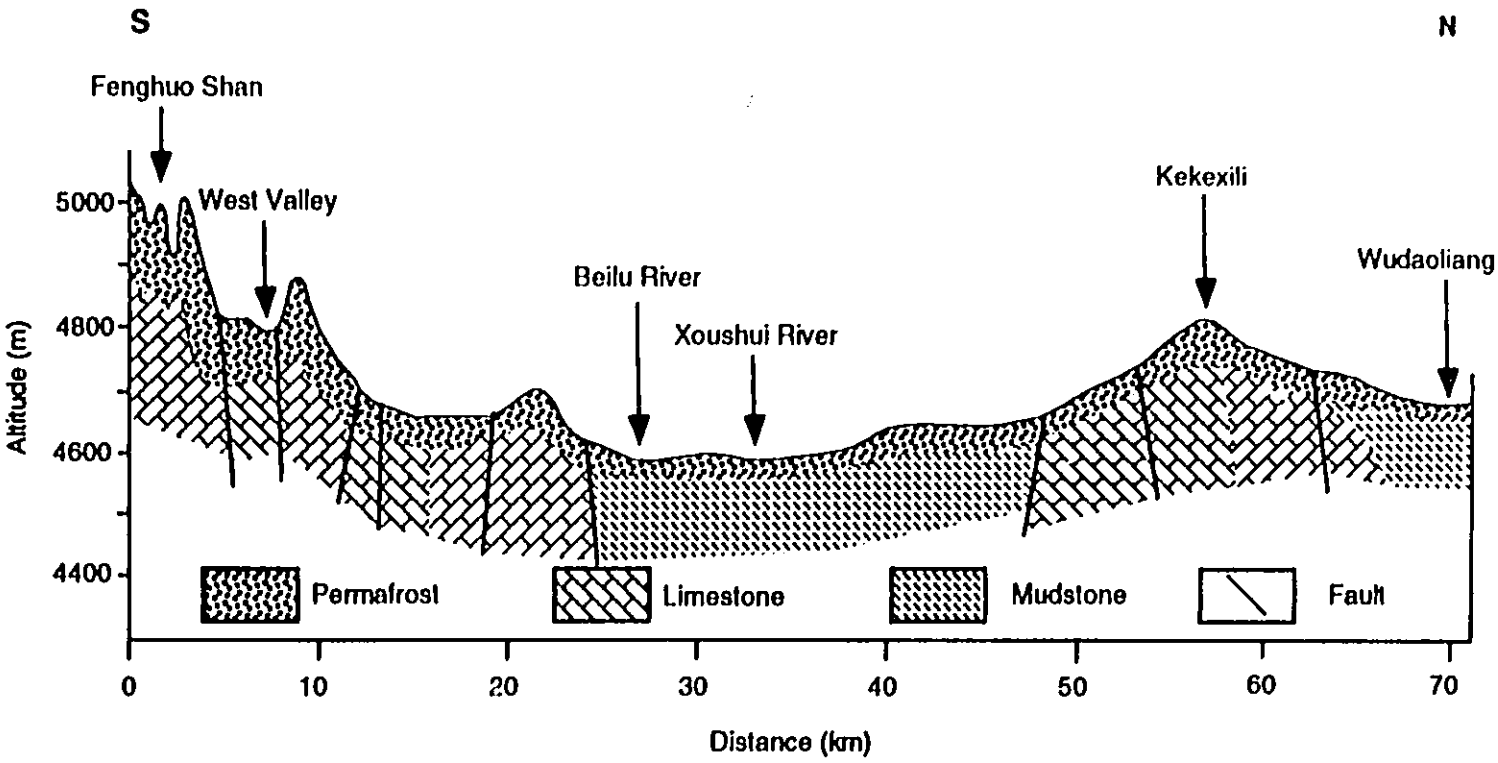

Figure 2.11 A geological cross-section (from Fenghuo Shan to Wudaoliang) on the Qinghai-Xizang Plateau (According to Tong *et al.* 1982).

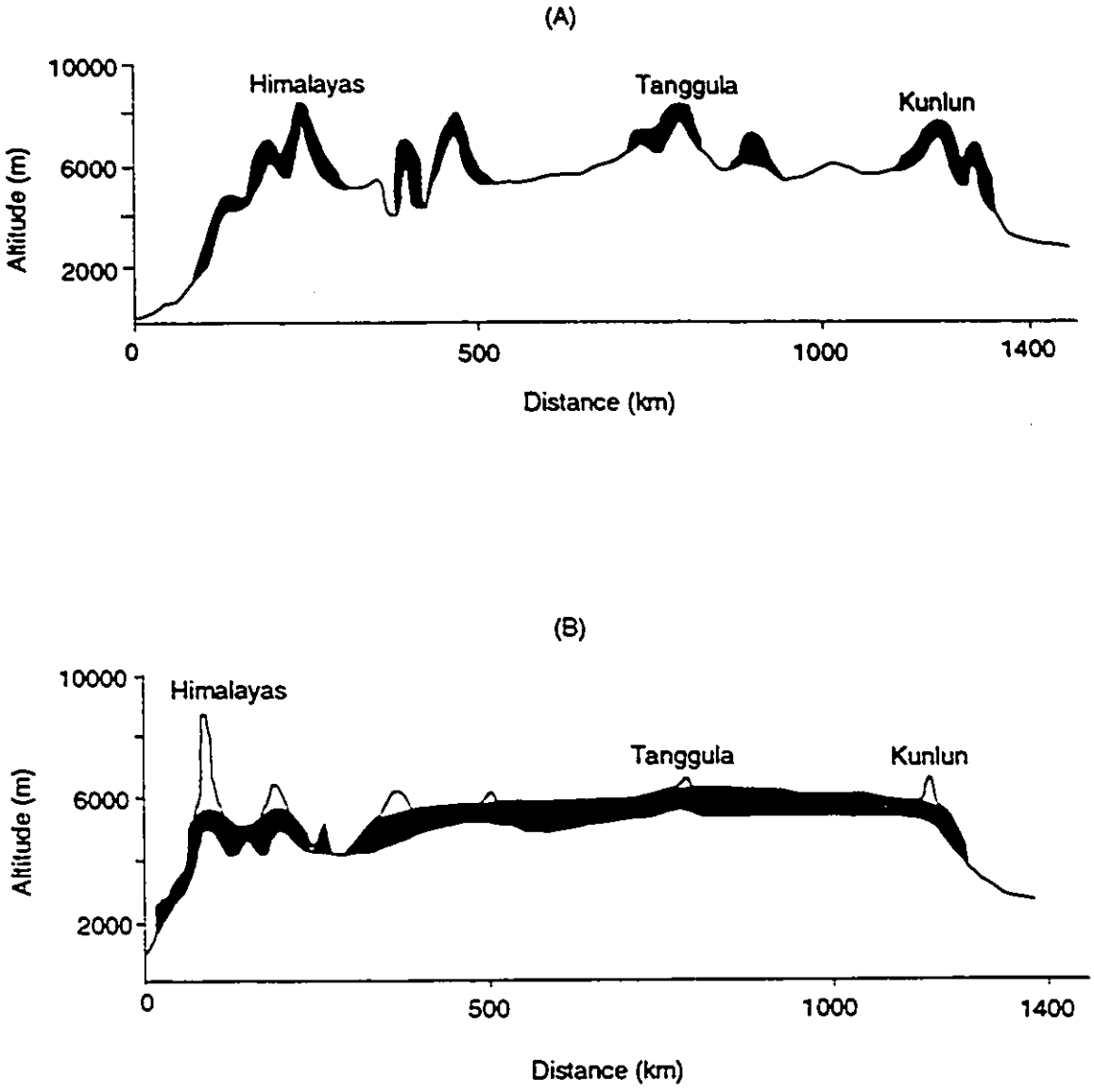

Figure 2.12 The maximum extension of the Pleistocene Glaciation on the Qinghai-Xizang Plateau: (A) the scattered ice-cap model of Shi *et al.* (1990), and (B) the unified ice-sheet model of Kuhle (1985).

2.3.3 Vegetation

Unlike the southern part of the Mackenzie Delta, the Qinghai-Xizang Plateau is devoid of trees, and it lacks a continuous vegetation cover. This is attributed to the high aridity and strong wind on the Plateau. The vegetation of the Plateau has been studied by Xu (1959) and Sun (1965). It falls into four categories: 1) mountain-tundra desert zone, 2) semi-arid steppe zone, 3) sub-mountain steppe zone, and 4) wet bog zone. These different zones are shown in Figure 2.13. The mountain-tundra desert zone, located at elevations above 4,900 m a.s.l., is characterized by cold and arid conditions, intense frost weathering and eolian action. The weathering products of local bedrock are widespread and soils are not well developed. Consequently, vegetation is limited to grasses (e.g. **Festuca** sp.).

A semi-arid steppe zone exists along river valleys, on floodplains and on some gentle slopes above 4,500 m a.s.l., especially where sand and gravel predominate. This zone is dominated by grasses(e.g. **Poarossberqiana**) and other herbs (e.g. **Stellaria decumbens** and **Myricaria hedinii**).

A sub-mountain steppe zone includes river terraces, alluvial fans and some gentle slopes. Typical alpine and sub-alpine species include: **Oxygraphis glacialis, Ranunculus involucratus, Anemone imbricata, Delphinium tanquticum, Nasturtium tibeticum, Potentilla subacaulis, Aster sp.,** and **Pedicularis sp.**.

The wet bog zone consists of poorly drained areas where sedges (**Kobresia robusta** and **Kobresia tibetica**) dominate.

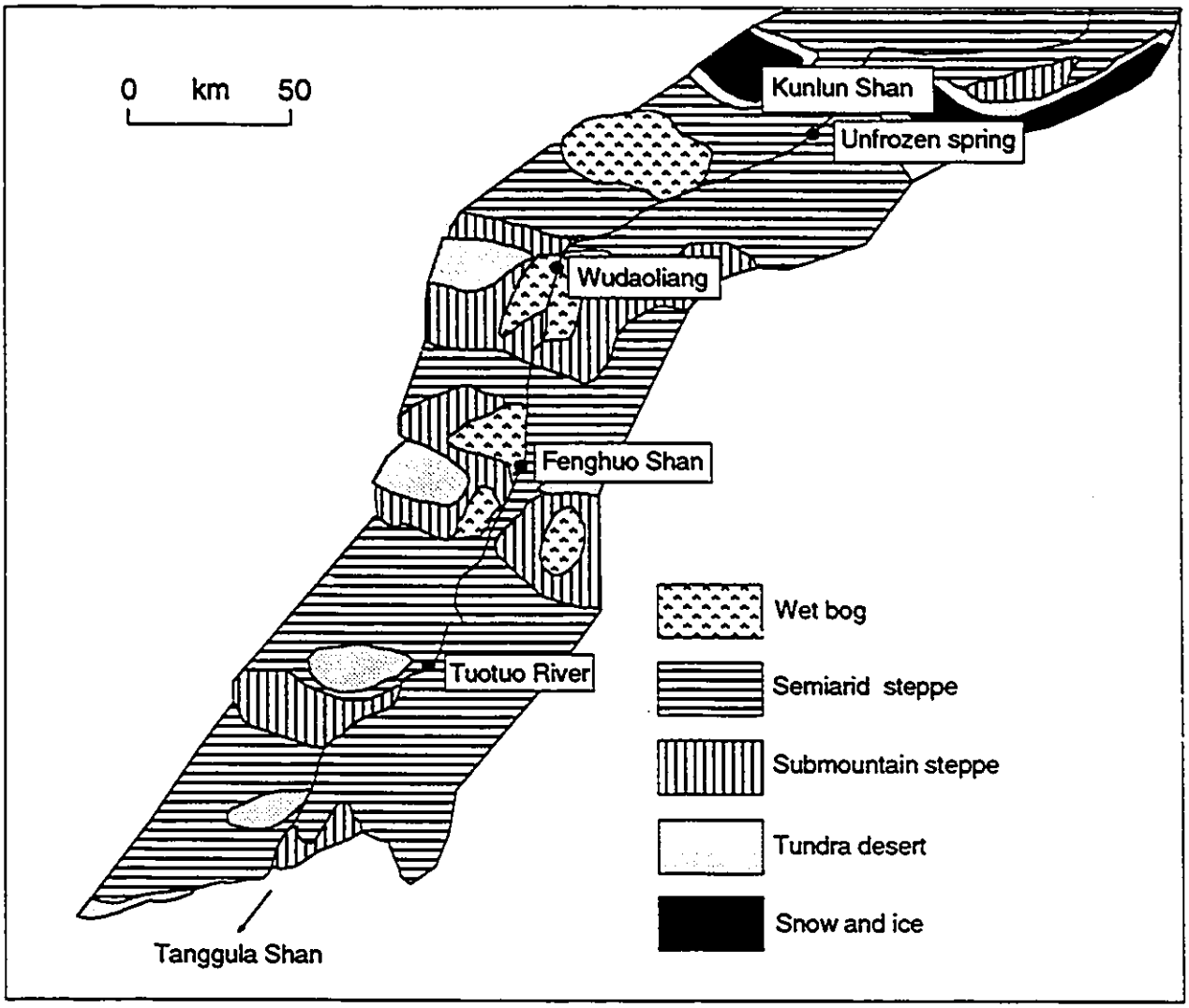

Figure 2.13 Distribution of vegetation along the Trans-Plateau Highway corridor (according to Sun 1965).

2.3.4 Permafrost history and geocryology

Permafrost history

The history of plateau permafrost is closely related to the uplift of the Plateau and to Quaternary climatic fluctuations (Ding and Guo 1982; Guo 1988; Guo and Li 1982; Pu *et al.* 1982; Zhou 1965).

Information concerning the inception of permafrost is sketchy, but numerical modelling indicates that permafrost first developed in the Early Pleistocene and then completely thawed (Ding and Guo 1982). Subsequently, permafrost reformed during the Middle Pleistocene and disappeared during the Middle Pleistocene interglacial when the MAAT was believed to be about 11°C higher than it is today (Guo 1988; Guo and Li 1982; Zhang and Cai 1981). Some argue that the Plateau was not high enough for permafrost to form before the Late Pleistocene (e.g. Li *et al.* 1979).

More data have become available for the Late Pleistocene. During this time period, the altitude of the Plateau was close to 4500 m a.s.l. This, coupled with the cooling trend of late Quaternary climate, produced a MAAT of -10°C or lower on the Plateau (Guo *et al.* 1982). Permafrost aggraded, and various ground wedges (originally reported as sand wedges, and/or ice-wedge pseudomorphs), and polygons formed. Radiocarbon dating of organic matter in these wedges produced ages varying from 23,500 to 15,340 years B.P. (Guo 1979; Guo and Li 1982; Liang and Cheng 1984; Wang 1989). Most of the ground wedges are found in fluvial terrace

sediments. The present author uses the term "ground wedge" as proposed by Harry and Gozdzik (1988) for these features. They are unlikely to be ice-wedge pseudomorphs because most are restricted to the active layer, to judge by their sizes. In any case, once a continental climate had been established in the Late Pleistocene, there was little water for the formation of ice wedges, although permafrost was more widespread and thermal contraction cracking was probably more active then (Guo and Li 1982).

Holocene permafrost history can be considered in two stages: 1) 10,000 - 3,000 year B.P., and 2) 3,000 - present (Wang 1989).

The first stage was marked by climatic warming and permafrost degradation. The hysithermal warm period (climatic optimum) on the Plateau occurred between 8,000 and 3,000 year B.P. during which time permafrost was subject to thaw. Thermokarst features, in the form of thaw lakes and depressions, and active layer detachments, developed (Guo and Li 1982). Because of its high elevation, permafrost did not disappear during this time period, but numerical modelling suggests that the permafrost table was lowered to a depth of 15 m below the ground surface (Ding and Guo 1982); and this conclusion is supported by a thaw unconformity at a depth of 16 m observed by Wang (1989). During the second stage, permafrost aggraded between 3,000 and 2,000 year B.P. (Little Ice Age), and newly formed permafrost and relict permafrost came into contact in many places (Ding and Guo 1982). Although the climate fluctuated after the Little Ice Age, permafrost conditions have not changed significantly.

If we consider uplift as the only cause for the formation of permafrost on the Qinghai-Xizang Plateau, then plateau permafrost did not come into existence until the Late Pleistocene. If correct, this means that during the Early and Middle Pleistocene, the Plateau was not high enough for permafrost to form (Li *et al.* 1979). One feature used to infer the presence of Early and Middle Pleistocene permafrost is the involutions. Because the formation of these structures does not necessarily require the presence of permafrost (e.g. French 1976), the existence and extent of Early and Middle Pleistocene permafrost is still open to debate.

Geocryology

Permafrost on the Qinghai-Xizang Plateau is mapped as 'predominantly continuous' (with 70 to 80% of area underlain by permafrost), and 'isolated' in distribution (less than 40 to 60% of area underlain by permafrost) by the Lanzhou Institute of Glaciology and Geocryology (1988). Those terms, often used in Chinese literature, are highly inconsistent with these in North America. Their equivalent terms in North American literature are the 'widespread zone' and 'sporadic zone' (e.g. ACGR 1988; Harris 1986, 1988).

Most permafrost investigations on the Qinghai-Xizang Plateau have been carried out along the Trans-Plateau Highway (i.e. Qinghai-Xizang Highway) which starts from Golmud in the north and ends at Lhasa in the south (Fig. 2.8). Plateau permafrost ranges from a few metres to 130 m in thickness, and the mean annual ground

temperature (at the depth of zero annual amplitude) is from a fraction of a degree below 0°C to -3.5°C (Li 1982). The distribution and thickness of permafrost, together with temperature and topography along the highway are shown in Fig. 2.14. The effect of elevation on the thickness of permafrost can be easily recognised from this graph.

One of the distinctive features of plateau permafrost is its combination of both vertical (altitude) and horizontal (latitude) zonation. Permafrost thickness increases with latitude at a rate of between 10 to 30 m per degree. Also permafrost thickens approximately 15 to 20 m for each increase of 100 m in elevation (e.g. Shang 1982; Tong and Li 1983; Zhou and Guo 1982). A unique characteristic of plateau permafrost is its lower altitudinal limit (i.e. the zone above which permafrost occurs). The lower limit becomes higher from north (4,150 m a.s.l.) to south (4,800 m a.s.l.) on the Plateau, at a rate of about 110 m per latitudinal degree. There is also a relationship between the lower limit and latitude. For instance, it decreases from 5,300 m a.s.l. on the north-facing slope of Himalayas to about 4,200 m a.s.l. at Xidatan (i.e., the northern edge of the Plateau). The lower altitudinal limit of permafrost on the Plateau is usually 800 to 1,100 m lower than the snowline (e.g. Tong and Li 1983; Zhou and Guo 1982). The mean annual air temperature at the lower limit is in the range of -2.5 to -3.6°C (Tong and Li 1983), considerably lower than that of the Rocky Mountains in North America (0 to -1°C) (Pèwè 1983) and that of the southern boundary of high latitude permafrost in Canada

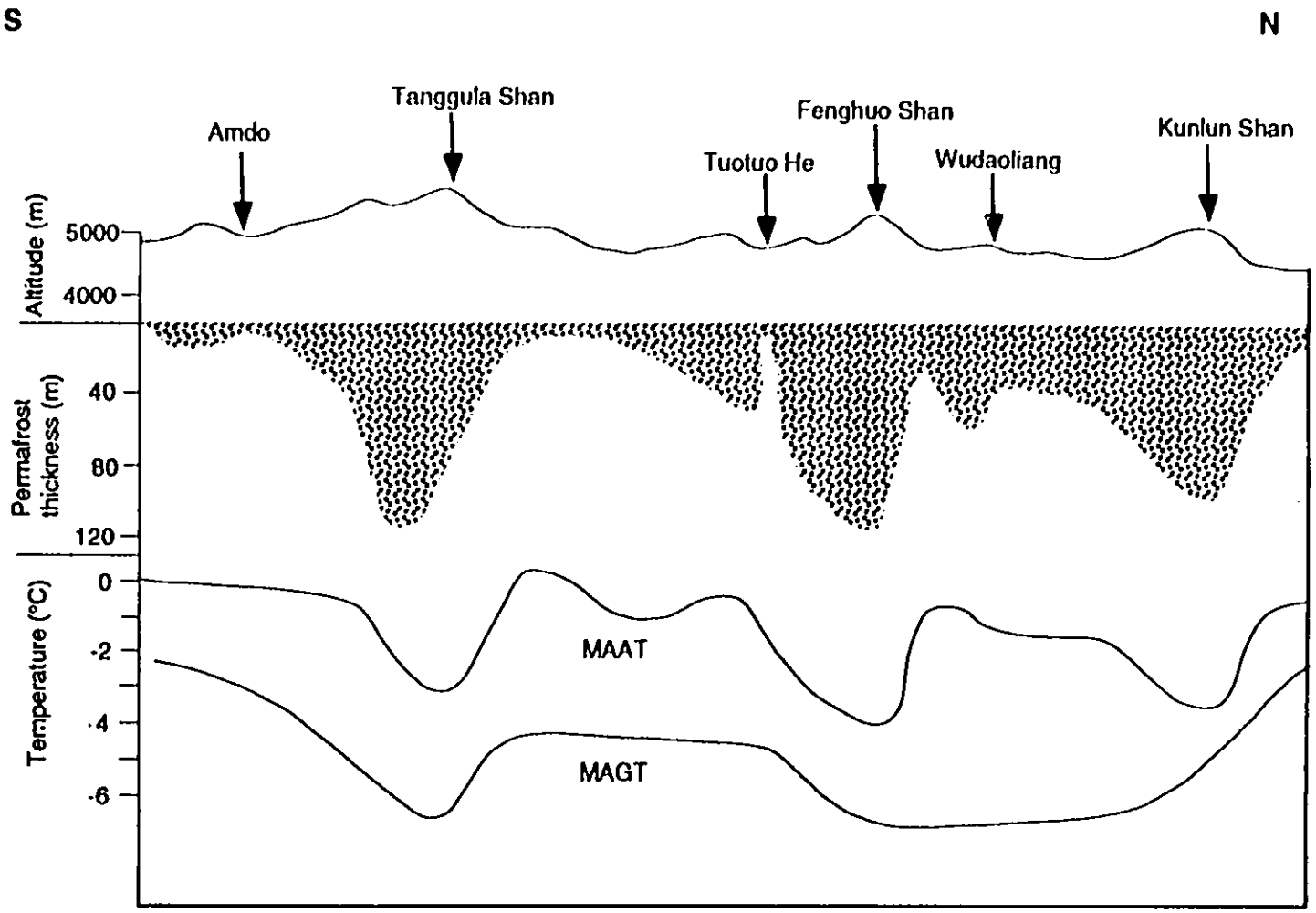

Figure 2.14 Graph showing changes in permafrost thickness, mean annual ground temperature (MAGT), mean annual air temperature (MAAT), and topography across the Qinghai-Xizang Plateau (according to Li 1982).

(about -1.1°C) (Brown 1967, 1969, 1970; Brown and Pèwè 1973; Ives 1973). A recent survey by Harris (1989) indicates that the MAAT at the lower elevational limit of permafrost in the Canadian Rocky Mountains is lower than that suggested by previous studies.

Ground-ice distribution is controlled largely by topographic location and soil type (Qinghai-Xizang Highway Research Group 1983). Although ice-rich permafrost is frequently encountered (e.g. Guo *et al.* 1982; Cheng 1982, 1983), tabular ice bodies and ice wedges like those reported from the Mackenzie Delta region (e.g. French and Harry 1990; Mackay 1989) have not been observed on the Qinghai-Xizang Plateau. Pingos are rare on the Plateau. Temperature conditions in the middle portion of the Plateau are suitable for the formation of thermal-contraction cracks (see Burn 1990a; Romanovskiy 1973; Harris 1988), but it appears that the aridity limits the growth of ice wedges. According to Harris (1988), thermal-contraction cracking occurs only at suitable sites north of 50°N in North American Cordillera. This is because of the general rule that mountains are drier than the polar regions due to better drainage conditions.

2.4 Conclusions

The Mackenzie Delta region and the Qinghai-Xizang Plateau are two quite different permafrost environments. The Mackenzie Delta is a subpolar area, characterized by high latitude and low elevation. The Qinghai-Xizang Plateau, however, is a mid-latitude high elevation area. Thus, both vertical and horizontal variations in

air temperature and permafrost conditions are evident and contrast sharply with the Mackenzie Delta region. Moreover, because of the lower values of solar radiation, the MAAT in the Mackenzie Delta region is lower. Although precipitation on the Plateau is slightly greater than in the delta region, the evaporation rate is several times higher. Thus, the Plateau is more arid.

The most fundamental difference relates to the Quaternary histories of the two areas. Tectonically, the Qinghai-Xizang Plateau is very active; at the end of the Tertiary, the altitude of the Plateau is estimated to have been only 1,000 m a.s.l. Therefore, the Plateau has experienced uplift of at least 3,000 m during the last 2 million years. Accordingly, plateau permafrost can be viewed as being the direct result of uplift of the land mass, and did not exist until the late Pleistocene when the Plateau reached approximately its present level. Under present climatic conditions, the altitude of the lower limit of plateau permafrost along the northern edge is at 4,150 m a.s.l. This suggests that if the Plateau were 1,000 m lower than its present elevation, there would be no permafrost. By contrast, the Quaternary history of the Mackenzie Delta region is most closely related to its Pleistocene Glaciation. During the Middle Pleistocene and the Early Wisconsinan age, the delta region was covered by the northwesterly flowing ice sheet, and during this period of time, permafrost was thin, if it existed at all. Following the deglaciation, uplift has been minimal and the Mackenzie Delta has been formed by ongoing fluvial deposition.

PART TWO

GEOTHERMAL MODELLING

CHAPTER THREE - THE GROUND THERMAL REGIME

3.1 Introduction

This part (Part Two) examines some basic aspects of the geothermal regimes and their differences between the Qinghai-Xizang Plateau and the Mackenzie Delta region. Here, in this chapter, the surface energy exchange is considered. In chapter four, details of some of the more obvious site-specific modifications are given.

3.2 Surface energy exchanges

Factors influencing the permafrost thermal regime include variables both above and below the ground surface; the most fundamental variable above the ground surface is the radiant energy from the sun. Potential insolation, often used in solar radiation studies, is the quantity of solar radiation that the ground surface receives in a specified time period, neglecting all other atmospheric influences, vegetation and topographic shading (Dingman and Koutz 1974). Primary dependence is upon the angle of incidence of the sun's rays on the surface, and hence upon latitude. For example, Figure 3.1A shows the potential insolation, expressed as a percentage of the amount received at the equator, as a function of latitude. Accordingly, if the potential insolation at the equator is 3.12×10^5 ly/yr, then the potential insolation values calculated from Figure 3.1A for the Mackenzie Delta (lat. 68-70°N) and the Qinghai-Xizang Plateau (lat. 29-38°N) are 1.56×10^5 ly/yr and 2.68×10^5 ly/yr, respectively.

Elevation is another factor influencing solar radiation. For example, the Fenghuo Shan area on the Plateau is at the same

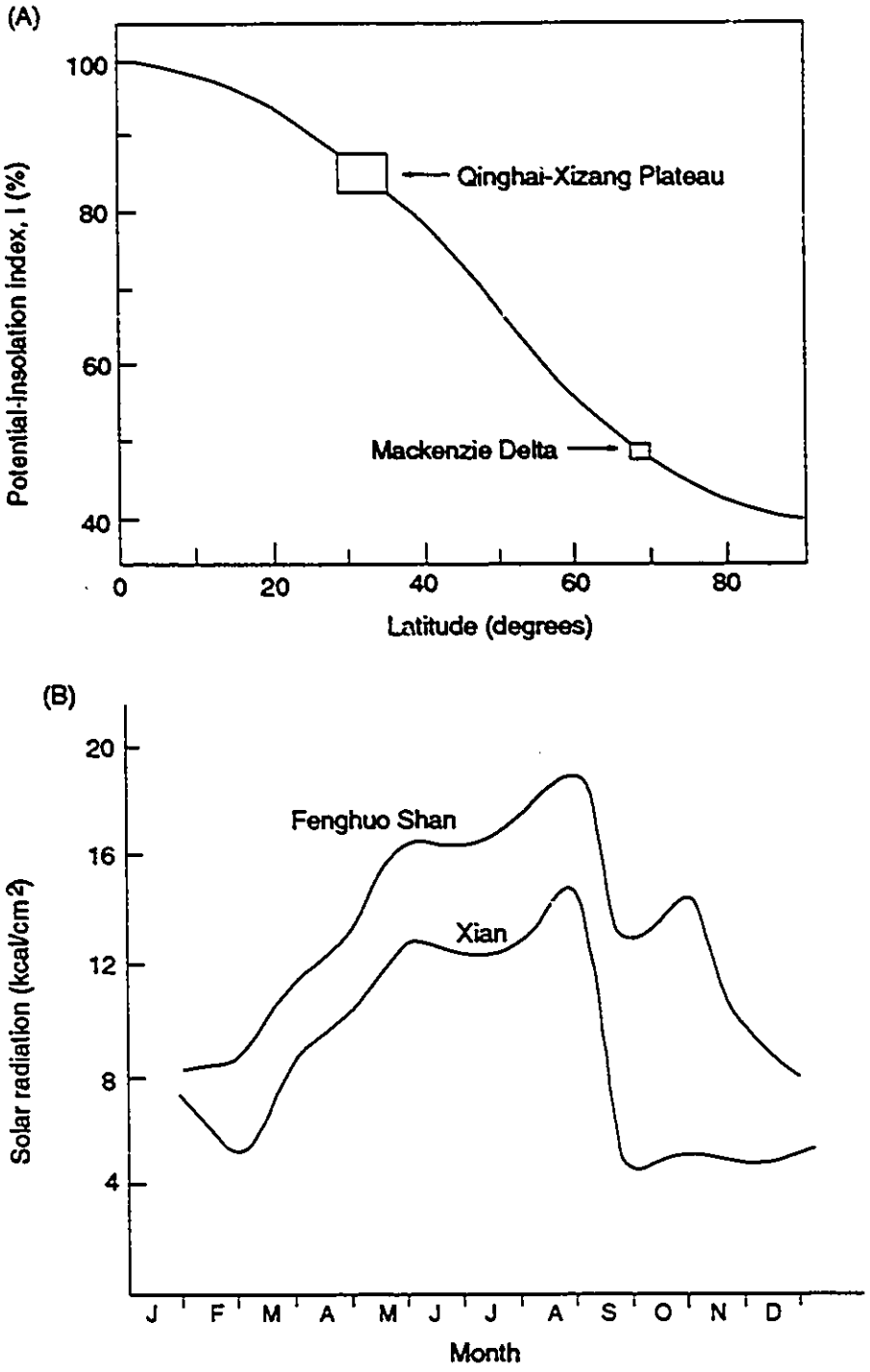

Figure 3.1 (A) Potential-insolation index, I, expressed as a percentage of the potential insolation at the equator (According to Dingman and Koutz 1974), and (B) Variation of actual incoming solar radiation over a year at the same latitude (34°N) but different altitude, Fenghuo Shan - 4,800 m a.s.l., Xian - 1,300 m a.s.l. (source: Kou et al. 1982).

latitude as, but 3500 m higher than, Xian in central China. Actual solar radiation on the Plateau is much higher than at Xian (Fig. 3.1B). This is because the water vapour and aerosol content in the atmosphere decrease with increasing elevation, which in turn causes less cloud cover and greater transparency in the atmosphere at high elevations (e.g. Kou *et al.* 1982; Zeng *et al.* 1982). The same principle applies to the Tibet Plateau and the Mackenzie Delta region, except that the Mackenzie Delta region is located at a much higher latitude and much lower elevation (≈sea level), which makes the difference in solar radiation between the two areas even greater. For example, the net radiation on the Qinghai-Xizang Plateau is 60 to 80 kly/yr; while it is only 10 to 20 kly/yr in the Mackenzie Delta.

The annual fluctuation of solar radiation and air temperature create unique and quite different freezing and thawing conditions for both the Mackenzie Delta and the Qinghai-Xizang Plateau. Freezing and thaw conditions for Tuktoyaktuk in the Mackenzie Delta region (B) and Fenghuo Shan on the Qinghai-Xizang Plateau (D), together with other periglacial regions of the globe are given in Figure 3.2.

In polar latitudes, the diurnal thermal pattern is extremely weak, while the seasonal pattern is strong. By contrast, the plateau and alpine permafrost environments of low to middle latitudes possess a well-developed diurnal and seasonal thermal pattern. Another difference between polar permafrost areas and alpine/plateau permafrost areas is that the number of frost-free days in the polar

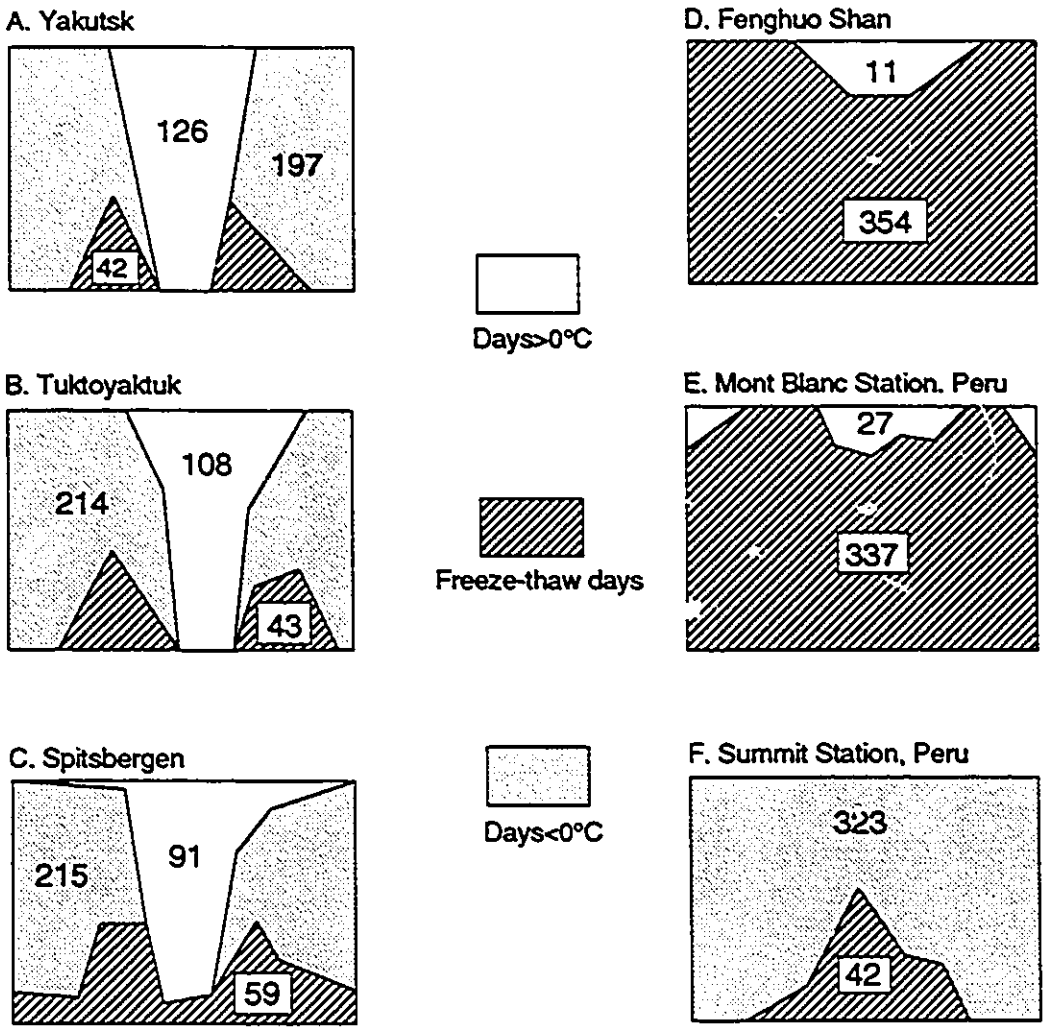

Figure 3.2 Freezing and thawing conditions in various periglacial environments of the world. A-Yakutsk (Lat. 62°01'N, Long. 129°43'E, altitude 108 m), Siberia, B-Tuktoyaktuk (Lat. 69° 27'N, Long. 133°02'W, altitude <10m), Mackenzie Delta, C-Spitsbergen (Lat. 78°02'N, Long. 14°14'E, altitude 7 m), D-Fenghuo Shan (Lat. 34°20'N, Long. 92°52'E, altitude 4,800 m), Qinghai-Tibet Plateau, E-El Misti (Mont BlancStation), South Peru (Lat. 16°16'S, Long. 71° 25'W, altitude 4760 m), and F-El Misti (Summit Station), South Peru (Lat. 16°16'S, Long. 71°25'W, altitude 5850 m) (A, C, E, and F from Troll 1958).

regions are greater. For example, the average annual number of frost-free days in Fenghuo Shan area is 11, while in Tuktoyaktuk it is 108. This is in spite of the fact that the MAAT (mean annual air temperature) at Tuktoyaktuk is about 4.7°C lower than in Fenghuo Shan area. This reflects the extremely low winter temperatures which occur for a long period of time in the polar environments. This suggests a smaller annual temperature range for the plateau environment than for polar regions. This is probably another reason why thermal-contraction cracking on the Tibet Plateau is not as frequently reported as in the Mackenzie Delta region.

3.3 Active-layer thermal regime

Although the mean annual surface temperature in permafrost areas may be below 0°C, the surface temperature will fluctuate during the year, causing the surface layer of ground to thaw in the summer and freeze in the winter. This layer of ground that is subject to annual freezing and thawing in areas underlain by permafrost is termed the 'active layer' in North America (ACGR 1988), and sometimes the 'seasonally thawed layer' in China (Lanzhou Institute of Glaciology, Geocryology and Desert Research 1975) and the former USSR (Melnikov and Tolstikhin 1988). The thermal regime of the active layer is complicated because of the effects of the periodic freezing and thawing (Lachenbruch 1959), and the surface canopy (vegetation and snow cover, for example). From both engineering and geomorphic viewpoints, the nature and rate of the spring thaw and the fall freeze-back are of interest (French 1988).

The spring thaw influences the nature of spring runoff and the amount of surficial water into the ground. Together they both influence the nature of frost heaving and ice segregation in the soil, as well as the stability of near-surface soil bodies.

For the Tibet Plateau, Figure 3.3 shows variations of shallow ground temperature with time in the active layer and the upper few metres of permafrost in the Fenghuo Shan area. Figure 3.4 shows detailed thawing and freeze-back conditions. The latter also indicates that the ground begins to thaw (i.e. the active layer begins to develop) in middle April. This is almost a month earlier than in Inuvik, N.W.T., where thawing begins in middle May (see Figure 3.5). Thawing progresses until early October for both Fenghuo Shan and Inuvik. The thawing process is one-sided, from the surface downwards.

The fall freeze-back process of the active layer begins in early October at both Fenghuo Shan (Figure 3.4) and Inuvik (Figure 3.5). In permafrost areas where there is no thawed layer sandwiched between the active layer and the underlying permafrost, the freezing is two-sided, occurring both downwards from the surface and upwards from the permafrost table (Figure 3.6). In other words, two freezing fronts co-exist in the active or seasonally frozen layer, and move towards each other as the freezing proceeds. The downward-advancing front usually moves faster, because of the colder air temperature and steeper temperature gradient. The two fronts can be regarded as the lower and upper boundaries for a thawed layer in between. Theoretically, since temperature at the two fronts remains at 0°C

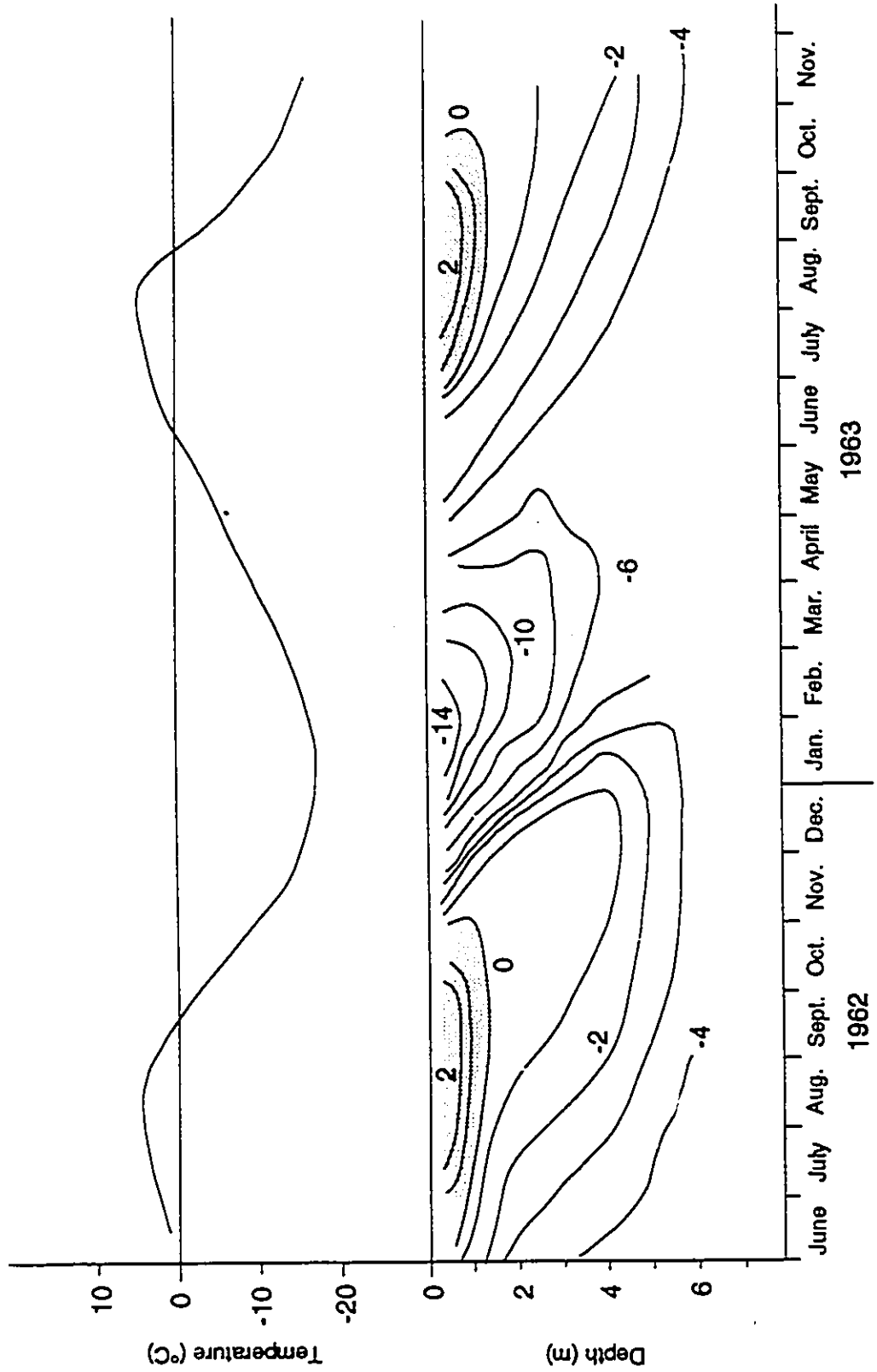

Figure 3.3 Ground thermal regime in a gentle slope of Fenghuo Shan area, together with mean monthly air temperature (Ground temperature data from Zhou 1965).

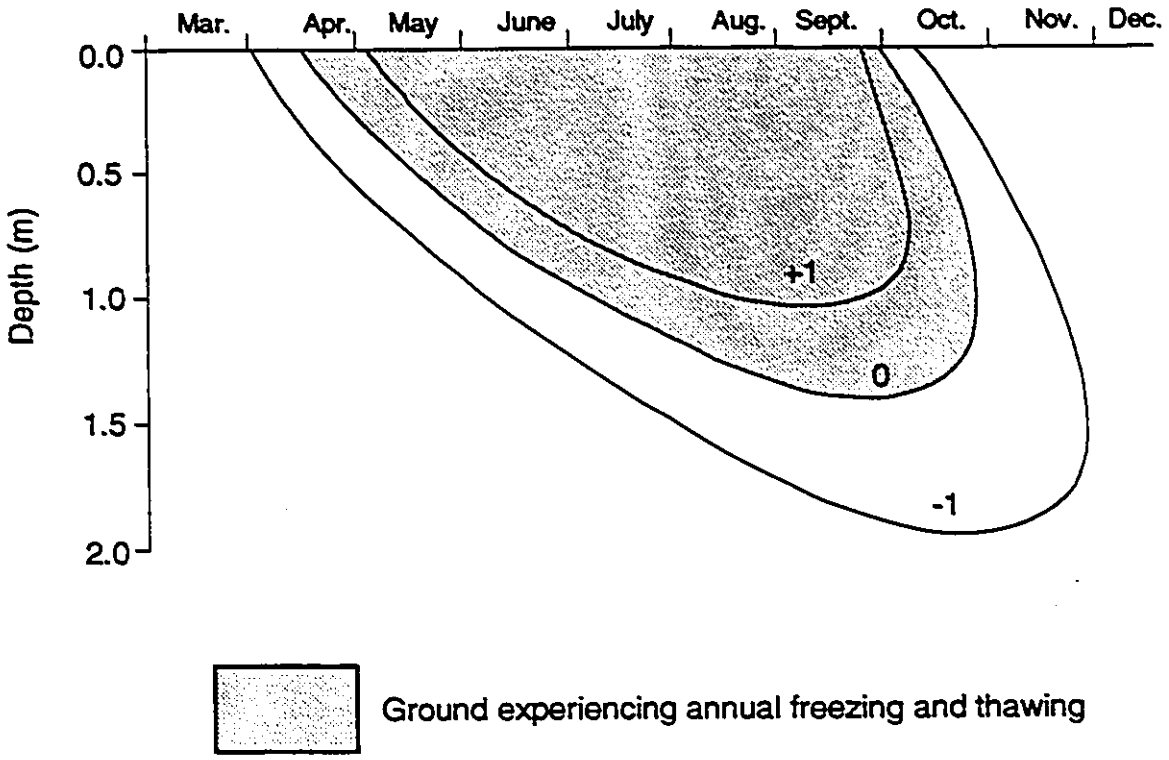

Figure 3.4 Thermal process of the active-layer development in 1983 for a gentle slope of Fenghuo Shan area, Qinghai-Xizang Plateau. The temperature data were thermistor readings from a 30 m borehole at the Fenghuo Shan Permafrost Research Station of the Lanzhou Northwest Railway Institute (According to B.Wang 1984).

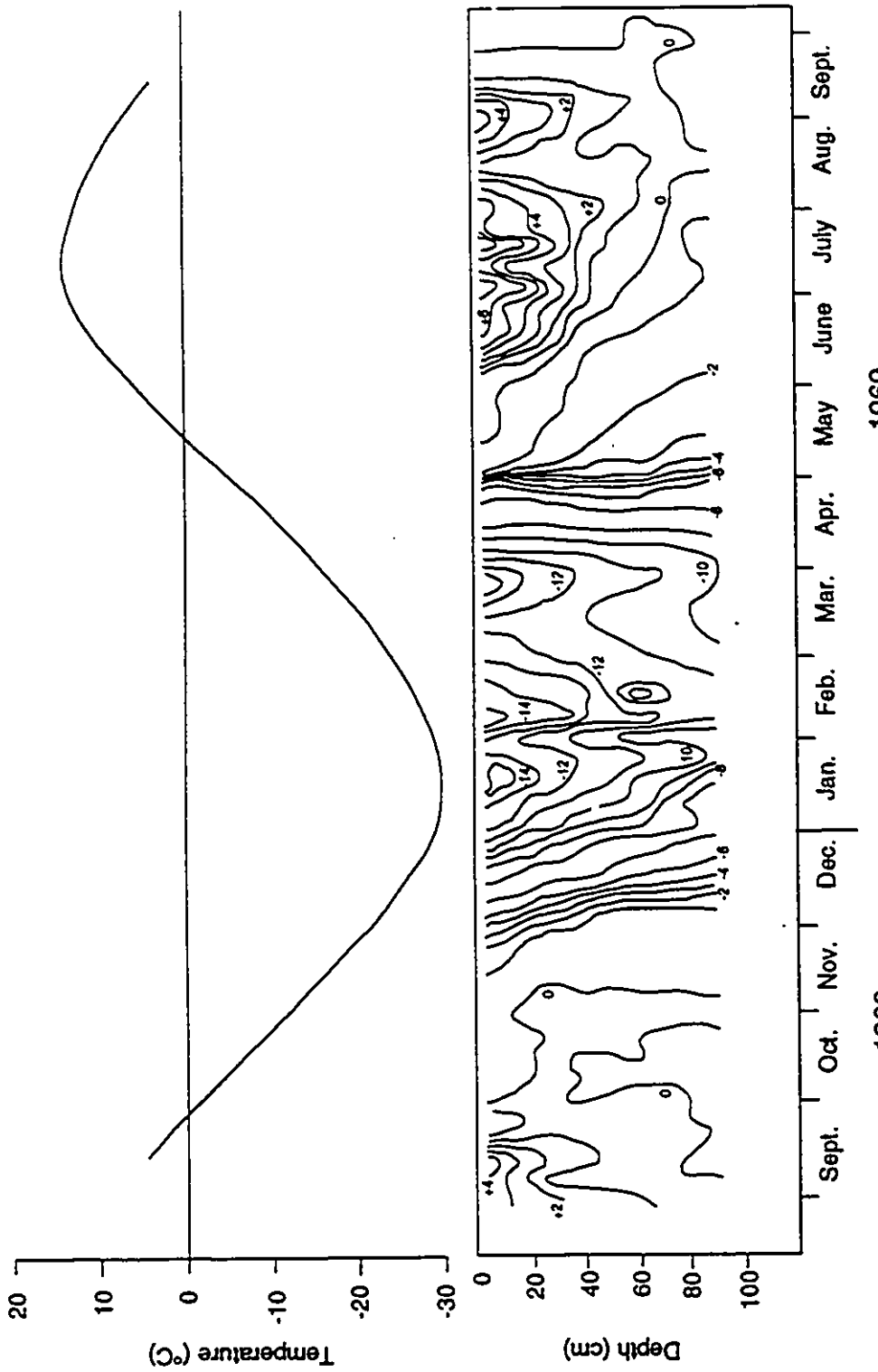

Figure 3.5 Ground thermal regime in the active layer of a mud hummock at Inuvik (According to Mackay and MacKay 1976), and monthly mean air temperature at Inuvik.

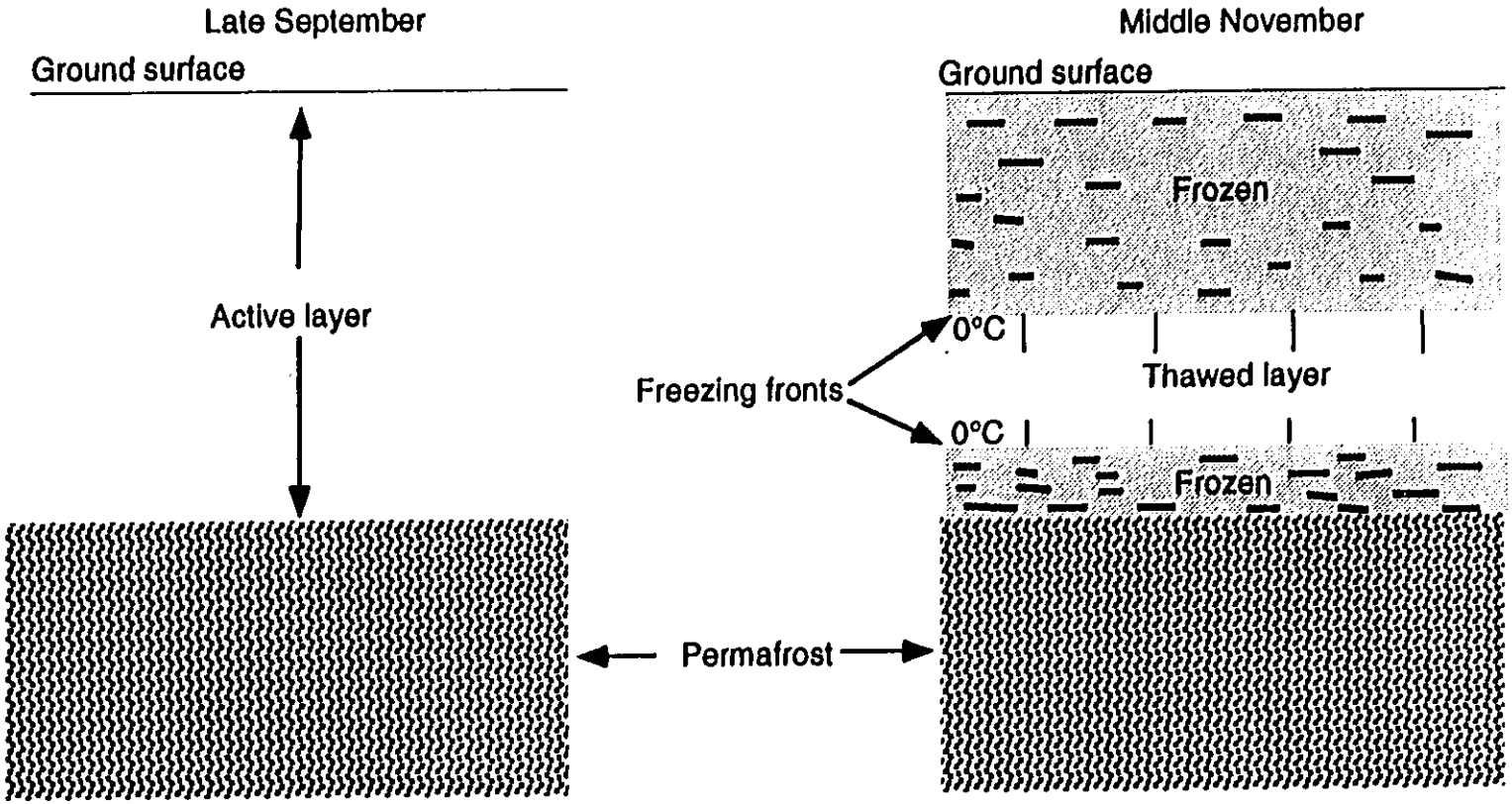

Figure 3.6 Graph showing the two-sided freezing in the active layer. Two freezing fronts move towards each other with zero curtain phenomenon in between.

throughout the freezing process (indicating a zero thermal gradient in the thawed layer between the two fronts), there is no heat flux through this layer. As a result, the layer remains isothermal for as long as it takes to freeze the active layer. This retarded residency of 0°C (assuming freezing point=0°C) in the soil has been termed the 'zero curtain' phenomenon (ACGR 1988; Melnikov and Tolstikhin 1988). It can be visualized clearly in figure 3.5 (the temperature during the period from late September to November).

Kudryavtsev (1961) believes that upward freezing in the active layer occurs only in permafrost areas where the mean annual ground temperature (MAGT) is colder than -3.5°C. However, studies in the People's Republic of China provide proof that it also takes place in warmer permafrost areas (see Table 3.1). Table 3.1 indicates that the thickness of the soil layer frozen by the upward freezing process can be substantial. This layer amounts to 32% of the total thickness of the active layer at Garry Island, N.W.T., Canada (Mackay 1973, Figure 1), greater than the percentage for the Fenghuo Shan area of the Qinghai-Xizang (Tibet) Plateau (Table 3.1). This is because (a) the MAGT at Garry Island is much lower, and (b) Garry Island is located in a maritime environment where the downward freezing of the active layer is slower due to higher moisture content in the soil, other conditions being the same.

The thickness of the active layer varies intimately with the surface energy exchanges. In the Pleistocene Mackenzie Delta, the combination of low air temperature in winter, the short summer thaw period, and relatively thick organic cover leads to the development

Table 3.1 Downward and upward freezing rates during the fall freeze-back of the active layer in the permafrost areas of the People's Republic of China (from Zhou and Guo 1982).

Location	Lithology	MAGT (°C)	AL thickness (m)	Downward freezing (cm/day)	Upward freezing (cm/day)	P
Fenghuo Shan, Tibet Plateau	Silty clay	-3.5	1.3	3.6	1.6	23.5
Tulihe, N.E. China	Silty clay	-1.2 to -2.0	2.2	4.7	1.9	17.4
Yakeshi, N.E. China	Silty clay	-0.5 to -0.7	2.5	3.3	0.5	10.0

Notes: (1) MAGT= Mean annual ground temperature, (2) AL = Active layer, and (3) P = Percentage of the thickness of the soil layer frozen by upward freezing over the total thickness of the active layer.

of a thin active layer (usually less than 0.5 m). On the Tibet Plateau, however, the thickness of the active layer varies between 1.3 and 3 m or more because of sparse vegetation, lack of organic cover, high solar insolation, and less moisture in the soil.

Monitoring the thickness of the active layer is a good way to study short-term climatic changes. For example, measurements by J.R. Mackay of the active layer at Garry Island and Inuvik, N.W.T. in the summer of 1990 suggested that the active layer in the Mackenzie Delta region reached the maximum depth in 1990 of the last 25 years (Mackay 1990, personal communication). Above-normal air temperature during that summer also initiated many skin flows in the region. The nature of these, and other mass-wasting processes operating in the active layer, have been summarized recently by French (1988).

3.4 Geothermal gradients

The term "mean annual ground temperature" (MAGT) has often been used to describe permafrost conditions. It refers to the ground temperature measured at the depth of zero annual amplitude, the level beneath which there is practically no annual fluctuation in ground temperature (ACGR 1988). Field measurements of ground temperature illustrate that MAGT is -7°C at Tuktoyaktuk, N.W.T. (Fujino *et al.* 1988), and -3.0°C at Fenghuo Shan, Tibet Plateau (Li 1982; Tong and Li 1983).

Below the level of zero annual amplitude, the ground temperature distribution is controlled largely by the geothermal gradient and thermal conductivity of the soil, for geothermal heat

flow depends upon these two parameters. This generalization assumes no complicating factors such as water bodies, geological irregularities, etc.

3.4.1 Mackenzie Delta region

The deep ground temperature data shown in Figure 3.7 were taken from five exploratory boreholes in the Mackenzie Delta region. Boreholes 1 and 2 are located in the Modern Delta; the rest are in the Pleistocene Delta (borehole 3 on Richards Island and boreholes 4 and 5 on the Tuktoyaktuk Peninsula). They indicates a temperature drop and an increase in thickness of permafrost from the Modern Delta to the Tuktoyaktuk Peninsula. The reason for this phenomenon is 1) the youthness of the Modern Delta sediments which have not been exposed to the cold air for as long as in the Pleistocene Delta, and 2) the Mackenzie River channels have been a source of heat.

The temperature profiles also indicate a departure from linearity in the upper 100 to 300 m. The almost linear portions of the curves at depth represent a steady heat flow from the earth through relatively homogeneous unconsolidated materials. Extrapolation of these curves to the surface yields a temperature of about -10°C for the Pleistocene Delta and 0 to +1°C for the Modern Delta. Today, in the Pleistocene Delta, the ground surface temperature is approximately -8°C (Judge 1973). In the Modern Delta, extrapolation of the measured temperatures suggests a present surface temperature of -5°C (Fig. 3.7). Thus, the curvature in the

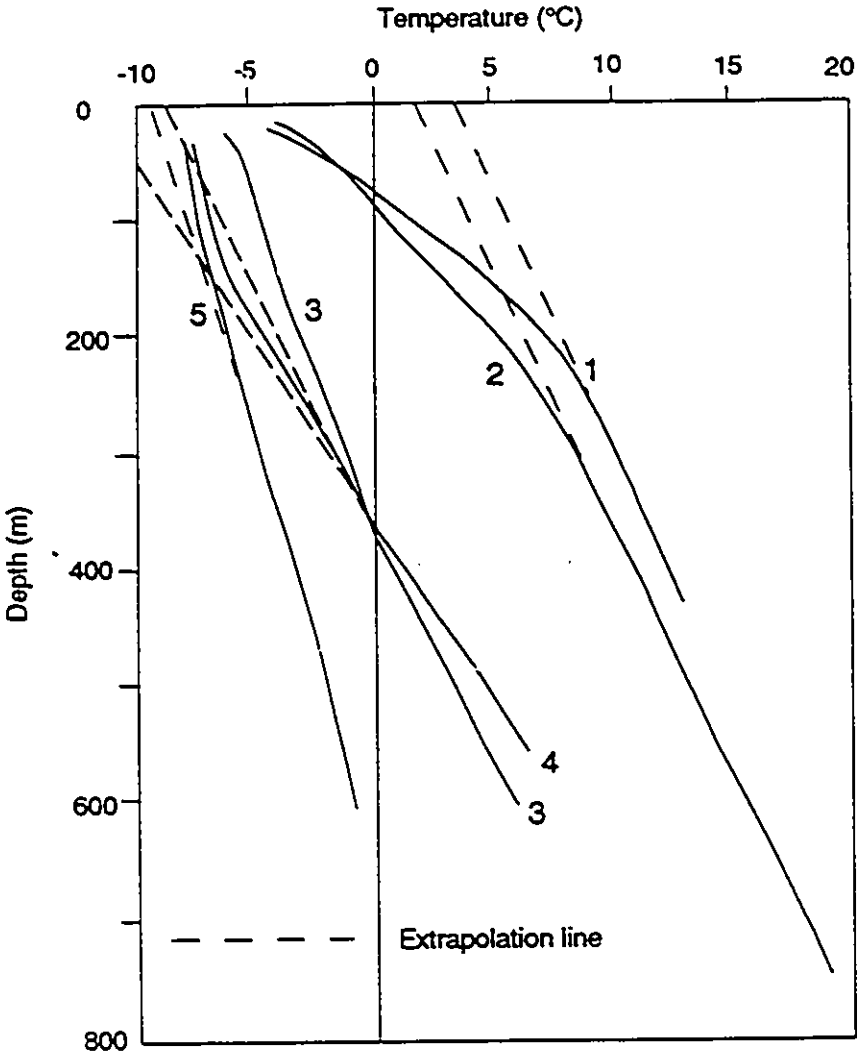

Fig. 3.7 Measured ground temperatures in the Mackenzie Delta region. Curves 1 and 2 are from the Modern Delta, while 3, 4 and 5 from the Pleistocene Coastal Plain (Data source: Judge *et al.* 1979; Taylor and Judge 1976; Taylor *et al.* 1982).

upper portion of the temperature profiles of boreholes 3 to 5 evidently represents a departure from equilibrium caused by a recent trend toward higher mean ground-surface temperatures. In other words, the curvature suggests an increase in temperature at the top of permafrost of about 2°C. Similar temperature trends have been reported by Lachenbruch *et al.* (1966, 1982, 1986, 1988) from the arctic slope and coastal plain of Alaska. According to Lachenbruch *et al.* (1986, 1988), this temperature increase commenced several decades to a century ago.

The ground temperature profiles for the Modern Delta (profiles 1 and 2 in Fig. 3.7), however, show an opposite trend (i.e. a cooling trend); the lower portions of the temperature profiles in Fig. 3.7 were established when the mean ground-surface temperature was between 0 and +1°C. Because the present ground surface temperature is about -5°C, this indicates a decrease in mean annual surface temperature of about 6°C in the Modern Delta. A change of this magnitude is unlikely to have been caused by climatic change. More plausible is that the changes are related to the development of the Delta itself. During the time when the lower portion of the ground temperature profile developed, the sediments must have been submerged, and water bottom temperature was probably about 0 to +1°C. With the continued sedimentation, delta growth, and probably channel shifting, the sediments emerged to experience colder ground-surface temperature, but still under the influence of periodic (i.e. annual) submergence. Thus, the cooling trend indicated by the borehole temperature profiles in the Modern Delta has little to do

with the large scale climatic change. Instead, the data are probably associated with the thermal effects of water body and sedimentation.

3.4.2 Qinghai-Xizang (Tibet) Plateau

Ground thermal conditions on the Qinghai-Xizang Plateau are illustrated in Fig. 3.8. Curves 1, 2 and 3 represent the ground temperatures in predominantly continuous permafrost areas. Curve 4 shows the higher ground temperature and thinner permafrost due to the thermal effect of Buqu River. Fig. 3.8 indicates that permafrost thicknesses on the Plateau are usually less than 100 m, except for the mountain ranges (see Fig. 2.14). Because of the higher permafrost temperature on the Plateau, the influence of thermal disturbances, such as those caused by water bodies and faults, is believed to be more important than in the Mackenzie Delta. For example, much greater areas of permafrost would disappear in Tibet than in the Mackenzie Delta region if the MAGT increased by 1°C, because about 75% of Tibetan plateau permafrost has a MAGT of between -0.5 and -1.5°C (see Figure 2.8).

The average geothermal gradient on the Qinghai-Xizang Plateau is 4.6/100 °C/m in permafrost, and 5.1/100 °C/m below permafrost. This is higher than in the Mackenzie Delta region where it is usually less than 2/100 °C/m in permafrost, and about 3/100 °C/m below permafrost. The higher geothermal gradient on the Plateau reflects the fact that the Plateau is geologically young and active.

Available boreholes on the Qinghai-Xizang Plateau are not suitable for studying changes in near-surface ground temperatures

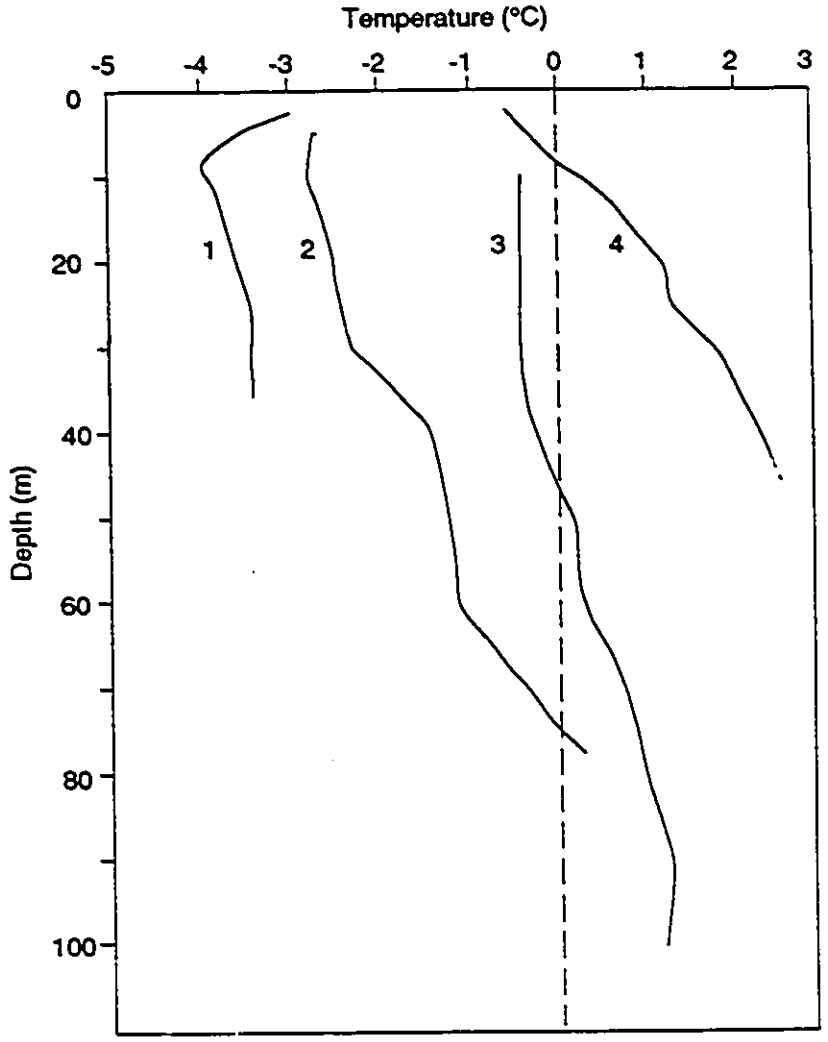

Figure 3.8 Measured ground temperatures in the Qinghai-Xizang Plateau: 1-FenghuoShan area, 2-Kunlun Shan Pass, 3-Wudaoliang, and 4-Buqu River valley (Data source: Tong and Li 1983; Wang and Li 1983; Zhou and Guo 1982).

since they are too shallow to show changes in geothermal gradient. According to the distribution of ground temperatures vs depth, boreholes drilled for the purpose of paleoclimatic reconstruction should be at least 200 to 300 m deep (Gold and Lachenbruch 1973). Thus, deep boreholes are needed in order to investigate the geothermal history on the Plateau.

3.5 Discussion and conclusions

The net radiation on the Tibet Plateau is much higher than that in the Mackenzie Delta region. This is due to the higher elevation and lower latitude of the Plateau. The differences in surface energy exchanges in both areas lead to different active layer regimes. The active layer on the Plateau begins to thaw almost a month earlier than in the Delta region. However, upward freezing in the Delta region is more significant; up to 32% of the active layer freezes from below. As a consequence of these differences in surface energy exchanges, the active layer on the Plateau is much thicker than in the Mackenzie Delta region.

The surface energy exchanges also influence ground temperatures at depth. Ground-temperature data indicate that the MAGT varies from above -4°C in the Modern Delta to at least -7°C in the Pleistocene Delta region, and from -0.5°C to -3.0°C on the Tibet Plateau.

The geothermal gradient on the Tibet Plateau is roughly 2 and 3 times higher than that in the Mackenzie Delta region. This is because the Plateau is geologically young and active.

Deep temperature measurements both in the Pleistocene Mackenzie

Delta, and in Alaska, point out some of the systematic temperature changes which have taken place in the North American Arctic. These changes are indicated by the anomalous curvatures in the upper 200 m or so of temperature-depth profiles. The anomalies can be interpreted confidently in terms of the surface temperature history. This is because of a special property of cold continuous permafrost: unlike most near-surface earth materials, it is unaffected by circulating groundwater. Thus heat transfer within it is exclusively by conduction. According to Lachenbruch *et al.* (1986, 1988), the 'surface' whose temperature is being analyzed is the upper surface of permafrost that lies beneath the active layer. This temperature differs from the standard 'surface air temperature' frequently analyzed by climatologists. It also differs from the mean ground temperature taken at the top of the snow pack, when it is present, or the ground surface when it is not. It is believed, however, that change in temperature at the top or bottom of permafrost represents secular change in climatic processes.

Temperature data from the Pleistocene Delta indicate an increase of 2°C at the top of permafrost; this increase is believed to have commenced several decades to a century ago. Although comparable data from the Modern Mackenzie Delta suggest a cooling trend, this has little to do with large scale climatic changes, since it is related to the thermal effect of the Mackenzie River and sedimentation.

Unfortunately, no deep ground temperature data are available on the Qinghai-Xizang Plateau to investigate the geothermal history

and /or to identify any global climatic warming.

CHAPTER FOUR - GEOTHERMAL DISTURBANCES

4.1 Introduction

Chapter three examined certain common aspects of the ground thermal regimes in both areas. The regional pattern so described is complicated and disturbed, however, by a number of important, site-specific controls. In certain circumstances, these controlling factors assume dominance and cannot be ignored. Accordingly, this chapter now examines the impact that site-specific variables have on permafrost.

4.2 Geological structure, Tibet Plateau

On the Qinghai-Xizang Plateau geological structure constitutes the most important control over permafrost distribution. This is because the Qinghai-Xizang Plateau is geologically active.

There is evidence that faulting has a close relationship with permafrost thickness. By using DC-electrical sounding methods, Huang and Mi (1983) have demonstrated that the permafrost thickness in the fault zone can be 100 m thinner than the surrounding areas (Figure 4.1). Based on geotechnical and hydrogeological investigations on the Plateau, Tong and Li (1983) conclude that faults have a significant effect on the thickness of permafrost. Their survey indicates that ground temperatures on the upthrust block of a reverse fault are higher than on the downthrust block (Table 4.1).

There is also a clear relationship between faults, taliks and hot springs. A large number of hot springs (Table 4.2) on the Qinghai-Xizang Plateau are the direct result of faulting. The kind

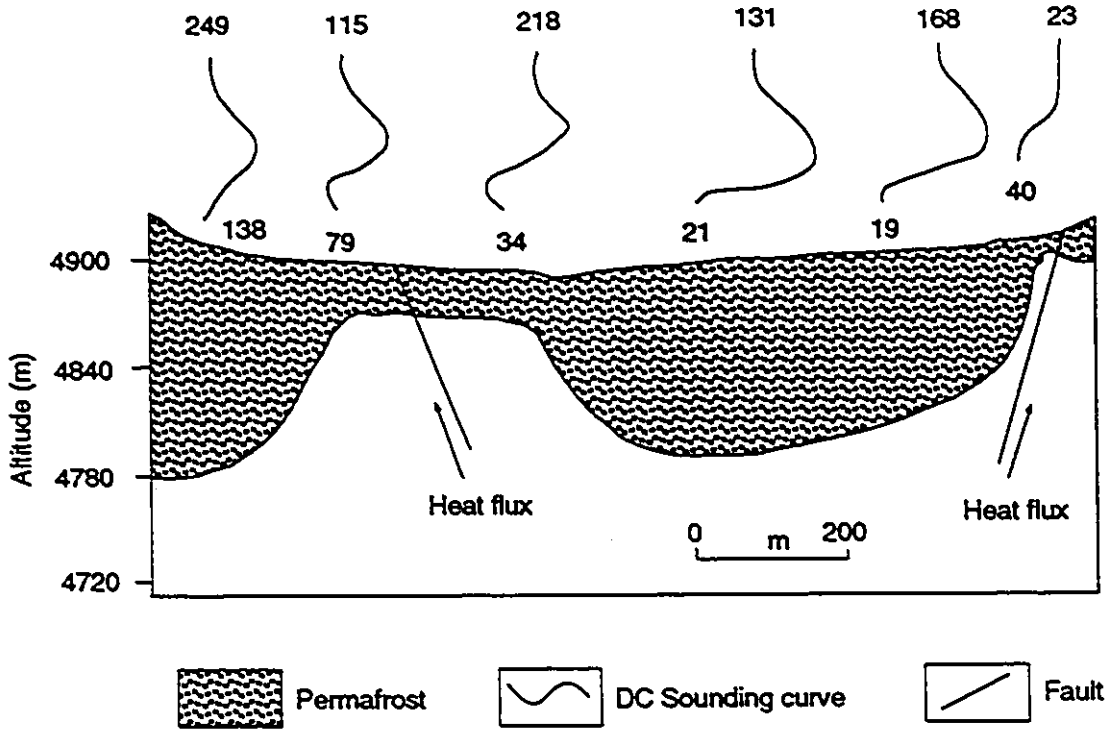

Figure 4.1 Effect of faults on the thickness of permafrost in the Fenghuo Shan area, as revealed by the DC Sounding method (Source: Huang and Mi 1983).

Table 4.1 Effects of reverse faults on permafrost
(Source: Tong and Li 1983)

Location	Part of fault	Groundwater discharge (l/sec.m)	Permafrost thickness, m
Budong-Quan	Upthrust side Downthrust side	15.3 0.004	0.0 55.0
Wuli	Upthrust side Downthrust side	4.3 0.6	0.0 8.1
Erdao-Gou	Upthrust side	4.3	0.0

Table 4.2 Water temperatures and origin of hot springs
(Source: Guo 1985)

Locality	Water temperature,°C	Intersecting faults and their strikes
Xidatan	0.3 to 3	EW/NS faults
Budong Spring	2.0	NW/NE faults
Kanxin range	20.5	NW faults
Buqu river valley	18 to 68	NW faults
Tanggula mountain	15 to 20	NW/NNE faults
Cuena lake	15 to 83	NE/NEE faults

of taliks associated with geological structures and volcanic activities are termed "structural-geothermal taliks". These hot springs and taliks are often located at the intersecting zone of faults of different strikes.

The effect of geological structure upon permafrost can best be described in terms of the geothermal heat flux. Investigations indicate that the geothermal flux in younger and active geological units is higher than in older and geologically stable units (Table 4.3). Because the uplift of the Qinghai-Xizang Plateau is a late Cenozoic event (post-Pliocene), the average geothermal flux is believed to be higher than 2.2 $\mu calcm^{-2}s^{-1}$. This is especially true along the fault zones. Groundwater is usually under great pressure and rises along the faults, bringing geothermal heat to the surface.

Sometimes, the formation of frost mounds on the Tibet Plateau is associated with faults. An example is the pingo located in the Kunlun Shan Pass along the Trans-Plateau Highway (Figure 4.2). Groundwater (mud) emerged from a borehole drilled through the pingo, to a depth of >57 m (the permafrost base). It seems unlikely that a subpingo water lens exists because the groundwater did not come immediately from beneath the ice core, but from the aquifer below the permafrost base (water (mud) jetted up to the air more than 20 m high when the borehole penetrated the permafrost) Investigations have confirmed that the pingo lies at the intersection of two faults. One is a normal fault with a NE strike, the other is a reverse one with a NNW strike. It is hypothesized,

Table 4.3 Mean geothermal flux in geological units of different age (Source: Geothermal Group 1978).

Geological age	Geothermal flux, $\mu cal cm^{-2}s^{-1}$
Precambrian	0.93
Palaeozoic	1.11 to 1.24
Mesozoic	1.42
Cenozoic	2.20

Figure 4.2 A photo showing the collapsed pingo at the Kunlun Shan Pass. It is the largest one found on the Tibet Plateau. The road by the pingo is the Trans-Plateau Highway (Photo taken by Wang Shaoling in the1970's).

therefore, that the pingo was formed by the freezing of artesian groundwater injected up through the fault zone (An 1980). This process is also responsible for the origin of many other pingos on the Plateau. Thus, Guo (1985) has tabulated several pingo groups formed in this manner. In all probability, similar pingos occur on Prince Patrick Island (Pissart 1967) and Amund Ringnes Island (Balkwill *et al.* 1974) in the Canadian Arctic.

4.3 Coastal retreat, Mackenzie Delta

In the Mackenzie Delta region, the proximity of the Beaufort Sea is an important influence upon permafrost. First, thermal erosion and rapid coastal retreat of unconsolidated ice-rich sediments leaves an offshore zone of relict permafrost beneath shallow water. and second the thermal regime in such areas progressively adjusts to the new upper boundary zone created by the coastal retreat. A numerical modelling was employed to better understand these changes. Moreover, the possibility of hydrocarbon development on the Beaufort Sea shelf and the location of processing and transportation facilities at the coast necessitates an understanding of permafrost conditions in these dynamic littoral environments.

4.3.1 Evidence for coastal retreat

Coastal recession, caused by thermal erosion and ablation of ice-rich sediments, has been reported from many areas of northern Alaska (e.g. Hume *et al.* 1972; Reimnitz and Maurer 1979; Vigdorchik

1980; Walker 1988), northern Siberia (e.g. Are 1983; Molochushkin 1978; Novikov and Fedorova 1989), and the Western Canadian Arctic (e.g. Dalllimore *et al.* 1988; Harry, *et al.* 1983; Mackay 1986a, 1987). In the Laptev Sea, certain islands have disappeared in historic times, on account of extremely rapid coastal recession (Barr 1976). On the Yukon Coastal Plain, the grave of a member of Amundsen's expedition had to be moved landward several times due to coastal retreat (Mackay 1963b). Recent field investigations along the Beaufort Sea coast in the Mackenzie Delta indicate that the retreat rate varies between less than one metre to 8 m/year, depending mainly on ice content, degree of lithification of the sediments and the activity of storm surges and longshore currents. For example, typical rates of coastal retreat are 8 m/year for high centred polygons underlain by a high ice content diamicton at Tuk 3 site; 7 m/year for tabular body of massive ground ice at Peninsula Point (Figure 4.3) (Mackay 1986a); 3 m/year for ice-rich sandy coastal bluffs (Figure 4.4); and 1 m/year or less for ice-poor sandy bluff and sand bars (Dallimore *et al.* 1988)). Elsewhere, maximum retreat rates as great as 15 to 20 m/year have been documented for parts of the Laptev Sea, Siberia (Molochushkin 1978).

4.3.2 Numerical simulation

Numerical modelling of seafloor temperatures is useful since it enables prediction of permafrost changes without expensive offshore measurements. Mean annual seafloor temperature (MAST) is

Figure 4.3 A 1971 air photo (A22535) of Peninsula Point, 6 km southwest of Tuktoyaktuk, N.W.T., showing the shoreline positions at different times (Source: Mackay 1986a).

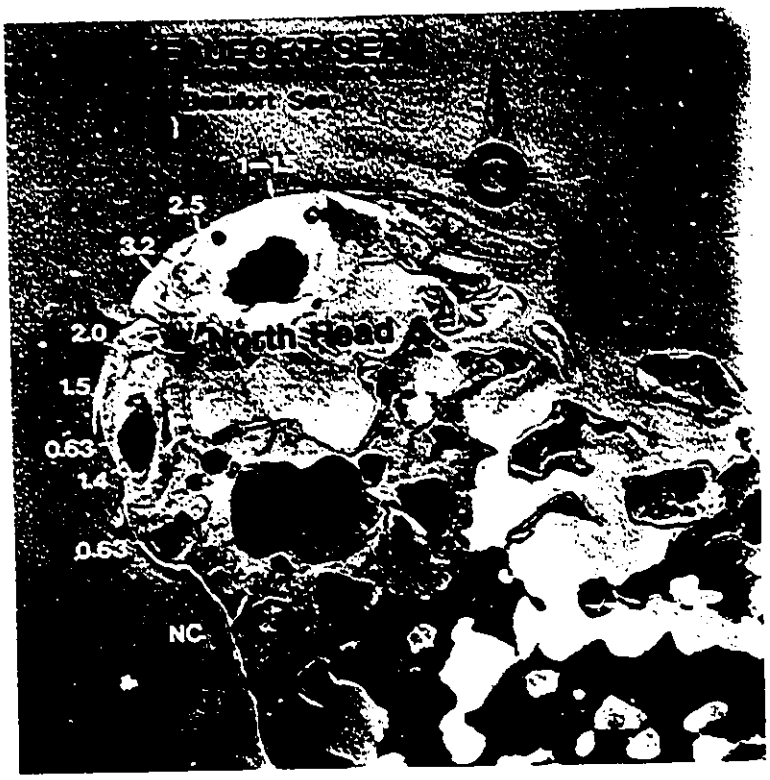

Figure 4.4 Rates of coastal retreat at North Head, Richards Island, Mackenzie Delta region (Source: Dallimore *ei al.* 1988).

taken as a boundary condition. For the Mackenzie Delta region, a mean ground surface temperature (Ts) of -8.0°C is typical (Judge 1973). Recent studies indicate that seafloor temperature decreases with increasing water depth and remains below 0°C for much of the year (Dyke 1991; Hunter 1988; Sellmann *et al.* 1992). In the Mackenzie Delta region of the Beaufort Sea the MAST ranges mostly between 0 and -2°C. In this study, values of between -1 and -2°C are assumed for all areas between Herschel Island and King Point, plus the offshore areas of the Pleistocene Mackenzie Delta. The discharge of the Mackenzie River mixes with sea water to give above 0°C temperatures, but this effect is restricted to shallow depths only (Dyke 1991; Hunter 1988). The MAST in this area is assumed to be 0 to -1°C. Following shoreline retreat the submerged permafrost is subject to degradation although MAST can be below 0°C (Nixon 1986). The depth of thaw has been discussed by Dyke (1991), Hunter (1988) and Nixon (1986). This section, however, focuses mainly upon the temperature variations of nearshore permafrost after rapid coastal retreat, regardless of the phase change.

The model

The first problem to consider is the thermal disturbance due to the ocean, where the shoreline is supposed to have shifted during some brief interval of time in the past, and to have since remained stable. The earth's surface can be considered as a plane (z=0), composed of the land surface and the ocean bottom. Neglecting relief in this way can be justified along the Western

Arctic Coast of Canada because of the gentle sloping continental shelf and low relative relief. In a two-dimensional model, the shoreline is represented by a vertical line (Z=0, X=0), the land surface by Z=0, X<0, and the ocean bottom by Z=0, X>0 (Figure 4.5). The basic equation describing the heat distribution is the two dimensional Fourier equation (Lachenbruch 1957a):

$$\frac{\partial^2\theta}{\partial x^2}+\frac{\partial^2\theta}{\partial z^2}=\frac{1}{\alpha}\frac{\partial\theta}{\partial t}, z>0 \qquad (4.1)$$

The problem is to find the increase in temperature caused by coastal retreat at any subsurface point (x, z) that satisfies equation (4.1). At the same time, Equation (4.1) needs to satisfy several conditions. First, it is assumed that prior to initiation of coastal retreat, there was no thermal disturbance, i.e.:

$$\theta(x,z,t)=0, (z>0, t=0) \qquad (4.2)$$

Second, after the beginning of retreat, although thermal disturbance at the sea bottom occurs, it is assumed that there is no change in ground surface temperature (i.e. Ts remains constant). The sea bottom disturbance is the difference between the mean annual temperatures of the land surface and seafloor, represented by A. Furthermore, at an infinite depth beneath land ($z=\infty$), it is assumed that the thermal disturbance caused by coastal retreat is zero:

$$\theta(x,0,t)=0, (t>0, x<0, z=0) \qquad (4.3)$$

$$\theta(x,0,t)=A, (t>0, x>0, z=0) \qquad (4.4)$$

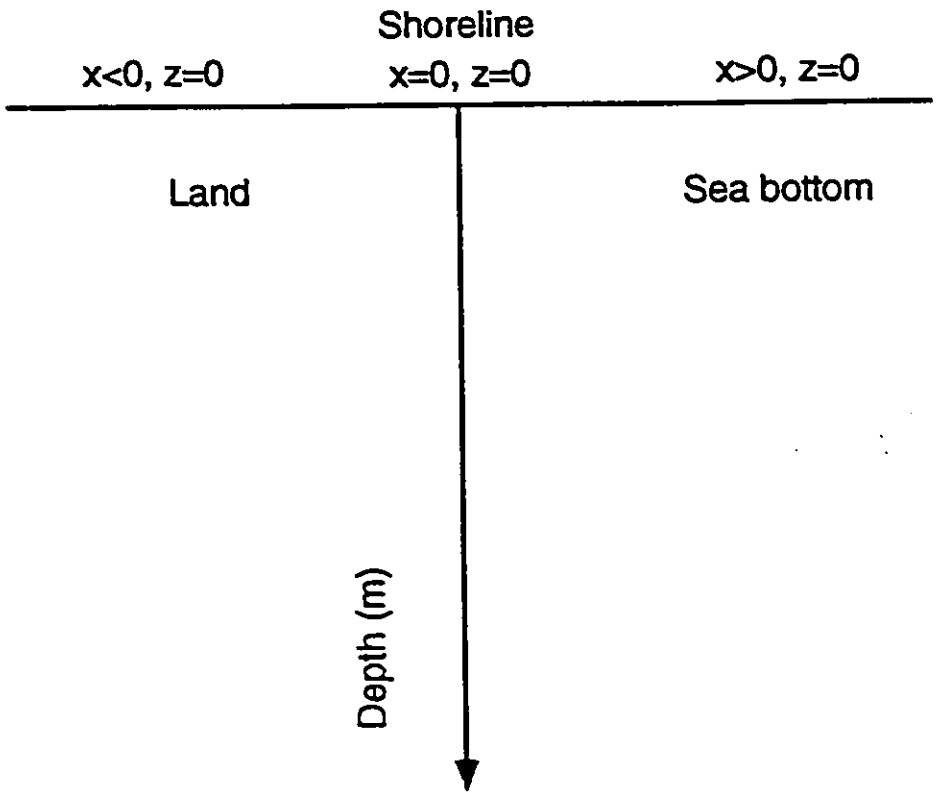

Figure 4.5 Coordinates used in the model.

$$\theta(x,\infty,t)=0,\ (t>0,x<0) \tag{4.5}$$

Equation (4.2) is an initial condition, while (4.3) to (4.5) are boundary conditions.

Stationary shorelines

For a stationary coastline, the thermal disturbance can be solved from the foregoing equations as follows (Lachenbruch 1957a):

$$\theta(x,z,t)=A\Psi\left(\frac{x}{z},m\right) \tag{4.6}$$

where

$$\Psi\left(\frac{x}{z},m\right)=\frac{1}{2}erfc\sqrt{m}+\frac{1}{\pi}\int_0^{x/z}\exp\left[-m(1+v^2)\right]\frac{dv}{1+v^2} \tag{4.7}$$

and

$$m=\frac{z^2}{4\alpha t} \tag{4.8}$$

where α=thermal diffusivity (cm^2/sec), t=time since coastline retreat (yr), v=integration variable, A=difference in temperature between the ocean bottom and land surface, and m=coefficient. Therefore, the thermal regime at any point (x,z) is the temperature before disturbance (Tu) plus the temperature increase caused by shoreline retreat:

$$T(x,z) = Tu + \theta(x,z,t) = (Ts + Ggz) + A\Psi\left(\frac{x}{z}, m\right) \qquad (4.9)$$

Retreating shorelines

An unstable (i.e., retreating) coastline is a more realistic scenario for the ice-rich unconsolidated sediments of the Mackenzie Delta. The restriction that a shoreline moves suddenly, at t = 0, to a new position, x = 0, can be removed by superposition of solutions of the form of (4.6) so that a numerical simulation of permafrost conditions can be made for retreating shorelines. In the general case when n stages of shoreline retreat are considered, solution (4.6) becomes:

$$\theta = A\left[\sum_{i=1}^{n-1}\left[\Psi\left(\frac{x-x_{i+1}}{z}, m_i\right) - \Psi\left(\frac{x-x_i}{z}, m_i\right)\right] + \Psi\left(\frac{x-x_1}{z}, m\right)\right] \qquad (4.10)$$

The model here simulates the thermal regime of permafrost by tracing shoreline retreat over the last 300 years. Assuming a maximum retreat rate of 8 m/yr as typical of exceptional rapid retreat, the coastline of certain part of the Mackenzie Delta region would have been 2,400 m seaward of its present position.

This shoreline retreat during the last 300 years can be divided into several stages: when the coastline moves from (1) $x_0 = \infty$ to x_1 = 2,400 m at t_0 = 0; (2) x_1 = 2,400 m to x_2 = 1,600 m at t_1 =100 years; (3) x_2 = 1,600 m to x_3 = 800 m at t_2 = 200 years; and (4) x_3 = 800 m to x_4 = 0 at t_3 = 300 years. For such a four-stage

retreat model from t_o = 0 (i.e. 300 years ago) to t_3= 300 year (i.e. present), solution (4.10) becomes (Lachenbruch 1957a):

$$\theta = A[[\Psi(\frac{x-x_2}{z}, m_1) - \Psi(\frac{x-x_1}{z}, m_1)] + [\Psi(\frac{x-x_3}{z}, m_2) - \Psi(\frac{x-x_2}{z}, m_2]$$

$$+ [\Psi(\frac{x-x_4}{z}, m_3) - \Psi(\frac{x-x_3}{z}, m_3)] + \Psi(\frac{x-x_1}{z}, m)] \qquad (4.11)$$

where

$$m_i = \frac{z^2}{4\alpha(t-t_i)} \qquad (4.12)$$

Solution to the equations is made by routine calculations following the methods of Smith (1953) and Lachenbruch (1957a). A major problem in this model is the calculation of the disturbance function Ψ from equation (4.7). This involves the complementary function erfc(x) which itself relates to an error function erf(x):

$$erfc(x) = 1 - erf(x) \qquad (4.13)$$

where

$$erf(x) = \frac{2}{\sqrt{\pi}} \int_0^x \exp(-t^2)\, dt \qquad (4.14)$$

Solution of these functions can be found in engineering mathematics textbooks (e.g. Kreyszig 1966). A second problem relates to the second term of equation (4.7) which is an integral. Smith (1953)

has made a solution in the form of a series expansion:

$$\int_0^{x/z} \exp[-m(1+v^2)] \frac{dv}{1+v^2}$$

$$= \exp(-m) \sum_{n=0}^{\infty} \frac{(-1)^n (\frac{x}{z})^{2n+1}}{2n+1} (1+\frac{m}{1!}+\ldots.\frac{m^n}{n!}) \qquad (4.15)$$

for x/z<=1, and

$$= \frac{\pi}{2} (1-erf\sqrt{m} erf(\frac{x}{z}\sqrt{m}) - \exp[-m(\frac{x}{z})^2] \times$$

$$\sum_{n=0}^{\infty} \frac{(-1)^n}{(2n+1)(\frac{x}{z})^{2n+1}} (1+\frac{m(\frac{x}{z})^2}{1!}+\ldots.+\frac{[m(\frac{x}{z})^2]^n}{n!}) \qquad (4.16)$$

for x/z>1.

Results

The thermal regime of nearshore permafrost in the coastal retreating zone is finally predicted by equation (4.9) under three different seafloor temperatures (Tsf). The results are shown in Figures 4.6 and 4.7. Predictably, these diagrams indicate that, although there is a minor difference in permafrost thickness between land and sea, the temperature beneath the sea is warmer than beneath land. For example, the offshore ground temperature predicted under the condition of Tsf=0°C is mostly above -4°C. By contrast, the temperature beneath land 500 m away from the shoreline may be as low as -6°C.

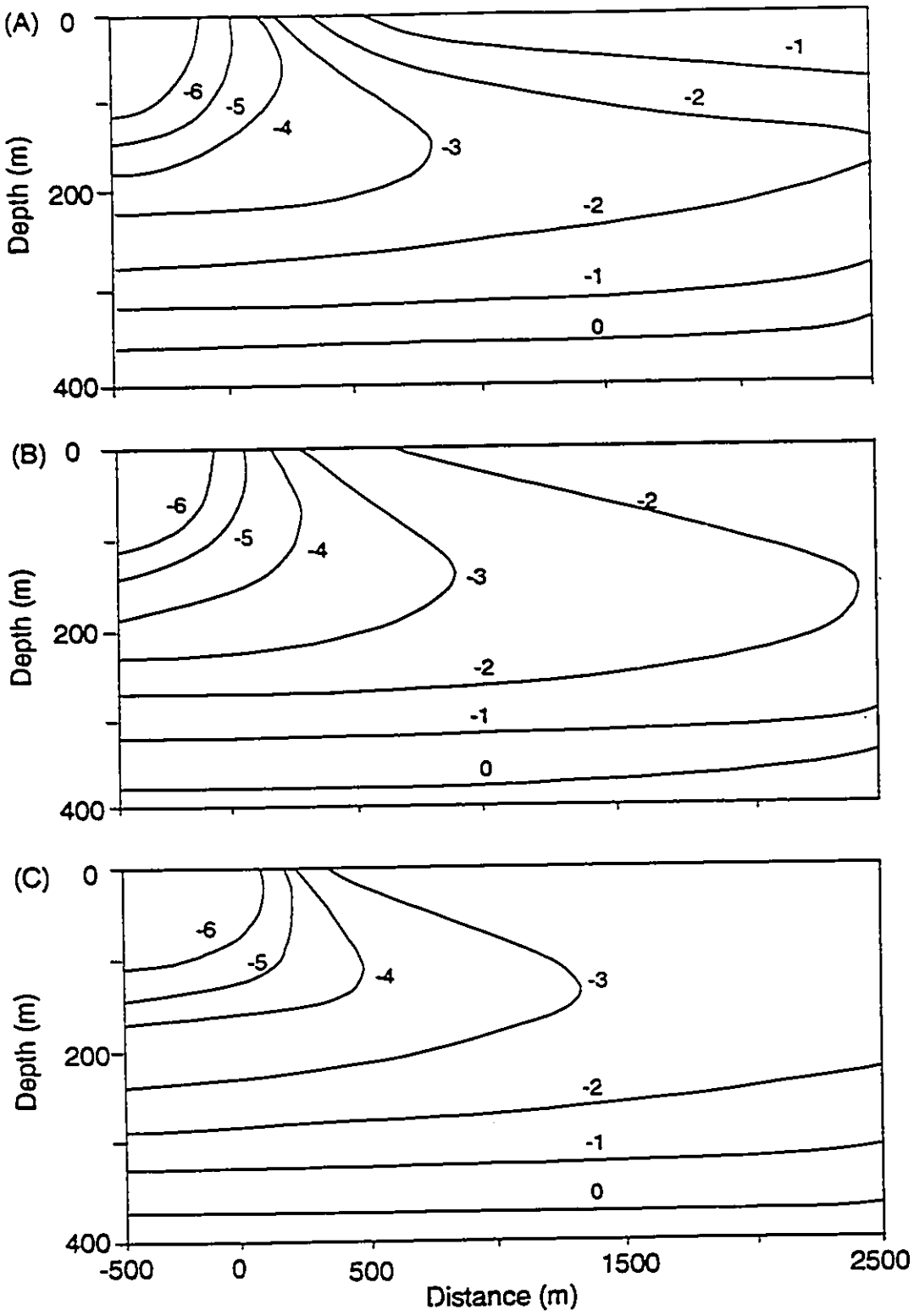

Figure 4.6 Predicted ground temperatures for the near-shore permafrost under three different seafloor temperatures Tsf (A: Tsf = 0°C, B: Tsf = -1°C, C: Tsf = -2°C).

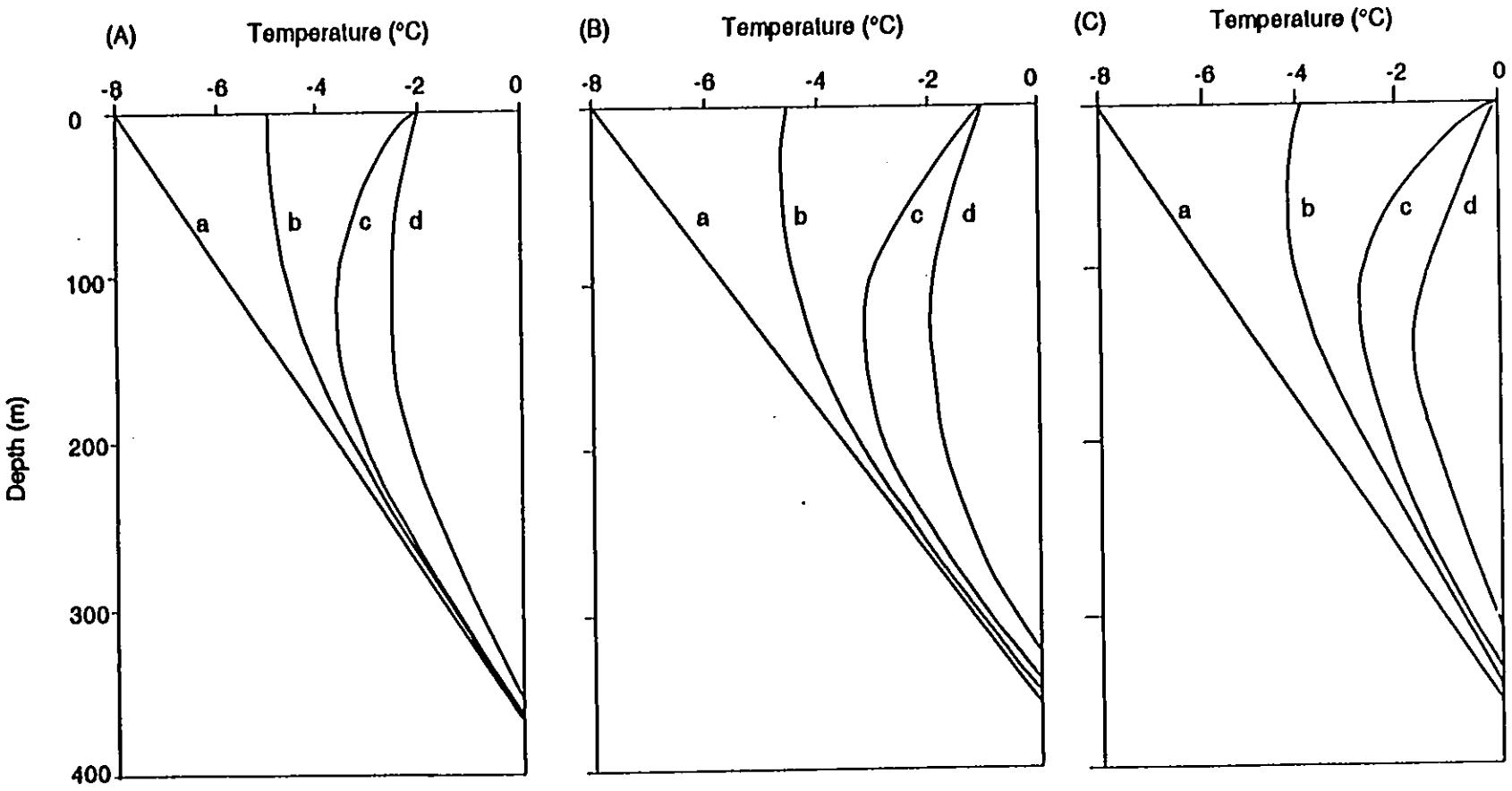

Figure 4.7 Predicted ground temperature ditribution vs depth for the nearshore region, Mackenzie Delta, A: Tsf=0°C, B: Tsf=-1°C, and C: Tsf=-2°C; curve a: on undisturbed land far from the sea, b: at the shoreline, c: 500 m offshore, and d: 2500 m offshore.

Figure 4.6 shows that permafrost can be expected to persist at a significant distance offshore following rapid coastal retreat. This has been proven in the offshore areas of the Pleistocene Mackenzie Delta where drilling has indicated subsea permafrost several tens of km offshore (Hunter *et al.* 1976; Mackay 1972). Such extensive subsea permafrost may be due partly to rapid coastal retreat. This inference is supported by the temperature data measured from Norton Sound area of the Bering Sea, where nearshore subsea permafrost is present only in areas of rapid coastal retreat (Osterkamp and Harrison 1982).

Figure 4.7 indicates that with rapid coastal retreat the extent and thickness of subsea permafrost within 2,500 m of the shoreline (curve D) can be almost as thick as that on land (curve A), but warmer. The most significant increase in temperature occurs near the surface (i.e., the seafloor). The temperature increase within 100 m of sea bottom may be as much as 4-6°C during the first several hundred years of submergence caused by coastal retreat. Data which support this model have been reported from the Laptev Sea, USSR (Molochushkin 1978), and from Prudhoe Bay, Alaska (Lachenbruch and Marshall 1977). Another phenomenon associated with coastal retreat is the presence of a negative geothermal gradient in the upper 100 m of subsea permafrost (Figure 4.7).

4.3.3 Discussion

This analysis identifies several problems concerning offshore permafrost. The first relates to the thickness of relict offshore

permafrost. Given the rate of coastal retreat used in this model, the thickness of subsea permafrost 2,000 m offshore is predicted to be about the same as that on land. However, its temperature would be higher. The model shows that the equilibrium thickness of permafrost beneath land, under current ground surface temperatures (Ts = -8°C), is about 350 m. Because seafloor temperatures (Tsf) are mostly between -1 and -2°C, (i.e. about 6 to 7°C higher than Ts) much subsea permafrost must be relict and is degrading. If a geothermal gradient of 0.01 °C/m is assumed for the sea bottom, the equilibrium thickness of permafrost would be 200 m. Thus, one can infer that the thickness of relict degrading offshore permafrost may be as much as 350-200 m (i.e., 150 m). As a regional maximum rate of coastal retreat has been assumed in this simulation, areas with slower retreat rates will have thinner relict permafrost.

A second problem concerns the origin of offshore permafrost. This has been discussed by many investigators (e.g. Mackay 1972; Osterkamp 1975; Vigdorchik 1980). One mechanism relates to the emergence-submergence of the land during the Pleistocene. Because most of the coastlands of the Western Canadian Arctic were unglaciated during Late Wisconsinan times (Rampton 1988), shallow areas below present sea level were exposed as dry land. Permafrost would have grown in response to cold air temperature, the thickness of which would depend on the duration of exposure (Mackay 1972). Upon submergence, terrestrial permafrost would have become subsea permafrost. But subsea permafrost may also originate in a number of other ways. As demonstrated by this simulation, extensive and rapid

coastal retreat can result in relict permafrost existing in offshore areas. Since continuing and rapid coastal retreat is a widespread geomorphic phenomenon of the western arctic coast of Canada, it may have played a more important role in the formation of offshore permafrost than originally thought.

By definition, permafrost, or perennially cryotic ground, need not contain ice even though its temperature remains below 0°C (ACGR 1988). Therefore, the permafrost base does not always coincide with the lower limit of ice-bonded permafrost. This model delineates the boundary between cryotic and noncryotic ground in the seafloor using the 0°C isotherm. However, the lower limit of ice-bonded permafrost cannot be directly predicted by the model because the freezing point of the seafloor changes considerably with soil type, salinity, pressure, etc.

The simulated results of this model also lend insight into the relationship between the deep ground temperature and surface climatic change. Figure 4.8 shows measured ground-temperature profiles from four drillholes at separate localities along the Alaskan arctic coast. Lachenbruch *et al.* (1969, 1982) conclude that the curvature in the upper 100 m or so of these temperature profiles represent a climatic warming trend. However, caution must be exercised, because these boreholes are located along the coast and the curvature may be caused partly by the thermal effect of the ocean and coastal retreat. Curve b in Fig. 4.7 represents the temperature profiles predicted at the shoreline. Although climatic warming over the last several hundred years is not explicitly

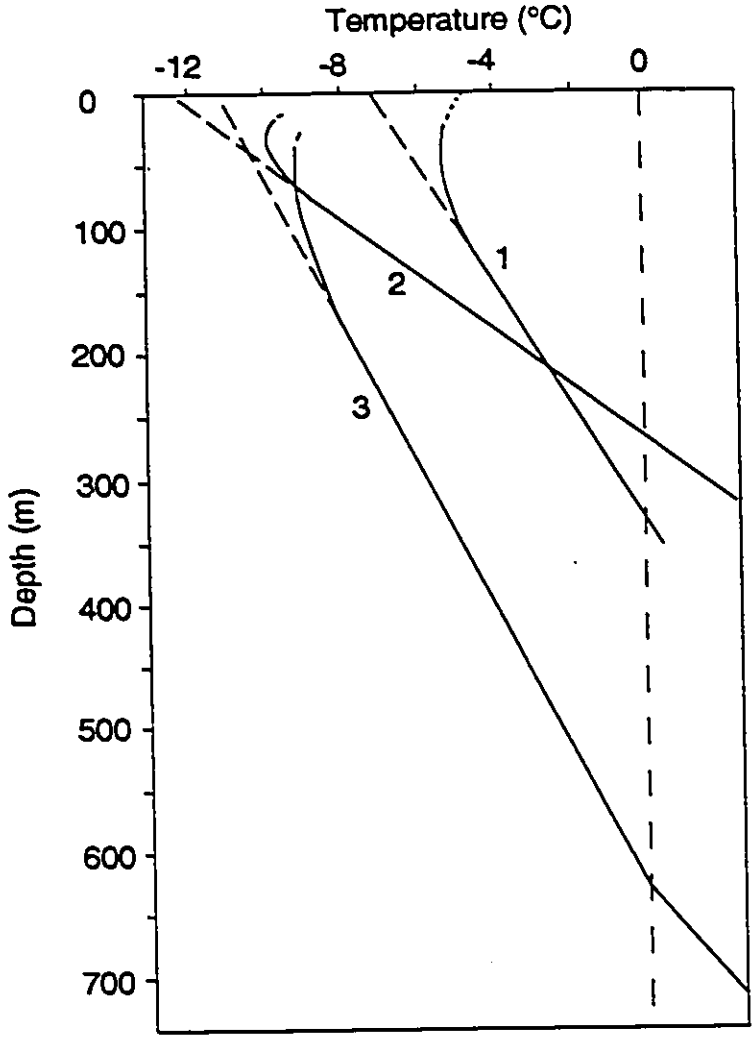

Figure 4.8. Generalized profiles of measured ground temperature on the Alaskan arctic coast (solid lines). Dashed lines represent extrapolations,1-Cape Thompson, 2-Cape Simpson, and 3-Prodhoe Bay (Source: Gold and Lachenbruch 1973).

considered in the model, the curvature of the ground temperature profiles beneath the coast is evident. This may be because of the significant warming effect produced by shoreline retreat in the upper layers of permafrost. It follows that ground temperature profiles in coastal areas are not good indicators of climatic change.

Finally, a disadvantage of this model is the neglect of the effect of unfrozen water content on the thermal diffusivity of the sediments. Since the thermal diffusivity is equal to the ratio k/c (where k is thermal conductivity; c is heat capacity), its variation with water content and temperature depends on the interplay of these two defining properties. The thermal diffusivity of frozen soil is highly temperature dependent and is dominated by the heat capacity term, especially within the range of 0°C to -3°C. The thermal diffusivity increases with decreasing unfrozen water content of the soil, within certain temperature range (e.g. from freezing point to -4°C) (cf. Williams and Smith 1989, pp. 89-94). For seabed sediments, this relationship is complicated by the infiltration of salt water into sediments. This infiltration is especially important for recently submerged terrestrial sediments due to sea-level rise and/or rapid coastal retreat. This means that the unfrozen water content in the submerged sediments will increase, and that the value of the thermal conductivity is likely to decrease. The neglect of the variations of the thermal diffusivity with unfrozen water content and temperature may exert a significant impact on, but unlikely alter the order of magnitude

of, the results of the model.

4.4 Other disturbances

4.4.1 Lakes

In the Mackenzie Delta region, several studies upon the effects of lakes on the permafrost thermal regime have been carried out (e.g. Johnston and Brown 1963, 1964; W.G. Brown *et al.* 1964; Smith 1972, 1976). According to Johnston and Brown (1964), even relatively shallow lakes do not freeze to the bottom, because of the presence of snow cover on the lake ice during winter, although the MAAT is as low as -10°C. Mackay (1978) also reports that open (through) taliks exist beneath some of the big lakes in this region.

If one assumes a constant value of the geothermal gradient, the linear variation of temperature with depth is:

$$T_u\ (z) = T_s + G_g\ Z \qquad (4.17)$$

where Tu(z) is undisturbed ground temperature at depth Z; Ts is mean annual ground surface temperature, °C; Gg is geothermal gradient, °C/m.

In the vicinity of a lake, however, ground temperature (Tu) is modified by the thermal influence of the lake. An important and intriguing geothermal problem, is to determine the disturbance that results when the surface temperature within some finite region such as a lake differs from that of the surrounding. A solution to this problem has been derived by Lachenbruch (1957b) as follows:

$$\theta(x,y,z,t) = (Tw-Ts)\sum\frac{\lambda}{360}\times\Phi(x,y,z,t) \qquad (4.18)$$

where

$$\Phi = [\frac{1}{\sqrt{1+(\frac{R_1}{Z})^2}}erfc[\frac{\sqrt{Z^2+R_1^2}}{2\sqrt{\alpha t}}] - \frac{1}{\sqrt{1+(\frac{R_2^2}{Z^2})}}erfc[\frac{\sqrt{Z^2+R_2^2}}{2\sqrt{\alpha t}}]] \qquad (4.19)$$

Under steady-state conditions this disturbance function can be simplified as the following equation for the case of a circular lake:

$$\theta(z) = (Tw-Ts)\,[1-\frac{z}{\sqrt{Z^2+R^2}}] \qquad (4.20)$$

Therefore, the ground temperature in the vicinity of a circular lake with a radius of R is:

$$T(z) = Tu(z) + (Tw-Ts)\,[1-\frac{z}{\sqrt{Z^2+R^2}}] \qquad (4.21)$$

Application of this heat conduction theory to the upper Mackenzie Delta led Smith (1976) to conclude that permafrost is absent beneath lakes that are wider than 80 to 100 m. In his calculations, he assumed Ts = -4.2°C, Tw = 3.2°C for lake water temperature, and Gg = 2.5/100 °C/m. The maximum thickness of

permafrost in his study area was about 100 m (Smith 1975a). This means that if the width of a lake is roughly equal to the thickness of permafrost, an open talik might be expected beneath the lake centre. However, in the Russian literature, it is known that through taliks occur beneath lake centres only if the width of the lake is more than twice the permafrost thickness (e.g. Kudryavtsev 1959, 1978).

The same model can be applied to the lower Mackenzie Delta region by assuming Ts = -8.0°C, Tw = 2°C, and Gg = 2.2/100 °C/m. Figure 4.9 shows ground temperature profiles which are predicted for lakes of different sizes for the lower Mackenzie Delta region. Curve 1 is the undisturbed ground temperature, and curves 2, 3, 4, and 5 are the computed curves when the lake radius is assumed to be 100, 200, 300, and 400 m, respectively. It is seen from this diagram that, under current conditions, permafrost still exists under a 200m-radius lake in the lower delta region. In the Mackenzie Delta, the critical radius of a lake beneath which a through-going (open) talik would develop is 250 m. This indicates that the Russian value of the critical size of a lake to produce an open talik is greater than needed, unless different conditions prevail.

Figure 4.10 illustrates the ground temperatures beneath lakes of different sizes in Fenghuo Shan area on the Qinghai-Xizang Plateau (in calculation, Ts = -4.2°C, Tw = 2°C, Gg = 5.4/100 °C/m). The straight line represents undisturbed ground thermal regime, and lines 2, 3, 4, and 5 are predicted ground temperatures when the

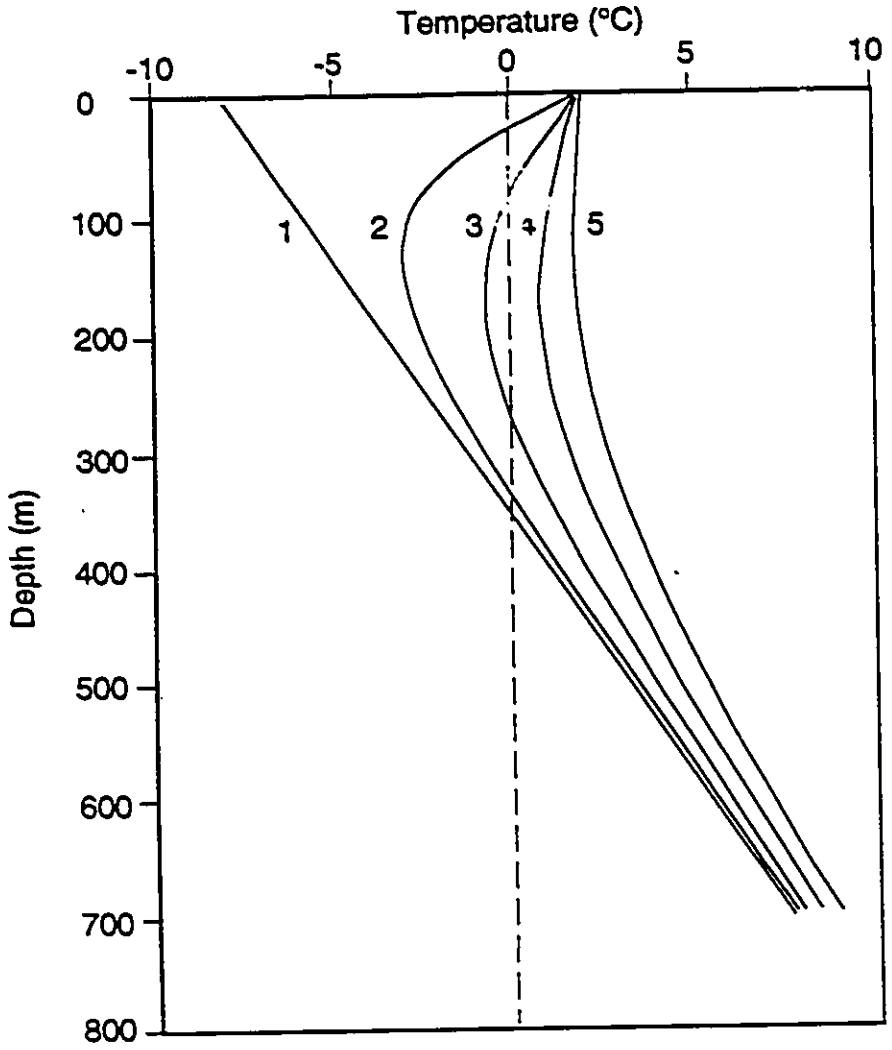

Figure 4.9 Predicted ground temperature beneath lakes of different sizes for the Mackenzie Delta region, 1-undisturbed ground remperature, 2, 3, 4, and 5 are lake bottom temperatures when the lake radius is assumed to be 100, 200, 300, and 400 m.

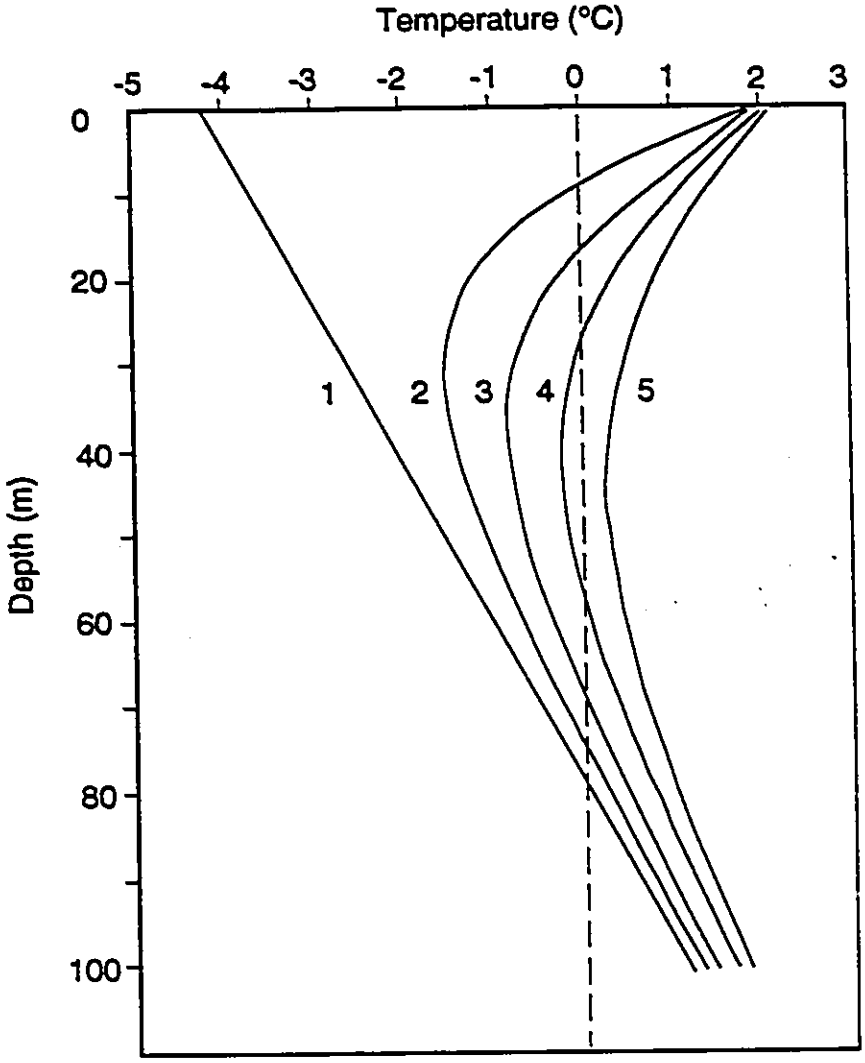

Figure 4.10 Predicted ground temperatures beneath lakes of different sizes in the Fenghuo Shan area, Qinghai-Xizang Plateau, 1-undisturbed temperature, 2, 3, 4, and 5 are lake bottom temperatures when the assumed sizes of the lakesare 20, 30, 40, and 50 m in radius, respectively.

lake radius is assumed to be 20, 30, 40, and 50 m, respectively. It is indicated in Figure 4.10 that the critical radius of a lake beneath which an open talik forms is 45 m.

These numerical simulations suggest that, in both areas, the ground thermal regimes under a lake are severely modified, especially in the upper portion of the profiles. The increase in temperature at a depth of 100 m can be as much as 5°C or more, depending upon the size of the lake.

4.4.2 Snow

The influence of snow cover on permafrost thermal regime is far-reaching in the Mackenzie Delta region, and discussed in great detail by a number of researchers (e.g. Brown 1970, 1973, 1978; Goodrich 1978; Mackay and MacKay 1974, 1976; Smith 1975a, 1975b, 1976). However, this effect is neglectable on the Plateau since there is little snow accumulation on the ground surface in winter. Therefore, analysis of the manner in which snow affects the geothermal regime is excluded from this thesis.

4.4.3 Elevation

An important characteristic of plateau permafrost in Tibet is that permafrost conditions change not only with latitude but also with relief and slope aspects. First, the effect of topography relates to the lapse rate of air temperature change with elevation. The lapse rate on the Plateau ranges from 0.44 to 0.54 °C/100 m, with a mean of about 0.5 °C/100 m (Xie and Zeng 1983). The ground

surface temperature is roughly 2°C higher than the air temperature on the Plateau (Xie 1982). Therefore, the variation of permafrost thickness with elevation can be expressed by the following equation:

$$\xi = (T_a - 0.005\ \Delta H + 2) \ / \ G_g \qquad (4.22)$$

where ξ=changes in permafrost thickness (m), Ta=mean annual air temperature (°C), and ΔH=changes in elevation (m). According to this relationship, an increase of 100 m in elevation will cause an increase of about 15 m in permafrost thickness. This is consistent with field investigations carried out by Shang (1982).

The impact of topography on permafrost on the Plateau also relates to slope aspects. Permafrost investigations on the Plateau indicate that permafrost beneath north-facing slopes is usually thicker than beneath the south-facing slopes. Field investigations suggest that the difference in permafrost thickness between slopes of different aspects ranges between 50 and 70 m (Table 4.4).

4.4.4 Eolian sand

Sand dunes are widespread on the Qinghai-Tibet Plateau; this is because 1) the Plateau is arid and has a sparse vegetation cover, 2) winds are strong, as great as 28 m/sec, and 3) unconsolidated surficial sediment, altered by frost action, provides a material source for the formation of sand cover and/or dunes.

Sand cover and dunes exert profound modifications to the

Table 4.4 Effect of slope aspects on permafrost, Qinghai-Tibet Plateau (Source: Tong and Li 1983)

Topographic location	Elevation a.s.l., m	Ground temp., °C	Permafrost thickness, m
SW-facing slope	4712.8	-2.2	72.8
Valley floor	4676.7	-2.8	94.0
NE-facing slope	4710.5	-4.4	146

ground thermal regime. Figure 4.11A indicates that the depth of thaw under 20 cm sand cover is 1.85 m greater than the ground without a sand cover. At some localities, permafrost shrinks greatly in thickness, even disappears under large sand dunes (Figure 4.11B). This is because the thermal conductivity of sand is greater than the surrounding ground. As a consequence, the sand absorbs more solar heat, which in turn, increases ground temperature.

Some of the sand dunes on the Plateau move quite fast. Airphoto studies indicate that one dune has moved 88.4 m in the last 22 years, approximately 4 m/year. Exceptional rates of migration has been witnessed along the Trans-Plateau Highway. One sand dune (Figure 4.12) moved from one side of the highway to the other side (a distance of at least 100 m) in four years (1987 - 1991). The influence of migratory sand dunes on permafrost differs, depending upon their rates of migration. Fast moving sand dunes will cause a transient geothermal regime to certain depth of permafrost, but will not thin the permafrost. Slow moving ones, however, may also cause the permafrost to degrade temporarily.

4.5 Conclusions

Some of the variables that affect the geothermal regime are unique to each area. Only lakes are common modifiers of ground temperature. On the Qinghai-Xizang Plateau, although elevation (topography) and sand dunes play a part in influencing the geothermal regime, faults constitute the most important and

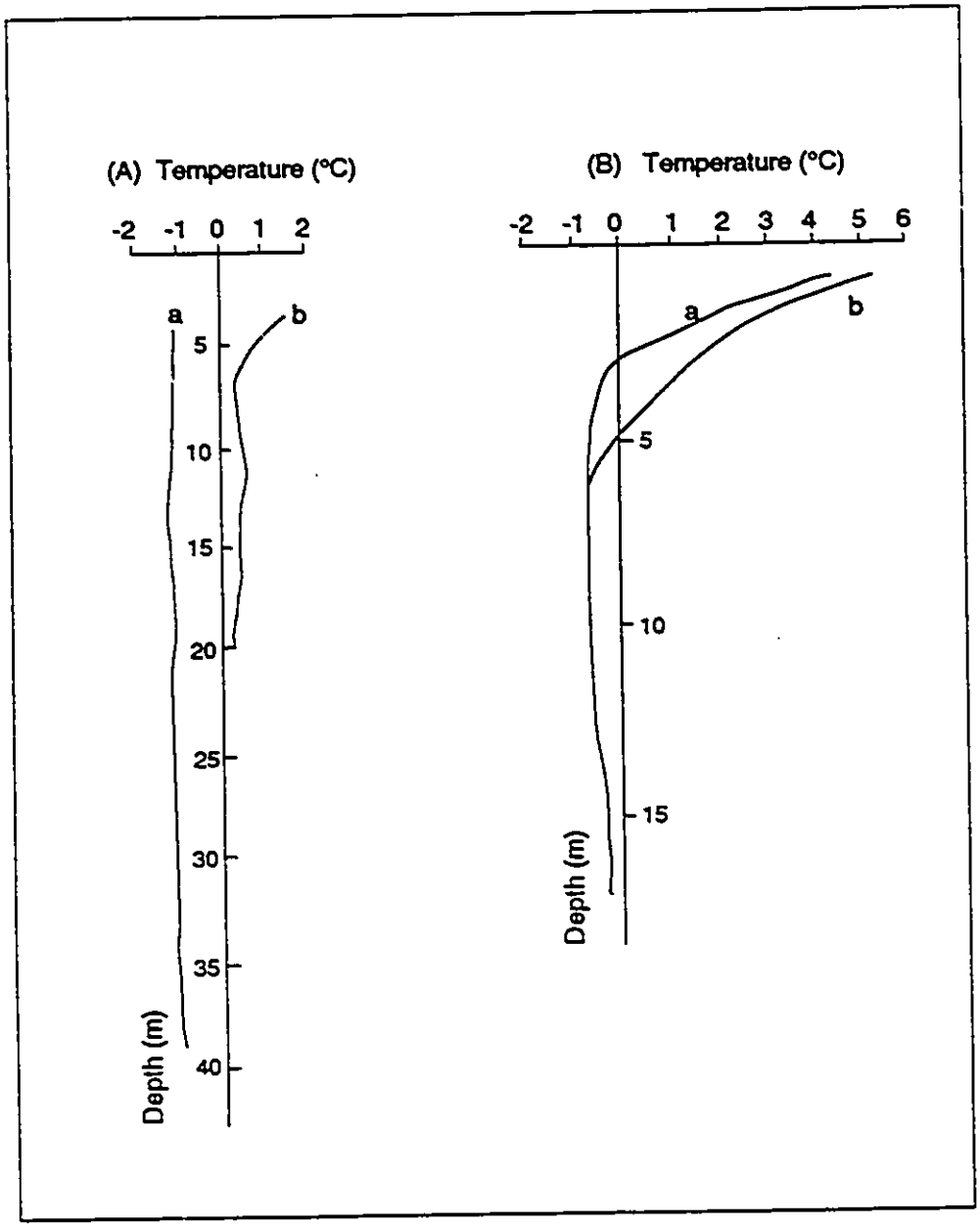

Figure 4.11 Measured ground temperature curves, showing effect of sand accumulation on the surface, Qinghai-Xizang PLateau, (A): Liangdao He area, a-swampy area, and b-ground surface covered with 2.5 m sand; (B): Cumaer He area, a-natural surface, and b-with 0.2 m sand cover (Source: Huang 1991).

Figure 4.12 A migratory sand dune in Wudaoliang area, Tibet Plateau. It was on the other side of the road in 1987 (Photo taken in September 1991).

powerful control. Along the fault zones permafrost is usually thinner and temperatures are higher. Sometimes groundwater, often under pressure, moves up along fault zones to form pingos, and even hot springs.

The presence of the Beaufort Sea and rapid coastal retreat in the Mackenzie Delta region provide an interesting field of study in terms of geothermal regime and subsea permafrost. A very fast rate of coastal retreat was used in the modelling of nearshore permafrost thermal regime. Following the retreat, ground temperature undergoes a increase of 4 to 6 °C within 100 m of the sea bottom during the first several hundred years. Although the emergence-submergence process of land during the Pleistocene is the primary origin of subsea permafrost, in areas where the shoreline undergoes rapid retreat, subsea permafrost is currently forming.

PART THREE

IN SITU PERMAFROST CREEP

CHAPTER FIVE - FIELD SITES AND INSTRUMENTATION

5.1 Introduction

This section describes a field project on the Tibet Plateau aimed at quantifying the nature of plateau permafrost so that it can be compared to the high-latitude permafrost of northern Canada.

Instrumentation, installed in the West Valley of the Fenghuo Shan area, Qinghai-Xizang (Tibet) Plateau in the summer of 1991 investigated the geothermal nature of the Tibet permafrost and magnitude of mass wasting and *in situ* permafrost creep. Ultimately, ground temperatures and ground-ice contents were related to site-specific permafrost creep. This chapter describes the instrumentation and geotechnical conditions of the field sites. The next chapter provides a discussion of the results.

5.2 Field sites and instrumentation

5.2.1 Field sites

Fieldwork undertaken in early August 1991 identified sites for study while actual drilling and instrumentation was accomplished in late September 1991.

The West Valley of Fenghuo Shan (Figure 5.1) was chosen because previous investigations had indicated the permafrost in this area to be ice-rich. As a consequence, it is especially prone to creep deformation. In addition, the area possesses good logistics since the Permafrost Research Station built by the Northwest Institute of Railway exists close to the Trans-Plateau Highway at this point. The disadvantage of the area was that disturbance and even damage (made

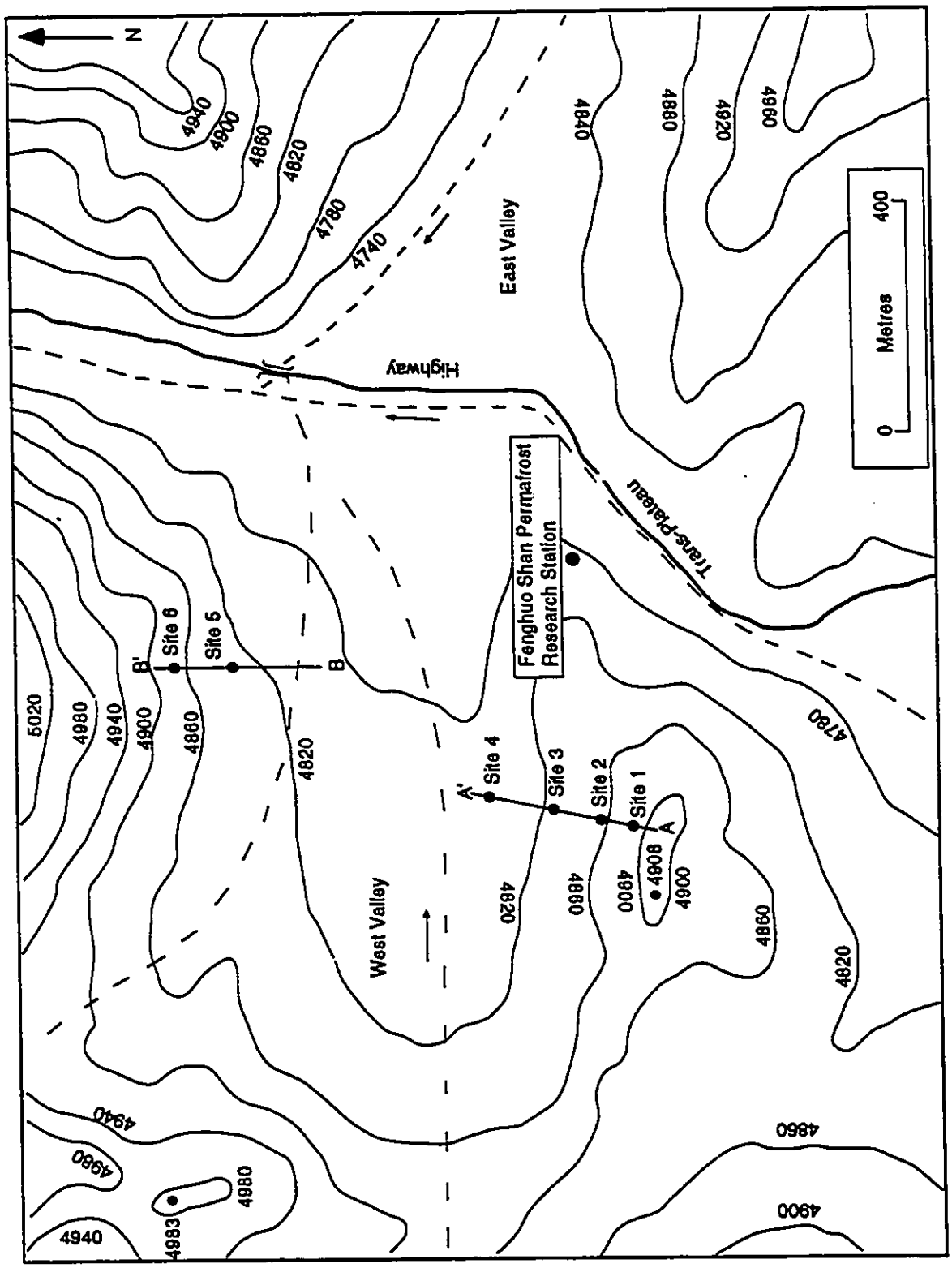

Fig. 5.1 Topographic map of the West Valley area, Tibet Plateau, also showing the field sites.

by humans and/or animals) to instrumentation can be a problem.

The Fenghuo Shan terrain is characterized by undulating hills and valleys. It is one of the few hilly areas between the Kunlun Shan Mountains to the north and the Tangula Shan Mountains of the Plateau to the south. The altitudes of the instrumented sites range between 4,780 and 4,900 m a.s.l. (Figure 5.1). The highest elevation in the area is approximately 5,200 m. The hills on either side of the West Valley trend in a nearly east-west direction, and probably reflect structural control.

Bedrock underlying the unconsolidated deposits in this area is Tertiary-age sandstone, siltstone and shale. The surficial deposits are thin and derived primarily from the cryogenic weathering of these bedrock strata. Cryogenic weathering leads to the development of considerable quantities of silt and silty clay materials; these are particularly frost-susceptible and conducive to the growth of ice lenses and/or frost heave.

In order to investigate the nature and magnitude of *in situ* permafrost creep, six sites were selected (four on the north-facing slope, and 2 on south-facing slope) in the West Valley of Fenghuo Shan (Figure 5.1). Profiles of the instrumented slopes are given in Figure 5.2.

The slopes of the West Valley are moderate in angle (Fig. 5.3). The north-facing slope (transect A-A') rises from the valley bottom at an angle of 10° at site #4 and changes to 25° at site #1, while the south-facing slope ranges from 11° at the toe, 15° at site #5 to 21° at site #6 (5.2).

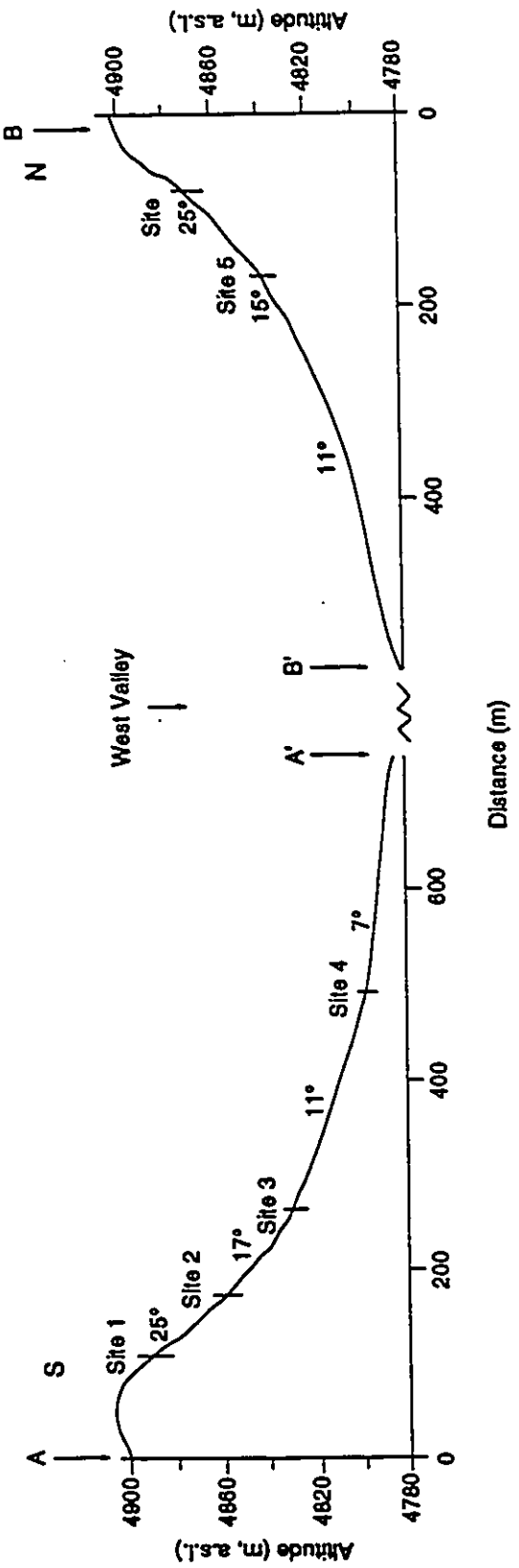

Figure 5.2 A diagram showing transects A-A' and B-B' of the instrumented sites, with indication of slope angles. The slope angles are average values.

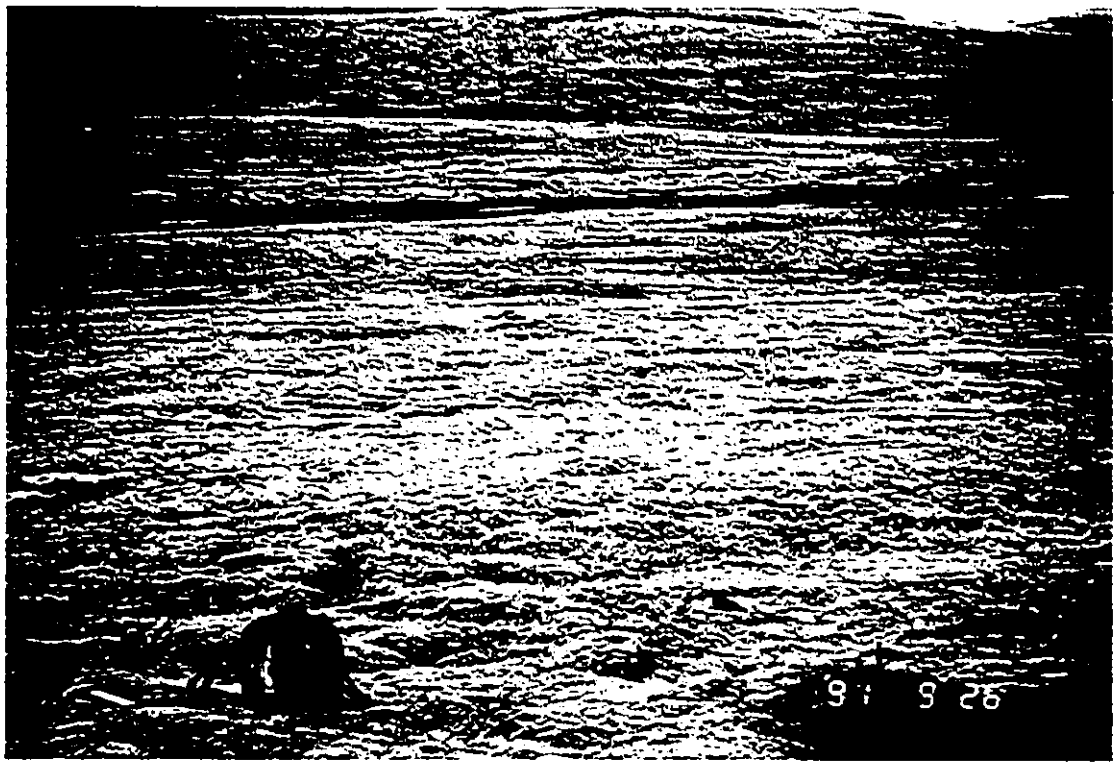

Fig. 5.3 The terrain of the West Valley of the Fenghuo Shan area, Tibet Plateau.

5.2.2 Instrumentation

An important constraint was to instrument in a manner which allowed direct comparison with North American data.

Numerous instruments and techniques are available for the investigation of rock/soil lateral movement (Dunnicliff and Green 1988), but only borehole inclinometer systems provide data over a full vertical profile with the accuracy necessary to resolve creep deformation. Inclinometer systems have already proven reliable in the study of soil creep (e.g. Wilson 1970), glacier movement (e.g. Meier 1960, Savage and Paterson 1963), and of particular relevance here, in the *in situ* creep of permafrost (Bennett 1989, Savigny 1980). Multi-string YSI thermistor cables were used in conjunction with the inclinometer system in order to correlate movement with thermal regime. Upward movement (presumably frost heave) was measured by heavemeters which were manufactured at LIGG.

To complement this approach, near-surface downslope movement (i.e. solifluction) was monitored by measuring small objects (metal rings, in this case) inserted into the seasonally thawed layer. However, these data are not yet available for presentation in the thesis, because a minimum 2-3 year period of observation is required. LIGG personnel will obtain these data in 1994 and 1995.

Inclinometer system

Inclinometer systems fall within the category of transverse deformation gauges. Inclinometers are defined as devices for monitoring deformation normal to the axis of a pipe (or casing) by

means of a probe passing along the pipe. The pipe contains gravity-sensing transducers designed to measure inclination with respect to the vertical. The pipe or casing may be installed either in a borehole or in fill. Inclinometers are also referred to as slope inclinometers, probe inclinometers, and slope indicators (Dunnicliff and Green 1988). Although many types of inclinometers exist, a Terra Technology MP-20 mini-probe inclinometer (Figure 5.4) was used in this study. This inclinometer, manufactured by Terra Technology Corp in Redmond, Washington, D.C., is designed to generate reliable data in case of very limited deformation. It provides accurate data at the extreme sub-zero temperatures experienced in permafrost environments. Similar equipment has been used by both Savigny (1980) and Bennett (1989).

The MP-20 inclinometer has four primary components. These are: the inclinometer probe itself or torpedo, the readout unit, the interconnecting cable, and the grooved inclinometer casing. In the mini-probe, two fluid-damped, metal flexure suspension servo accelerometers are mounted in the sensor housing. The sensitive axis of the two accelerometers are aligned at 90 degrees to each other so that one (the A axis sensor) measures the component of tilt towards or away from the probe's spring loaded wheel, while the other (B axis sensor) measures the tilt component aligned at 90 degrees to the spring loaded wheels. The system is designed to detect changes in the downslope configuration of slope soils to 0.0003 cm over a 30 cm vertical distance. Accuracy of the system, however, as measured in field test is demonstrated by maximum

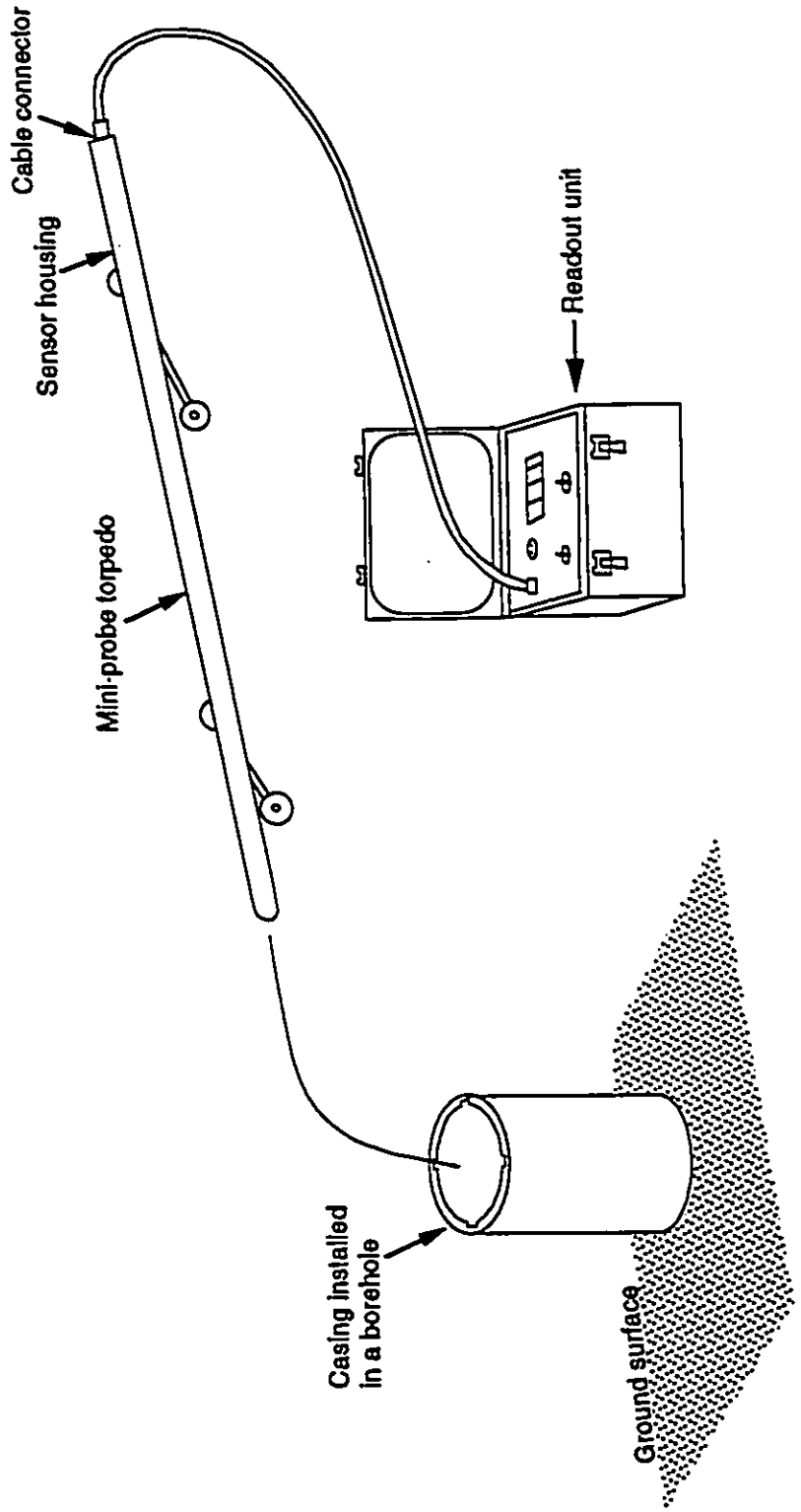

Figure 5.4 A diagram showing the Terra Technology MP - 20 mini-probe inclinometer system.

variability of 0.0061 cm for repeated readings at a single point. Results are well inside the resolution of the system (e.g. Bennett 1989). The inclinometer is connected to a digital readout unit (Terra Technology, Model TPC-101) by a 15 m-flexible, epoxy-encased cable.

PVC casing was purchased from RST Instruments, Port Coquitlam, B.C., Canada and shipped by air direct to Lanzhou, China. The casing came with an outside diameter of 7.09 cm and a length of 3 m. The casing contains 4 longitudinal pre-cut grooves which are located equidistance around the interior. The bottom of the casing was sealed by the manufacturer, and the top was capped. The grooves within the casing keep the inclinometer from rotating and allowed a precise directional positioning of the inclinometer each time a site was monitored. Markings of the cable at 1 foot intervals (30.48 cm) allowed for a precise depth positioning of the probe.

Thermistor cables

Five multi-thermistor strings with a length of 3 m were constructed of a nine-pair conductor cable. Thermistors were placed at intervals of 0.5 m (6 thermistors for each string). YSI (Yellow Springs Instrument Co, U.S.A.) 44033 thermistors with an accuracy of ± 0.05 °C were used. These multi-thermistor cables were tied on the outside of the casing and lowered into boreholes. Ground temperatures were measured at six levels (0.5, 1.0, 1.5, 2.0, 2.5, and 3.0 m) at sites from #2 to #5, inclusive, but at 5 levels (0.0, 0.5, 1.0, 1.5, and 2.0 m) at site #6. Site #1 was not installed with

a thermistor cable. Pre-existing ground temperature observations of deep boreholes in this area were employed to estimate the mean annual ground temperature.

Heavemeters

Since the inclinometer system provides only horizontal displacement, five telescoping tube heavemeters made of aluminum and steel were installed at sites #1, #2, #3, #4, and #5 to estimate upward (vertical) movement. It should be emphasized that the (vertical) direction of the measured heave by the tubes is not normal to the slopes. The heavemeters were made up of three heave tubes and a central rod (Figure 5.5 and Table 5.1) to measure frost heave at three different levels in the active layer. For each site, the heavemeter was located within 1 m distance from the inclinometer casing. An installed heavemeter is shown in Figure 5.6. Telescoping tube heavemeters have been proven to be an effective tool for the measurement of frost heave in the field (e.g. Mackay *et al.* 1979; Smith 1985; Bennett 1989; Burn 1989, 1990b).

Drilling and installation

Drilling was undertaken in late September 1991 using a QPC-30 Drill manufactured by Changsha Mineral Exploration Machinery Co., P.R. China (see Figure 5.7). The drill is owned by the Qinghai-Xizang Plateau Comprehensive Research Station of LIGG at Golmud and was transported to field sites by truck. It is an auger-type drill and no water was used during drilling. Two holes were drilled for

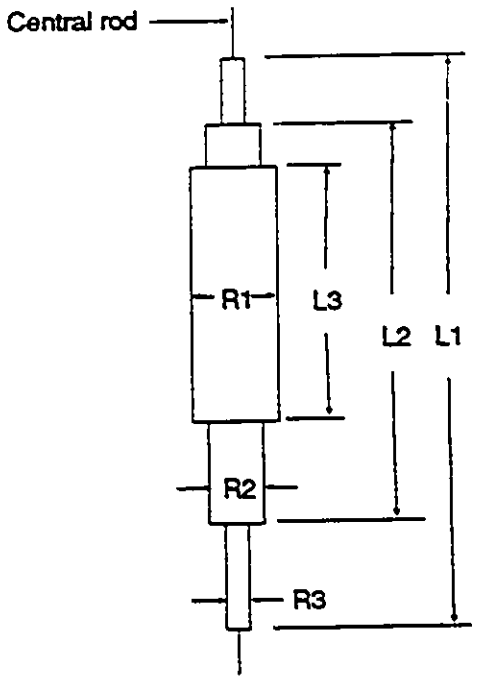

Figure 5.5. Design of the heavemeters (see Table 5.1 for details).

Table 5.1. Details of the five self-made heavemeters.

Unit: mm

Number		HM1	HM2	HM3	HM4	HM5
Length	L1	1370	1450	1350	1400	1400
	L2	1170	980	1060	970	1170
	L3	750	650	500	560	550
Outer diameter	R1	33	33	42	42	42
	R2	25	25	30	30	30
	R3	10	20	25	21	21
Thickness of the tube wall	D1	3.5	3.5	3.0	3.0	3.0
	D2	2.0	2.0	2.0	1.5	2.0
	D3	1.5	1.5	1.5	1.5	1.5

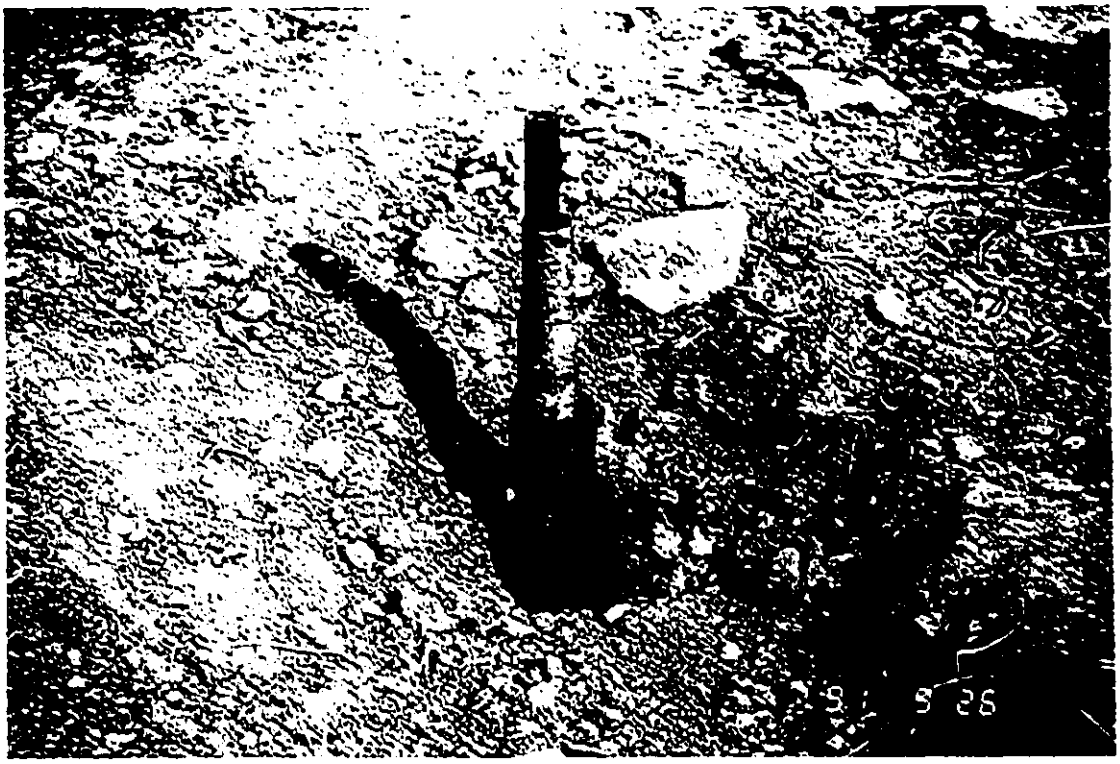

Figure 5.6 An installed heavemeter at site #1.

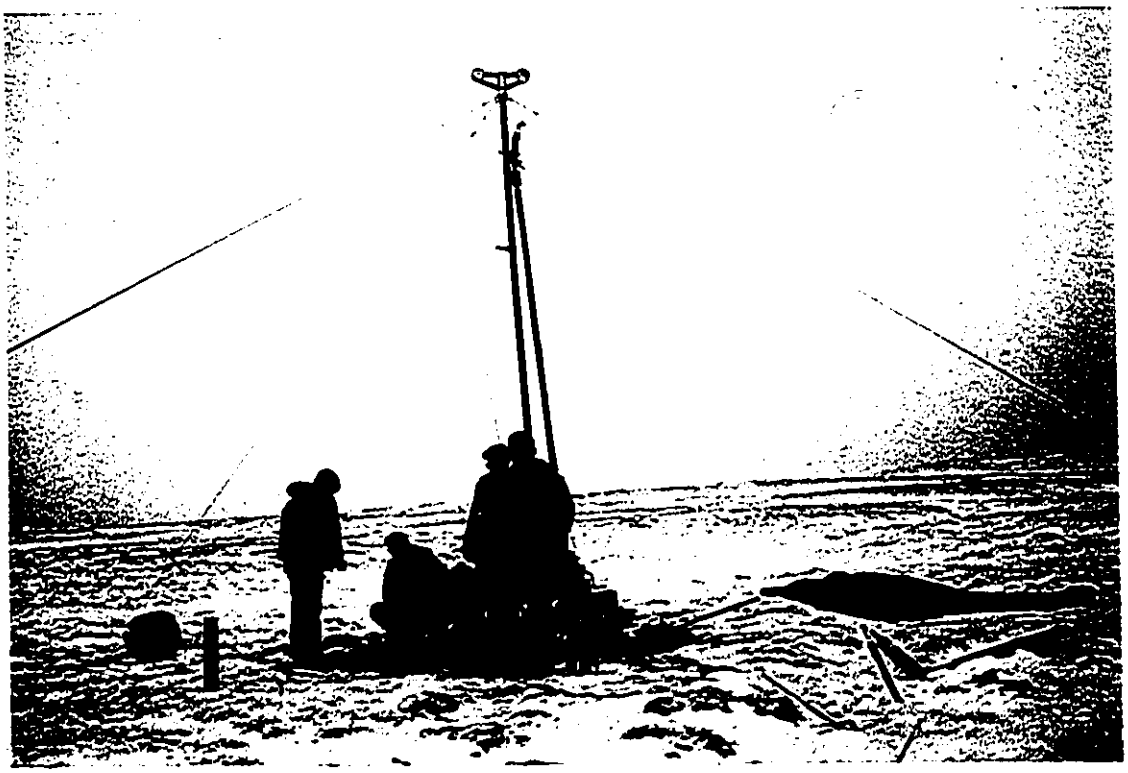

Figure 5.7 The QPC - 30 Drill in operation in the West Valley, Tibet Plateau.

each site, one for the inclinometer casing and thermistor cable, and another for the heavemeter. The boreholes were 10.5 cm in diameter.

At the time of drilling, borehole logs were made for each site, and soil samples taken for the determination of water/ice content and bulk density.

Upon completion of each borehole to a depth of 3 m, inclinometer casings and thermistor cables were installed into place. The thermistor strings were wrapped to the outside of the casing and lowered into the boreholes together with the casings. Since the casing was sealed at the base a clean interior for the inside operation of the inclinometer torpedo is assured. The space between the PVC casing and the borehole wall was backfilled with the soils that were dug out by drilling. Long thin metal rods were used to tamp the backfill soil. The installation allowed 10 to 20 cm of casing to be exposed above the ground surface. After the first reading was taken, the casing and thermistor strings (but the heavemeters) were buried in order that damage and disturbances can be avoided.

Heavemeters were installed in separate boreholes at each site. At site 5 the hole for the installation of the heavemeter was made by a thick metal rod. Careful backfilling assured contact between the meter and the wall. At the instrumented sites, where the depth of the active layer ranges from 1.25 m at site #4 to 1.60 m at site #6, different depths were chosen for the heave measurements. Certain tube lengths were exposed above the ground surface so that readings could be made easily. Subsequent measurements of the distance

between the tubes determined whether heave or settlement had occurred. An installed site is shown in Figure 5.8.

5.2.3 Measurement procedures

The field sites were visited twice during the remainder of 1991 and 7 times in 1992. For permafrost creep measurements, a borehole is surveyed initially by lowering the inclinometer torpedo to the bottom of the casing with successive readings taken from there up to the ground surface. At each reading point, the A and B axis displacement measurements are recorded. Then the torpedo is raised by the wheel base length, 24 inches (60 cm) and the A and B axis readings are again recorded through the readout unit. This process is repeated until the torpedo reaches the ground surface. The torpedo is then rotated 180 degrees and lowered back to the bottom of the hole and brought up as before. The readings are then averaged and are ready for interpretation or further reduction.

On each site visit, the heavemeters were surveyed by measuring the exposed length of different tubes by tape measure. In calculating the heave, measurements from one set of readings were compared with those from the previous set, thereby indicating whether heave or settlement occurred. The resistance measurement of the thermistors was made by a Beckman Tech 310 multimeter, and temperatures are obtained by a resistance-temperature relationship. Measurements continue to be made by LIGG personnel and will continue into 1994 and 1995.

Figure 5.8 A photo showing the exposed portion of the inclinometer casing, heavemeter and thermistor cable at site #5.

5.3 Thermal conditions

5.3.1 Soils

Surficial material in the West Valley consist of silt/stoney silt, silty clay/stoney silty clay, clay/stoney clay, and sandstone fragments (see drillhole logs, Figures 5.9 to 5.11). The upper slopes, as revealed by boreholes at sites #1, #2, and #6, are covered by a layer of silt/stoney silt whose thickness ranges between 20 to 85 cm. Sandstone fragments were encountered during the drilling on upper slopes, for example at sites #1, #2, and #6. Drillhole logs at sites #3, #4 and #5, however, show that the lower slopes are covered by silty clay/stoney silty clay which is underlain by clay/stoney clay. Sandstone fragments were not encountered.

Bulk densities were determined in the field for the top metre or so at sites #3, #4, and #5, and ranged from 2.16 to 2.45 g/cm^3.

5.3.2 Ground temperature

The mean annual ground temperature at Fenghuo Shan is approximately -3.0°C. This is obtained from previous direct measurements in deep drillholes (Wang 1984).

Ground-temperature measurements were made in the present study by using thermistors arranged in a multi-conductor cable. Direct readings, in ohms, were taken by a multimeter and converted to temperatures. Although a resistance (R) versus temperature (T) table is attached to each thermistors, this conversion still cannot be

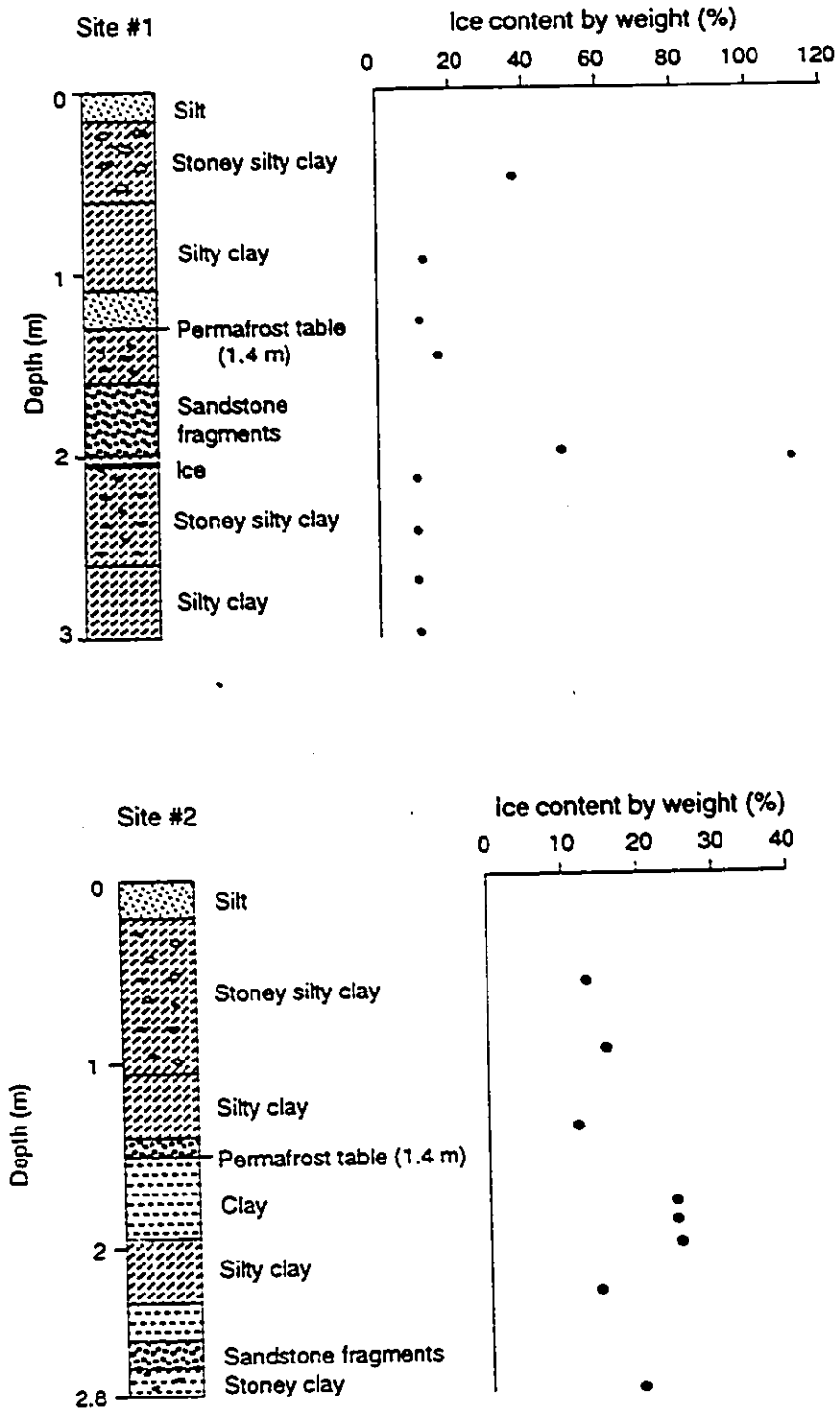

Figure 5. 9 Drillhole logs and ice contents at sites #1 and #2

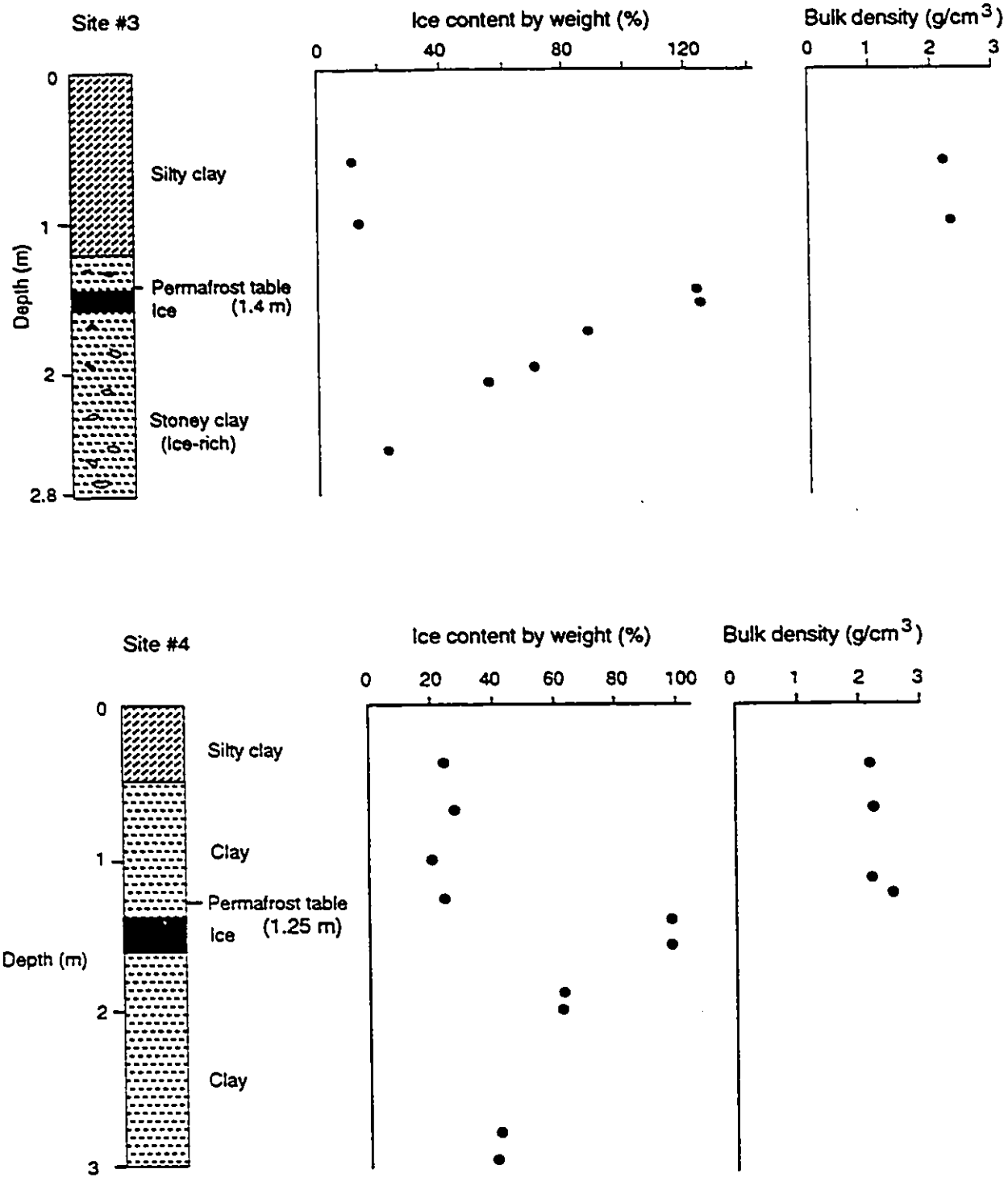

Figure 5.10 Drillhole logs, ice contents and bulk densities at sites #3 and #4.

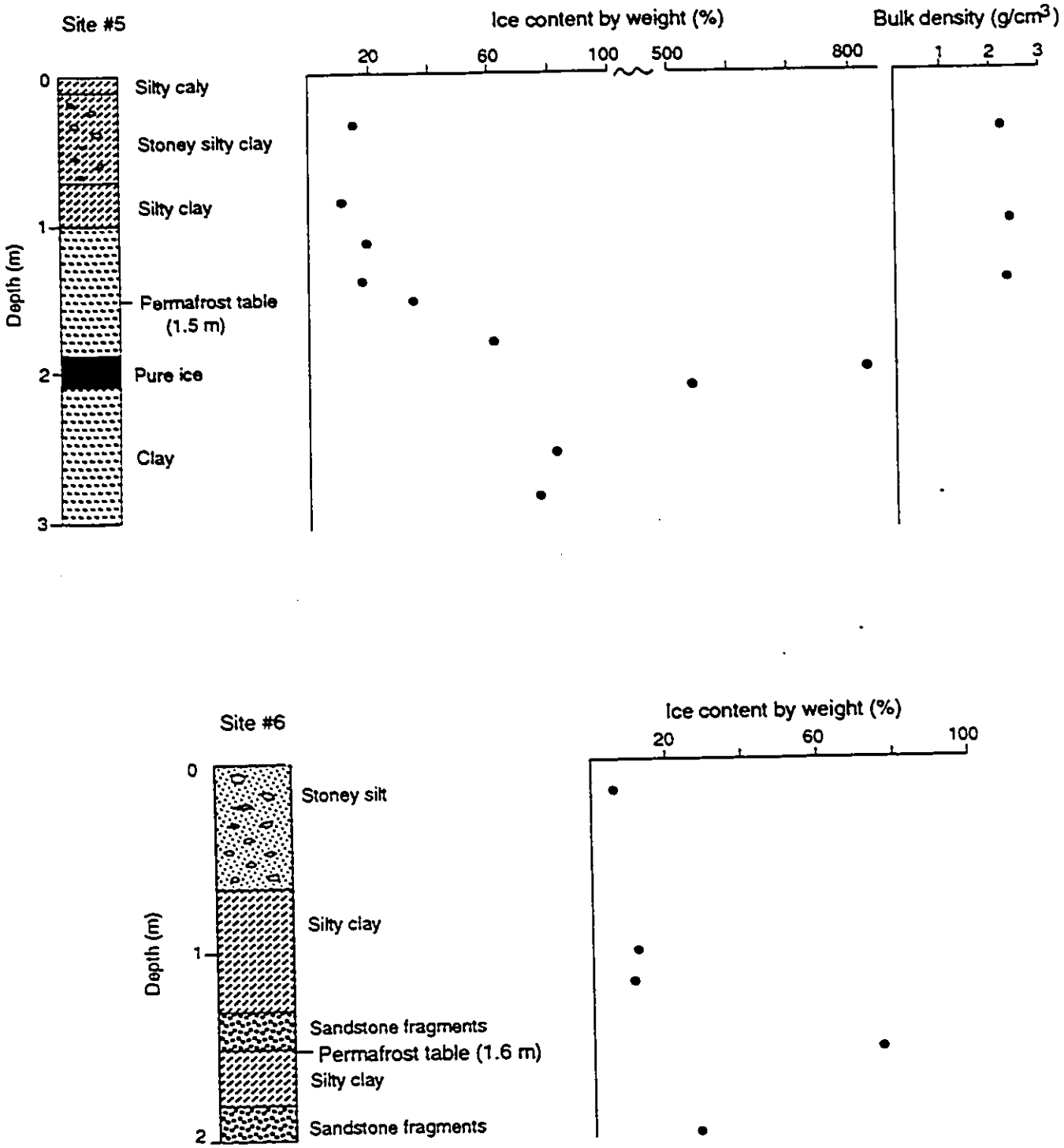

Figure 5.11 Drillhole logs, ice content, and bulk density at sites #5 and #6.

made easily because the relationship between T and R is nonlinear, and there has been no equation developed for this conversion. A converting equation is developed in this study and presented here for the future convenience of others. Resistance values were converted into temperatures with the SAS (Statistical Analysis System) program. The equation that best fits the T - R curve is in the form of

$$T = 585.14 - 281.80(\ln R)^{1/2} + 29.82(\ln R) - 0.12(\ln R)^2 \quad (5.1)$$

Temperatures for each site are given in Figures 5.12 and 5.13. Figure 5.12 presents ground temperatures measured from the north-facing slope (transect A-A'), while Figure 5.13 from the south-facing slope (transect B-B'). These ground-temperature profiles show a similar range and trend of temperature variation. The near surface temperature changes between 7 and -12 °C at the times of recording; this range attenuates to -1.0 to -9.0 °C in permafrost. Near-surface permafrost presumably creeps faster in summer when the temperature is highest. The temperature ranges during the warm period from slightly below 0°C to about -3°C. These values constitute an important temperature range for permafrost creep. The temperature data also indicate that the south-facing slope is 0.3 to 1.0°C warmer than the north-facing one.

5.4 Ground ice

Soil samples were collected at each site during drilling in

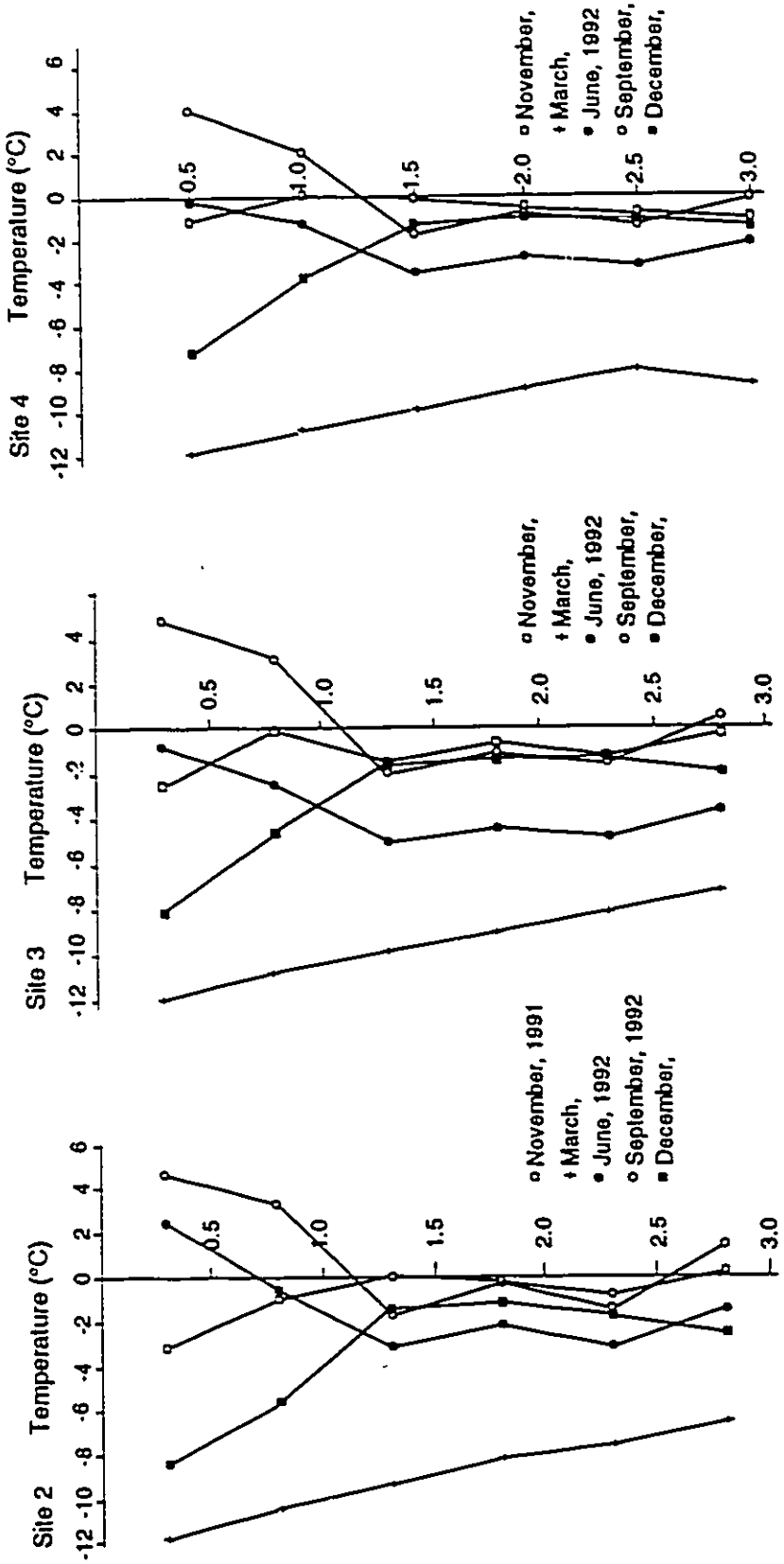

Figure 5.12 Representative ground temperatures measured at sites #2, #3 and #4.

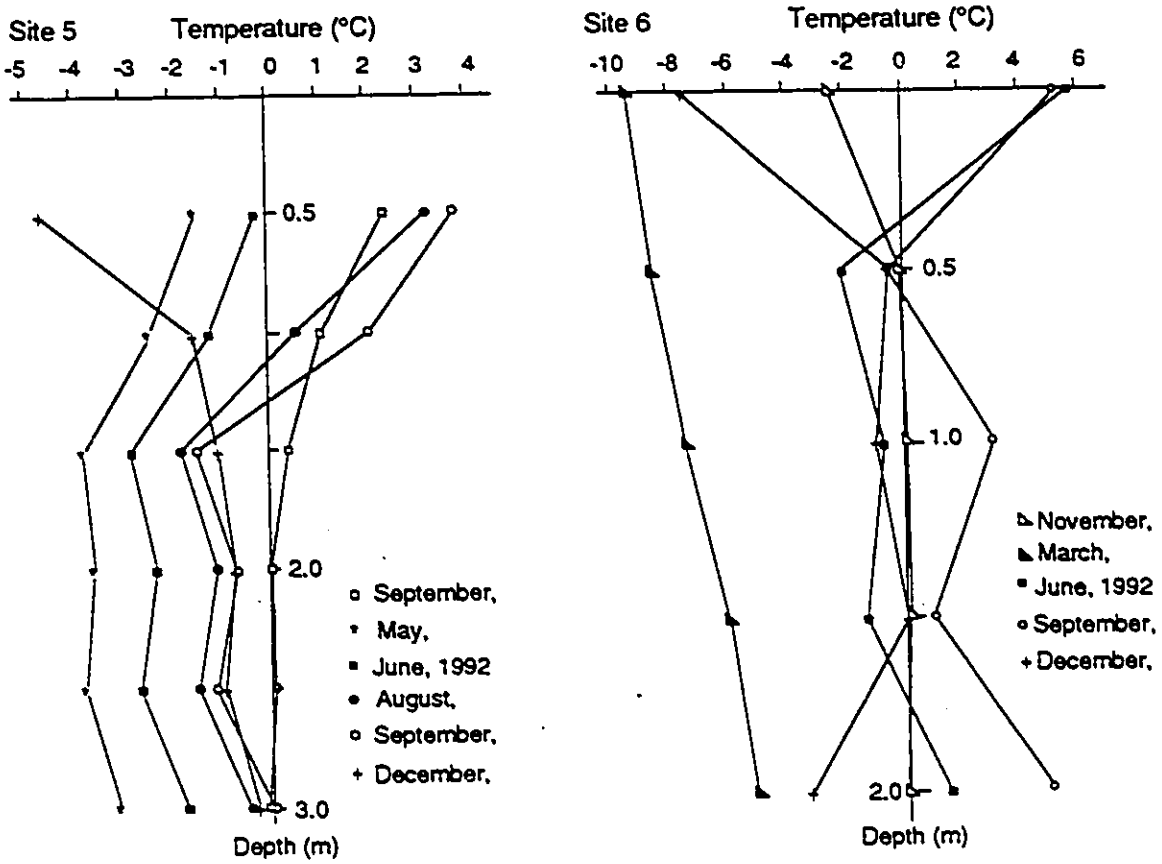

Figure 5.13 Ground temperatures measured at sites #5 and #6.

order to determine ice contents. A power generator and a microwave oven were brought to the field for this purpose. However, because of the malfunction of the generator, some of the samples were dried by a coal-burning stove which was used primarily for heating purposes. Ice contents are finally calculated by the following relationship:

$$IC = \frac{loss\ of\ moisture}{dry\ mass} \times 100\% = \frac{m_2 - m_3}{m_3 - m_1} \times 100\% \qquad (5.2)$$

where IC is ice content (%); m_1 is mass of container (g); m_2 is mass of container and wet soil (g); and m_3 is mass of container and dry soil (g).

Ice contents for six sites are given in Figures 5.9 to 5.11. The data indicate that ice content ranges from 10% up to 837%. Icy layers were encountered at sites #3, #4 and #5, and permafrost at these three sites is regarded, therefore, as being ice-rich (Tsytovich 1975; Phukan 1985). For each site, the maximum ice content occurs at or near the permafrost table, as commonly found in high-latitude permafrost (e.g. Pollard and French 1980). Since the drilling took place in late September, the frost table was regarded as the permafrost table. Comparisons of the cryostratigraphies at the six sites demonstrate that ice layers develop preferentially on the lower slopes. The highest ice content was from site #5 located in the south-facing slope of the West Valley. This is probably because the grain size is finer in the lower part (see drillhole logs), and the lower portion of slopes is more gentle (Figure 5.2). This gives rise to a poor drainage

condition, and thus, favours ground-ice growth.

5.4.1 Frost heave

Details of the emplacement of the five heavemeters is shown in Table 5.2. Frost heave was measured at three different levels in the active layer. The central iron rods (anchor rods) of the heavemeters extended below the permafrost table for approximately 50 cm.

The first set of readings, taken on 26 September, 1991, is treated as a datum mark for subsequent readings. Unfortunately by 12 September, 1992, heavemeters at sites #1, #2, and #3 had been destroyed (the heave tubes were taken away because they were not buried). Frost-heave measurements at the five sites of the West Valley are tabulated in Table 5.3. The maximum heave recorded in this study was 3 cm over an individual layer, and the average heave over an entire winter was 2 cm for certain layers.

The heave data shown in Table 5.3 are approximately of the order of magnitudes as those obtained by Smith (1985), but smaller than those of Mackay *et al.* (1979) and Burn (1990b) for the Mackenzie Delta region.

Peak values of frost heave occur at different times from site to site; these different times lend insight into the relationship between frost heave and the hydrological regime in the active layer. It is plausible that meltwater accumulates in summer at site #4, located near the bottom of the West Valley where the hydraulic gradient is small. Thus, water migrates from the base of the active layer to the top layer of permafrost to form segregated ice lenses

Table 5.2. Emplacement of the heavemeters at the instrumented sites, West Valley, Fenghuo Shan area, Tibetan Plateau.

	Site #1	Site #2	Site #3	Site #4	Site #5
Level of measurement (cm)	0 - 59 59 - 86 86 - 126	0 - 41 41 - 92 92 - 116	0 - 68 68 - 104 104 - 119	0 - 56 56 - 88 88 - 129	0 - 50 50 - 106 106 - 120
Thickness of active layer (cm)	130	140	140	125	150
Length of centre rod below permafrost table (cm)	54.1	46.3	47.4	64.9	32.0

Table 5.3 Frost heave (cm) in the active layer of the instrumented sites of the West Valley, Fenghuo Shan area, Tibetan Plateau

Site	Depth (cm)	1991			1992						
		26/09	05/11	04/12	08/03	10/05	09/06	10/08	12/09	05/11	04/12
#1 (25°)	0 - 59	0	0.7	2.4	2.4	2.0	1.7	1.2			
	59 - 86	0	0.9	2.3	2.5	2.0	1.8	1.4			
	86 - 126	0	1.0	2.3	2.7	2.1	1.2	1.5			
#2 (17°)	0 - 41	0	0.1	0.6	0.7	0.6	1.1	0.3			
	41 - 92	0	0.4	0.4	0.5	0.4	0.9	0.1			
	92 - 116	0	0.4	0.4	0.5	0.4	0.9	0.1			
#3 (11°)	0 - 68	0	0.5	2.3	2.4	3.0	0.8	0.3			
	68 - 104	0	-0.4	2.0	1.7	2.1	0.3	-0.7			
	104 - 119	0	-0.2	2.2	2.0	2.3	0.3	-0.4			
#4 (7°)	0 - 56	0	0.7	1.2	2.2	1.9	2.1	1.8	2.2	2.4	2.1
	56 -88	0	-0.4	-0.7	1.8	1.2	1.6	1.5	1.9	2.1	1.7
	* 88 - 129	0	-0.3	-0.6	2.0	1.5	1.9	1.7	2.1	2.7	2.1
#5 (15°)	0 - 50	0	0.3	0.7	1.4	1.1	1.8	1.3	1.2	0.7	1.3
	50 - 106	0	0.6	0.4	1.7	1.6	1.3	1.5	1.4	1.1	0.9
	106 - 120	0	0.7	0.8	1.3	1.2	0.8	1.2	1.0	0.8	0.5

* 4 cm of the heavemeter tube was in permafrost (see table 5.2).

(Cheng 1983; Mackay 1983). The drop in heave after August at site #5 may be caused by thaw consolidation.

5.4.2 Heave susceptibility

A frost-heave coefficient (η) was estimated as follows:

$$\eta = \frac{\Delta H}{H} \times 100\ \% \qquad (5.3)$$

where ΔH - increase in thickness by heaving, and H - total thickness of the frozen soil layer.

A maximum frost-heave coefficient value was calculated for each site by dividing the peak heave value by the corresponding depth range (Table 5.4). The coefficient ranges between 1.76% and 15.33%, with a mean of 5.6%, much higher than the values (1.0% to 4.0%) reported by Tong (1983) for the same area. For simplicity, the three depth ranges are marked from the surface downwards as level 1, level 2, and level 3 in Table 5.4. The data indicate that the frost-heave coefficient is greater in the lower portion of the active layer. According to Tong (1983), the materials of the West Valley are either heave-susceptible (η>3%)or very heave-susceptible (η>5.6%).

Frost-heave coefficients calculated from data of Burn (1990b) and Smith (1985) are about twice as much as on the Qinghai-Xizang (Tibet) Plateau; this is because less moisture is available for ice segregation (forst heaving) in the active layer of the Tibetan Plateau than in the Mackenzie Delta region.

Table 5.4. Maximum frost-heave coefficients (%) at the instrumented sites

	Site #1	Site #2	Site #3	Site #4	Site #5
Level 1	4.07	2.68	4.41	3.93	2.80
Level 2	9.26	1.76	5.83	5.94	3.04
Level 3	6.75	3.75	15.33	5.12	9.29

CHAPTER SIX - *IN SITU* PERMAFROST CREEP

6.1 Introduction

Investigations of *in situ* permafrost creep were carried out in the West Valley of Fenghuo Shan area. The investigation is restricted to the top 1.5 m of permafrost. This chapter presents the results of the *in situ* measurement of permafrost creep and determines the creep parameters as defined by the power flow law.

Numerous studies on solifluction have been carried out (e.g. Williams 1957, 1966; Dylik 1967; Benedict 1970; Price 1972; Jahn 1975; Washburn 1979; Mackay 1981; Smith 1988, 1992). It is not the intention of this thesis to review and summarize the massive literature on this topic, simply because solifluction is a process which is confined to the active layer, if permafrost is present, and is quite different from the permafrost creep.

6.2 Previous studies in high latitude

Several attempts have been made to monitor *in situ* permafrost creep. One of the first was by Thompson and Sayles (1972) who describe the *in situ* creep in the CRREL permafrost tunnel in Alaska. It was found that the ice-rich silt in which the tunnel was excavated deformed 3.3 times faster in the field than in the laboratory. Another study was by Ladanyi and Johnston (1973) who carried out a short-term *in situ* creep test of frozen ground at a permafrost site at Thompson, Manitoba by using a pressuremeter. A third study was by Haeberli (1985) and Wagner (1992), who have measured the *in situ* creep of rock glaciers in the Swiss Alps by using photogrammetric and geodetic techniques and a slope

indicator.

Of particular interest to the present study was the work done by Savigny (1980) and Bennett (1989) using inclinometer systems. Savigny measured creep in fine-grained, ice-rich and relatively 'warm' permafrost in the Mackenzie Valley. In terms of ground temperature, the Mackenzie Valley permafrost conditions resemble these of the Tibet Plateau. The results, published in a series of papers (Savigny and Morgenstern 1986a, 1986b, 1986c) indicate systematic downslope movement in the range of 0.1 - 0.3 cm/year for a slope (15°-31° in angle). *In situ* near-surface permafrost creep was also measured by Bennett (1989) in 'cold' permafrost at Rea Point, Melville Island, N.W.T.. This study shows that soil creep rates of between 0.03 to 0.05 cm/year are typical of four sites on a low angle (5°) west-facing slope (Bennett and French 1988, 1990, 1991). These data confirm that deformation occurs at a significantly slower rate in relatively 'cold' permafrost.

The *in situ* determination of permafrost creep on the Tibet Plateau adds to this data base and represents the first such study in China.

6.3 Principles and data reduction

Slope movement is reflected in the displacement measurements obtained with the torpedo. Grooves in the casing keep the torpedo from rotating as it is lowered and raised in the casing, thereby keeping the torpedo aligned. In this way the direction of casing tilt (i.e., the direction of the ground movement) can be

determined.

The signals out of the sensors are proportional to the sine of the angle between the torpedo's axis and the earth's gravity vector (vertical). The readout unit scales these signals and displays them as horizontal displacement values relative to base length of the probe. Figure 6.1 illustrates how the output relates to the position of the torpedo and how the total displacement is calculated.

Readings for both A and B axes were recorded on a field data sheet such as shown in Figure 6.2. The recording procedure includes: 1) record the data in columns 1 (A_0) and 5 (B_0) every time when the probe is raised by its base length, keeping track of the sign (plus or minus) until the torpedo reaches the top of the borehole, and 2) take the torpedo out of the casing, rotate it 180 degrees, lower it back to the initial low point and record readings in columns 2 (A_{180}) and 6 (B_{180}) at the same intervals and locations as before. This completes the field measurement. The third and seventh columns (A_{avg} and B_{avg}) are generated by subtracting the second column from the first and the sixth from the fifth and dividing each by two:

$$A_{avg} = \frac{A_0 - A_{180}}{2} \qquad (6.1)$$

$$B_{avg} = \frac{B_0 - B_{180}}{2} \qquad (6.2)$$

These equations generate the absolute horizontal displacement for both axes and for each of the data points. In this study the

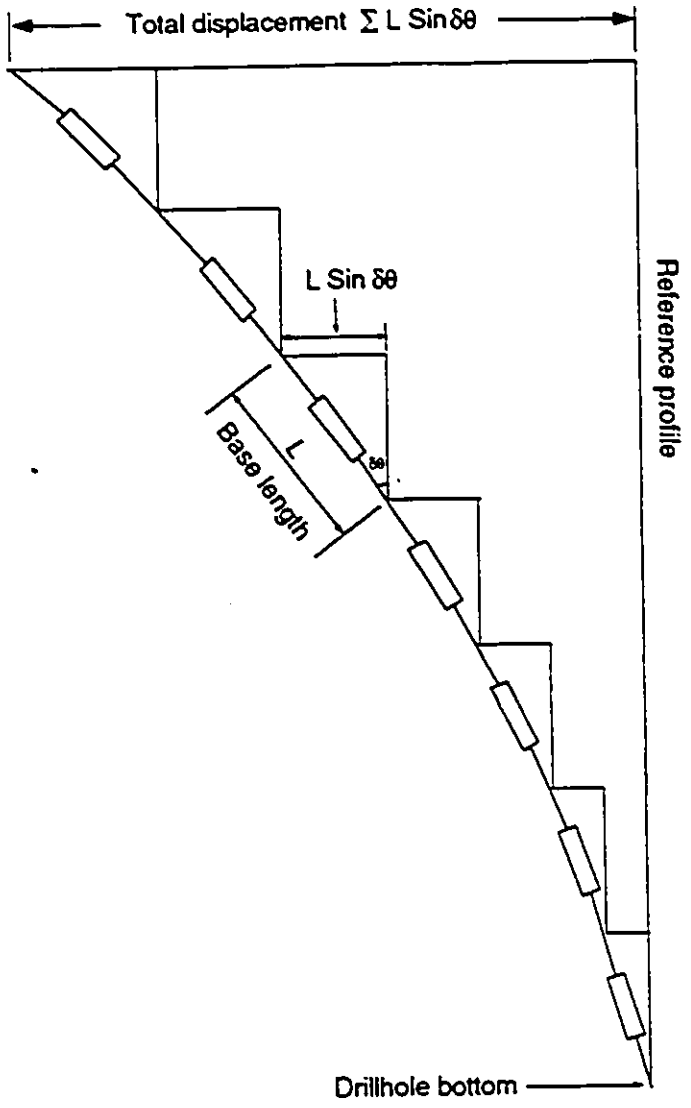

Figure 6.1 A diagram showing the relationship between the torpedo base length (L) and the incremental displacement (L Sin δθ). The calculation of total displacement is also shown.

1	2	3	4	5	6	7	8
A0	A180	Aavg	Acum	B0	B180	Bavg	Bcum
-0.554	0.322	-0.438	-0.438	-0.622	0.547	-0.5845	-0.5845
-0.435	0.249	-0.342	-0.78	-0.573	0.476	-0.5245	-1.109
-0.405	0.192	-0.2985	-1.0785	-0.563	0.482	-0.5225	-1.6315
-0.38	0.142	-0.261	-1.3395	-0.525	0.429	-0.477	-2.1085
-0.402	0.169	-0.2855	-1.625	-0.499	0.425	-0.462	-2.5705
November 5, 1991			Site #1				
A0	A180	Aavg	Acum	B0	B180	Bavg	Bcum
-0.549	0.332	-0.4405	-0.4405	-0.634	0.553	-0.5935	-0.5935
-0.407	0.188	-0.2975	-0.738	-0.554	0.469	-0.5115	-1.105
-0.413	0.198	-0.3055	-1.0435	-0.552	0.472	-0.512	-1.617
-0.375	0.157	-0.266	-1.3095	-0.502	0.424	-0.463	-2.08
-0.383	0.17	-0.2765	-1.586	-0.516	0.444	-0.48	-2.56
December 4, 1991			Site #1				
A0	A180	Aavg	Acum	B0	B180	Bavg	Bcum
-0.5674	0.3076	-0.4375	-0.4375	-0.752	0.4431	-0.5976	-0.5976
-0.4371	0.1527	-0.2949	-0.7324	-0.7021	0.2954	-0.4988	-1.0963
-0.4639	0.1483	-0.3061	-1.0385	-0.6537	0.3652	-0.5095	-1.6058
-0.4374	0.1004	-0.2689	-1.3074	-0.6249	0.3156	-0.4703	-2.076
-0.5026	0.088	-0.2953	-1.6027	-0.6031	0.291	-0.4471	-2.5231
March 8, 1992			Site #1				
A0	A180	Aavg	Acum	B0	B180	Bavg	Bcum
-0.604	0.22	-0.412	-0.412	-0.842	0.34	-0.591	-0.591
-0.48	0.095	-0.2875	-0.6995	-0.76	0.252	-0.506	-1.097
-0.469	0.122	-0.3055	-1.005	-0.75	0.253	-0.5015	-1.5985
-0.459	0.062	-0.2605	-1.2655	-0.722	0.218	-0.47	-2.0685
-0.61	0.06	-0.335	-1.6005	-0.7	0.105	-0.4025	-2.471

Figure 6.2 A sample page of the field data sheet.

initial data set is used as a reference profile for each borehole, and more recent data are adjusted to this profile. This reflects the total amount of movement and an average rate. The values in columns 4 (A_{cum}) and 8 (B_{cum}) represent the horizontal displacement of the borehole relative to the starting measurement point (the bottom of the borehole). The relative displacement is determined by subtracting the current cumulative values from the initial cumulative values and plotting the difference.

6.4 Inclinometer data

Depths at which measurements have been taken were established on 26 September, 1991 and all subsequent readings were taken at the same levels. Nine field visits were made to the instrumented sites between 26 September, 1991 and 5 December 1992.

One basic factor has to be considered in order to delineate creep deformation of the boreholes: recovery of equilibrium conditions. Drilling and installation disturb the natural equilibrium conditions of the slopes and cause small and random deformation within a certain time period following the installation. In Savigny's case where mud-rotary drilling was used, the random deformation approached negligible magnitudes seven months after the installation (Savigny and Morgenstern 1986b). Since no mud-rotary drilling was used in this project, the random deformation caused by drilling and installation should terminate in a shorter time period.

There have been concerns that the casing may be too stiff to

follow soil movement in soft soils. This concern implies that soil might flow around the casing. However, available evidence suggests that the casing conforms with soil movement (cf. Dunnicliff and Green 1988). This problem is unlikely to happen in permafrost because the casing and surrounding soils are "frozen" together.

Results for the six sites are presented in Figures 6.3 to 6.8. The initial position in these diagrams is the September, 1991 readings. Deflection data for the A- and B- direction of each site are illustrated on the same diagram.

To minimize the effects of transient temperature and stress field, which developed most rapidly within a short time period immediately following placement, the first set of readings (the September, 1991 readings) is rejected in calculations. Figs. 6.3 to 6.8 indicate that the amount of permafrost creep varies not only from site to site, but also seasonally. The greatest downslope displacement occurs in the summer when permafrost temperatures are warmest. During the winter, upslope movement is measured. This backward movement was also noticed by both Savigny (1980) and Bennett (1989). Savigny attributed it to frost heave; while Bennett and French (1988) believe that the backward movement is caused by frost heave and thermal contraction. Because permafrost undergoes constant creep deformation throughout the year, the net displacement of the boreholes depends upon the offset between the upslope and downslope components of the movement. The following analysis focuses upon the *in situ* creep measured immediately below the permafrost table which ranges from 1.25 m to 1.60 m below the

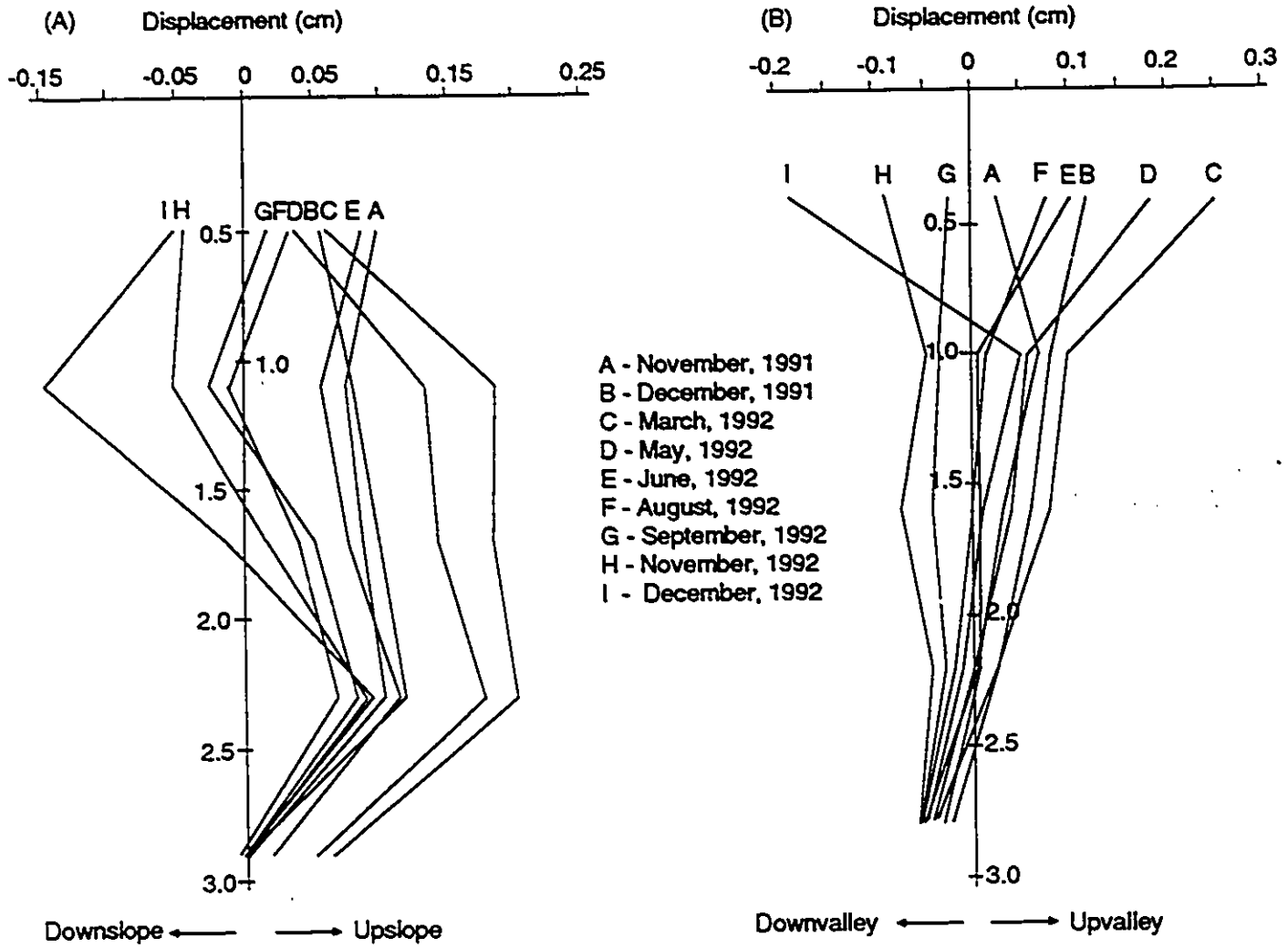

Figure 6.3 Displacement in permafrost in both A (parallel to slope) and B (cross slope) directions at site #1. The depth to permafrost table at this site is 1.4 m.

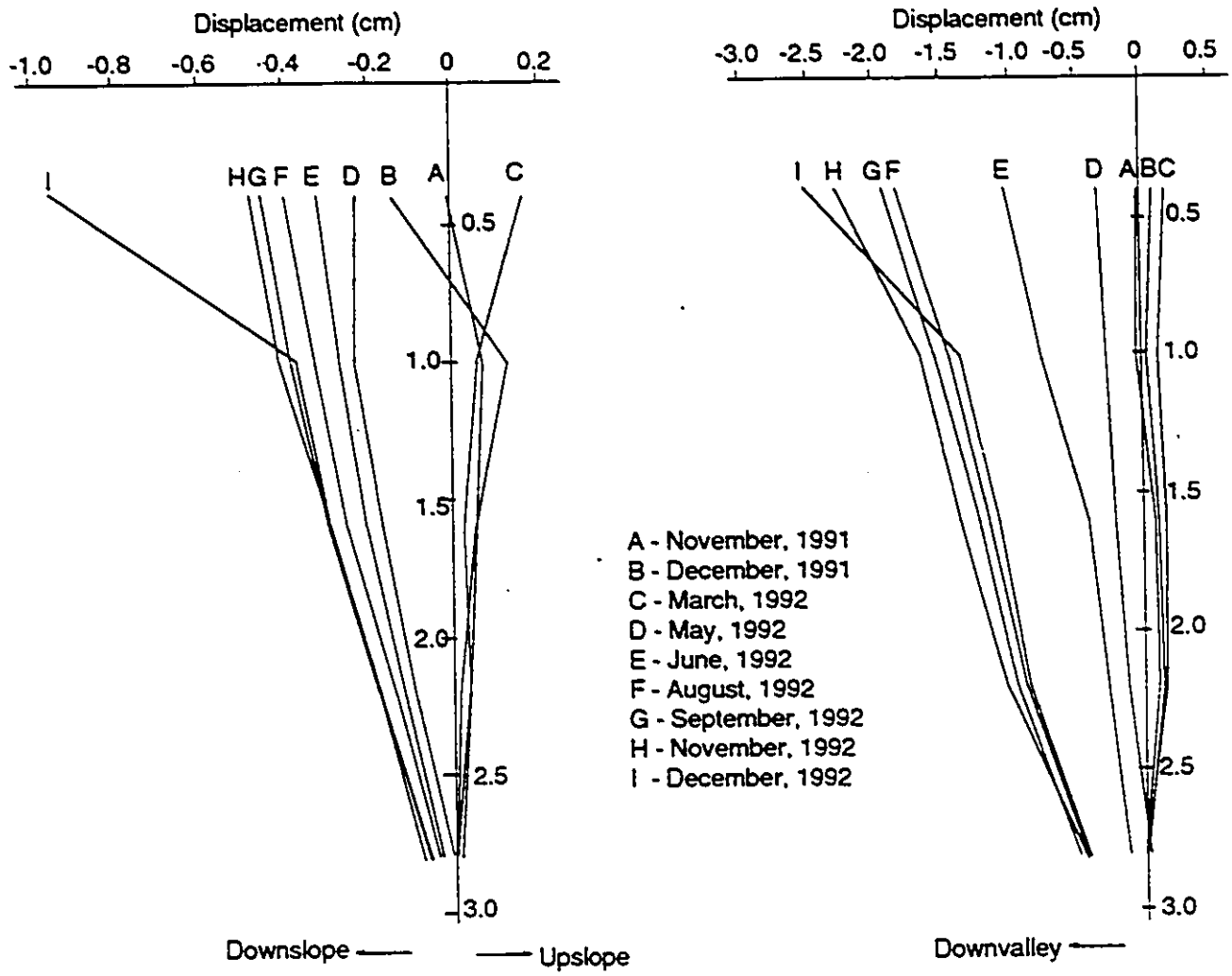

Figure 6.4 Displacement in permafrost in both A (parallel to slope) and B (cross slope) directions at site #2. The depth to permafrost table at this site is 1.4 m.

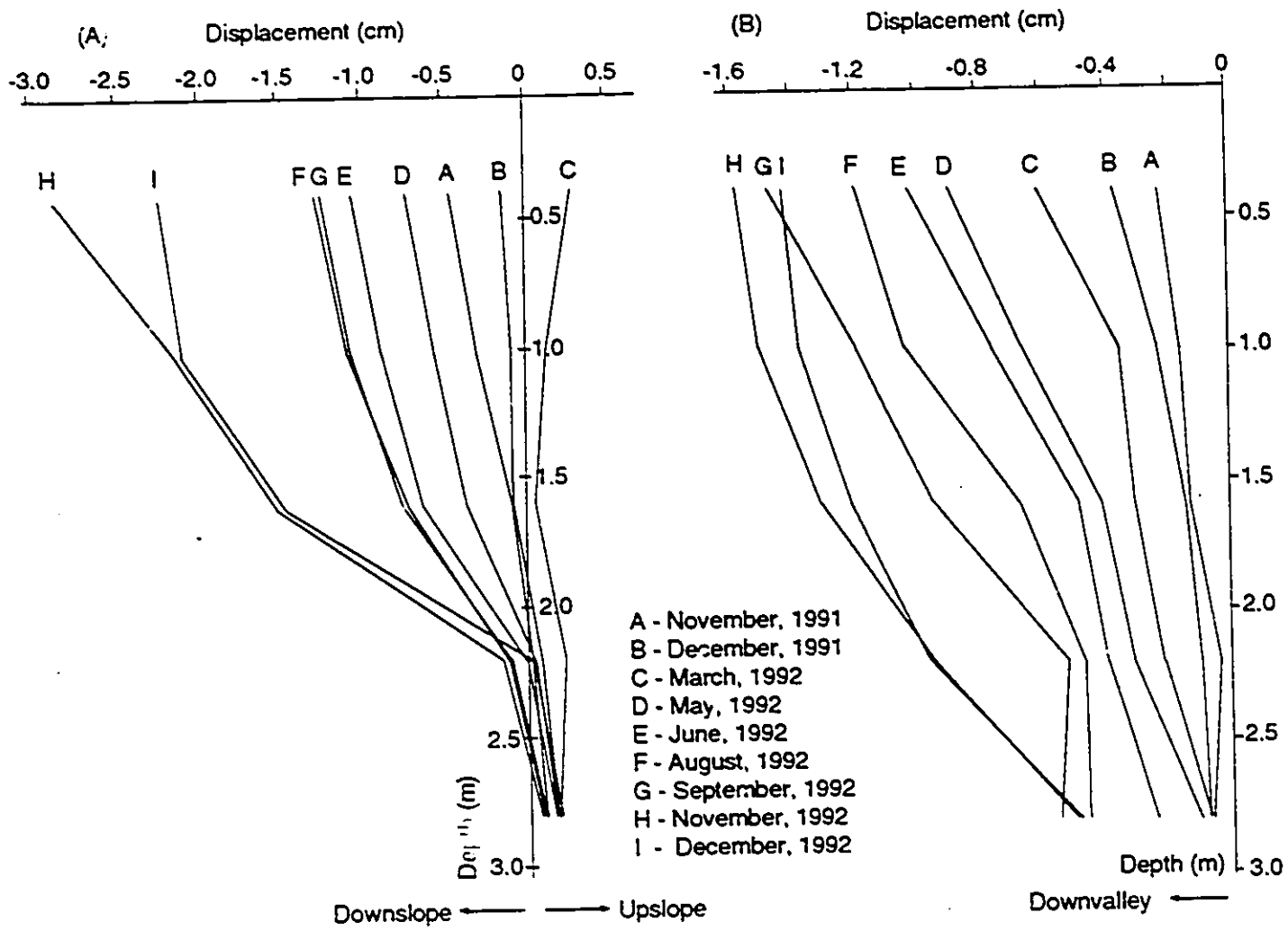

Figure 6.5 Displacement in permafrost in both A (parallel to slope) and B (cross slope) directions at site #3. The depth to permafrost table at this site is 1.4 m.

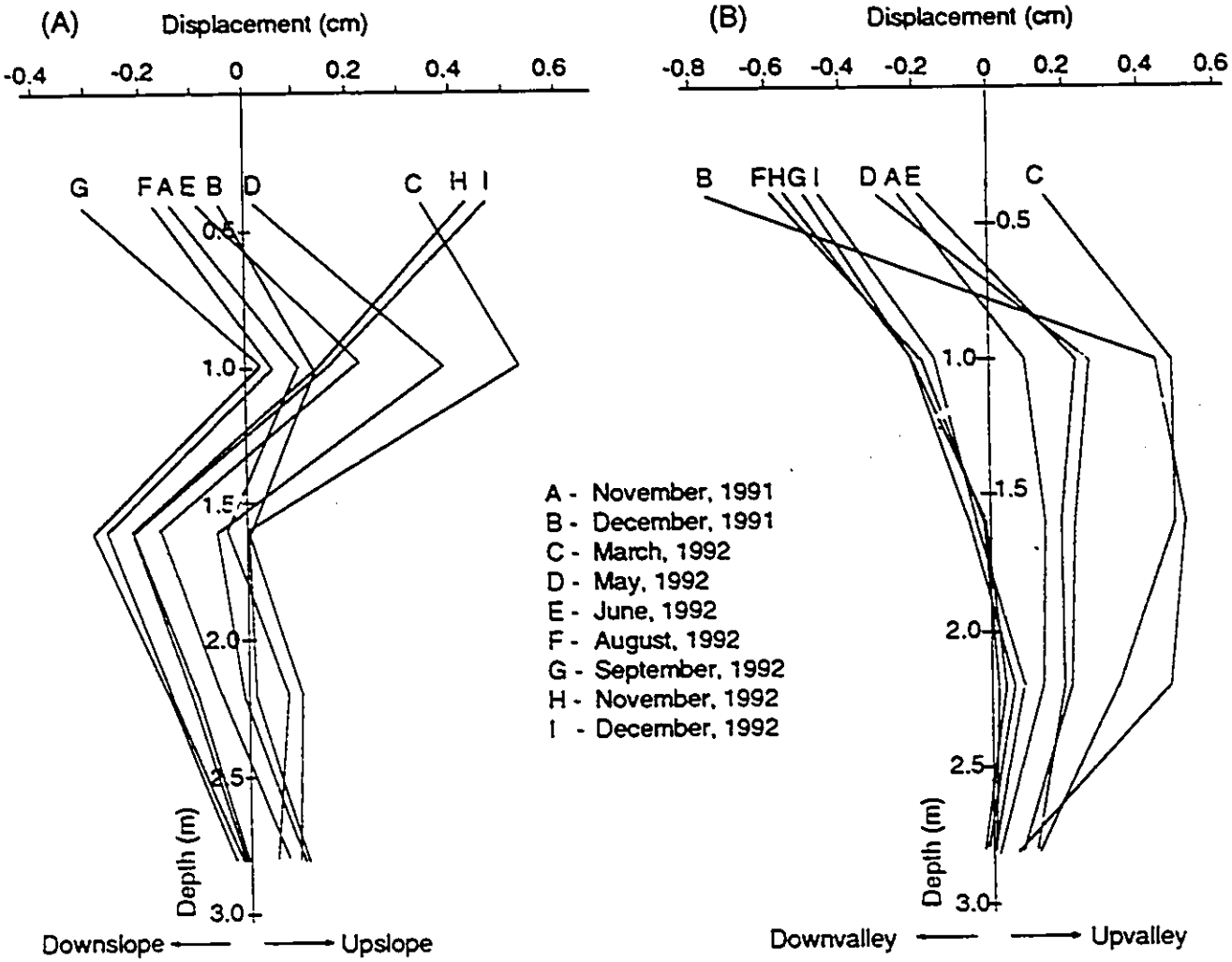

Figure 6.6 Displacement in permafrost for both A (parallel to slope) and B (cross slope) directions at site #4. The depth to permafrost table at this site is 1.25 m.

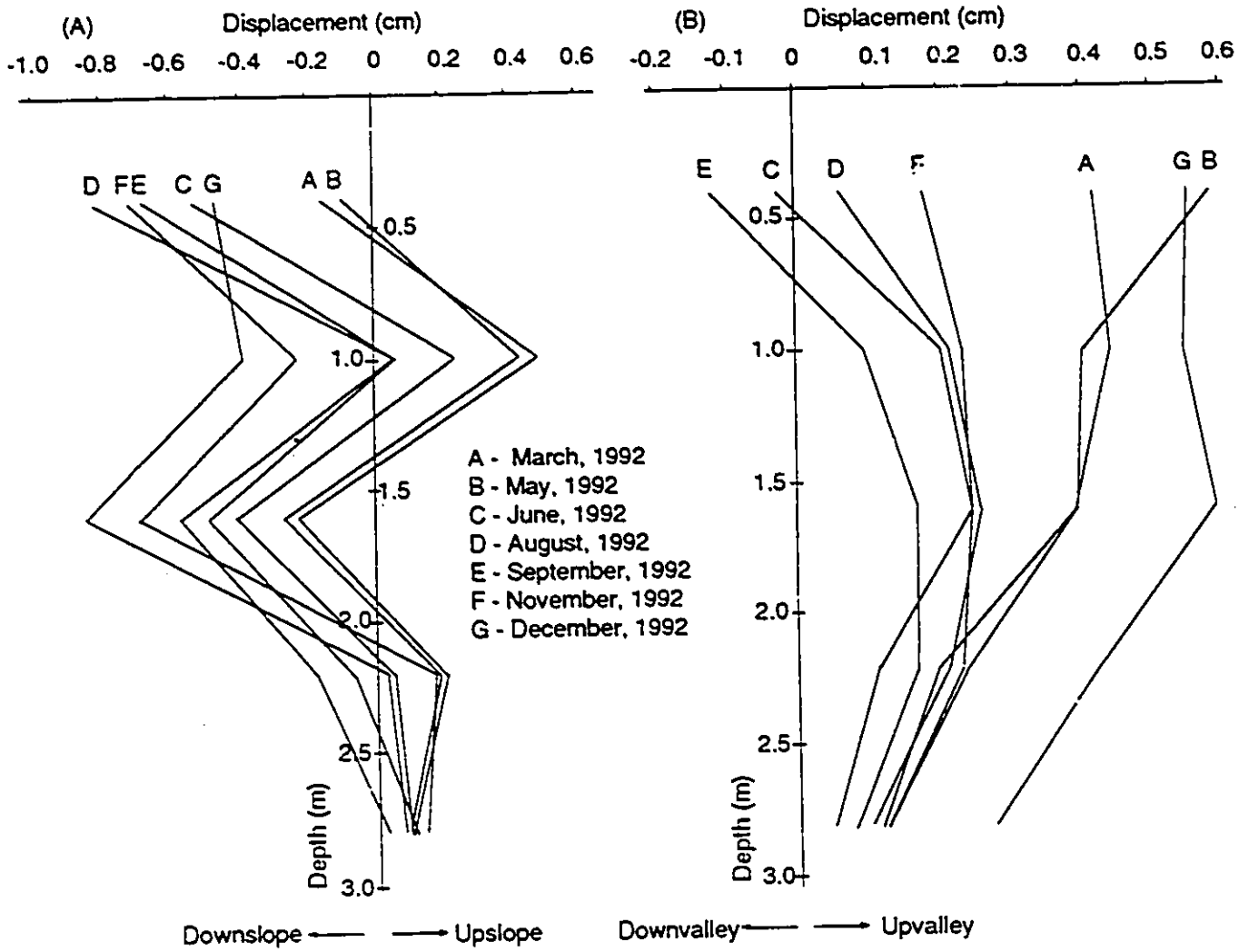

Figure 6.7 Displacement in permafrost for both A (parallel to slope) and B (cross slope) directions at site #5. The depth to permafrost table at this site is 1.5 m.

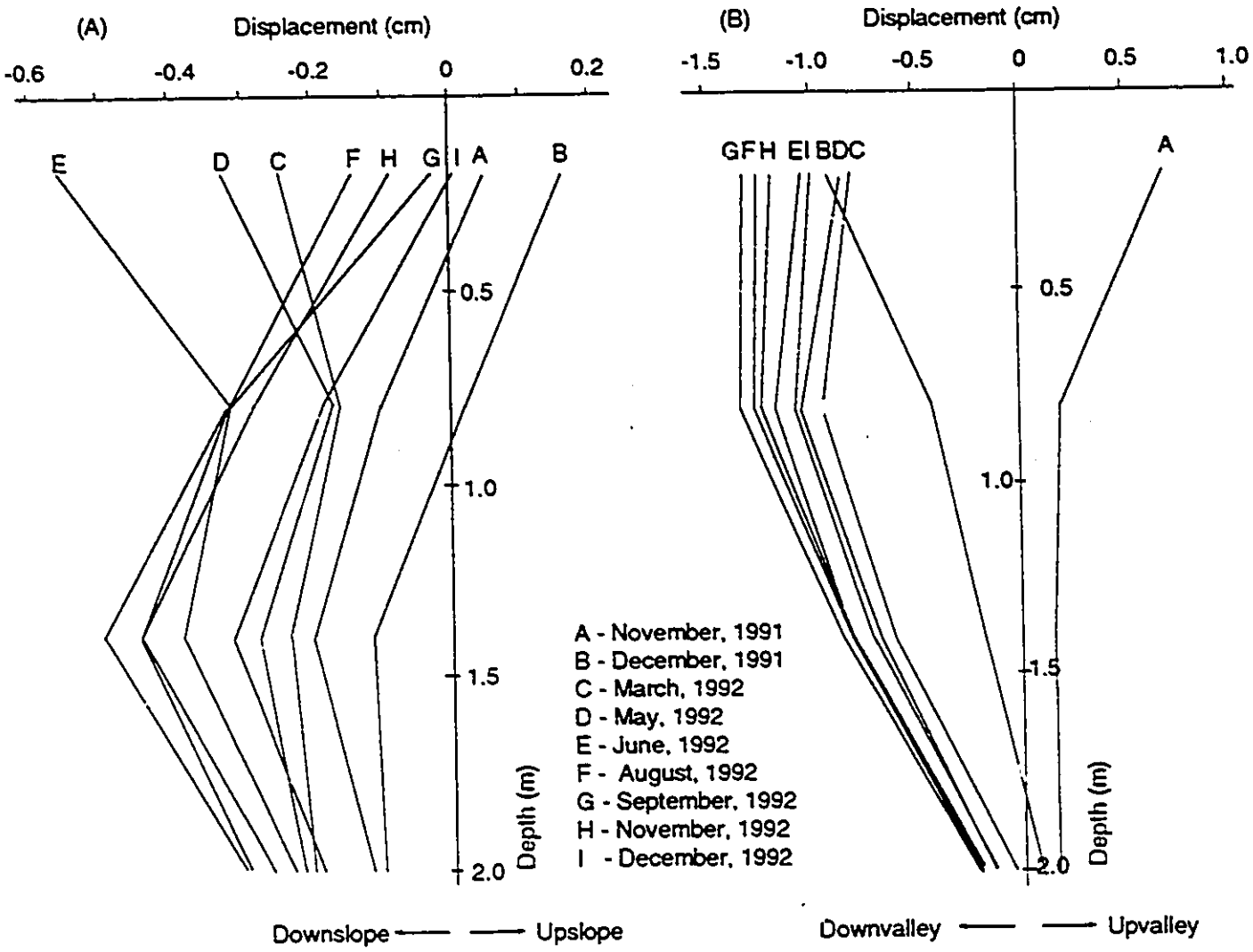

Figure 6.8 Displacement in permafrost in both A (parallel to slope) and B (cross slope) directions at site #6. The depth to permafrost table at this site is 1.6 m.

surface in the West Valley. This movement has nothing to do with solifluction.

6.5 Upslope movement

Upslope movement of permafrost has been detected in winter at all the instrumented sites of the West Valley, Fenghuo Shan area. The magnitudes of upslope (and upvalley) movement over certain periods of time are shown in Table 6.1.

The net upslope movement ranged from less than 0.01 cm up to 0.34 cm during the specified time period, and decreased with depth. The greatest upvalley displacement was monitored at site #5 where ice content is the greatest of all the six sites (Figure 5.11).

In solifluction investigations, the upslope or retrograde soil movement has been attributed to a number of origins such as soil cohesion, interference of soil particles with each other, capillary pressure, greater desiccation at top of the slope, etc. (cf. Washburn 1979). It is unlikely that these hypotheses are applicable to the interpretation of the upslope movement in permafrost because the retrograde component in solifluction has been detected only during thawing season; while the upslope displacement in permafrost has always been reported to occur during winter months. Frost heave has been theoretically considered as an initiator of the potential frost creep (downslope) (cf. Jahn 1975; French 1976; Washburn 1979). Therefore, anyone trying to explain the backward movement of permafrost by frost heaving will soon find himself in a major dilemma. The backward movements were also recorded by Meier (1960)

Table 6.1 Upslope displacement (cm) at various sites, West Valley, Fenghuo Shan area, Tibetan Plateau.

Site	Depth (m)	Upslope (cm)	Upvalley (cm)	Period
#1 (25°)	1.6	0.10	0.05	11/91 - 03/92
		0.03	0.08	11/92 - 12/92
	2.2	0.10	0.02	11/91 - 03/92
		0.01	0.05	11/91 - 12/92
	2.8	0.07	<0.01	11/91 - 03/92
		<0.01	<0.01	11/92 - 12/92
#2 (17°)	1.6	-0.03	0.08	11/91 - 03/92
		0.01	0.30	11/92 - 12/92
	2.2	0.01	0.04	11/91 - 03/92
		<0.01	0.16	11/92 - 12/92
	2.8	0.01	0.03	11/91 - 03/92
		0.01	0.00	11/92 - 12/92
#3 (11°)	1.6	0.14	- 0.18	11/91 - 03/92
		0.07	0.10	11/92 - 12/92
	2.2	0.20	- 0.19	11/91 - 03/92
		0.18	- 0.20	11/92 - 12/92
	2.8	0.06	-0.01	11/91 - 03/92
		0.13	0.01	11/92 - 12/92
#4 (7°)	1.6	0.04	0.08	11/91 - 03/92
		<0.01	0.02	11/92 - 12/92
	2.2	-0.06	0.08	11/91 - 03/92
		<0.01	0.03	11/92 - 12/92
	2.8	0.06	0.07	11/91 - 03/92
		<0.01	0.02	11/92 - 12/92
#5 (15°)	1.6	-0.06	0.34	11/92 - 12/92
	2.2	-0.06	0.31	11/92 - 12/92
	2.8	-0.02	0.22	11/92 - 12/92
#6 (25°)	1.6	0.01	-0.08	11/91 - 12/91
		0.10	0.02	11/92 - 12/92
	2.0	0.04	-0.07	11/91 - 12/91
		0.06	0.03	11/92 - 12/92

for Saskatchewan glaciers.

Thermal contraction cracking can be a mechanism for the upslope permafrost creep where the ground undergoes cracking. However, neither polygons nor thermal contraction cracks have been developed on the slope of the West Valley, Fenghuo Shan area. Thus, it is also hard to interpret the upslope movement by thermal contraction cracking.

One possibility is that the direction of frost heaving in reality is not quite normal, but vertical, to the slope surface. This means that the upslope movement is caused by the upslope component of frost heaving during winter months. This hypothesis contradicts with the conventional "frost creep" mechanism.

6.6 *In situ* creep velocity

Annual creep rates are calculated according to the readings over the whole year period of November 5, 1991 to November 5, 1992. The data indicate that downslope permafrost creep for transect A - A' (the north-facing slope) of the West Valley ranges from 0.07 to 1.44 cm/year at 1.6 m depth (with a mean of 0.50 cm/year), from 0.02 to 1.13 cm/year at 2.2 m depth (with a mean of 0.15 cm/year), and from 0.02 to 0.08 cm/year at 2.8 m depth (with a mean of 0.04 cm/year)(see Table 6.2 and Figure 6.9A).

Downvalley permafrost creep rates, shown in Table 6.3 and Figure 6.9B, are greater than the downslope rates. This contrasts with the *in situ* creep data obtained by Savigny (1980, also Savigny and Morgenstern 1986b) for the Mackenzie Valley and by Bennett

Table 6.2 Downslope permafrost creep rates for transect A-A' (cm/year)

Depth, m	Site #1	Site #2	Site #3	Site #4	Mean
1.6	0.072	0.340	1.420	0.183	0.504
2.2	0.018	0.212	0.188	0.178	0.149
2.8	0.020	0.076	0.033	0.057	0.040
slope angle	25°	17°	11°	7°	15°

Table 6.3 Down-valley permafrost creep rates for transect A-A' (cm/year)

Depth, m	Site #1	Site #2	Site #3	Site #4	Mean
1.6	0.107	1.440	1.182	0.204	0.733
2.2	0.046	1.130	0.911	0.081	0.542
2.8	0.025	0.429	0.437	0.033	0.231

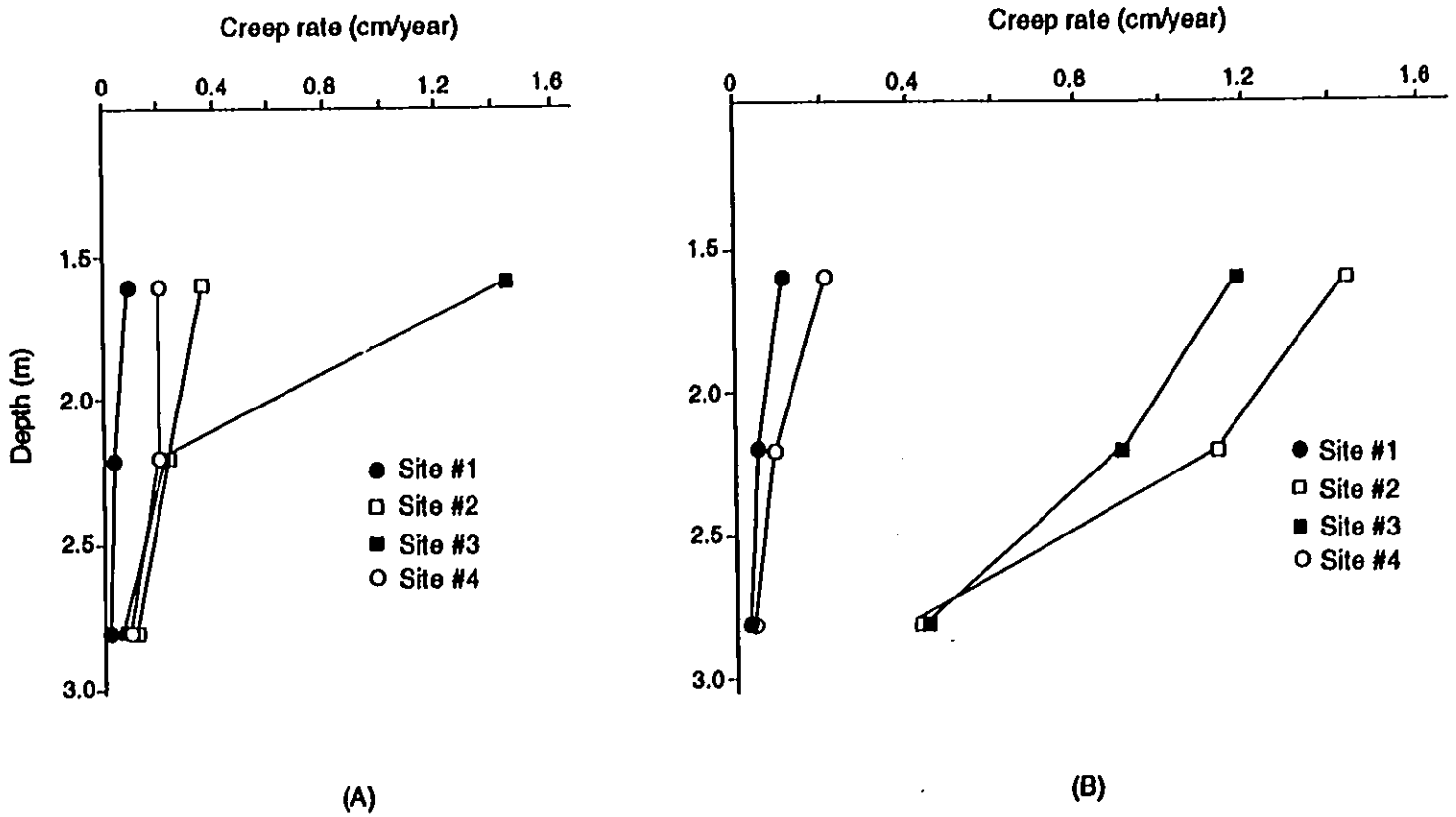

Figure 6.9 Annual (November 1991 - November 1992) creep rates for transect A-A': (A) - Downslope, and (B) - Downvalley.

(1989, also Bennett and French 1988, 1990) for the high Arctic of Canada. In all probability, this is likely related to local topography; the instrumented sites are close to (approximately 500 m) the ends of the hills on either side of the West Valley. Thus, the terrain slopes naturally towards both the valley bottom and the downvalley (or cross-slope) direction.

The abrupt increase in creep rate at site #3 (Fig. 6.9) seems related to an increase in ice content (Fig. 5.10); however, the high ice content at site #4 (Fig. 5.10) is not reflected in the magnitude of the creep rate. Both downslope and downvalley creep rates at site #1 are the smallest along the transect A-A' (Fig. 6.9), reflecting the low ice content at this site (Fig. 5.9). However, correlation between creep rate and ice content is poor at sites #2 and #6. The increase in downslope creep rate at site #5 from 2.2 to 1.6 m (Fig. 6.10 and Table 6.4) appears to relate to the existence of an ice layer (Fig. 5.11).

The *in situ* creep data indicate no clear differences in creep rates between the two slopes although the south-facing slope is slightly warmer as suggested by ground temperature measurements. Therefore, no significant inference can be made as to slope aspect on creep rate. The same is true for slope angle.

It is useful to compare these data with those of Savigny (1980) and of Bennett (1989). Savigny measured permafrost creep in ice-rich sediments in the Mackenzie Valley. The mean annual ground temperatures were -2.5 °C, and creep rates of between 0.10 and 0.3 cm/year were detected at depths of between 5 m to 32 m (Savigny

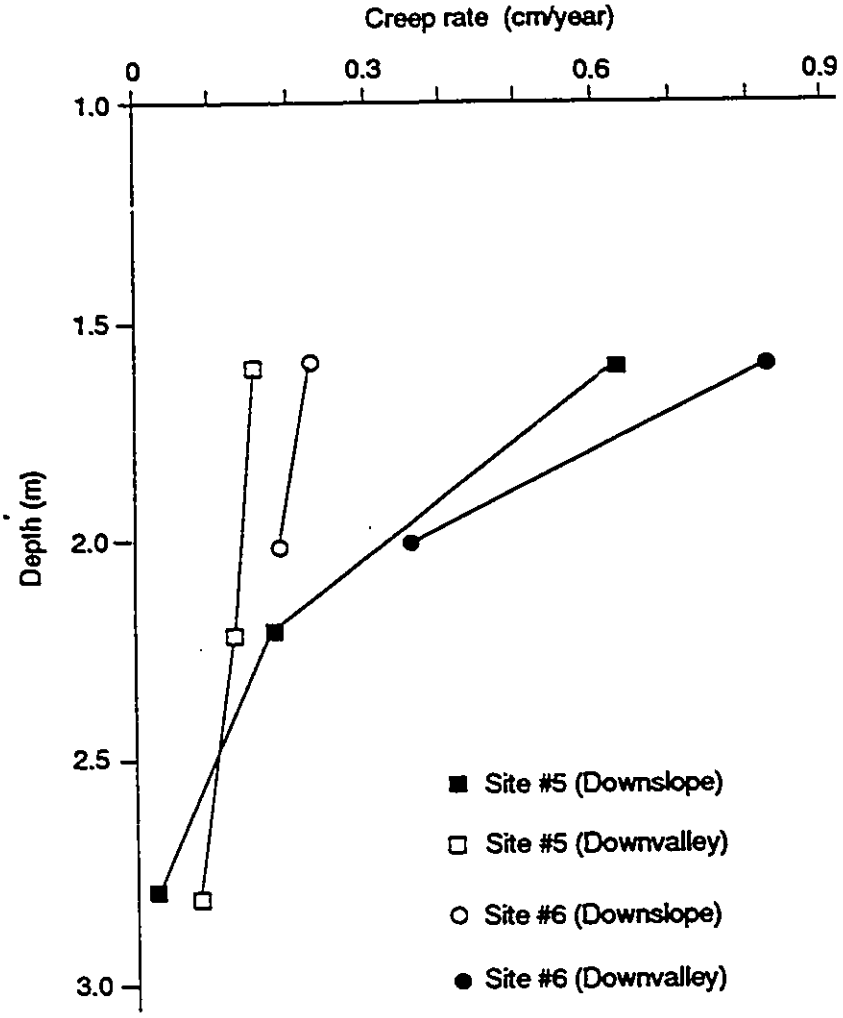

Figure 6.10 Creep rate of transect B-B' (creep rates of site #5 were calculated for the period of March, 1991 to November, 1992; from November 1991 to November 1992 for site #4).

Table 6.4 In situ permafrost creep data for transect B - B'

Depth (m)	Site #5 (cm)		Depth (m)	Site #6 (cm/year)	
	Downslope	Downvalley		Downslope	Downvalley
1.6	0.622	0.147	1.6	0.220	0.820
2.2	0.170	0.124	2.0	0.178	0.356
2.8	0.020	0.072			

1980). Creep rate as high as 0.5 cm/year was monitored at the top metre or so of permafrost (see Fig. 10 of Savigny and Morgenstern 1986b).

Bennett (1989) monitored *in situ* permafrost creep on eastern Melville Island of Arctic Canada. At his sites, the mean annual ground temperature was -16.5°C, and maximum annual rates ranged from 0.3 cm/year at 35 cm depth to 0.1 cm/year at 65 cm depth. Average annual rates were less and ranged from 0.11 cm/year at 35 cm to 0.04 cm/year at 65 cm (Bennett 1989). No measurable creep deformation was noted at depths below 1.0 m.

The permafrost creep rates measured in the West Valley of Fenghuo Shan area, Tibet Plateau are greater than those detected by Bennett (1989), but approximately of the same magnitude as those reported by Savigny (1980). This reflects the basic control of ground temperature over *in situ* permafrost creep. The MAGT in the West Valley of Fenghuo Shan area, Tibet Plateau is much higher than that on Melville Island of Arctic Canada, thus, the creep rates for the West Valley are much greater than those on Melville Island. When compared with the data from the Mackenzie Valley, the West Valley on the Plateau shows similar creep rates. This is because the terrain in both areas experiences a similar temperature range. The difference in MAGT between both areas is just 0.5°C.

A cautious conclusion, derived from this limited data base, is that the regional magnitude of naturally-occurring permafrost creep is controlled largely by temperature (i.e. climate), although creep rate may vary from site to site due to changes in ground-ice

conditions.

6.7 Constitutive relationship

Laboratory studies have indicated that the constitutive relationship for the secondary creep of ice and ice-rich frozen soil is in the form of (e.g. Glen 1952, 1955; Nixon 1978, 1990; Nixon and McRoberts 1976):

$$\dot{\varepsilon} = A\,\tau^{n} \tag{6.3}$$

where $\dot{\varepsilon}$ denotes strain rate; τ denotes shear stress; A and n are creep parameters.

A comprehensive literature review by Morgenstern *et al.* (1980) concludes that the flow law for ice constitutes an upper bound to creep tests on ice-rich soils. Using the flow law (6.3), pile velocities in ice and ice-rich soils have been predicted and the predictions are shown to be in good agreement with available long-term creep data for piles in ice and ice-rich soils. A laboratory investigation by McRoberts (1988) indicates that most samples exhibited a secondary creep mode of deformation similar to that of ice even with water (ice) contents as low as 22%. Because the water (ice) contents of the soil samples in this study are mostly greater than 22%, the slopes of the West Valley are regarded as ice-rich. Thus, the secondary power flow law (6.3) is assumed to be applicable to the creep sites in the West Valley.

6.7.1 The model

In order to carry out modelling of creep parameters A and n in equation (6.3) for the slopes in the West Valley, Fenghuo Shan area, it is necessary to work out the formulation of the shear stress and strain rate. It can be assumed, following Meier (1960) and McRoberts (1975), that the strain rate is a function of the deviator stress and the magnitude of the deviator stress is, in turn, measured by the octahedral shear stress:

$$\tau_o = \frac{1}{3}\sqrt{(\sigma_1-\sigma_2)^2+(\sigma_2-\sigma_3)^2+(\sigma_3-\sigma_1)^2} \qquad (6.4)$$

where (σ_1, σ_2, σ_3) are principal stresses.

Similarly, an octahedral shear strain rate $\dot{\varepsilon}_o$ is defined as:

$$\dot{\varepsilon}_o = \frac{1}{3}\sqrt{(\dot{\varepsilon}_1-\dot{\varepsilon}_2)^2+(\dot{\varepsilon}_2-\dot{\varepsilon}_3)^2+(\dot{\varepsilon}_3-\dot{\varepsilon}_1)^2} \qquad (6.5)$$

where ($\dot{\varepsilon}_1$, $\dot{\varepsilon}_2$, $\dot{\varepsilon}_3$) are the principal strain rates. The power flow law (or Glen's flow law) then can be rewritten as:

$$\dot{\varepsilon}_o = A\,\tau_o^{\,n} \qquad (6.6)$$

If we assume that the slopes in the West Valley to be "ideal" (i.e. they are uniform in material and geometry), the shear stress

acting parallel to the straight slope and thus tending to cause downslope movement is given by (cf. Williams 1982; Williams and Smith 1989, p124):

$$\tau_s = \rho\, z\, g \sin\beta \cos\beta \qquad (6.7)$$

where ρ is bulk density, g is gravitational acceleration, β is the slope angle, and z is depth.

As the principal stresses are $(\sigma_z + \tau_s,\ \sigma_z,\ \sigma_z - \tau_s)$, then we get the following expression by substituting these principal stresses into equation (6.4):

$$\tau_0 = \sqrt{\frac{2}{3}}\ \rho\, z\, g \sin\beta \cos\beta \qquad (6.8)$$

If the creep velocity at any depth is assumed to be V_x, then the engineering shear strain rate can be written as (cf. McRoberts 1975):

$$\dot{\gamma} = \frac{\partial v_x}{\partial z} \qquad (6.9)$$

where x is taken parallel to the slope. This is also an expression of creep velocity gradient ($year^{-1}$), which is what Savigny and Morgenstern (1986b) regarded as the shear strain rate. All values

of shear strain rate are calculated based upon (6.9), which is a linear regression fit to velocity data over the specified depth interval (see footnote on page 513 of Savigny and Morgenstern 1986b). The same method is employed here to calculate the strain rate from the field creep velocity data, although the classic textbook definition of "strain" can not be easily visualized in the slopes.

Because the principal strain rates are ($\dot{\gamma}/2$, 0, $-\dot{\gamma}/2$), the following relationship is obtained by substituting these principal strain rates into equation (6.5):

$$\dot{e}_0 = \sqrt{\frac{1}{6}} \frac{\partial V_x}{\partial Z} \qquad (6.10)$$

Thus, for the slopes the flow law (6.6) becomes:

$$\sqrt{\frac{1}{6}} \frac{\partial V_x}{\partial Z} = A \left(\sqrt{\frac{2}{3}} \rho z g \sin\beta \cos\beta\right)^n \qquad (6.11)$$

This equation is used to analyze the field data from the West Valley of the Plateau and to calculate the creep parameters A and n.

6.7.2 Creep parameters A and n

The shear stress in the slopes acts on soil in two directions

(i.e. downslope and downvalley) due to local topography of the field sites. Soils at different depths are subject to different stresses and yield different deformation; thus it is necessary to establish separate constitutive relationships for each of the three depths (1.6 m, 2.2 m, and 2.8 m) at which permafrost creep was measured.

Shear strain rates so defined were calculated by equation (6.9). The results indicate that the strain rate measured in the West Valley ranges mostly between 0.33×10^{-4} year^{-1} and 20.0×10^{-4} year^{-1}. But large strain rates ranging from 45.20×10^{-4} year^{-1} to 200.00×10^{-4} year^{-1} were also indicated. These variations of strain rate were between different boreholes on the slopes of the West Valley. They are much greater than the values of Savigny and Morgenstern (1986b). Shear stress levels were estimated by equation (6.7). The shear stress ranges between 5 kPa and 20 kPa over the depths that this study is concerned. In order to calculate the creep parameters A and n from the creep power flow law (6.6), a series of vector analyses was carried out for the shear stresses and strain rates to achieve their resultants. A vector sum was obtained for each pair of stresses and strain rates at each depth respectively. The horizontal movement was calculated from the readings of the readout unit. Further calculations were then made to get the profile of the borehole (casing) and the displacement parallel to the slopes. The calculated resultants of strain rates and shear stresses were introduced into equation (6.11); then both sides of equation (6.11) were plotted against each other in a log-

log coordinate (Figure 6.11) in order to convert an exponent curve into a straight line. Linear regressions carried out for each depth indicates the following constitutive relationships:

$$\dot{\varepsilon} = 1.93 \times 10^{-4}\ \tau^{1.70} \qquad (6.12)$$

$$\dot{\varepsilon} = 8.24 \times 10^{-5}\ \tau^{1.72} \qquad (6.13)$$

$$\dot{\varepsilon} = 9.9 \times 10^{-6}\ \tau^{2.0} \qquad (6.14)$$

Where $\dot{\varepsilon}$ is expressed in $year^{-1}$ and τ in kPa (kN/m^{-2}). Therefore, equations (6.12), (6.13), and (6.14) are the power flow laws governing permafrost creep at depths of 1.6 m, 2.2 m, and 2.8 m, respectively. They demonstrate that the value of n is stress-dependent and tends to increase with increasing stress level, which is in good agreement with many other studies (e.g. Morgenstern 1985; Nixon and Neukirchner 1984; McRoberts *et al.* 1978).

Laboratory studies on ice and ice-rich soils indicate that the exponent n ranges between 1 and 3 for strain rate less than 1×10^{-2} $year^{-1}$ and for temperatures between 0 and -5°C (e.g. Morgenstern *et al.* 1980) and can be as high as 6 at high stresses (e.g. Hooke 1981; Paterson 1977; McRoberts *et al.* 1978). Although a value of 3 has been proposed by several investigators for ice-rich soils at temperatures colder than -1°C and at stress levels lower than 100

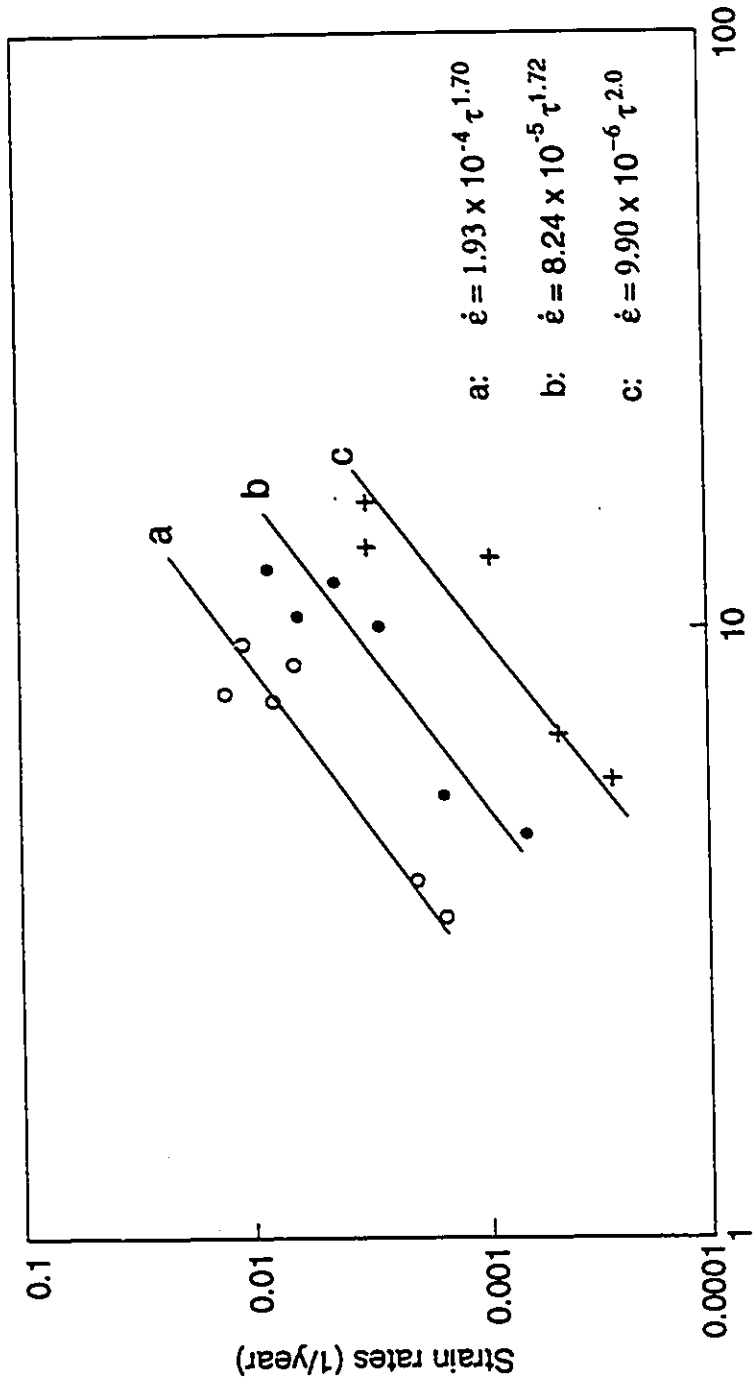

Figure 6.11 A log-log plot of shear stresses vs strain rates: a - 1.6 m depth, b - 2.2 m depth, and c - 2.8 m depth.

kPa (e.g. McRoberts 1988; Morgenstern *et al.* 1980; Neukirchner and Nixon 1987; Nixon 1990; Savigny and Morgenstern 1986c), a best-fit flow law to all available creep data takes the following form (Morgenstern 1981; Savigny and Morgenstern 1986c):

$$\dot{\varepsilon} = 1.9 \times 10^{-5} \tau^{1.70} \qquad (6.15)$$

where $\dot{\varepsilon}$ is in year^{-1} and τ in kPa. The constitutive relationships (6.12), (6.13), and (6.14) which were derived from the *in situ* creep data measured in the West Valley of the Qinghai-Xizang (Tibet) Plateau are comparable with the power flow law (6.15). It is believed therefore that the flow laws (6.12), (6.13), and (6.14) can be used to predict creep deformation of permafrost in the Fenghuo Shan area.

6.8 Discussion and conclusions

Investigations into the nature of *in situ* permafrost creep suggest that it is a complex process. The direction and magnitude of the movement is dependent upon a number of factors, among which temperature, frost heave, and ground-ice conditions are the most important ones. This study indicates that, for plateau permafrost, the net displacement is upslope during winter and downslope during summer. The upslope displacement has been previously interpreted as being caused by "conventional" frost heave and thermal contraction in Canada. Analysis suggests that neither of these two mechanisms

is applicable to the West Valley, Tibetan Plateau. It may be that, in reality, the direction of frost heaving is not quite normal, but vertical, to the surface of the slope. If this is the case, the upslope displacement of permafrost is then caused by the upslope component of frost heaving. This interpretation seems tangible because the timing of upslope movement coincides with that of frost heaving. The net upslope displacement in permafrost at the instrumented sites of the West Valley ranged from less than 0.01 cm up to 0.34 cm, much less than the amount of heave measured from the active layer.

The permafrost slopes in the West Valley exhibit significant down-valley (cross-slope) creep rates which range, in average, from 0.15 cm/year at 2.8 m depth to 0.63 cm/year at 1.6 m depth. Downslope creep rates between 0.16 cm/year at 2.8 m depth and 0.44 cm/year at 1.6 m depth have been detected at the instrumented sites on the Tibetan Plateau.

Inter-continental comparisons of the creep rates suggest that climate is the most important factor controlling the regional magnitude of *in situ* permafrost creep. However, when comparisons are made between different sites over the same general area, ground ice, and frost heave also play an important role. The best-fit constitutive relationships (flow laws) were determined with the Glen's flow law for the field creep data, which are the equations (6.12), (6.13), and (6.14).

PART FOUR: SYNTHESIS

CHAPTER SEVEN - CONCLUSIONS

7.1 Geocryology

Differences in Quaternary history and climate cause quite unique and different permafrost conditions on the Tibetan Plateau and in the Mackenzie Delta. Plateau permafrost in Tibet is discontinuous and belongs to the 'widespread' and 'sporadic' categories in distribution, and is less continuous than the permafrost in the Mackenzie Delta. Because of its high elevation, plateau permafrost conditions vary with both latitude and altitude.

Ground-ice conditions in both areas differ considerably; ice contents are much higher in the Mackenzie Delta region. Ice wedges and tabular bodies of ground ice are widespread in the Delta, but neither have been reported from the Tibetan Plateau. This relates to differences in glacial history between the two areas. During the Quaternary, the Tibetan Plateau remained unglaciated, with valley glaciers rarely extending far from the surrounding mountain ranges. This has meant that there has been little water for the formation of massive ice on the Plateau. By contrast, the Mackenzie Delta region has been glaciated, and, during retreat, the glaciers provided meltwater to the thick unconsolidated deltaic sediments. Thus, conditions favoured the formation of massive ground ice, ice wedges, and pingos in the Mackenzie Delta region. However, pingos on the Plateau are rare and usually associated with faults and geological irregularities.

7.2 Geothermal regime

The ground thermal regime is a major characteristic of the

permafrost conditions at any one site since it not only reflects the sensitivity and stability of permafrost to thermal disturbances, but also contains information on permafrost thermal history.

In both areas, the active layer operates in a similar manner during the spring thaw and the fall freeze-back, except that it starts to thaw roughly a month earlier on the Plateau than in the Mackenzie Delta. Temperature data from Inuvik, N.W.T., show a better development of the 'zero curtain' phenomenon.

Plateau permafrost is both warmer and thinner than that in the Mackenzie Delta region. This is primarily because of the higher amount of solar radiation on the Plateau. Deep ground temperature data indicate a warming trend at the permafrost table for the Pleistocene Coastal Plain and a cooling trend for the Modern Delta. The warming is perhaps caused by large scale climatic change, while the cooling by site-specific factors such as channel shifting and sedimentation which are irrelevant to large scale climatic event. Boreholes on the Qinghai-Xizang (Tibet) Plateau are not deep enough for similar geothermal history studies. Data which are available indicate that the geothermal gradient on the Plateau is twice as high as in the Mackenzie Delta region. This is because the Plateau is geologically young and active. The present thickness of permafrost on the Plateau is in equilibrium with thermal conditions, implying that the permafrost on the Plateau is not relict. However, the actual thickness of permafrost in some areas of the Pleistocene Mackenzie Delta is much greater than the

equilibrium thickness. Therefore, relict permafrost exists in the Delta region.

7.3 Geothermal disturbances

Faults constitute the most important and powerful geothermal disturbances to permafrost on the Tibetan Plateau. Along fault zones, permafrost is thinner and warmer; sometimes hot springs, taliks, and even pingos form. The effects of water bodies (ocean, lakes and river channels) and coastal retreat are more important in the Mackenzie Delta region. Sand accumulation on the ground surface of the Qinghai-Xizang (Tibet) Plateau causes an increase in ground temperature, sometimes an absence of permafrost. There, migratory sand dunes are the cause of transient geothermal regimes in the same way as shifting meandering channels influence ground temperatures on floodplains in the Mackenzie Delta.

7.4 *In situ* permafrost creep

Investigations of *in situ* permafrost creep in the West Valley indicate an average velocity of 0.16 cm/year at 2.8 m depth and 0.54 cm/year at 1.6 m depth. The creep velocities are greater than those of Arctic Canada, and in about the same range as those of the Mackenzie Valley. Inter-continental comparison of creep data suggests that climate is a dominant factor controlling the regional (large-scale) magnitude of creep, while other factors such as ground ice play a part at a local scale. Creep parameters were determined; and constitutive equations were established from the

field creep data for each of the three different depths (1.6 m, 2.2 m, and 2.8 m).

7.5 Limitations and future research

One limitation of the present study on *in situ* permafrost creep is its relatively short duration of measurements. As this project will continue into 1994 and 1995, the results reported here will be checked and compared with the long-term values. Future research on *in situ* permafrost creep should still focus upon the accumulation of the data base and comparisons with creep rates of non-permafrost regions so that a better knowledge of the controls over creep can be achieved.

If one assumes that the Tibetan Plateau is experiencing a climatic warming trend, permafrost would degrade. A consequence is that the ground surface will become drier. This will increase the intensity of eolian action and form a potential risk of desertification on the Tibet Plateau. Thus, one aspect of future research in Tibet is to investigate the relationships between global warming, permafrost, and desertification. For this purpose, deep boreholes are required.

Frost mounds are another periglacial phenomenonon on the Tibetan Plateau that merits further investigation. Is their origin all related to faults? How do they fit the North American classification of frost mounds proposed by J. Ross Mackay (1986b)?

7.6 Recommendations for casing selection

There are several types of casing available: plastic, aluminum alloy, fiberglass, and steel, each of which has distinctive properties. PVC (polyvinylchloride) casing tends to be brittle, especially at low temperatures. Aluminum alloy casing is subject to corrosion, and several cases of total corrosion within a period of a few months have been reported (Dunnicliff and Green 1988). Sometimes, the casing needs to be treated both inside and outside with proper coating.

Deformation in a distinct shear zone may cause bending of the casing, and excessive localized bending will prevent passage of probe. If substantial deformation is predicted, a large-diameter casing and small-diameter probe should be used. The greater is the diameter of a borehole, the more expensive is the drilling operation.

If the casing will be installed in deep boreholes, steel casing is preferred because plastic casing may be damaged by external pressure.

REFERENCES

ACGR 1988. Glossary of permafrost and Related Ground-Ice Terms. Permafrost Subcommittee, Association Committee on Geotechnical Research, National Research Council of Canada, 156 pp.

Allen, D., Michel, F. and Judge, A. 1988a. Palaeoclimate and permafrost in the Mackenzie Delta. In: Proceedings, Fifth International Conference on Permafrost. Trondheim, Norway, Tapir Publications, Vol.1, 33-38.

Allen, D.M., Michel, F.A., and Judge, A.S. 1988b. The permafrost regime in the Mackenzie Delta, Beaufort Sea region, N.W.T. and its significance to the reconstruction of the palaeoclimatic history. Journal of Quaternary Science, 3(1), 3-13.

An, Zhengyuan 1980. Formation and evolution of permafrost ice mounds the Qinghai-Xizang Plateau. Journal of Glaciology and pedology, 2(2): 25-30 (in Chinese).

Are, F.E. 1983. Thermal abrasion of coasts. In: Permafrost: Proceedings of Fourth International Conference on Permafrost, Fairbanks, Alaska. National Academy Press, Washington, D.C., 24-28.

Balkwill, H.R., Roy, K.J., Hopkins, W.S., and Sliter, W.V. 1974. Glacial features and pingos, Amund Ringnes Island, Arctic Archipelogo. Canadian Journal of Earth Sciences, 11, 1319-1325.

Barr, W. 1976. Retreating coasts and disappearing islands in the Arctic. Musk-Ox, 18, 103-111.

Benedict, J.B. 1970. Downslope soil movement in a Colorado alpine region: rates, processes, and climatic significance. Arctic

and Alpine Research, 2, 165-226.

Bennett, L.P. 1989. *In situ* creep of perennially cryotic ground, Rea Point, Eastern Melville Island, N.W.T. Unpublished Ph.D. thesis, University of Ottawa, 171 pp.

Bennett, L.P. and French, H.M. 1988. Observations on near-surface creep in permafrost, Eastern Melville Island, Arctic Canada. In: Permafrost, Proceedings of the Fifth International Conference on Permafrost, Trondheim, Norway, Tapir Publications, volume 2, 683-688.

Bennett, L.P. and French, H.M. 1990. *In situ* permafrost creep, Melville Island, and implications for global change. In: Proceedings of the Fifth Canadian Permafrost Conference, Quèbec City, Collection Nordicana, 54, 119-123.

Bennett, L.P. and French, H.M. 1991. Solifluction and the role of permafrost creep, Eastern Melville Island, N.W.T., Canada. Permafrost and Periglacial Processes, Vol. 3: 95-102.

Bozhinskiy, A.N. and Konishchev, V.N. 1982. On the possible formation mechanism of inclined ice wedges in the Yedoma sequence of North Yakutiya. (in Russian) Academy of Sciences of the USSR, Section of Glaciology and of the Soviet Geophysical Committee and Institute of Geography, Data of Glaciological Studies, Publication 43, 139-142.

Brown, R.J.E. 1967. Comparison of permafrost conditions in Canada and the USSR. The Polar Record, 13(87), 741-751.

Brown, R.J.E. 1969. Factors influencing discontinuous permafrost in Canada. In: The periglacial Environment (edited by Péwé,

T.L.), McGill-Queen's University Press, Montreal, 11-53.

Brown, R.J.E. 1970. Permafrost in Canada. University of Toronto Press, 234 p.

Brown, R.J.E. 1973. Ground ice as an initiator of landforms in permafrost regions. In: Proceedings, Third Guelph Symposium on Geomorphology, 1973. Geo Abstract Ltd., 25-42.

Brown, R.J.E. 1978. Influence of climate and terrain on ground temperatures in the continuous permafrost zone of northern Manitoba and Keewatin District, Canada. In: Proceedings of the Third International Conference on Permafrost, Edmonton, National Research Council of Canada, 15-21.

Brown, R.J.E. and Péwé, T.L. 1973. Distribution of permafrost in North America and its relationship to the environments: a review, 1963 to 1973. In: Permafrost, Proceedings of the Second International Conference on Permafrost, Yakutsk, U.S.S.R. National Academy Press, Washington, D.C., 2115, 71-100.

Brown, W.G., Johnston, G.H. and Brown, R.J.E. 1964. Comparison of observed and calculated ground temperatures with permafrost distribution under a northern lake. Canadian Geotechnical Journal, Vol. 1, 147-154.

Büdel, J. 1982. Climatic Geomorphology. Princeton University Press, Princeton, N.J., 443 pp.

Burn, C.R. 1989. Frost heave of subaqueous lake-bottom sediments, Mackenzie Delta, Northwest Territories. In: Current Research, Part D, Geological Survey of Canada, Paper 89-1D, 85-93.

Burn, C.R. 1990a. Implications for palaeoenvironmental reconstruction of recent ice-wedge development at Mayo, Yukon Territory. Permafrost and Periglacial Processes, Vol.1, 3-14.

Burn, C.R. 1990b. Frost heave in lake-bottom sediments, Mackenzie Delta, Northwest Territories. In: Proceedings of the Fifth Canadian Permafrost Conference, Quèbec city. Collection Nordicana, No. 54, 103-109.

Burns, B.M. 1973a. The Climate of the Mackenzie Valley - Beaufort Sea, Volume I, Environment Canada, Climatological Studies No. 24.

Burns, B.M. 1973b. The Climate of the Mackenzie Valley - Beaufort Sea, Volume II, Environment Canada, Climatological Studies No. 24.

Cheng, Guodong. 1979. Rock pingos. Journal of Glaciology and Cryopedology, 1(1): 49-50 (in Chinese).

Cheng, Guodong. 1982. The forming process of thick-layered ground ice. Scientia Sinica, Series B, Vol. 25, No. 7, 777-788.

Cheng, Guodong. 1983. The mechanism of repeated segregation for the formation of thick layered ground ice. Cold Regions Science and Technology, 8, 57-66.

Cheng, Guodong. 1988. Review and prospect of regional geocryology in China. Journal of Glaciology and Geocryology, Vol. 10, 296-299 (in Chinese).

Cheng Guodong and F. Dramis. 1992. Distribution of mountain permafrost and climate. Permafrost and Periglacial Processes, Vol. 3: 83-91.

Cheng, Guodong and Qiu, Guoqing. 1983. Classification of frost heave terrain on the Qinghai-Xizang Plateau. In: Professional papers on permafrost studies of the Qinghai-Xizang Plateau. Science Press, 12-22 (in Chinese).

Cheng, Guodong and Wang, Shaoling. 1982. On the zonation of high-altitude permafrost in China. Journal of Glaciology and Cryopedology, Vol. 4, 1-17 (in Chinese).

Cheng, Guodong and Wu, Bangjun. 1984. Approach to the mathematical model of zonality of high-altitude permafrost. Journal of Glaciology and Cryopedology, vol. 5, 1-8 (in Chinese).

Chinese Academy of Sciences, 1965. Permafrost Investigations along the Qinghai-Xizang Plateau. Science Press, Beijing, China, pp. 108 (in Chinese).

Cui, Zhijun, 1983. The Kunlun mountain type rock glaciers. In: Proceedings, Second National Conference on Frozen Ground of China, Gansu People's Publishing House, Lanzhou, China, 65-74 (in Chinese).

Dallimore, S.R., Kurfurst, P.J., and Hunter, J.A.M. 1988. Geotechnical and geothermal conditions of near-shore sediments, southern Beaufort Sea, Northwest Territories, Canada. In: Proceedings, Fifth International Conference on Permafrost, Trondheim-Norway, Tapir publications, volume 1, 127-131.

Ding, Dewen and Guo, Dongxin. 1982. Permafrost history, Qinghai-Xizang Plateau. In: Proceedings, Second Chinese Conference on Glaciology and Geocryology, Gansu People's Publishing House,

Lanzhou, 78-82 (in Chinese).

Ding, Dewen and Xu, Xuezu. 1982. Zonation parameters of frozen ground in China. In: Proceedings, First National Conference on Frozen Ground and glaciology of China, Science Press, Beijing 70-73 (in Chinese).

Dingman, S.L. and Koutz, F.R. 1974. Relations among vegetation, permafrost and potential insolation in central Alaska. Arctic and Alpine Research, Vol. 6, No. 1, 37-42.

Dredge, L.A. and Thorleifson, L.H. 1987. The Middle Wisconsinan history of the Laurentide Ice Sheet. Géographie physique et Quaternaire, Vol. XLI, No. 2, 215-236.

Du, Renhuan and Xie, Zicu. 1965. Periglacial geomorphological characteristics along the Qinghai-Xizang Highway. In: Permafrost Investigations along the Qinghai-Xizang Highway, Academia Sinica, Science Press, 44-60 (in Chinese).

Dunnicliff, J. and Green, G.E. 1988. Geotechnical instrumentation for monitoring field performance. John Wiley & Sons, 577pp.

Dyke, A.S. and Prest, V.K. 1986. Late Wisconsin and Holocene Retreat of the Laurentide Ice Sheet. Geological Survey of Canada, Map 1702A, Scale: 1:5,000,000.

Dyke, A.S. and Prest, V.K. 1987. Paleogeography of northern North America 18,000 to 5,000 years ago. Geological Survey of Canada, Map 1703A, Scale: 1:12,500,000.

Dyke, L.D. 1991. Temperature changes and thaw of permafrost adjacent to Richards Island, Mackenzie Delta, N.W.T. Canadian Journal of Earth Sciences, 28, 1834-1842.

Dylik, Jan. 1967. Solifluxion, congelifluction and related slope processes. Geografiska Annalar, 49,A, 167-177.

French, H.M. 1976. The periglacial environment. Longman, 309 pp.

French, H.M. 1988. Active layer processes. In: Advances in periglacial geomorphology (edited by M.J. Clark). John Wiley & Sons, U.K., 151-177.

French, H.M. and Gozdzik, J.S. 1988. Pleistocene epigenetic and syngenetic frost fissures, Belchatow, Poland. Canadian Journal of Earth Sciences, 25, 2017-2027.

French, H.M. and Harry, D.G. 1990. Observations on buried glacier ice and massive segregated ice, Western Arctic Coast, Canada. Permafrost and Periglacial Processes, Vol. 1, 31-44.

Fujino, K., Sato, S., Matsuda, K., Shimuzi, O. and Kato, K. 1988. Characteristics of the massive ice body in the Western Canadian Arctic related to palaeoclimatology. In: Fujino, K. (ed.) Characteristics of the massive ground ice in the Western Canadian Arctic related to palaeoclimatology, 1986-1987. Institute of Low Temperature Science, Hokkaido University, Kosoku Printing Centre, Sapporo, Japan, 10-23.

Fyles, J.G., J.A. Heginbottom, and V.N. Rampton. 1972. Quaternary geology and geomorphology, Mackenzie Delta to Hudson Bay. In: Guidebook, 24th International Geological Congress, Field excursion A30, 23 pp.

Gasanov, Sh.Sh. 1981. Flow deformation of permafrost in ice-ground system. (in Russian) Academy of Sciences of the USSR, Section of Glaciology and Soviet Geophysical Committee and Institute

of Geography, Data of glaciological studies, Publication 41, 55-58.

Geothermal Research Group, 1978. Investigations on geothermal energy. Geothermal monograph. Institute of Geology, Academia Sinica, Science Press, Beijing, 34 pp (in Chinese).

Glen, J.W. 1952. Experiments on the deformation of ice. Journal of Glaciology, 1(12), 111-114.

Glen, J.W. 1955. The creep of polycrystalline ice. Proceedings of the Royal Society of London, Series A, Vol. 228, 519-538.

Gold, L.W. and Lachenbruch, A.H. 1973. Thermal conditions in permafrost: A review of North American literature. in: Proceedings of the Second International Conference on Permafrost, Yakutsk, USSR, July 1973, North American contribution, National Academy of Sciences, Washington, 2115, 3-25.

Goodrich, L.E. 1978. Some results of a numerical study of ground thermal regimes. In: Proceedings of the Third International Conference on Permafrost, Edmonton, Canada, National Research Council of Canada, 30-34.

Guo, Dongxin 1979. Sand wedges on the Qinghai-Xizang Plateau, Journal of Glaciology and Cryopedology, 1, 51 (in Chinese).

Guo, Dongxin. 1981. An Introduction to the permafrost map along the Qinghai-Xizang Highway. Journal of Glaciology and Cryopedology, Vol. 3, 77 (in Chinese).

Guo, Dongxin. 1985. Influence of geologic structure of permafrost. Scientia Geographica, 5(2): 98-105 (in Chinese).

Guo, Dongxin, 1988. Some progress and existing problems in historical geocryology in China. Journal of Glaciology and Geocryology, 10(3), 300-303 (in Chinese).

Guo, Dongxin, Huang Yizhi, Xu Shuying and Zhang Linyuan. 1982. Taliks in the Buqu river valley area, north slope of Tangula Mountain. In: Proceedings, First Chinese Conference on Glaciology and Geocryology, Science Press, Beijing, 11-18 (in Chinese).

Guo, D-X. and Li, S-D. 1982. Formation and history of thick-layered ground ice, Fenghuo Shan area, Qinghai-Xizang Plateau. In: Proceedings of the Second Chinese Conference on Glaciology and Geocryology, 60-66 (in Chinese).

Haeberli, W. 1985. Creep of mountain permafrost: internal structure and flow of alpine rock glaciers. Mitteilungen der Versuchsanstalt fur Wasserbau, Hydrologie und Glaziologie, Nr. 77, Zurich, 142 pp.

Harris, S.A. 1986. The permafrost environment. Croom Helm, Beckenham, Kent, 276 pp.

Harris, S.A. 1988. The alpine periglacial zone. in: Advances in periglacial geomorphology (ed. M.J. Clark), John Wiley & Sons Ltd, U.K., 369-413.

Harris, S.A. 1989. Continentality Index: its uses and limitations applied to permafrost in the Canadian Cordillera. Physical Geography, 13, 367-390.

Harris, S.A. and A.E. Corte. 1992. Interactions and relations between mountain permafrost, glacier, snow and water.

Permafrost and Periglacial Processes, Vol. 3: 103-110.

Harry, D.G., French, H.M., and Clark, M.J. 1983. Coastal conditions and processes, Sachs Harbour, Banks Island, Western Canadian Arctic. Zeitschrift fur Geomorphologie, N.F., Supplementband 47, 1-26.

Harry, D.G., French, H.M. and Pollard, W.H. 1988. Massive ground ice and ice-cored terrain near Sabine Point, Yukon Coastal Plain. Canadian Journal of Earth Sciences, 25, 1846-1856.

Harry, D.G. and Gozdizk, J.S. 1988. Ice wedges: growth, thaw transformation, and palaeoenvironmental significance. Journal of Quaternary Science, 3 (1), 39-55.

Heginbottom, J.A. and Tarnocai, C. 1983. Mackenzie Delta and Inuvik. In: Guidebook to permafrost and related features of the northern Yukon Territories and Mackenzie Delta, Canada (edited by French, H.M. and J.A. Heginbottom). Guidebook No. 3, Fourth International Conference on Permafrost, Fairbanks, Alaska, 113-146.

Heim, Arnolad. 1936. The glaciation and solifluction at Minya Gongkar. Geographical Journal, Vol. 87, 444-454.

Heim, A. and Gansser, A. 1939. Central Himalaya: geological observations of the Swiss expedition 1936. Kommissionsverlag Von Gebruder Fretz A.G. Zürich, pp. 246.

Hooke, R.L. 1981. Flow law for polycrystalline ice in glaciers: comparison of theoretical predictions, laboratory data, and field measurements. Reviews of Geophysics and Space Physics. VOL. 19, 664-672.

Hu, Haitao and Xu, Gueisen. 1982. The control of geological structures over groundwater on the Qinghai-Xizang Plateau. In: Professional Geological Papers on the Qinghai-Xizang Plateau (5)-Hydrogeology and Engineering Geology. Geological Publishing House of China, Beijing, 130-144 (in Chinese).

Huang, Y.-Z. 1991. Desertification of the permafrost zone on the Qinghai-Xizang (Tibet) Plateau. Encyclopedic Knowledge, 6, 48-49.

Huang, Y-Z. and Mi, F-R. 1983. Geological structure and permafrost thickness, Fenghuo Shan area, Qinghai-Xizang Plateau. Journal of Glaciology and Geocryology, 5(1), 55-62 (in Chinese).

Hume, J.D., Schalk, M., and Hume, P.W. 1972. Short-term climatic changes and coastal erosion, Barrow, Alaska. Arctic, Vol. 25, 272-278.

Hunter, J.A. 1988. Permafrost aggradation on arctic coasts of North America. In: Permafrost, Proceedings of the Fifth International Conference on Permafrost, Trondheim, Norway, Tapir Publications, Vol. 3, 27-33.

Hunter, J.A.M., Judge, A.S., MacAulay, H.A., Good, R.L., Gagne, R.M., and Burns, R.A. 1976. The occurrence of permafrost and frozen subsea bottom materials in the southern Beaufort Sea. Canada Department of Environment, Beaufort Sea project Technical report no.22, 174 pp.

Ives, J.D. 1973. Permafrost and its relationship to other environmental parameters in a mid-latitude, high-altitude setting, Front Range, Colorado Rocky Mountains. In:

Permafrost, Second International Conference on Permafrost, North America Contribution. National Academy of Sciences, Washington, 2115, 121-125.

Jahn, Alfred. 1975. Problems of the periglacial zone (Zagadnienia strefy peryglacjalnej). Warsaw, Panstwowe Wydawnictwo Naukowe, 223 pp.

Johnston, G.H. and Brown, R.J.E. 1963. Effect of a lake on distribution of permafrost in the Mackenzie River Delta. In: Proceedings, First Canadian Conference on Permafrost (17 and 18 April 1962), Associate Committee on Soil and Snow Mechanics, National Research Council of Canada, 218-225.

Johnston, G.H. and Brown, R.J.E. 1964. Some observations on permafrost distribution at a lake in the Mackenzie Delta, N.W.T., Canada. Arctic, 17, 162-175.

Judge, A.S. 1973. Thermal regime of the Mackenzie Valley. Information Canada 177 pp.

Judge, A.S., Taylor, A.E. and Burgess, M. 1979. Canadian Geothermal Data Collection--Northern Wells 1977-78, Geothermal Series Number 11, Earth Physics Branch, Energy,Mines and Resources Canada, 188 pp.

Kou, Yuguan, Zeng, Qunzhu, Xie, W.-R., and Xian, S. 1982. Investigation of global radiation on the Qinghai-Xizang Plateau. In: Lanzhou Institute of Glaciology and Geocryology, Memoir No. 3, 1-12 (in Chinese).

Kuhle, M. 1985. Glaciation research in the Himalayas: a new ice age theory. Universitas, 27(4), 281-294.

Kreyszig, E. 1966. Advanced engineering mathematics. John Wiley and Sons, 777 pp.

Kudryavtsev, V.A. 1959. Temperature, thickness and discontinuity of permafrost. In: Principle of geocryology, Part I, General Geocryology, Chapter VIII. USSR Academy of Sciences, V.A. Obruchev Institute of Permafrost Study, Moscow, National Research Council of Canada, Technical translation, 1187.

Kudryavtsev, V.A. 1961. Znachyene myerzlotno-temperaturnoy zonalinochi v formirovani singyenetitseckoy myerzloy tolistoy tyekstury. sp. Merzlotni isslyedovania, vip.I., Izd-vo MGU (in Russian).

Kudryavtsev, V.A. 1978. General geocryology, Moscow State University, 463 pp (in Russian).

Lachenbruch, A.H. 1957a. Thermal effect of the ocean on permafrost; Bulletin of the geological Society of America, Vol.68, 1515-1530.

Lachenbruch, A.H. 1957b. Three-dimensional heat conduction in permafrost beneath heated buildings; U.S. Geological Survey, Washington, D.C., Bulletin, 1052-B, 19 pp.

Lachenbruch, A.H. 1959. Periodic heat flow in a stratified medium with application to permafrost problems. U.S. Geological Survey, Bulletin, #1083-A, 36 pp.

Lachenbruch, A.H., Greene, G.W. and Marshall, B.V. 1966. Permafrost and the geothermal regimes. In: Environment of the Cape Thompson region, Alaska: USAEC Division of Technical Information, 149-165.

Lachenbruch, A.H. 1968. Permafrost. in: Encyclopedia of Geomorphology, (edited by R.W. Fairbridge), 833-839.

Lachenbruch, A.H. and Marshall, B.V., 1969. Heat flow in the Arctic. Arctic, Vol.22, 300-311.

Lachenbruch, A.H. and Marshall, B.V., 1977. Sub-sea temperature and a tentative model for offshore permafrost at Prudhoe Bay, Alaska. United States Department of the Interior Geological Survey, Open-file report 77-395, 54 pp.

Lachenbruch, A.H., Sass, J.H., Marshall, B.V. and Moses, T.H. Jr., 1982. Permafrost, heat flow, and the geothermal regime at Prudhoe Bay, Alaska. Journal of Geophysical Research, Vol.87, 9301-9316.

Lachenbruch, A.H. and Marshall, B.V., 1986. Changing climate: geothermal evidence from permafrost in the Alaskan Arctic. Science, Vol.234, 7 November, 689-696.

Lachenbruch, A.H., Cladouhos, T.T. and Saltus, R.W., 1988. Permafrost temperature and the changing climate. In: Permafrost, Fifth International Conference on Permafrost, Trondheim, Norway, Tapir Publications Vol. 3, 9-17.

Ladanyi, B. and Johnston, G.H. 1973. Evaluation of *in situ* creep properties of frozen soils with the pressuremeter. In: Proceedings of the Second International Conference on Permafrost, Yakutsk, U.S.S.R., North American Contribution, National Academy of Sciences, Washington, 2115, 310-317.

Lambert, J.D.H. 1972. Vegetation patterns in the Mackenzie Delta area, N.W.T. In: Mackenzie Delta Area Monograph (edited By

D.E. Kerfoot), 51-68.

Lanzhou Institute of Glaciology and Geocryology. 1982a. Proceedings of the First National Conference on Glaciology and Frozen Ground (frozen ground volume), Science Press, Beijing, 206 pp (in Chinese).

Lanzhou Institute of Glaciology and Geocryology. 1982b. Thermal conditions for the development of permafrost and glaciers in West China. Memoir 3, Science Press, Beijing, 120 pp (in Chinese).

Lanzhou Institute of Glaciology and Geocryology. 1983a. Proceedings of the Second Chinese Conference of Frozen Ground, Gansu People's Publishing House, Lanzhou, Gansu 493 pp (in Chinese).

Lanzhou Institute of Glaciology and Geocryolog Professional papers on permafrost studies of the Qinghai-Xizang Plateau, Science Press, Beijing, 269 pp (in Chinese).

Lanzhou Institute of Glaciology and Geocryology. 1988. Map of snow, ice and frozen ground in China (1:4,000,000). With explanatory notes. China Cartographic Publishing House.

Lanzhou Institute of Glaciology and Geocryology. 1989a. Interaction among temperature, moisture and stress fields in frozen soil. Lanzhou University Press, Lanzhou, China, 292 pp (in Chinese).

Lanzhou Institute of Glaciology and Geocryology 1989b. Proceedings of the Third Chinese Conference on Frozen Ground (held in Harbin, 1986). Science Press, Beijing, 215 pp (in Chinese).

Lanzhou Institute of Glaciology, Geocryology, and Desert Research, 1975. Permafrost. Science Press, Beijing, 124 pp (in Chinese).

Liang, Fengxian and Cheng, Guodong 1984. Polygon-veins along the Qinghai-Xizng Highway. Journal of Glaciology and Geocryology, 6(4), 49-60 (in Chinese).

Lewkowicz, A.G. 1988. Slope processes. In: Advances in Periglacial Geomorphology (ed. M.J. Clark), John Wiley & Sons Ltd, U.K., 325-368.

Li, Jijun, Wen, Shixuan, Zhang, Qingsong, Wang, Fubao, Zheng, Benxing, and Li, Bingyuan. 1979. Time and magnitude of the uplift of the Qinghai-Xizang Plateau. Scientia Sinica (series B), 6, 608-616 (in Chinese).

Li, Lie, 1982. Physical-chemical characteristics of ground ice, Fenghuo Shan area, Qinghai-Xizang Plateau, China (Abstract,in Chinese). In: Proceedings, First National Conference on Glaciology and Geocryology (permafrost volume), Science Press, Beijing, 54-59 (in Chinese).

Li. Lie and Xing. Zemin. 1980. Preliminary studies on ground ice characteristics of Fenghuo Shan area, Qinghai-Xizang Plateau. Journal of Glaciology and Cryopedology, Vol. 2, 31-35 (in Chinese).

Li, Shude 1982. Permafrost temperature and thickness, Qinghai-Xizang Plateau. In: Proceedings, Second Chinese Conference on Glaciology and Geocryology, Gansu People's Publishing House, Lanzhou, Gansu, 7-10 (in Chinese).

Mackay, J.R. 1962. Pingos in the Pleistocene Mackenzie Delta area. Geographical Bulletin, 18, 21-63.

Mackay, J.R. 1963a. The Mackenzie Delta area, N.W.T. Geographical

Branch, Memoir 8, 202 pp.

Mackay, J.R. 1963b. Notes on the shoreline recession along the coast of Yukon Territory. Arctic, 16, 195-197.

Mackay, J.R. 1971. The origin of massive icy beds in permafrost, western Arctic coast, Canada. Canadian Journal of Earth Sciences, 8, 397-422.

Mackay, J.R. 1972. Offshore permafrost and ground ice, southern Beaufort Sea, Canada. Canadian Journal of Earth Sciences, 9(11), 1550-1561.

Mackay, J.R. 1973. The growth of pingos, western Arctic coast, Canada. Canadian Journal of Earth Sciences. 10,979-1004.

Mackay, J.R. 1975. Freezing processes at the bottom of permafrost, Tuktoyaktuk Peninsula area, District of Mackenzie (107C). Geological Survey of Canada, Paper 75-1, Part A: 471-474.

Mackay, J.R. 1978. Quaternary and permafrost features, Mackenzie Delta area. In: International Conference on Facts and Principles of World Oil Occurrence. Geological and geographical guide to the Mackenzie Delta area (edited by F.G. Young), CSPG Publication, Calgary, 42-50.

Mackay, J.R. 1979. Pingos of the Tuktoyaktuk Peninsula area, Northwest Territories. Gèographie physique et Quaternaire, 33: 3-61.

Mackay, J.R. 1981. Active layer slope movement in a continuous permafrost environment, Garry Island, Northwest Territories, Canada. Canadian Journal of Earth Sciences, 18, 1666-1680.

Mackay, J.R. 1983. Downward water movement into frozen ground,

western arctic coast, Canada. Canadian Journal of Earth Sciences, 20, 120-134.

Mackay, J.R. 1986a. Fifty years (1935 to 1985) of coastal retreat west of Tuktoyaktuk, District of Mackenzie. In: Current Research, Part A, Geological Survey of Canada, Paper 86-1A, 727-735.

Mackay, J.R. 1986b. Frost mounds. The Canadian Geographers, 30 (4), 363-364.

Mackay, J.R. 1987. Pingos of the western Arctic coast, Canada. Ymer'87, Swedish Society of Anthropology and Geography, Vol. 107, 155-170.

Mackay, J.R. 1988. Pingo collapse and paleoclimatic reconstruction. Canadian Journal of Earth Sciences, 25, 495-511.

Mackay, J.R. 1989. Massive ice : some field criteria for the identification of ice types. In: Current Research, Part G, Geological Survey of Canada, Paper 89-1G, 5-11.

Mackay, J.R. 1990a. Some observations on the growth and deformation of epigenetic, syngenetic and antisyngenetic ice wedges. Permafrost and Periglacial Processes, 1, 15-30.

Mackay, J.R. 1990b. Seasonal growth bands in pingo ice. Canadian Journal of Earth Sciences, 27, 1115-1125.

Mackay, J.R. 1992. Lake stability in an ice-rich permafrost environment: examples from the western Arctic coast. In (eds. R.D. Robarts and M.L. Bothwell) Aquatic Ecosystem in Semi-arid Regions: Implications for Resource Management, N.H.R.I. Symposium Series 7, Environment Canada, Saskatoon, 1-26.

Mackay, J.R. and Black, R.F. 1973. Origin, composition, and structure of perennially frozen ground and ground ice: a review. In: Permafrost: North America contribution to the Second International Conference on Permafrost, National Academy of Sciences, Washington, 2115, 185-192.

Mackay, J.R. and Dallimore, S.R. 1992. Massive ice of the Tuktoyaktuk area, western Arctic coast, Canada. Canadian Journal of Earth Sciences, 29, 1235-1249.

Mackay, J.R. and MacKay, D. 1974. Snow cover and ground temperatures, Garry Island, N.W.T. Arctic, Vol. 27, 287-296.

Mackay, J.R. and MacKay, D.K. 1976. Cryostatic pressures in nonsorted circles (mud hummocks), Inuvik, Northwest Territories. Canadian Journal of Earth Sciences, 13(7), 889-897.

Mackay, J.R., J. Ostrick, C.P. Lewis, and D.K. MacKay. 1979. Frost heave at ground temperatures below 0°C, Inuvik, Northwest Territories. In: Current Research, Part A, Geological Survey of Canada, Paper 79-1A, 403-405.

Mackay, J.R., Rampton, V.N. and Fyles, J.G. 1972. Relic Pleistocene permafrost, Western Arctic, Canada. Science, 176, No. 4041, 1321-1323.

McRoberts, E.C. 1975. Some aspects of a simple secondary creep model for deformations in permafrost slopes. Canadian Geotechnical Journal, 12, 98-105.

McRoberts, E.C. 1988. Secondary creep interpretation of ice-rich permafrost. In: Permafrost: Proceedings of the Fifth

International Conference on Permafrost, Trondheim, Norway, Tapir Publications, 2: 1137-1142.

McRoberts, E.C., Law, T.C., and Murray, T.K. 1978. Creep tests on undisturbed ice-rich silt. In: Proceedings of the Third International Conference on Permafrost, Edmonton, Canada, National Research Council of Canada, 540-545.

Meier, M.F. 1960. Model of flow of Saskatchewan glacier, Alberta, Canada. U.S. Geological Survey Professional Paper, 351.

Melnikov, P.I. and Tolstikhin, O.N. 1988. General Geocryology (Chinese version). The USSR Academy of Sciences, Siberian Branch. USSR Academy of Sciences, Siberian Branch, Novosibirsk. Translated by Lanzhou Institute of Glaciology and Geocryology, Science Press, Beijing, 318 pp.

Molochushkin, E.N. 1978. The effect of thermal abrasion on the temperature of the permafrost in the coastal zone of the Laptev Sea. In: Permafrost, Second International Conference, USSR contribution, National Academy Press, 90-93.

Morgenstern, N.R. 1981. Geotechnical engineering and frontier resource development. Geotechnique, 31, 305-365.

Morgenstern, N.R. 1985. Recent observations on the deformation of ice and ice-rich permafrost. In: Field and theory: Lectures in geocryology (eds: M. Church and O. Slaymaker), University of British Columbia, Vancouver, 133-153.

Morgenstern, N.R., Roggensack, W.D., and Weaver, J.S. 1980. The behaviour of friction piles in ice and ice-rich soils. Canadian Geotechnical Journal, 17, 405-415.

Nixon, J.F. 1978. Foundation design approaches in permafrost areas. Canadian Geotechnical Journal, 15, 96-112.

Nixon, J.F. 1986. Thermal simulation of subsea permafrost. Canadian Journal of Earth Sciences, 23, 2039-2046.

Nixon, J.F. 1990. Seasonal and climatic warming effects on pile creep in permafrost. In: Proceedings of the Fifth Canadian Permafrost Conference, Quèbec City, Collection Nordicana, 54, 335-340.

Nixon, J.F. and McRoberts, E.C. 1976. A design approach for pile foundations in permafrost. Canadian Geotechnical Journal, 13, 40-57.

Nixon, J.F. and Neukirchner, R.J. 1984. Design of vertical and laterally loaded piles in saline permafrost. In: Proceedings of the Third International Specialty Conference: Cold Regions Engineering, Vol. 1, 131-144.

Nuekirchner, R.J. and Nixon, J.F. 1987. Behaviour of laterally loaded piles in permafrost. Journal of Geotechnical Engineering, Vol. 113, 1-14.

Novikov, V.N. and Fedorova, Ye.V. 1989. Coastal erosion in the southeastern part of the Barents Sea. Polar Geography and Geology, 13(1), 46-50.

Odell, N.E. 1925. Observations on the rocks and glaciers of Mt. Everest. The Geographical Journal, Vol. 66, 289-315.

Osterkamp, T.E. 1975. A conceptual model of offshore permafrost. Geophysical Institute, University of Alaska, Fairbanks, Report AG R-234.

Osterkamp, T.E. and Harrison, W.D. 1982. Temperature measurements in subsea permafrost off the coast of Alaska. In: The Roger J.E. Brown Memorial Volume: Proceedings of the Fourth Canadian Permafrost Conference (ed. H.M. French), National Research Council of Canada, 238-248.

Parameswaran, V.R. 1982. Strength and deformation of frozen saturated sand at -30°C. Canadian Geotechnical Journal, 19, 104-107.

Paterson, W.S.B. 1977. Secondary and tertiary creep of glacier ice as measured by borehole closure rates. Reviews of Geophysics and Space Physics, Vol. 15, 47-55.

Péwé, T.L. 1983. Alpine permafrost in the contiguous United States: a review. Arctic and Alpine Research, 15(2), 145-156.

Phukan, A. 1985. Frozen Ground Engineering. Prentice-Hall, Inc., 333 pp.

Pissart, A. 1967. Les pingos de l'Ile Prince Patrick (76°N-120°W). Geographical Bulletin, 9, 189-217.

Pollard, W.H. and French, H.M. 1980. A first approximation of the volume of ground ice, Richards Island, Pleistocene Mackenzie Delta, Northwest Territories, Canada. Canadian Geotechnical Journal, 17, 509-516.

Price, L.W. 1972. The periglacial environment, permafrost, and man. Association of American Geographers, Comm. on College Geography Resource Paper 14, 88pp.

Proceedings, Fifth Canadian Permafrost Conference, Québec city, June, 1990. National Research Council of Canada, and Centre

d'etudes nordiques, Universite Laval, Collection Nordicana, No. 54, 424 pp.

Pu, Q-Y., Wu, X-H, and Qian, F. 1982. Historical change of permafrost along the Qinghai-Xizang Highway. In: Proceedings of the Second Chinese Conference on Glaciology and Geocryology, 74-77 (in Chinese).

Qinghai-Xizang Highway Research Group, 1983, Distribution of ice-rich permafrost along the Qinghai-Xizang Highway. In: Proceedings, Second National Conference on Frozen Ground, Gansu People's Publishing House, Lanzhou, Gansu, 43-51 (in Chinese).

Qiu, Guoqing. 1980. Problems in permafrost engineering geological survey in the western mountain and plateau areas. Journal of Glaciology and Cryopedology, vol. 2, 17-23 (in Chinese).

Qiu, G-Q. 1982. Distribution of taliks in the Tuo-tuo river basin, Qinghai-Xizang Plateau. In: Proceedings, Second Chinese Conference on Glaciology and Geocryology, 19-28 (in Chinese).

Qiu, Guoqing and Guo, Dongxin. 1983. Taliks along the Qinghai-Xizang Highway. In: Professional papers on permafrost on the Qinghai-Xizang Plateau, Science Press, Beijing, 30-37 (in Chinese).

Rampton, V.N. 1972. An outline of the Quaternary geology of the lower Mackenzie Region. In: Mackenzie Delta area monograph (ed. D.E. Kerfoot), Brock University, 7-14.

Rampton, V.N. 1974. The influence of ground ice and thermokarst upon the geomorphology of the Mackenzie-Beaufort region. In:

Research in Polar and Alpine Geomorphology (eds. B.D. Fahey and R.D. Thompson). Proceedings, Third Guelph Symposium on Geomorphology, 43-59.

Rampton, V.N. 1988. Quaternary geology of the Tuktoyaktuk Coastlands, Northwest Territories. Memoir 423, Geological Survey of Canada, 98 pp.

Reimnitz, E. and Maurer, D.K. 1979. Effect of storm surges on the Beaufort Sea Coast, northern Alaska; Arctic, Vol. 32, 329-344.

Ritchie, J.C. 1972. Pollen analysis of late-Quaternary sediments from the arctic treeline of the Mackenzie Delta region, N.W.T. In: Mackenzie Delta Area Monograph (edited by Kerfoot, D.E.). Brock University, 29-50.

Ritchie, J.C. 1984. Past and Present Vegetation of the Far Northwest Canada. University of Toronto Press, 251 pp.

Romanovskiy, N.N. 1973. Regularities in formation of frost-fissures and development of frost-fissure polygons. Biuletyn Periglacjalny, 23, 237-277.

Savage, J.C. and Paterson, W.S.B. 1963. Measurements of the Athabasca Glacier relating to the flow of ice. Journal of Physical Research, 68 (15), 4521-4543.

Savigny, K.W. 1980. *In situ* analysis of naturally occurring creep in ice-rich permafrost soil. Ph.D. thesis, University of Alberta, Edmonton, Alberta, 439 pp.

Savigny, K.W. and Morgenstern, N.R. 1986a. Geotechnical conditions of slopes as a proposed pipeline crossing, Great Bear River valley, Northwest Territories. Canadian Geotechnical Journal,

23, 490-503.

Savigny, K.W. and Morgenstern, N.R. 1986b. *In situ* creep properties in ice-rich permafrost soil. Canadian Geotechnical Journal, 23, 504-514.

Savigny, K. W. and Morgenstern, N.R. 1986c. Creep behaviour of undisturbed clay permafrost. Canadian Geotechnical Journal, 23, 515-527.

Sellmann, P.V., Delaney, A.J., Champlain, E.J. and Dunton, K.H. 1992. Seafloor temperature and conductivity data from Steffansson Sound, Alaska. Cold Regions Science and Technology, 20, 271-288.

Shang, Jianyi. 1982. Some characteristics of permafrost along the Qinghai-Xizang Plateau. In: Proceedings of the First Chinese Conference on Glaciology and Frozen Ground (Frozen Ground Volume), Science Press, Beijing, 38-43 (in Chinese).

Shi, Yafeng. 1988. Review and lessons of the last thirty years. Journal of Glaciology and Geocryology, Vol. 10, 201-214 (in Chinese).

Shi, Yafeng, Zheng, Benxing and Li, Shijie 1990. Last glaciation and maximum glaciation on the Qinghai-Xizang Plateau. Journal of Glaciology and Geocryology, 12(1), 1-29 (in Chinese).

Skinner and Porter, 1989. Physical geology. John Wiley & Sons, pp. 750.

Smith, D.J. 1988. Rates and controls of soil movement on a solifluction slope in the Mt. Rae area, Canadian Rocky Mountains, Zeitschrift für Geomorphologie Supplemenband, 71,

25-44.

Smith, D.J. 1992. Long-term rates of contemporary solifluction in the Canadian Rocky Mountains. In: Periglacial Geomorphology (edited by Dixon, J.C. and A.D. Abrahams), John Wiley and Sons Ltd, 203-221.

Smith, M.W. 1972. Observed and predicted ground temperature, Mackenzie Delta, N.W.T. In: Mackenzie Delta Area Monograph (ed. D.E. Kerfoot), Brock University, 95-106.

Smith, M.W. 1975a. Microclimatic influences on ground temperatures and permafrost distribution, Mackenzie Delta, Northwest Territories. Canadian Journal of Earth Sciences, 12, 1421-1438.

Smith, M.W. 1975b. Numerical simulation of microclimatic and active layer regimes in a High Arctic environment. Department of Indian and Northern Affairs, Ottawa, ALUR 74-75-72, 29 pp.

Smith, M.W. 1976. Permafrost in the Mackenzie Delta, N.W.T. Geological Survey of Canada. Paper 75-28, 34 pp.

Smith, M.W. 1985. Observations of soil freezing and frost heave at Inuvik, Northwest Territories, Canada. Canadian Journal of Earth Sciences, 22, 283-290.

Smith, R.C.T. 1953. Conduction of heat in the semi-infinite solid,with a short table of an important integral. Australian Journal of Physics, vol.6, 127-129.

Sun, X-B. 1965. Vegetation along the Qinghai-Xizang Highway. In: Permafrost investigations along the Qinghai-Xizang Highway, Science Press, 83-86 (in Chinese).

Tarnocai, C. and Hill, R.W. 1978. Earth hummocks and the Mackenzie Delta area. In: Guidebook for a tour of soil, permafrost and vegetation relationship, Eleventh Congress of the International Society of Soil Science, Edmonton, Canada, 70-78.

Taylor, A.E. and Judge, A.S. 1976. Canadian Geothermal Data Collection: Northern Wells 1975. Geothermal Survey of Canada, Geothermal Series Number 6, Earth Physics Branch, Energy, Mines and Resources Canada, 142 pp.

Taylor, A.E., Burgess, M. Judge, A.S. and Allen, V.S. 1982. Canadian Geothermal Data Collection--Northern Wells 1981. Geothermal Series Number 13, Earth Physics Branch, Energy, Mines and Resources Canada, 153 pp.

Thompson, E.C. and Sayles, F.H. 1972. In-situ creep analysis of room in frozen soil. Journal of soil mechanics and foundation division (ASCE) 98: 899-916.

Tong, Boliang. 1965. Permafrost conditions in the Xidatan area, Qinghai-Xizang Plateau. In: Permafrost investigations along the Qinghai-Xizang Highway, Science Press, 20-30 (in Chinese).

Tong, Boliang, Li, Shude, Pu, Jueying, Qiu, Guoqing, Wu, Ziwang, Cheng, Guodong, Guo, Dongxin, Wang, Jiachang, Wang, Shaoling, Liang Fengxian, Luo, Xiangrui, Yen, Shichong, and Ding, Linglong. 1982. Permafrost map along the Trans-Plateau Highway corridor. Shanghai Xinhua Press, Scale: 1:600,000.

Tong, Boliang and Li, Shude. 1983. Permafrost characteristics and factors affecting them, Qinghai-Xizang Plateau. In:

Professional paper on Qinghai-Xizang Plateau permafrost, Science Press, 1-11 (in Chinese).

Tong, Boliang, Li, Shude, Pu, Jueying and Qiu, Guoqing. 1983. Permafrost map (1:600,000) along the Qinghai-Xizang Plateau. In: Proceedings, Second Chinese Conference on Frozen Ground, Gansu People's Publishing House, Lanzhou, 75-80 (in Chinese).

Tong, Changjiang. 1982. Frost heaving force of foundation. In: Proceedings, First Chinese Conference on Glaciology and Frozen Ground, Science Press, 113-119 (in Chinese).

Tong, Changjiang. 1983. Tangential frost-heaving forces of soils and their classification. In: Professional papers on permafrost studies of the Qinghai-Xizang Plateau. China Science Press, Beijing, 75-79.

Tong. Changjiang and Yu, Chongyuen. 1983. Investigation on frost heave. In: Proceedings, Second Chinese Conference on Frozen Ground, 240-244 (in Chinese).

Troll, C. 1958. Structure soils, solifluction, and frost climates of the world. Translation 43, US Army Snow, Ice and Permafrost Research Establishment, Corps of Engineers, Wilmette, Illinois, pp. 121.

Tsytovich, N.A. 1975. The mechanics of frozen ground. New York: McGill-Hill Book Co., 426 pp.

Vigdorchik, M.E. 1980. Submarine permafrost on the Alaskan continental shelf; Boulder, Colorado, Westview Press, 118 pp.

Wagner, S. 1992. Creep of alpine permafrost, investigated on the Murtel rock glacier. Permafrost and Periglacial Processes,

Vol.3: 157-162.

Walker, H.J. 1988. Permafrost and coastal processes. In: Permafrost, Proceedings of the Fifth International Conference on Permafrost, Trondheim, Norway, Tapir Publications, Vol. 3, 35-42.

Wang, Baolai. 1984. Permafrost conditions in Fenghuo Shan area, Tibet Plateau: An internal fieldwork report, the Lanzhou Institute of Glaciology and Geocryology, 24 pp (in Chinese).

Wang, Jiacheng and Li, Shude. 1983. Thermal regime of near the permafrost base, along the Qinghai-Xizang Highway. In: Professional papers on Qinghai-Xizang Plateau permafrost. Science Press, 38-43 (in Chinese).

Wang. Jiacheng, Wang. Shaoling and Qiu, Guoqing. 1979. Permafrost along the Qinghai-Xizang Highway. Scientia Geographica, 34(1), 18-32 (in Chinese).

Wang, Shaoling. 1983a. The pingos along the Qinghai-Xizang Highway. In: Professional papers on permafrost studies of the Qinghai-Xizang Plateau. Science Press, 23-29 (in Chinese).

Wang, Shaoling. 1983b. Thermokarst along the Qinghai-Xiznag Highway. In: Second Chinese Conference on Frozen Ground. Science Press, 58-64 (in Chinese).

Wang, Shaoling. 1986. Types and characteristics of modern periglaciation along the Qinghai-Xizang Highway. Journal of Glaciology and Geocryology, 157-164 (in Chinese).

Wang, Shaoling 1989. Formation and evolution of permafrost on the Qinghai-Xizang Plateau since the Late Pleistocene. Journal of

Glaciology and Geocryology, 11(2), 69-75 (in Chinese).

Wang. Shaoling. 1990. Thaw slides and subsidence in Fenghuo Shan area, Qinghai-Xizang Plateau. Journal of Glaciology and Geocryology, Vol. 12, 63-70 (in Chinese).

Wang, Shaoling and Yao, Heqing. 1981. On the pingos along both banks of the Qing-Shui River on the Qinghai-Xizang Plateau. Journal of Glaciology and Cryopedology, 3(3): 58-62 (in Chinese).

Wang, Shaoling and Zhang, Weixin. 1985. Permafrost evolution since the late Pleistocene, Qingsui River region, Qinghai-Xizang Plateau. Journal of Glaciology and Geocryology, Vol. 7, 15-25 (in Chinese).

Wang, Yaqing. 1983. Moisture content and density of frozen soils. In: Professional papers on permafrost studies of the Qinghai-Xizang Plateau, Science Press, 60-66 (in Chinese).

Washburn, A.L. 1979. Geocryology, a survey of periglacial processes and environments. Edward Arnold, 406 pp.

Washburn, A.L. 1981. Permafrost features as evidence of climatic change. Earth Science Review, 327-402.

Williams, P.J. 1957. Sonme investigations into solifluction features in Norway. Geographical Journal, 123, 42-58.

Willaims, P.J. 1966. Downslope soil movement at a sub-arctic location with regard to variations with epth. Canadian Geotechnical Journal, 3, 191-203.

Williams, P.J. 1982. The surface of the earth: an introduction to geotechnical science. London, Longman, 212 pp.

Williams, P.J. and Smith, M.W. 1989. The frozen earth: fundamentals of geocryology. Cambridge University Press, 306 pp.

Wilson, S.D. 1970. Observational data on ground movements related to slope stability. ASCE Journal of the Soil Mechanics and Foundations Division, 96(SM5), 285-310.

Wu, Ziwang. 1965a. Ground water characteristics along the Qinghai-Xizang Highway. In: Permafrost investigations along the Qinghai-Xizang Highway, 61-72 (in Chinese).

Wu, Ziwang. 1965b. Chemical composition and structure of ground ice along the Qinghai-Xizang Highway. In: Permafrost investigations along the Qinghai-Xizang Plateau, 73-82 (in Chinese).

Wu, Ziwang. 1979. An engineering classification of permafrost. Journal of Glaciology and Cryopedology, Vol. 1, 52-60 (in Chinese).

Wu, Ziwang. 1982. Engineering classification of frozen ground. Journal of Glaciology and cryopedology, Vol. 4, 43-48 (in Chinese).

Wu, Ziwang, Liu Yongzhi and Zhang Jiayi. 1982. Experimantal studies on permafrost creep. In: Proceedings, First Chinese Confernece on Glaciology and Frozen Ground, 128-132 (in Chinese).

Wu, Ziwang, Zhang Jiayi and Liu Yongzhi. 1983a. *In situ* studies on the bearing capacity of permafrost. In: Professional papers on Qinghai-Xizang Plateau permafrost, Science Press, 112-119 (in Chinese).

Wu, Ziwang et al. 1983b. Experimental studies on the methods of

determining long-term strength. In: Professional papers on Qinghai-Xizang Plateau, Science Press, 120-123 (in Chinese).

Xie, Yingqen. 1982. Temperature conditions for the development of permafrost on the Qinghai-Xizang Plateau. In: Proceedings, First Chinese Conference on Glaciology and Frozen Ground, 1-6 (in Chinese).

Xie, Yingqen and Zeng, Quenzhu. 1983. Climatic conditions for the development of permafrost on the Qinghai-Xizang plateau. In: Proceedings, Second Chinese Conference on Frozen Ground, 13-20 (in Chinese).

Xu, Jinzhi, 1959. Physical geography of the Qinghai and Xizang (Tibet) (Vegetation of the Plateau: 49-51). Science Press, 91 pp.

Xu, Xiaozu, Fu, Liandi and Zhu, Linnan. 1981. Determination of permafrost table by latitude and altitude. in: Lanzhou Institute of Glaciology and Geocryology Memoir No.2, 17-25 (in Chinese).

Zeng, Q-Z, Kou, Y-G, Xie, W-R and Xian S. 1982. Investigations on radiation balance, Qinghai-Xizang Plateau. In: Lanzhou Institute of Glaciology and Geocryology Memoir 3, 32-52 (in Chinese).

Zhai, Rongting. 1982. Hot ground water along the Qinghai-Xizang Highway. In: Professional geological papers on the Qinghai-Xizang Plateau (5)--Hydrogeology and Engineering Geology, 72-81. (in Chinese).

Zhang, Y. and Cai, S-Q. 1981. Permafrost history on the Qinghai-

Xizang Plateau. Journal of Glaciology and Cryopedology, 3(1), 32-36 (in Chinese).

Zhang, Weixin. 1983. Sand wedges and their chronology along the Qinghai-Xizang Highway. In: Proceedings, Second Chinese Conference on Glaciology and Geocryology, 52-57 (in Chinese).

Zhou, Youwu. 1965. Permafrost along the Qinghai-Xizang Highway. In: Permafrost investigations along the Qinghai-Xizang Highway, Science Press, 1-19 (in Chinese).

Zhou, Youwu and Guo, Dongxin. 1982. Principal characteristics of permafrost in China. Journal of Glaciology and Geocryology, 4(1): 1-19 (in Chinese).

Zhou, Youwu and Guo, Dongxin. 1983. Some features of permafrost in China. In: Proceedings, Fourth International Conference on Permafrost, National Academy Press, Washington, 2115, 1496-1501.

Zhu, Yunlin and Zhang, Jiayi. 1982a. Thaw subsidence of permafrost. In: Proceedings, First Chinese Conference on Glaciology and Frozen Ground, 145-150 (in Chinese).

Zhu, Yunlin and Zhang, Jiayi. 1982b. Elastic and compressive deformation of frozen soil. Journal of Glaciology and Cryopedology, Vol. 4, 29-39 (in Chinese).

APPENDIX

IN SITU PERMAFROST CREEP DATA

Summary of creep data for the West Valley of Fenghuo Shan area, Tibet Plateau

			Site #1				
Sept. 26, 1991			Aavg=(A0-A180)/2		Bavg=(B0-B180)/2		
A0	A180	Aavg	Acum	B0	B180	Bavg	Bcum
-0.554	0.322	-0.438	-0.438	-0.622	0.547	-0.5845	-0.5845
-0.435	0.249	-0.342	-0.78	-0.573	0.476	-0.5245	-1.109
-0.405	0.192	-0.2985	-1.0785	-0.563	0.482	-0.5225	-1.6315
-0.38	0.142	-0.261	-1.3395	-0.525	0.429	-0.477	-2.1085
-0.402	0.169	-0.2855	-1.625	-0.499	0.425	-0.462	-2.5705

			Site #1				
November 5, 1991							
A0	A180	Aavg	Acum	B0	B180	Bavg	Bcum
-0.549	0.332	-0.4405	-0.4405	-0.634	0.553	-0.5935	-0.5935
-0.407	0.188	-0.2975	-0.738	-0.554	0.469	-0.5115	-1.105
-0.413	0.198	-0.3055	-1.0435	-0.552	0.472	-0.512	-1.617
-0.375	0.157	-0.266	-1.3095	-0.502	0.424	-0.463	-2.08
-0.383	0.17	-0.2765	-1.586	-0.516	0.444	-0.48	-2.56

			Site #1				
December 4, 1991							
A0	A180	Aavg	Acum	B0	B180	Bavg	Bcum
-0.5674	0.3076	-0.4375	-0.4375	-0.752	0.4431	-0.5976	-0.5976
-0.4371	0.1527	-0.2949	-0.7324	-0.7021	0.2954	-0.4988	-1.0963
-0.4639	0.1483	-0.3061	-1.0385	-0.6537	0.3652	-0.5095	-1.6058
-0.4374	0.1004	-0.2689	-1.3074	-0.6249	0.3156	-0.4703	-2.076
-0.5026	0.088	-0.2953	-1.6027	-0.6031	0.291	-0.4471	-2.5231

			Site #1				
March 8, 1992							
A0	A180	Aavg	Acum	B0	B180	Bavg	Bcum
-0.604	0.22	-0.412	-0.412	-0.842	0.34	-0.591	-0.591
-0.48	0.095	-0.2875	-0.6995	-0.76	0.252	-0.506	-1.097
-0.489	0.122	-0.3055	-1.005	-0.75	0.253	-0.5015	-1.5985
-0.459	0.062	-0.2605	-1.2655	-0.722	0.218	-0.47	-2.0685
-0.61	0.06	-0.335	-1.6005	-0.7	0.105	-0.4025	-2.471

			Site #1				
92-0510							
-0.6047	0.2303	-0.4175	-0.4175	-0.8575	0.3402	-0.5989	-0.5989
-0.4807	0.1025	-0.2916	-0.7091	-0.7731	0.2407	-0.5069	-1.1058
-0.4872	0.137	-0.3121	-1.0212	-0.7642	0.2527	-0.5085	-1.6142
-0.453	0.0783	-0.2657	-1.2869	-0.7305	0.2103	-0.4704	-2.0846

-0.573	0.0743	-0.3237	-1.6105	-0.7032	0.1229	-0.4131	-2.4977
92-06-09			Site #1				
-0.6072	0.254	-0.4306	-0.4306	-0.8604	0.3423	-0.6014	-0.6014
-0.4818	0.1238	-0.3028	-0.7334	-0.7753	0.2419	-0.5086	-1.11
-0.4876	0.141	-0.3143	-1.0477	-0.7793	0.2517	-0.5155	-1.6255
-0.4509	0.0864	-0.2687	-1.3164	-0.7342	0.2238	-0.479	-2.1045
-0.4831	0.064	-0.2736	-1.5899	-0.7019	0.1473	-0.4246	-2.5291
13/08/92			Site #1				
-0.607	0.273	-0.44	-0.44	-0.865	0.344	-0.6045	-0.6045
-0.482	0.142	-0.312	-0.752	-0.778	0.24	-0.509	-1.1135
-0.478	0.142	-0.31	-1.062	-0.784	0.249	-0.5165	-1.63
-0.449	0.113	-0.281	-1.343	-0.742	0.2	-0.471	-2.101
-0.436	0.101	-0.2685	-1.6115	-0.706	0.169	-0.4375	-2.5385
92-09-12			Site #1			920912	
-0.602	0.275	-0.4385	-0.4385	-0.878	0.332	-0.605	-0.605
-0.474	0.144	-0.309	-0.7475	-0.788	0.237	-0.5125	-1.1175
-0.474	0.146	-0.31	-1.0575	-0.806	0.25	-0.528	-1.6455
-0.455	0.129	-0.292	-1.3495	-0.756	0.193	-0.4745	-2.12
-0.433	0.105	-0.269	-1.6185	-0.728	0.19	-0.459	-2.579
921105			Site #1				
-0.609	0.268	-0.4385	-0.4385	-0.864	0.343	-0.6035	-0.6035
-0.465	0.148	-0.3065	-0.745	-0.814	0.225	-0.5195	-1.123
-0.481	0.173	-0.327	-1.072	-0.848	0.224	-0.536	-1.659
-0.457	0.118	-0.2875	-1.3595	-0.768	0.166	-0.467	-2.126
-0.48	0.084	-0.282	-1.6415	-0.684	0.273	-0.4785	-2.6045
921204							
-0.591	0.287	-0.439	-0.439	-0.858	0.348	-0.603	-0.603
-0.463	0.143	-0.303	-0.742	-0.761	0.241	-0.501	-1.104
-0.494	0.188	-0.341	-1.083	-0.778	0.268	-0.523	-1.627
-0.467	0.16	-0.3135	-1.3965	-0.72	0.201	-0.4605	-2.0875
-0.409	0.088	-0.2485	-1.645	-0.668	0.443	-0.5555	-2.643

Summary for site #1

910926	911105	911204	920308	920510	920609	920813	920912	921105	921204

A axis			in inches						
-0.438	-0.0025	0.0005	0.026	0.0205	0.0074	-0.002	-0.0005	-0.0005	-0.001
-0.78	0.042	0.0476	0.0805	0.0709	0.0466	0.028	0.0325	0.035	0.038
-1.0785	0.035	0.04	0.0735	0.0573	0.0308	0.0165	0.021	0.0065	-0.0045
-1.3395	0.03	0.0321	0.074	0.05265	0.02315	-0.0035	-0.01	-0.02	-0.057
-1.625	0.039	0.0223	0.0245	0.0145	0.0351	0.0135	0.0065	-0.0165	-0.02
Recalculation		A axis	in inches						
2.8	-0.0025	0.0005	0.026	0.0205	0.0074	-0.002	-0.0005	-0.0005	-0.001
2.2	0.042	0.0476	0.0805	0.0709	0.0466	0.028	0.0325	0.035	0.038
1.6	0.035	0.04	0.0735	0.0573	0.0308	0.0165	0.021	0.0065	-0.0045
1	0.03	0.0321	0.074	0.05265	0.02315	-0.0035	-0.01	-0.02	-0.057
0.4	0.039	0.0223	0.0245	0.0145	0.0351	0.0135	0.0065	-0.0165	-0.02
	in cm (1	inch=2.54	cm)						
2.8	-0.0063	0.00127	0.06604	0.05207	0.0188	-0.0051	-0.0013	-0.0013	-0.0025
2.2	0.10668	0.1209	0.20447	0.18009	0.11836	0.07112	0.08255	0.0889	0.09652
1.6	0.0889	0.1016	0.18669	0.14554	0.07823	0.04191	0.05334	0.01651	-0.0114
1	0.0762	0.08153	0.18796	0.13373	0.0588	-0.0089	-0.0254	-0.0508	-0.1448
0.4	0.09906	0.05664	0.06223	0.03683	0.08915	0.03429	0.01651	-0.0419	-0.0508
Axis B	in inches			site #1					
2.8	-0.009	-0.013	-0.0065	-0.0143	-0.0168	-0.02	-0.0205	-0.019	-0.0185
2.2	0.004	0.0127	0.012	0.00325	-0.0009	-0.0045	-0.0085	-0.014	0.005
1.6	0.0145	0.02575	0.033	0.0173	0.00605	0.0015	-0.014	-0.0275	0.0045
1	0.0285	0.0325	0.04	0.0239	0.00405	0.0075	-0.0115	-0.0175	0.021
0.4	0.0105	0.04745	0.0995	0.07285	0.04145	0.032	-0.0085	-0.034	-0.0725
B aixs	in cm	1 inch=2.54	cm						
2.8	-0.0229	-0.0331	-0.0165	-0.0364	-0.0428	-0.0508	-0.0521	-0.0483	-0.047
2.2	0.01016	0.03226	0.03048	0.00826	-0.0024	-0.0114	-0.0216	-0.0356	0.0127
1.6	0.03683	0.06541	0.08382	0.04394	0.01537	0.00381	-0.0356	-0.0698	0.01143
1	0.07239	0.08255	0.1016	0.06071	0.01029	0.01905	-0.0292	-0.0445	0.05334
0.4	0.02667	0.12052	0.25273	0.18504	0.10528	0.08128	-0.0216	-0.0864	-0.1841

Site 2

September 26, 1991

A0	A180	Aavg	Acum	B0	B180	Bavg	Bcum
-0.023	0.255	-0.139	-0.139	-0.133	0.053	-0.093	-0.093
-0.071	0.161	-0.116	-0.255	-0.128	0.06	-0.094	-0.187

-0.11	0.12	-0.115	-0.37	-0.204	0.133	-0.1685	-0.3555
-0.247	0.014	-0.1305	-0.5005	-0.183	0.108	-0.1455	-0.501
-0.305	0.078	-0.1915	-0.692	-0.155	0.083	-0.119	-0.62

November 5,1991			Site #2				
A0	A180	Aavg	Acum	B0	B180	Bavg	Bcum
-0.03	0.238	-0.134	-0.134	-0.138	0.047	-0.0925	-0.0925
-0.062	0.149	-0.1055	-0.2395	-0.088	0.01	-0.049	-0.1415
-0.112	0.102	-0.107	-0.3465	-0.225	0.145	-0.185	-0.3265
-0.231	0.021	-0.126	-0.4725	-0.228	0.145	-0.1865	-0.513
-0.335	0.113	-0.224	-0.6965	-0.155	0.079	-0.117	-0.63

December 4, 1991			Site #2				
A0	A180	Aavg	Acum	B0	B180	Bavg	Bcum
-0.0285	0.2407	-0.1346	-0.1346	-0.1356	0.043	-0.0893	-0.0893
-0.0728	0.1507	-0.1118	-0.2464	-0.0843	0.0083	-0.0463	-0.1356
-0.1187	0.084	-0.1014	-0.3477	-0.2084	0.143	-0.1757	-0.3113
-0.168	0.0365	-0.1023	-0.45	-0.2174	0.1348	-0.1761	-0.4874
-0.3406	0.2538	-0.2972	-0.7472	-0.1437	0.055	-0.0994	-0.5868

March 8, 1992			Site #2				
A0	A180	Aavg	Acum	B0	B180	Bavg	Bcum
-0.028	0.2306	-0.1293	-0.1293	-0.1258	0.038	-0.0819	-0.0819
-0.0925	0.1206	-0.1066	-0.2359	-0.0753	0.012	-0.0437	-0.1256
-0.1508	0.093	-0.1219	-0.3578	-0.2031	0.134	-0.1686	-0.2941
-0.1943	0.0427	-0.1185	-0.4763	-0.2053	0.1257	-0.1655	-0.4596
-0.2507	0.05	-0.1504	-0.6266	-0.1348	0.0462	-0.0905	-0.5501

920510			Site #2				
-0.0243	0.2538	-0.1391	-0.1391	-0.1109	0.042	-0.0765	-0.0764
-0.1732	0.1248	-0.149	-0.2881	-0.1362	0.182	-0.1591	-0.2356
-0.1642	0.1258	-0.145	-0.4331	-0.2683	0.132	-0.2002	-0.4357
-0.2538	0.063	-0.1584	-0.5915	-0.1936	0.142	-0.1678	-0.6035
-0.3521	0.0285	-0.1903	-0.7818	-0.1202	0.163	-0.1416	-0.7451

920609			Site #2				
-0.0287	0.2671	-0.1479	-0.1479	-0.1372	0.128	-0.1326	-0.1326
-0.15	0.1507	-0.1504	-0.2983	-0.1362	0.173	-0.1546	-0.2872
-0.1653	0.1352	-0.1503	-0.4485	-0.326	0.126	-0.226	-0.5132
-0.2847	0.0285	-0.1566	-0.6051	-0.386	0.162	-0.274	-0.7872

-0.3926	0.0305	-0.2116	-0.8167	-0.328	0.13	-0.229	-1.0162
August13,1992			Site #2				
-0.031	0.2702	-0.1506	-0.1506	-0.355	0.177	-0.266	-0.266
-0.155	0.1538	-0.1544	-0.305	-0.302	0.23	-0.266	-0.532
-0.174	0.1492	-0.1616	-0.4666	-0.425	0.112	-0.2685	-0.8005
-0.292	0.0301	-0.1611	-0.6277	-0.45	0.083	-0.2665	-1.067
-0.409	0.0431	-0.218	-0.8457	-0.412	0.125	-0.2685	-1.3355
Sept.12,1992			Site #2				
-0.03	0.296	-0.163	-0.163	-0.374	0.187	-0.2805	-0.2805
-0.15	0.165	-0.1575	-0.3205	-0.308	0.246	-0.277	-0.5575
-0.194	0.133	-0.1635	-0.484	-0.437	0.113	-0.275	-0.8325
-0.275	0.055	-0.165	-0.649	-0.474	0.089	-0.2815	-1.114
-0.388	0.053	-0.2205	-0.8695	-0.414	0.122	-0.268	-1.382
921105			Site #2				
-0.048	0.28	-0.164	-0.164	-0.36	0.163	-0.2615	-0.2615
-0.177	0.141	-0.159	-0.323	-0.368	0.282	-0.325	-0.5865
-0.146	0.169	-0.1575	-0.4805	-0.382	0.232	-0.307	-0.8935
-0.219	0.143	-0.181	-0.6615	-0.327	0.198	-0.2625	-1.156
-0.323	0.113	-0.218	-0.8795	-0.398	0.336	-0.367	-1.523
921204			Site #2				
-0.049	0.268	-0.1585	-0.1585	-0.337	0.186	-0.2615	-0.2615
-0.176	0.148	-0.162	-0.3205	-0.298	0.223	-0.2605	-0.522
-0.205	0.119	-0.162	-0.4825	-0.454	0.05	-0.252	-0.774
-0.318	0.007	-0.1625	-0.645	-0.457	0.068	-0.2625	-1.0365
-0.388	0.45	-0.419	-1.064	-0.278	0.869	-0.5735	-1.61

Summary for site #2

910926	911105	911204	920308	920510	920609	920813	920912	921105	921204
A axis				in inches					
-0.139	0.005	0.0044	0.0097	-5E-05	-0.0089	-0.0116	-0.024	-0.025	-0.0195
-0.255	0.0155	0.00865	0.01915	-0.0331	-0.0432	-0.05	-0.0655	-0.068	-0.0655
-0.37	0.0235	0.0223	0.01225	-0.0631	-0.0785	-0.0966	-0.114	-0.1105	-0.1125
-0.5005	0.028	0.05055	0.02425	-0.091	-0.1046	-0.1272	-0.1485	-0.161	-0.1445
-0.692	-0.0045	-0.0551	0.0654	-0.0898	-0.1247	-0.1537	-0.1775	-0.1875	-0.372

A axis	in cm		site #2						
2.8	0.0127	0.01118	0.02464	-0.0001	-0.0226	-0.0295	-0.061	-0.0635	-0.0495
2.2	0.03937	0.02197	0.04864	-0.0839	-0.1099	-0.127	-0.1664	-0.1727	-0.1664
1.6	0.05969	0.05664	0.03112	-0.1601	-0.1994	-0.2454	-0.2896	-0.2807	-0.2858
1	0.07112	0.1284	0.0616	-0.231	-0.2657	-0.323	-0.3772	-0.4089	-0.367
0.4	-0.0114	-0.1401	0.16612	-0.228	-0.3166	-0.3903	-0.4509	-0.4763	-0.9449

B axis	site #2			in inches				B axis	
2.8	0.0005	0.0037	0.0111	0.01655	-0.0396	-0.173	-0.1875	-0.1685	-0.1685
2.2	0.0455	0.0514	0.06145	-0.0486	-0.1002	-0.345	-0.3705	-0.3995	-0.335
1.6	0.029	0.0442	0.0614	-0.0802	-0.1577	-0.445	-0.477	-0.538	-0.4185
1	-0.012	0.0136	0.0414	-0.1025	-0.2862	-0.566	-0.613	-0.655	-0.5355
0.4	-0.01	0.03325	0.0699	-0.1251	-0.3962	-0.7155	-0.762	-0.903	-0.99

B axis	in cm		Site #2					B axis	
2.8	0.00127	0.0094	0.02819	0.04204	-0.1006	-0.4394	-0.4763	-0.428	-0.428
2.2	0.11557	0.13056	0.15608	-0.1233	-0.2545	-0.8763	-0.9411	-1.0147	-0.8509
1.6	0.07366	0.11227	0.15596	-0.2037	-0.4006	-1.1303	-1.2116	-1.3665	-1.063
1	-0.0305	0.03454	0.10516	-0.2604	-0.7269	-1.4376	-1.557	-1.6637	-1.3602
0.4	-0.0254	0.08445	0.17755	-0.3178	-1.0063	-1.8174	-1.9355	-2.2936	-2.5146

Site #3

September 26, 1991

A0	A180	Aavg	Acum	B0	B180	Bavg	Bcum
-1.143	0.915	-1.029	-1.029	-0.103	0.035	-0.069	-0.069
-1.244	1.007	-1.1255	-2.1545	-0.113	0.038	-0.0755	-0.1445
-1.259	1.025	-1.142	-3.2965	-0.15	0.082	-0.116	-0.2605
-1.236	1.006	-1.121	-4.4175	-0.207	0.142	-0.1745	-0.435
-1.23	1.002	-1.116	-5.5335	-0.285	0.223	-0.254	-0.689

November 5, 1991

A0	A180	Aavg	Acum	B0	B180	Bavg	Bcum
-1.32	0.726	-1.023	-1.023	-0.127	0.042	-0.0845	-0.0845
-1.372	0.927	-1.1495	-2.1725	-0.1	0.03	-0.065	-0.1495
-1.492	0.872	-1.182	-3.3545	-0.185	0.125	-0.155	-0.3045
-1.372	1.02	-1.196	-4.5505	-0.222	0.16	-0.191	-0.4955
-1.472	0.872	-1.172	-5.7225	-0.324	0.238	-0.281	-0.7765

December 4, 1991

A0	A180	Aavg	Acum	B0	B180	Bavg	Bcum
-1.273	0.725	-0.999	-0.999	-0.138	0.042	-0.09	-0.09
-1.28	1.027	-1.1535	-2.1525	-0.12	0.051	-0.0855	-0.1755

-1.468	0.927	-1.1975	-3.35	-0.126	0.147	-0.1365	-0.312
-1.029	1.203	-1.116	-4.466	-0.248	0.172	-0.21	-0.522
-1.826	0.432	-1.129	-5.595	-0.352	0.27	-0.311	-0.833

March 8, 1992

A0	A180	Aavg	Acum	B0	B180	Bavg	Bcum
-1.172	0.825	-0.9985	-0.9985	-0.12	0.06	-0.09	-0.09
-1.274	0.92	-1.097	-2.0955	-0.126	0.142	-0.134	-0.224
-1.372	1.032	-1.202	-3.2975	-0.147	0.158	-0.1525	-0.3765
-1.203	0.97	-1.0865	-4.384	-0.219	0.169	-0.194	-0.5705
-1.784	0.302	-1.043	-5.427	-0.372	0.334	-0.353	-0.9235
920510				Site #3			
-1.132	0.914	-1.023	-1.023	-0.132	0.074	-0.103	-0.103
-1.252	1.043	-1.1475	-2.1705	-0.126	0.192	-0.159	-0.262
-1.398	1.183	-1.2905	-3.461	-0.158	0.152	-0.155	-0.417
-1.3	1.072	-1.186	-4.647	-0.262	0.283	-0.2725	-0.6895
-1.289	1.069	-1.179	-5.826	-0.351	0.342	-0.3465	-1.036
920609							
-1.192	0.817	-1.0045	-1.0045	-0.136	0.182	-0.159	-0.159
-1.37	0.992	-1.181	-2.1855	-0.119	0.151	-0.135	-0.294
-1.559	1.198	-1.3785	-3.564	-0.159	0.142	-0.1505	-0.4445
-1.408	1.005	-1.2065	-4.7705	-0.271	0.291	-0.281	-0.7255
-1.987	0.362	-1.1745	-5.945	-0.372	0.352	-0.362	-1.0875
920813							
-1.205	0.865	-1.035	-1.035	-0.305	0.184	-0.2445	-0.2445
-1.357	1.017	-1.187	-2.222	-0.106	0.043	-0.0745	-0.319
-1.552	1.209	-1.3805	-3.6025	-0.306	0.087	-0.1965	-0.5155
-1.42	1.079	-1.2495	-4.852	-0.306	0.339	-0.3225	-0.838
-1.342	0.997	-1.1695	-6.0215	-0.329	0.304	-0.3165	-1.1545
920912							
-1.196	0.874	-1.035	-1.035	-0.388	0.17	-0.279	-0.279
-1.356	1.028	-1.192	-2.227	-0.342	-0.208	-0.067	-0.346
-1.55	1.219	-1.3845	-3.6115	-0.434	0.127	-0.2805	-0.6265
-1.411	1.07	-1.2405	-4.852	-0.443	0.104	-0.2735	-0.9
-1.339	1.01	-1.1745	-6.0265	-0.408	0.325	-0.3665	-1.2665

921105				Site #3			
-1.186	0.886	-1.036	-1.036	-0.364	0.149	-0.2565	-0.2565
-1.358	1.063	-1.2105	-2.2465	-0.317	0.186	-0.2515	-0.508
-1.826	1.508	-1.667	-3.9135	-0.496	0.028	-0.262	-0.77
-1.507	1.206	-1.3565	-5.27	-0.434	0.073	-0.2535	-1.0235
-1.303	1.488	-1.3955	-6.6655	-0.54	0.023	-0.2815	-1.305
921204				Site #3			
-1.096	0.871	-0.9835	-0.9835	-0.343	0.162	-0.2525	-0.2525
-1.318	1.064	-1.191	-2.1745	-0.373	0.154	-0.2635	-0.516
-1.863	1.56	-1.7115	-3.886	-0.404	0.024	-0.214	-0.73
-1.519	1.224	-1.3715	-5.2575	-0.459	0.026	-0.2425	-0.9725
-1.308	1.004	-1.156	-6.4135	-0.487	0.062	-0.2745	-1.247

Summary for site #3

910926	911105	911204	920308	920510	920609	920813	920912	921105	911205
A axis		in inches							
-1.029	0.006	0.03	0.0305	0.006	0.0245	-0.006	-0.006	-0.007	0.0455
-2.1545	-0.018	0.002	0.059	-0.016	-0.031	-0.0675	-0.0725	-0.092	-0.02
-3.2965	-0.058	-0.0535	-0.001	-0.1645	-0.2675	-0.306	-0.315	-0.617	-0.5895
-4.4175	-0.133	-0.0485	0.0335	-0.2295	-0.353	-0.4345	-0.4345	-0.8525	-0.84
-5.5335	-0.189	-0.0615	0.1065	-0.2925	-0.4115	-0.488	-0.493	-1.132	-0.88

A axis	in cm		site #3			A axis		in cm	
2.8	0.01524	0.0762	0.07747	0.01524	0.06223	-0.0152	-0.0152	-0.0178	0.11557
2.2	-0.0457	0.00508	0.14986	-0.0406	-0.0787	-0.1714	-0.1841	-0.2337	-0.0508
1.6	-0.1473	-0.1359	-0.0025	-0.4178	-0.6794	-0.7772	-0.8001	-1.5672	-1.4973
1	-0.3378	-0.1232	0.08509	-0.5829	-0.8966	-1.1036	-1.1036	-2.1654	-2.1336
0.4	-0.4801	-0.1562	0.27051	-0.7429	-1.0452	-1.2395	-1.2522	-2.8753	-2.2352

B axis	in inches		site #3			B axis		in inches	
2.8	-0.0155	-0.021	-0.021	-0.034	-0.09	-0.1755	-0.21	-0.1875	-0.1835
2.2	-0.005	-0.031	-0.0795	-0.1175	-0.1495	-0.1745	-0.2015	-0.3635	-0.3715
1.6	-0.044	-0.0515	-0.116	-0.1565	-0.184	-0.255	-0.366	-0.5095	-0.4695
1	-0.0605	-0.087	-0.1355	-0.2545	-0.2905	-0.403	-0.465	-0.5885	-0.5375
0.4	-0.0875	-0.144	-0.2345	-0.347	-0.3985	-0.4655	-0.5775	-0.616	-0.558

B axis	in cm		site #3			B axis		in cm	
2.8	-0.0394	-0.0533	-0.0533	-0.0864	-0.2286	-0.4458	-0.5334	-0.4762	-0.4661

2.2	-0.0127	-0.0787	-0.2019	-0.2985	-0.3797	-0.4432	-0.5118	-0.9233	-0.9436
1.6	-0.1118	-0.1308	-0.2946	-0.3975	-0.4674	-0.6477	-0.9296	-1.2941	-1.1925
1	-0.1537	-0.221	-0.3442	-0.6464	-0.7379	-1.0236	-1.1811	-1.4948	-1.3653
0.4	-0.2223	-0.3658	-0.5956	-0.8814	-1.0122	-1.1824	-1.4669	-1.5646	-1.4173

Site #4

September 26, 1991

A0	A180	Aavg	Acum	B0	B180	Bavg	Bcum
-0.036	0.268	-0.152	-0.152	-0.769	0.71	-0.7395	-0.7395
-0.098	0.138	-0.118	-0.27	-0.667	0.609	-0.638	-1.3775
-0.215	0.01	-0.1125	-0.3825	-0.604	0.55	-0.577	-1.9545
-0.43	0.188	-0.309	-0.6915	-0.438	0.378	-0.408	-2.3625
-0.559	0.309	-0.434	-1.1255	-0.392	0.323	-0.3575	-2.72

November 5, 1991

A0	A180	Aavg	Acum	B0	B180	Bavg	Bcum
-0.012	0.26	-0.136	-0.136	-0.778	0.686	-0.732	-0.732
-0.094	0.12	-0.107	-0.243	-0.633	0.546	-0.5895	-1.3215
-0.162	0.151	-0.1565	-0.3995	-0.621	0.528	-0.5745	-1.896
-0.379	0.126	-0.2525	-0.652	-0.468	0.39	-0.429	-2.325
-0.484	0.578	-0.531	-1.183	-0.547	0.434	-0.4905	-2.8155

December 4, 1991

A0	A180	Aavg	Acum	B0	B180	Bavg	Bcum
-0.019	0.218	-0.1185	-0.1185	-0.284	1.14	-0.712	-0.712
-0.104	0.122	-0.113	-0.2315	-0.187	0.763	-0.475	-1.187
-0.148	0.155	-0.1515	-0.383	-0.558	0.563	-0.5605	-1.7475
-0.348	0.168	-0.258	-0.641	-0.498	0.379	-0.4385	-2.186
-0.419	0.589	-0.504	-1.145	-0.487	1.176	-0.8315	-3.0175

March 8, 1992

A0	A180	Aavg	Acum	B0	B180	Bavg	Bcum
-0.003	0.223	-0.113	-0.113	-0.936	0.474	-0.705	-0.705
-0.105	0.203	-0.154	-0.267	-0.829	0.343	-0.586	-1.291
-0.132	0.101	-0.1165	-0.3835	-0.809	0.337	-0.573	-1.864
-0.144	0.06	-0.102	-0.4855	-0.658	0.134	-0.396	-2.26
-0.582	0.429	-0.5055	-0.991	-0.907	0.243	-0.575	-2.835

920510							
-0.003	0.226	-0.1145	-0.1145	-1.045	0.332	-0.6885	-0.6885

-0.107	0.216	-0.1615	-0.276	-0.884	0.226	-0.555	-1.2435
-0.152	0.108	-0.13	-0.406	-0.865	0.168	-0.5165	-1.76
-0.246	0.027	-0.1365	-0.5425	-0.69	0.131	-0.4105	-2.1705
-0.508	0.644	-0.576	-1.1185	-0.766	0.213	-0.4895	-2.66
920609							
-0.008	0.243	-0.1255	-0.1255	-1.036	0.349	-0.6925	-0.6925
-0.102	0.233	-0.1675	-0.293	-0.927	0.283	-0.605	-1.2975
-0.164	0.15	-0.157	-0.45	-0.852	0.309	-0.5805	-1.878
-0.284	0.022	-0.153	-0.603	-0.714	0.067	-0.3905	-2.2685
-0.582	0.532	-0.557	-1.16	-0.835	0.209	-0.522	-2.7905
920813							
-0.001	0.326	-0.1635	-0.1635	-1.012	0.477	-0.7445	-0.7445
-0.122	0.212	-0.167	-0.3305	-0.886	0.36	-0.623	-1.3675
-0.17	0.149	-0.1595	-0.49	-0.862	0.319	-0.5905	-1.958
-0.346	0.016	-0.181	-0.671	-0.744	0.204	-0.474	-2.432
-0.506	0.541	-0.5235	-1.1945	-0.785	0.244	-0.5145	-2.9465
920912							
-0.005	0.33	-0.1675	-0.1675	-1.027	0.471	-0.749	-0.749
-0.112	0.221	-0.1665	-0.334	-0.89	0.334	-0.612	-1.361
-0.185	0.149	-0.167	-0.501	-0.876	0.323	-0.5995	-1.9605
-0.353	0.003	-0.178	-0.679	-0.767	0.2	-0.4835	-2.444
-0.598	0.54	-0.569	-1.248	-0.738	0.203	-0.4705	-2.9145
921105				Site #4			
-0.005	0.312	-0.1585	-0.1585	-1.008	0.482	-0.745	-0.745
-0.118	0.191	-0.1545	-0.313	-0.868	0.349	-0.6085	-1.3535
-0.049	0.268	-0.1585	-0.4715	-0.888	0.358	-0.623	-1.9765
-0.258	0.07	-0.164	-0.6355	-0.729	0.208	-0.4685	-2.445
-0.478	0.168	-0.323	-0.9585	-0.757	0.226	-0.4915	-2.9365
921204							
-0.002	0.317	-0.1595	-0.1595	-0.998	0.477	-0.7375	-0.7375
-0.128	0.186	-0.157	-0.3165	-0.858	0.349	-0.6035	-1.341
-0.03	0.278	-0.154	-0.4705	-0.888	0.368	-0.628	-1.969
-0.242	0.078	-0.16	-0.6305	-0.708	0.193	-0.4505	-2.4195
-0.48	0.146	-0.313	-0.9435	-0.742	0.215	-0.4785	-2.898

Summary for site #4

910926	911104	911205	920308	920510	920609	920813	920912	921104	921204
A axis				in inches					
-0.152	0.016	0.0335	0.039	0.0375	0.0265	-0.0115	-0.0155	-0.0065	-0.0075
-0.27	0.027	0.0385	0.003	-0.006	-0.023	-0.0605	-0.064	-0.043	-0.0465
-0.3825	-0.017	-0.0005	-0.001	-0.0235	-0.0675	-0.1075	-0.1185	-0.089	-0.088
-0.6915	0.0395	0.0505	0.206	0.149	0.0885	0.0205	0.0125	0.056	0.061
-1.1255	-0.0575	-0.0195	0.1345	0.007	-0.0345	-0.069	-0.1225	0.167	0.182
A axis	in cm								
2.8	0.04064	0.08509	0.09906	0.09525	0.06731	-0.0292	-0.0394	-0.0165	-0.019
2.2	0.06858	0.09779	0.00762	-0.0152	-0.0584	-0.1537	-0.1626	-0.1092	-0.1181
1.6	-0.0432	-0.0013	-0.0025	-0.0597	-0.1715	-0.2731	-0.301	-0.2261	-0.2235
1	0.10033	0.12827	0.52324	0.37846	0.22479	0.05207	0.03175	0.14224	0.15494
0.4	-0.146	-0.0495	0.34163	0.01778	-0.0876	-0.1753	-0.3112	0.42418	0.46228
Site #4		inches						B axis	
2.8	0.0075	0.0275	0.0345	0.051	0.047	-0.005	-0.0095	-0.0055	0.002
2.2	0.056	0.1905	0.0865	0.134	0.08	0.01	0.0165	0.024	0.0365
1.6	0.0585	0.207	0.0905	0.1945	0.0765	-0.0035	-0.006	-0.022	-0.0145
1	0.0375	0.1765	0.1025	0.192	0.094	-0.0695	-0.0815	-0.0825	-0.057
0.4	-0.0955	-0.2975	-0.115	0.06	-0.0705	-0.2265	-0.1945	-0.2165	-0.178
	B axis	in cm							
2.8	0.01905	0.06985	0.08763	0.12954	0.11938	-0.0127	-0.0241	-0.014	0.00508
2.2	0.14224	0.48387	0.21971	0.34036	0.2032	0.0254	0.04191	0.06096	0.09271
1.6	0.14859	0.52578	0.22987	0.49403	0.19431	-0.0089	-0.0152	-0.0559	-0.0368
1	0.09525	0.44831	0.26035	0.48768	0.23876	-0.1765	-0.207	-0.2096	-0.1448
0.4	-0.2426	-0.7557	-0.2921	0.1524	-0.1791	-0.5753	-0.494	-0.5499	-0.4521

Site #5

Sept. 26, 1991

A0	A180	Aavg	Acum	B0	B180	Bavg	Bcum
-1.282	1.047	-1.1645	-1.1645	-0.468	0.411	-0.4395	-0.4395
-1.331	1.093	-1.212	-2.3765	-0.457	0.396	-0.4265	-0.866
-1.266	1.022	-1.144	-3.5205	-0.421	0.353	-0.387	-1.253
-1.133	1.882	-1.5075	-5.028	-0.348	0.28	-0.314	-1.567
-1.049	0.808	-0.9285	-5.9565	-0.298	0.231	-0.2645	-1.8315

March 8, 1992			Site #5				
A0	A180	Aavg	Acum	B0	B180	Bavg	Bcum
-1.288	0.97	-1.129	-1.129	-0.65	0.135	-0.3925	-0.3925
-1.338	1.002	-1.17	-2.299	-0.652	0.14	-0.396	-0.7885
-1.479	1.148	-1.3135	-3.6125	-0.557	0.06	-0.3085	-1.097
-1.388	1.063	-1.2255	-4.838	-0.34	0.249	-0.2945	-1.3915
920510							
-1.299	0.972	-1.1355	-1.1355	-0.629	0.15	-0.3895	-0.3895
-1.336	1.007	-1.1715	-2.307	-0.625	0.139	-0.382	-0.7715
-1.488	1.159	-1.3235	-3.6305	-0.515	0.135	-0.325	-1.0965
-1.392	1.069	-1.2305	-4.861	-0.56	0.062	-0.311	-1.4075
-1.309	0.977	-1.143	-6.004	-0.218	0.171	-0.1945	-1.602
920609							
-1.321	0.944	-1.1325	-1.1325	-0.652	0.127	-0.3895	-0.3895
-1.438	1.016	-1.227	-2.3595	-0.637	0.134	-0.3855	-0.775
-1.502	1.15	-1.326	-3.6855	-0.631	0.129	-0.38	-1.155
-1.678	0.818	-1.248	-4.9335	-0.593	0.071	-0.332	-1.487
-1.492	0.974	-1.233	-6.1665	-0.578	0.129	-0.3535	-1.8405
920813				Site #5			
-1.305	0.944	-1.1245	-1.1245	-0.678	0.118	-0.398	-0.398
-1.426	1.138	-1.282	-2.4065	-0.659	0.109	-0.384	-0.782
-1.521	1.101	-1.311	-3.7175	-0.648	0.09	-0.369	-1.151
-1.493	1.087	-1.29	-5.0075	-0.61	0.052	-0.331	-1.482
-1.603	0.938	-1.2705	-6.278	-0.602	0.046	-0.324	-1.806
920912							
-1.362	0.953	-1.1575	-1.1575	-0.682	0.133	-0.4075	-0.4075
-1.48	1.103	-1.2915	-2.449	-0.658	0.123	-0.3905	-0.798
-1.496	1.103	-1.2995	-3.7485	-0.661	0.112	-0.3865	-1.1845
-1.505	1.004	-1.2545	-5.003	-0.615	0.07	-0.3425	-1.527
-1.492	0.974	-1.233	-6.236	-0.621	0.078	-0.3495	-1.8765
921105							
-1.274	0.953	-1.1135	-1.1135	-0.683	0.153	-0.418	-0.418
-1.344	1.048	-1.196	-2.3095	-0.669	0.136	-0.4025	-0.8205
-1.638	1.332	-1.485	-3.7945	-0.599	0.069	-0.334	-1.1545

-1.458	1.196	-1.327	-5.1215	-0.589	0.051	-0.32	-1.4745
-1.299	0.928	-1.1135	-6.235	-0.547	0.023	-0.285	-1.7595
921204							
-1.28	0.994	-1.137	-1.137	-0.675	-0.014	-0.3305	-0.3305
-1.379	1.079	-1.229	-2.366	-0.647	0.087	-0.367	-0.6975
-1.676	1.307	-1.4915	-3.8575	-0.569	0.075	-0.322	-1.0195
-1.489	1.168	-1.3285	-5.186	-0.596	0.067	-0.3315	-1.351
-1.281	0.633	-0.957	-6.143	-0.522	0.003	-0.2625	-1.6135

Summary for site #5

	910926	920308	920510	920609	920813	920912	921105	921204
A axis				in inches				
	2.8	0.0355	0.029	0.032	0.04	0.007	0.051	0.0275
	2.2	0.0775	0.0695	0.017	-0.03	-0.0725	0.067	0.0105
	1.6	-0.092	-0.11	-0.165	-0.197	-0.228	-0.274	-0.337
	1	0.19	0.167	0.0945	0.0205	0.025	-0.0935	-0.158
	0.4		-0.0475	-0.21	-0.3215	-0.2795	-0.2785	-0.1865
		A axis			in cm			
	2.8	0.09017	0.07366	0.08128	0.1016	0.01778	0.12954	0.06985
	2.2	0.19685	0.17653	0.04318	-0.0762	-0.1841	0.17018	0.02667
	1.6	-0.2337	-0.2794	-0.4191	-0.5004	-0.5791	-0.696	-0.856
	1	0.4826	0.42418	0.24003	0.05207	0.0635	-0.2375	-0.4013
	0.4	-0.1478	-0.1206	-0.5334	-0.8166	-0.7099	-0.7074	-0.4737
B axis		Site #5			inches			
	2.8	0.047	0.05	0.05	0.0415	0.032	0.0215	0.109
	2.2	0.0775	0.0945	0.091	0.084	0.068	0.0455	0.1685
	1.6	0.156	0.1565	0.098	0.102	0.0685	0.0985	0.2335
	1	0.1755	0.1595	0.08	0.085	0.04	0.0925	0.216
	0.4		0.2295	-0.009	0.0255	-0.045	0.072	0.218
					cm	B axis		
	2.8	0.11938	0.127	0.127	0.10541	0.08128	0.05461	0.27686
	2.2	0.19685	0.24003	0.23114	0.21336	0.17272	0.11557	0.42799
	1.6	0.39624	0.39751	0.24892	0.25908	0.17399	0.25019	0.59309
	1	0.44577	0.40513	0.2032	0.2159	0.1016	0.23495	0.54864
	0.4		0.58293	-0.0229	0.06477	-0.1143	0.18288	0.55372

Site #6

September 26, 1991

A0	A180	Aavg	Acum	B0	B180	Bavg	Bcum
-1.495	1.266	-1.3805	-1.3805	-0.201	0.132	-0.1665	-0.1665
-1.463	1.233	-1.348	-2.7285	-0.07	0.004	-0.037	-0.2035
-1.585	1.354	-1.4695	-4.198	-0.103	0.103	-0.103	-0.3065
-1.609	1.38	-1.4945	-5.6925	-0.45	0.118	-0.284	-0.5905

November 4, 1991

A0	A180	Aavg	Acum	B0	B180	Bavg	Bcum
-1.535	1.315	-1.425	-1.425	-0.091	0.158	-0.1245	-0.1245
-1.492	1.274	-1.383	-2.808	-0.025	0.038	-0.0315	-0.156
-1.541	1.318	-1.4295	-4.2375	-0.113	0.052	-0.0825	-0.2385
-1.543	1.328	-1.4355	-5.673	-0.122	0.035	-0.0785	-0.317

December 05, 1991

A0	A180	Aavg	Acum	B0	B180	Bavg	Bcum
-1.507	1.334	-1.4205	-1.4205	-0.128	0.183	-0.1555	-0.1555
-1.419	1.289	-1.354	-2.7745	-0.268	0.007	-0.1375	-0.293
-1.524	1.31	-1.417	-4.1915	-0.102	0.273	-0.1875	-0.4805
-1.513	1.364	-1.4385	-5.63	-0.187	0.754	-0.4705	-0.951

March 08, 1992

A0	A180	Aavg	Acum	B0	B180	Bavg	Bcum
-1.644	1.276	-1.46	-1.46	-0.274	0.142	-0.208	-0.208
-1.548	1.173	-1.3605	-2.8205	-0.231	0.271	-0.251	-0.459
-1.628	1.25	-1.439	-4.2595	-0.138	0.32	-0.229	-0.688
-1.468	1.588	-1.528	-5.7875	-0.162	0.319	-0.2405	-0.9285
920510							
-1.647	1.28	-1.4635	-1.4635	-0.388	0.108	-0.248	-0.248
-1.546	1.202	-1.374	-2.8375	-0.214	0.26	-0.237	-0.485
-1.621	1.23	-1.4255	-4.263	-0.125	0.368	-0.2465	-0.7315
-1.609	1.502	-1.5555	-5.8185	-0.187	0.207	-0.197	-0.9285
920609							
-1.635	1.302	-1.4685	-1.4685	-0.301	0.273	-0.287	-0.287
-1.582	1.24	-1.411	-2.8795	-0.253	0.254	-0.2535	-0.5405
-1.593	1.29	-1.4415	-4.321	-0.14	0.327	-0.2335	-0.774
-1.596	1.58	-1.588	-5.909	-0.201	0.232	-0.2165	-0.9905

920813							
-1.646	1.316	-1.481	-1.481	-0.13	0.412	-0.271	-0.271
-1.592	1.254	-1.423	-2.904	-0.258	0.289	-0.2735	-0.5445
-1.588	1.252	-1.42	-4.324	-0.35	0.188	-0.269	-0.8135
-1.584	1.26	-1.422	-5.746	-0.377	0.162	-0.2695	-1.083
920912							
-1.658	1.338	-1.498	-1.498	-0.132	0.423	-0.2775	-0.2775
-1.584	1.263	-1.4235	-2.9215	-0.252	0.308	-0.28	-0.5575
-1.562	1.24	-1.401	-4.3225	-0.366	0.198	-0.282	-0.8395
-1.571	1.17	-1.3705	-5.693	-0.373	0.17	-0.2715	-1.111
921105							
-1.648	1.342	-1.495	-1.495	-0.147	0.382	-0.2645	-0.2645
-1.569	1.248	-1.4085	-2.9035	-0.244	0.299	-0.2715	-0.536
-1.57	1.24	-1.405	-4.3085	-0.339	0.193	-0.266	-0.802
-1.583	1.253	-1.418	-5.7265	-0.328	0.185	-0.2565	-1.0585
921204							
-1.663	1.248	-1.4555	-1.4555	-0.123	0.368	-0.2455	-0.2455
-1.557	1.238	-1.3975	-2.853	-0.277	0.234	-0.2555	-0.501
-1.576	1.254	-1.415	-4.268	-0.29	0.184	-0.237	-0.738
-1.585	1.26	-1.4225	-5.6905	-0.276	0.219	-0.2475	-0.9855

Summary for site #6

910926	911104	911205	920308	920510	920609	920813	920913	921105	921204
A axis		in inches							
-1.3805	-0.0445	-0.04	-0.0795	-0.083	-0.088	-0.1005	-0.1175	-0.1145	-0.075
-2.7285	-0.0795	-0.046	-0.092	-0.109	-0.151	-0.1755	-0.193	-0.175	-0.1245
-4.198	-0.0395	0.0065	-0.0615	-0.065	-0.123	-0.126	-0.1245	-0.1105	-0.07
-5.6925	0.0195	0.0625	-0.095	-0.126	-0.2165	-0.0535	-0.0005	-0.034	0.002
A axis	in cm					A axis	in cm		
2	-0.113	-0.1016	-0.2019	-0.2108	-0.2235	-0.2553	-0.2984	-0.2908	-0.1905
1.4	-0.2019	-0.1168	-0.2337	-0.2769	-0.3835	-0.4458	-0.4902	-0.4445	-0.3162
0.8	-0.1003	0.01651	-0.1562	-0.1651	-0.3124	-0.32	-0.3162	-0.2807	-0.1778
0.2	0.04953	0.15875	-0.2413	-0.32	-0.5499	-0.1359	-0.0013	-0.0864	0.00508

B axis	Site #6	in inches		B axis		in inches			
2	0.042	0.011	-0.0415	-0.0815	-0.1205	-0.1045	-0.111	-0.098	-0.079
1.4	0.0475	-0.0895	-0.2555	-0.2815	-0.337	-0.341	-0.354	-0.3325	-0.2975
0.8	0.068	-0.174	-0.3815	-0.425	-0.4675	-0.507	-0.533	-0.4955	-0.4315
0.2	0.2735	-0.3605	-0.338	-0.338	-0.4	-0.4925	-0.5205	-0.468	-0.395
		in cm							
2	0.10668	0.02794	-0.1054	-0.207	-0.3061	-0.2654	-0.2819	-0.2489	-0.2007
1.4	0.12065	-0.2273	-0.649	-0.715	-0.856	-0.8661	-0.8992	-0.8446	-0.7557
0.8	0.17272	-0.442	-0.969	-1.0795	-1.1875	-1.2878	-1.3538	-1.2586	-1.096
0.2	0.69469	-0.9157	-0.8585	-0.8585	-1.016	-1.251	-1.3221	-1.1887	-1.0033